Erasmus+ PROGRAMME,

KEY ACTION: Cooperation for innovation and the exchange of good practices,

ACTION: Strategic Partnerships

FIELD: Strategic Partnerships for higher education, CALL: 2015

INNOVATIVE EUROPEAN STUDIES ON RENEWABLE ENERGY SYSTEMS

2015-1-TR01-KA203-021342

Real-time optimization of the Renewable Energy Sources / Fuel Cell Hybrid Power Systems

Nicu BIZON
University of Pitesti, Pitesti, Romania

Summary of Part 1 - FC HPS under test

1. FC HPS under test
2. Energy management strategies for FC vehicle
3. Advanced EMS for FC / Renewable HPS
4. Real-time Optimization of FC / Renewable HPS
5. Conclusions.

1. Hybrid architectures for the interconnection of Renewable Energy Sources (RES), Energy Storage Devices (ESD) and Fuel Cell (FC) system.

1.1. Hybrid architecture of multi-stages type

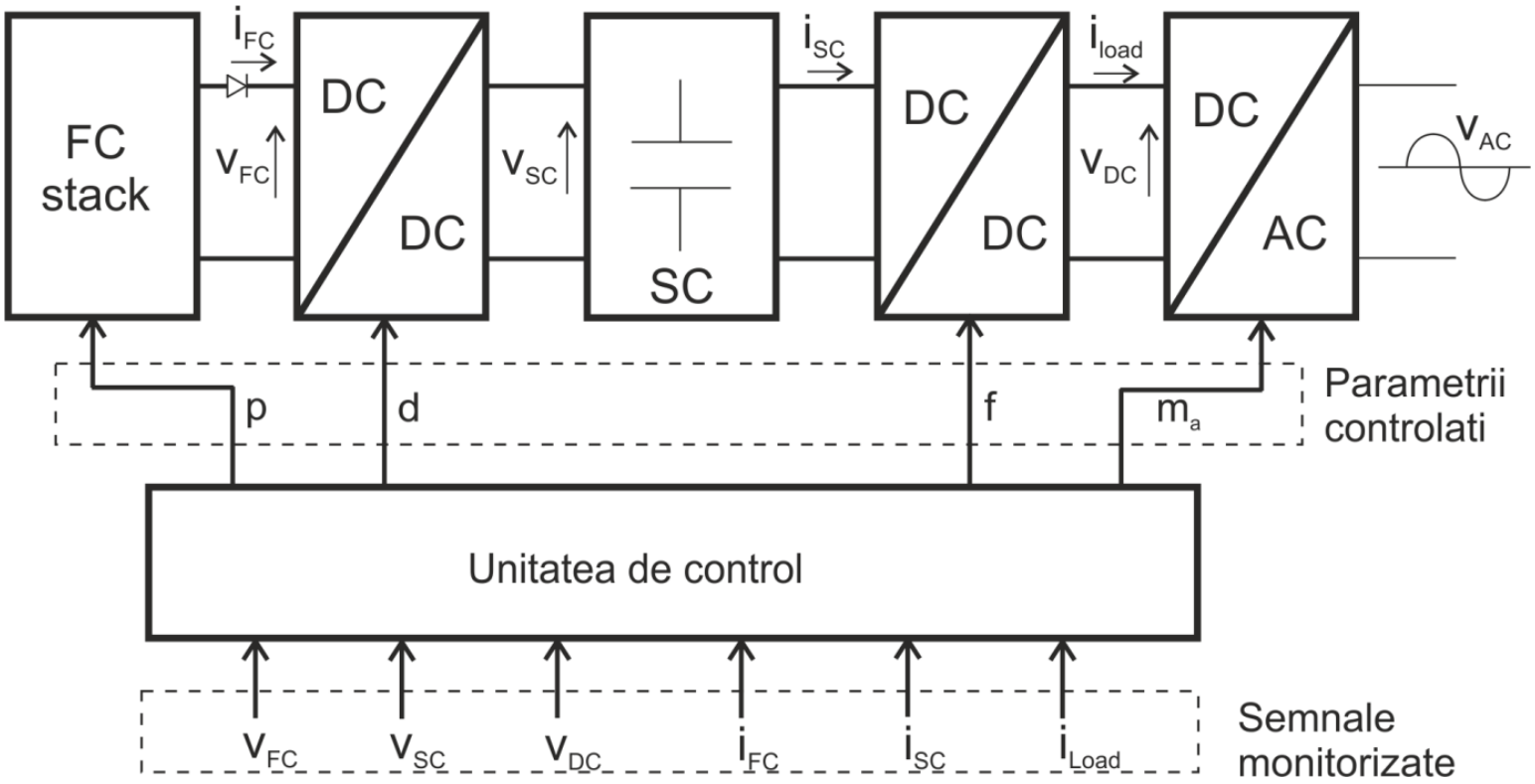

Figure 1.1. Diagram of Hybrid architecture of multi-stages type.

1. Hybrid architectures for the interconnection of Renewable Energy Sources (RES), Energy Storage Devices (ESD) and Fuel Cell (FC) system.

1.2. Hybrid architecture with DC bus

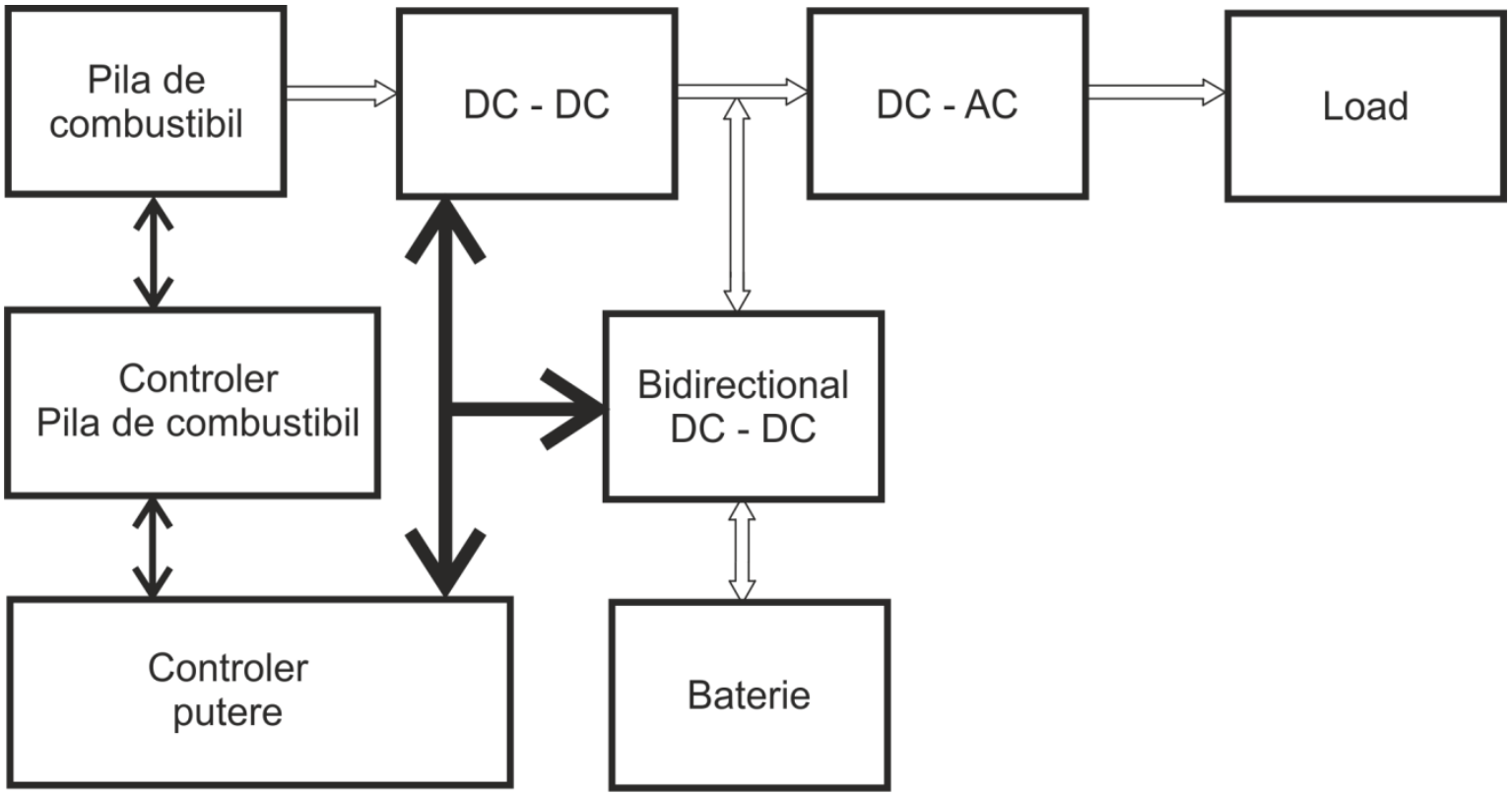

Figure 1.2a. Diagram of the Hybrid architecture with DC bus

1. Hybrid architectures for the interconnection of Renewable Energy Sources (RES), Energy Storage Devices (ESD) and Fuel Cell (FC) system.

1.2. Hybrid architecture with DC bus

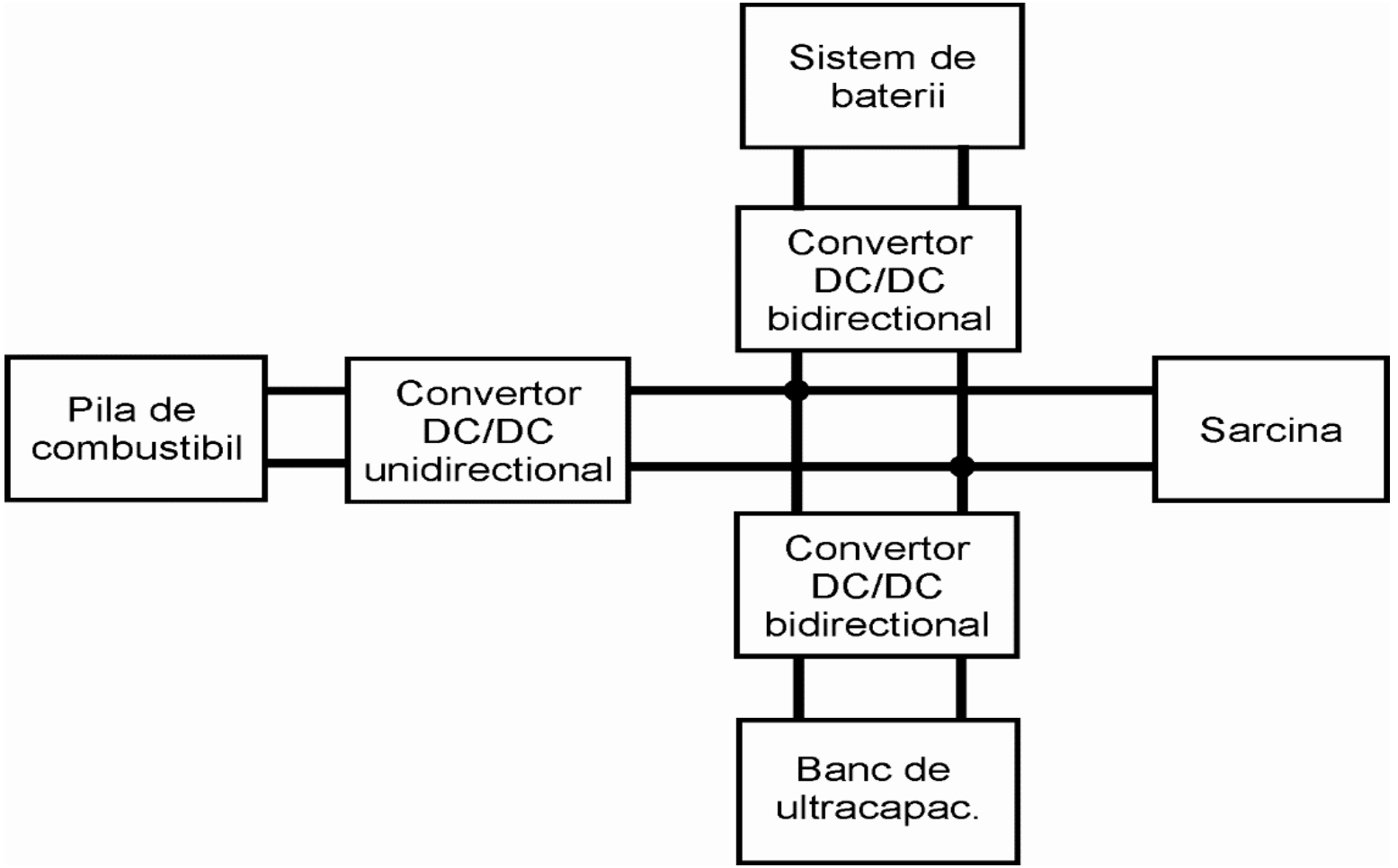

Figure 1.2b. Diagram of the Hybrid architecture with DC bus

1. Hybrid architectures for the interconnection of Renewable Energy Sources (RES), Energy Storage Devices (ESD) and Fuel Cell (FC) system.

1.2. Hybrid architecture with DC bus

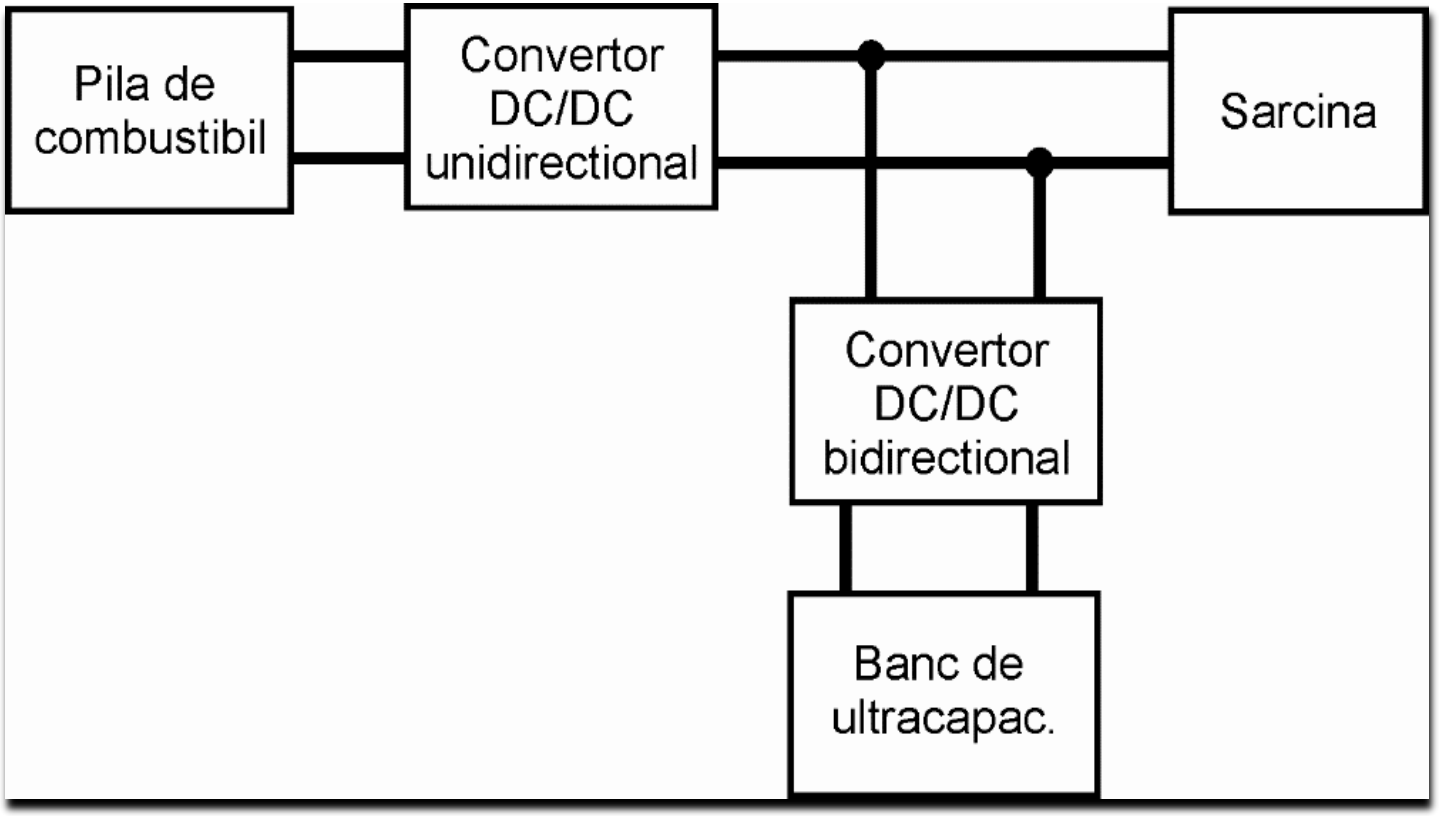

Figure 1.2c. Diagram of the Hybrid architecture with DC bus

1. Hybrid architectures for the interconnection of Renewable Energy Sources (RES), Energy Storage Devices (ESD) and Fuel Cell (FC) system.

1.2. Hybrid architecture with DC bus

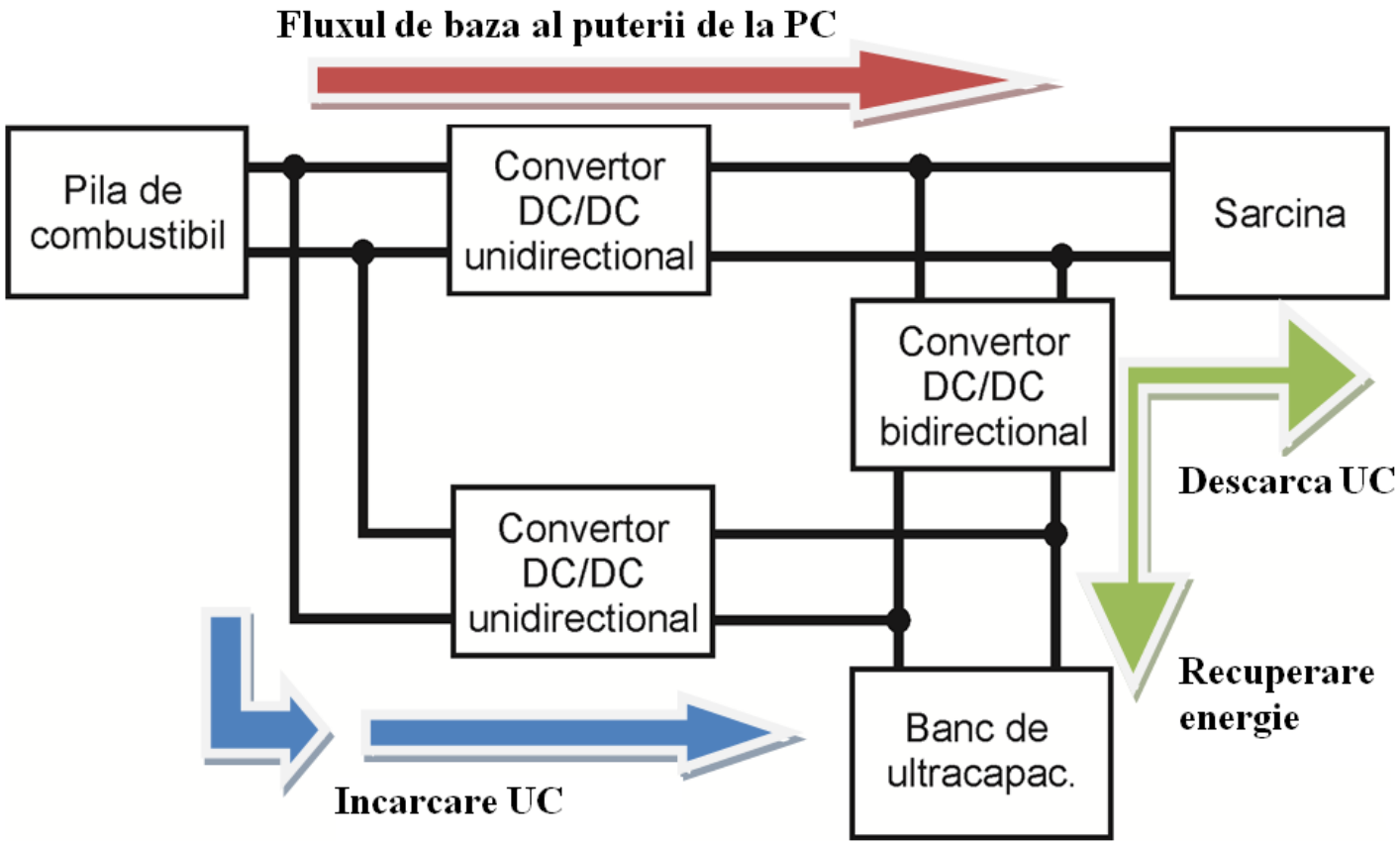

Figure 1.2d. Diagram of the Hybrid architecture with DC bus

1.3. Hybrid architecture of Multiport type

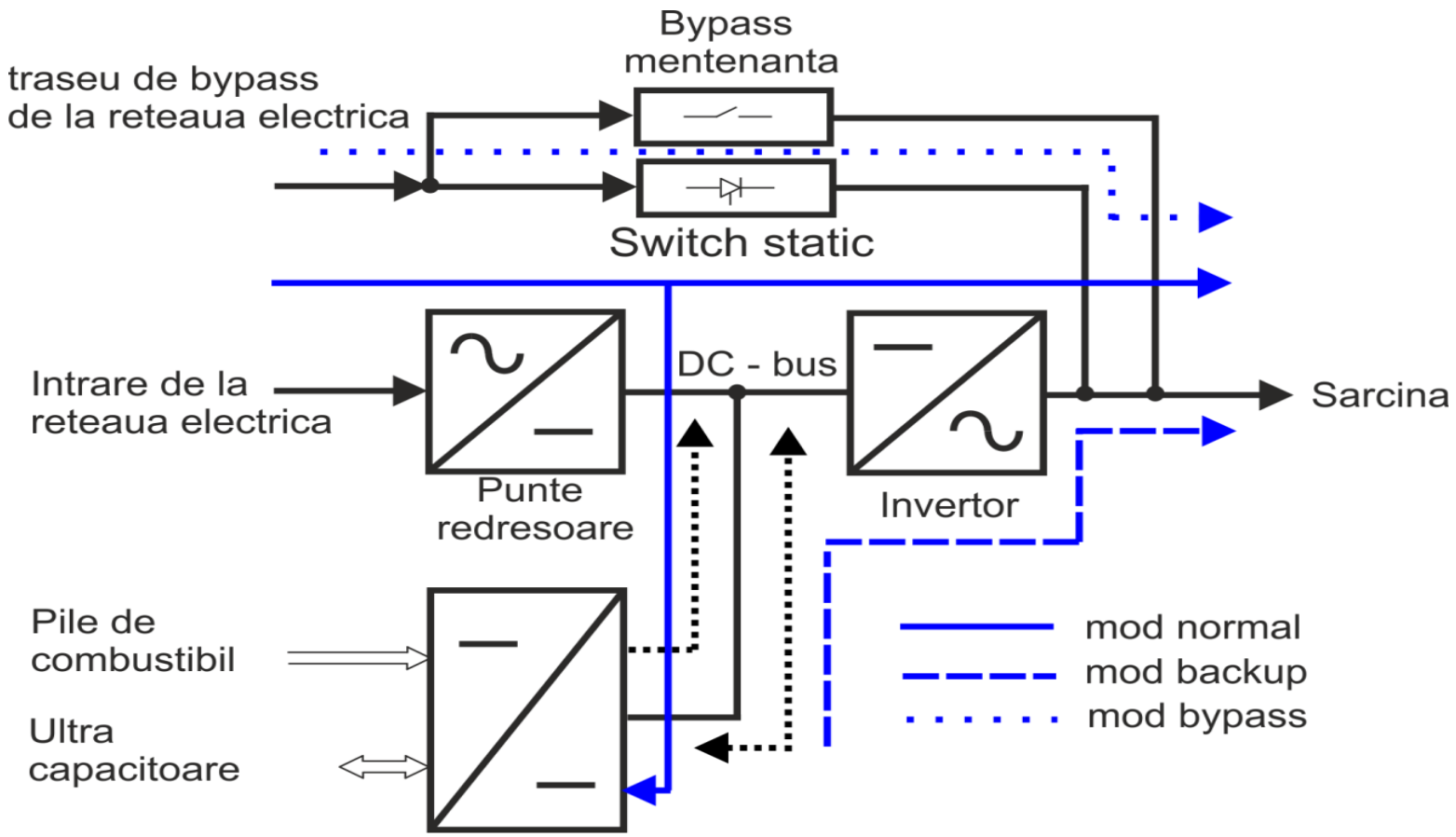

Figure 1.6. Diagram of the Hybrid UPS architecture of Multiport type

2. Energy management strategies of the Hybrid Power Source.

2.1. Power flow in Hybrid Power Source during different operating regimes

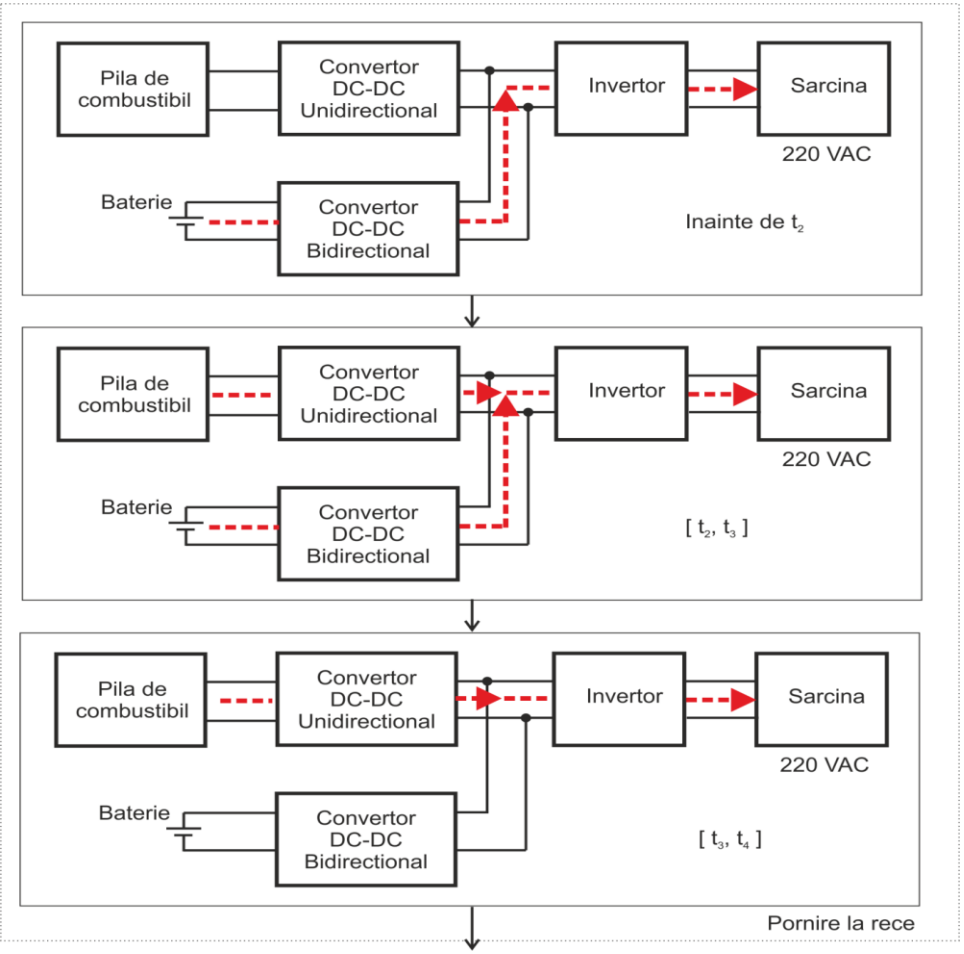

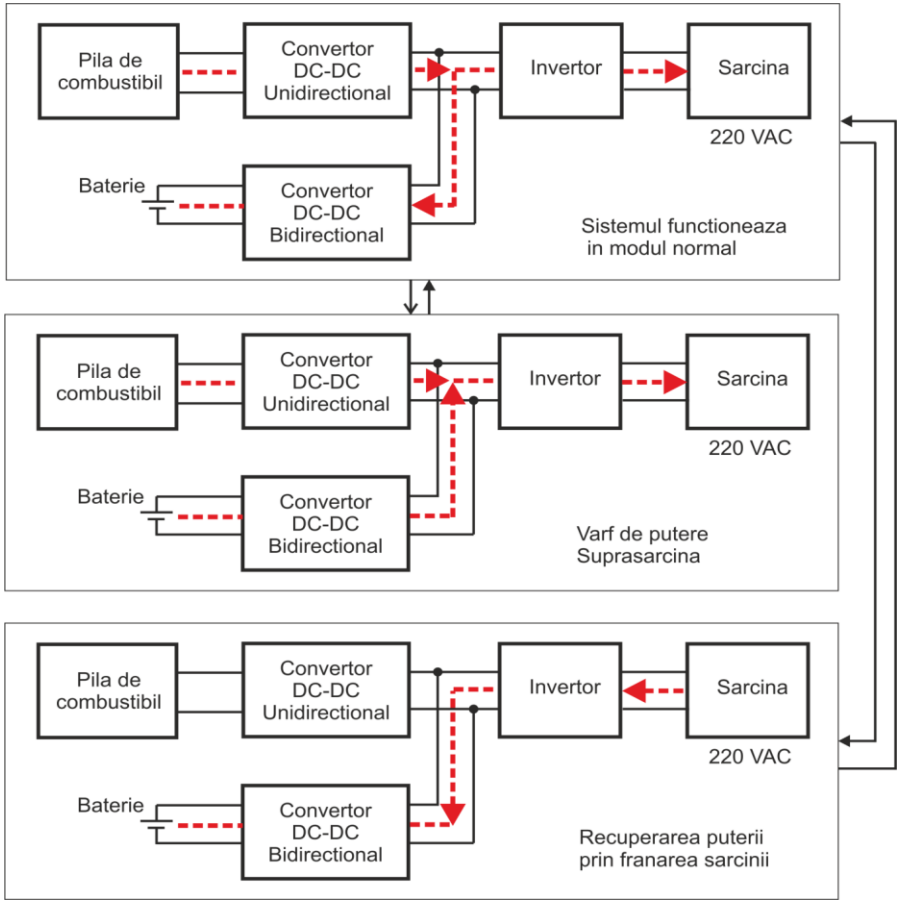

Figure 1.4. Power flow in Hybrid Power Source

2.2. Ragone diagram

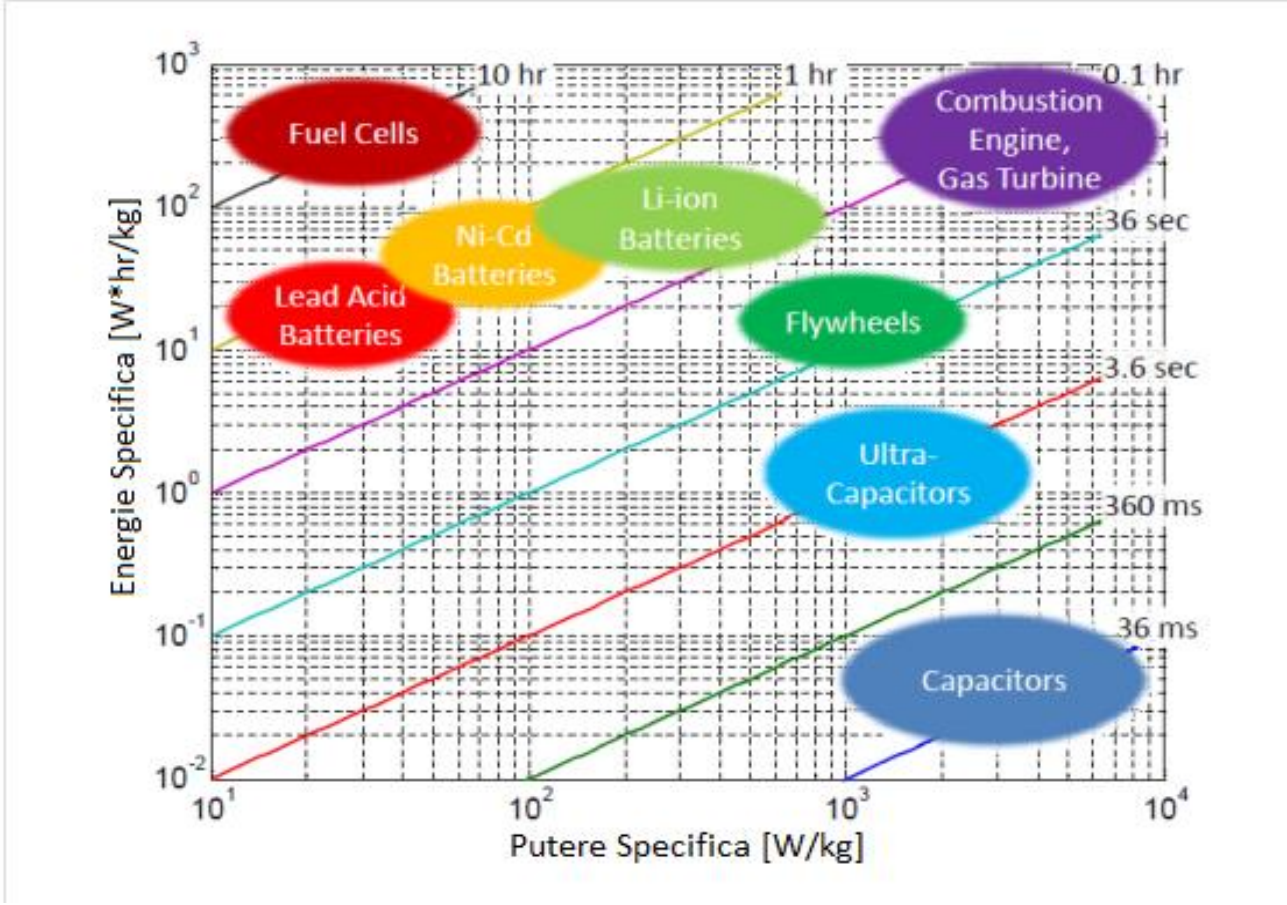

Figure 2.1. The Ragone diagram. Adapted from US Defense Logistics Agency Report [25].

2.3. Experimental study for a FC vehicle (ref. 29)

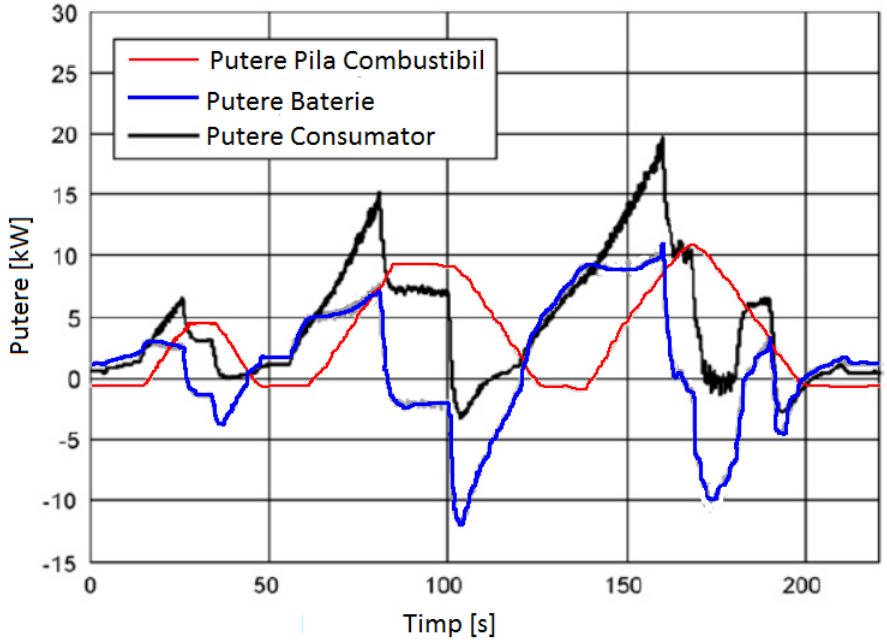

Figure 2.2. Power flow for the FC system, electrical motor and bateries stack with FC current rate limited 5A/sec

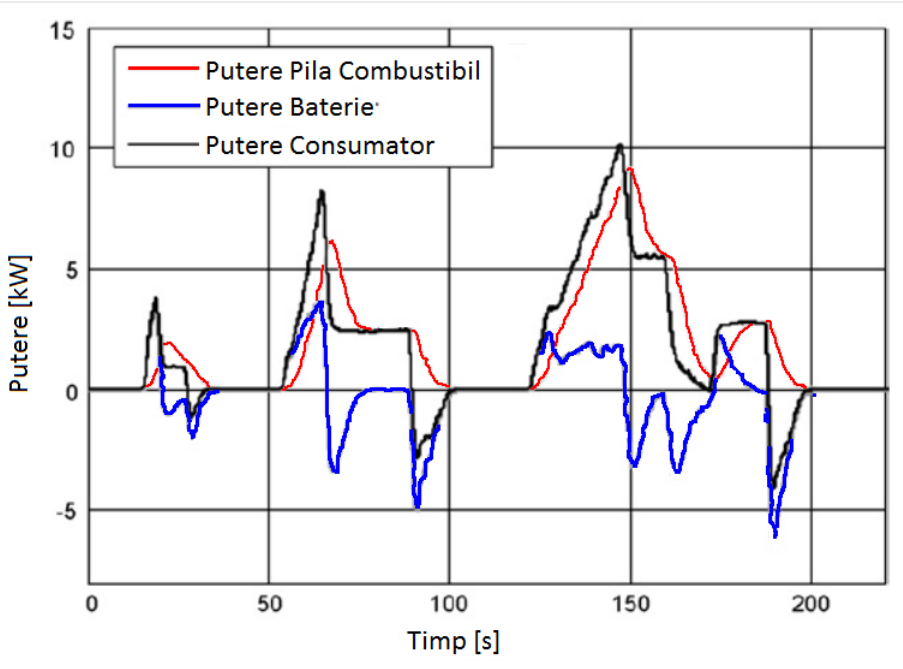

Figura 2.3. Power flow for the FC system, electrical motor and bateries stack with FC current rate limited 10A/sec

2.4. Control of the electrical motor supplied from the FC system (ref. 32)

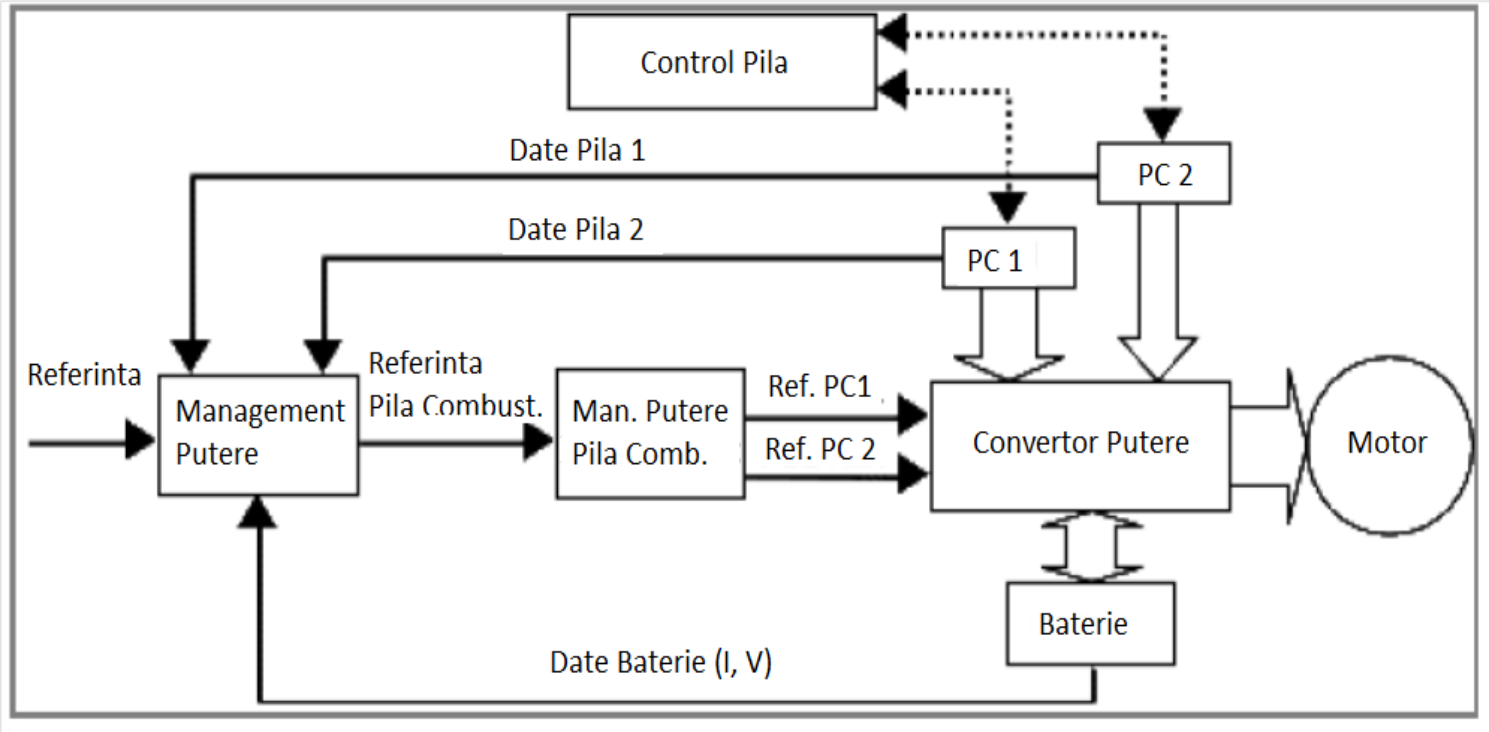

Figure 2.7. Control diagram of the electrical motor supplied from the FC system .

3. FC Hybrid Power Source (FC HPS) under test.

3.1. The components of the FC HPS under test

3.1.1 Ultracapacitor

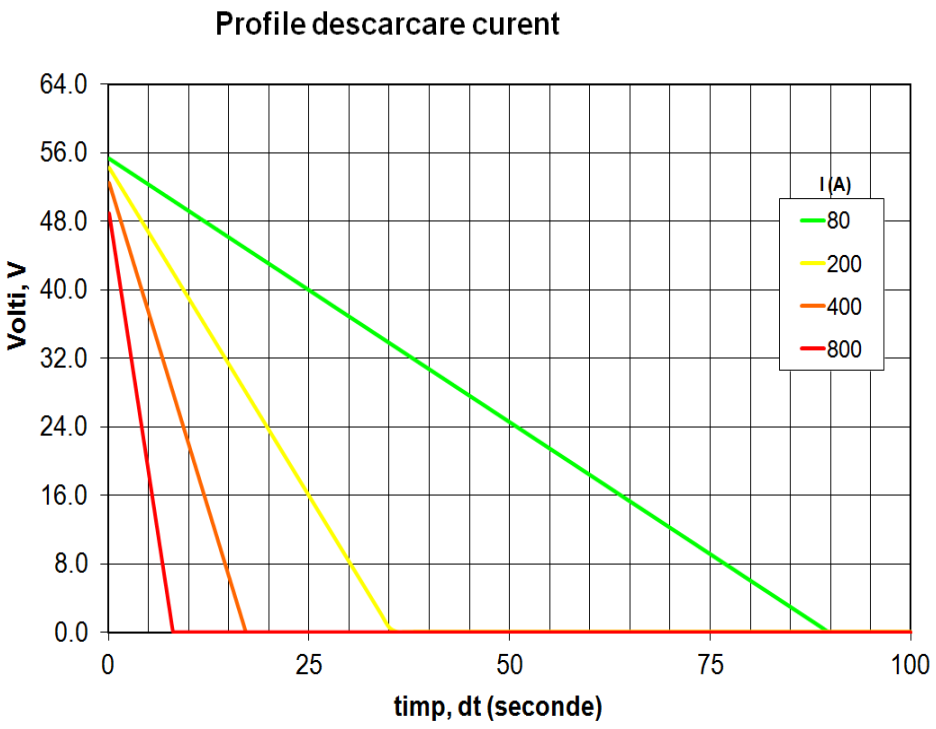

Table 3.1. Data sheet of the ultracapacitor

Producator	Maxwell
Tip	BMODO130-P056
Tensiune maxima $V_{UC,max}$	56V
Capacitate C_{UC}	130F
Rezistenta serie echivalenta	8.1 mΩ la 100Amp.
Densitatea specifica de energie	3.1 Wh/kg
Densitate specifica de putere	2600 W/kg
Numar de celule	23
Energie stocata	57Wh
Greutate	18kg

3. FC Hybrid Power Source (FC HPS) under test.

3.1. The components of the FC HPS under test

3.1.2. 5 kW FC system

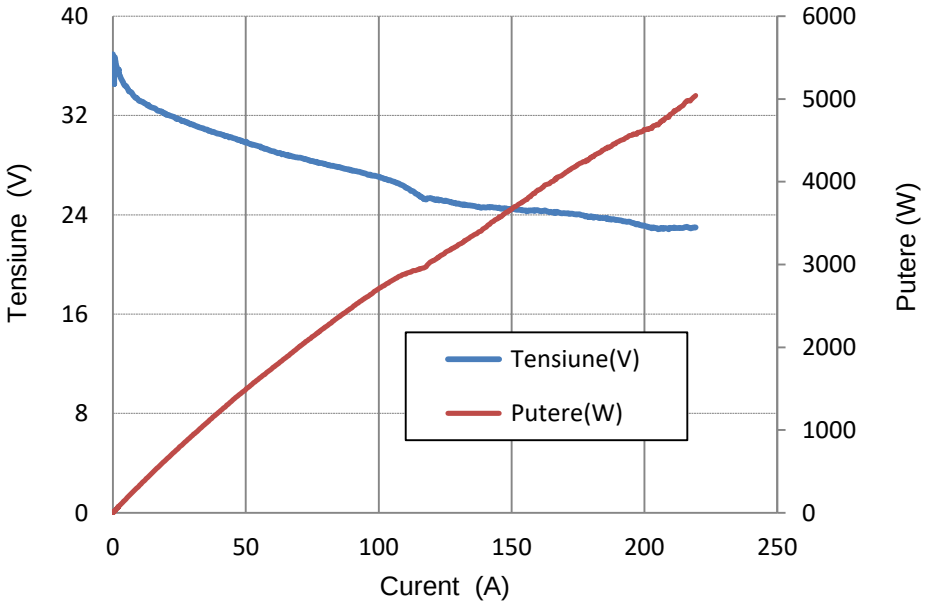

Table 3.2. Data sheet of the 5 kW FC system

Specificații	**Valoare**
Zona activa	250 cm2
Ieșirea nominala	5000 W @ 36VDC
Tensiunea maxima	40 VDC
Temperatura de funcț.	40-80 °C
Alimentarea anodului	H2 gazos cu puritate 99,99%
Alimentarea catodului	Aer ambiental
Lichidul de racire	Apa deionizata

3. FC Hybrid Power Source (FC HPS) under test.

3.1. The components of the FC HPS under test

3.1.3. The batteries stack : 4 x 12V-100A

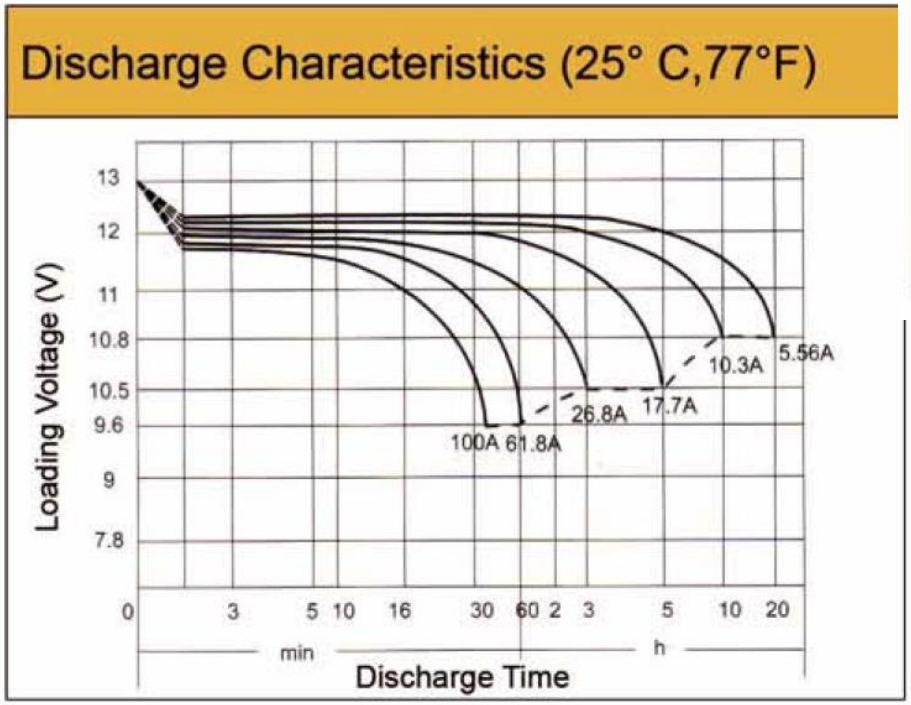

Electrical Specification					
Rated Capacity	20 hour rate (5.56A) 10 hour rate (10.3A) 5 hour rate (17.7A) 3 hour rate (26.8A) 1 hour rate (61,8A)	111 AH 103 AH 88,5AH 80.4AH 61,8AH	Constant-Voltage Charge	Cycle	Initial Charging Current less than 30A. Voltage 14.4 V- 15.0 V at 25°C (77°F) Temp. Corfficient -30mV/°C
Capacity affected by Temperature	40°C (104°F) 25°C (77°F) 0°C (32°F)	103% 100% 86%		Standby	No limit on Initial Charg-ing Current Voltage 13.5 V~13.8 V at 25°C (77°F) Temp. Corfficient -20mV/°C

3. FC Hybrid Power Source (FC HPS) under test.

3.1. The components of the FC HPS under test

3.1.4. DC/DC Converter

DC- DC Converter is produced by the Ripenergy company: model DCC5500.

Data sheet for the DC-DC converter:
Input: 23V- 35V
Output: 48-60V (controled with input variable 0-10V)
Power: 5000 W

3.1.5. Flow controllers for the air and fuel flows

Flow controllers are produced by the Brooks Instruments company: model 5850E.

Data sheet for the flow controllers:

DC voltage for supplying: 24VDC;
Control : 0 – 5 VDC;
Range for H2 : 0 250 SLPM;
Range for Air: 0 – 350 SLPM;

3. FC Hybrid Power Source (FC HPS) under test.

3.1. The components of the FC HPS under test

Ethernet VGA output	SLOT 1	SLOT 2	SLOT 3	SLOT 4	SLOT 5	SLOT 6	SLOT 7	SLOT 8
NI cRIO - 9082 Intel Core i7 FPGA Spartan	**NI - 9205** 250kS/s 16biti	**NI - 9264** ±10V 16biti	**NI - 9263** ±10V 16biti	**NI - 9206** 250kS/s 16biti Fuel Cell	**NI - 9206** 250kS/s 16biti Fuel Cell	**NI - 9213** 75S/s 16biti	**NI - 9213** 75S/s 16biti	**NI - 9213** 75S/s 16biti
Power Conector	16 canale citire tensiune	16 canale control tensiune	4 canale control tens. izolate	16 canale citire tensiune	16 canale citire tensiune	16 canale citire temperaturi	16 canale citire temperaturi	16 canale citire temperaturi

0 Vdc
+ 24 Vdc

3.1.6. Control and monitoring system

Control and monitoring system is based on controller cRIO-9082 with 8 NI modules:
Modul 1 citeste senzorii: are 16 canale diferentiale ;
Modul 2 comanda regulatoarele de H2 si Aer;
Modul 3 comanda cele patru module DC/DC canale izola
Modul 4 citeste tensiuni pe fiecare pila;
Modul 5 citeste tensiuni pe fiecare pila;
Modul 6 citeste temperaturi pe fiecare pila;
Modul 7 citeste temperaturi pe fiecare pila;
Modul 8 citeste temperaturi pe fiecare pila;

3. FC Hybrid Power Source (FC HPS) under test.

3.1. The components of the FC HPS under test

3.1.7. Software interface implemented in Labview

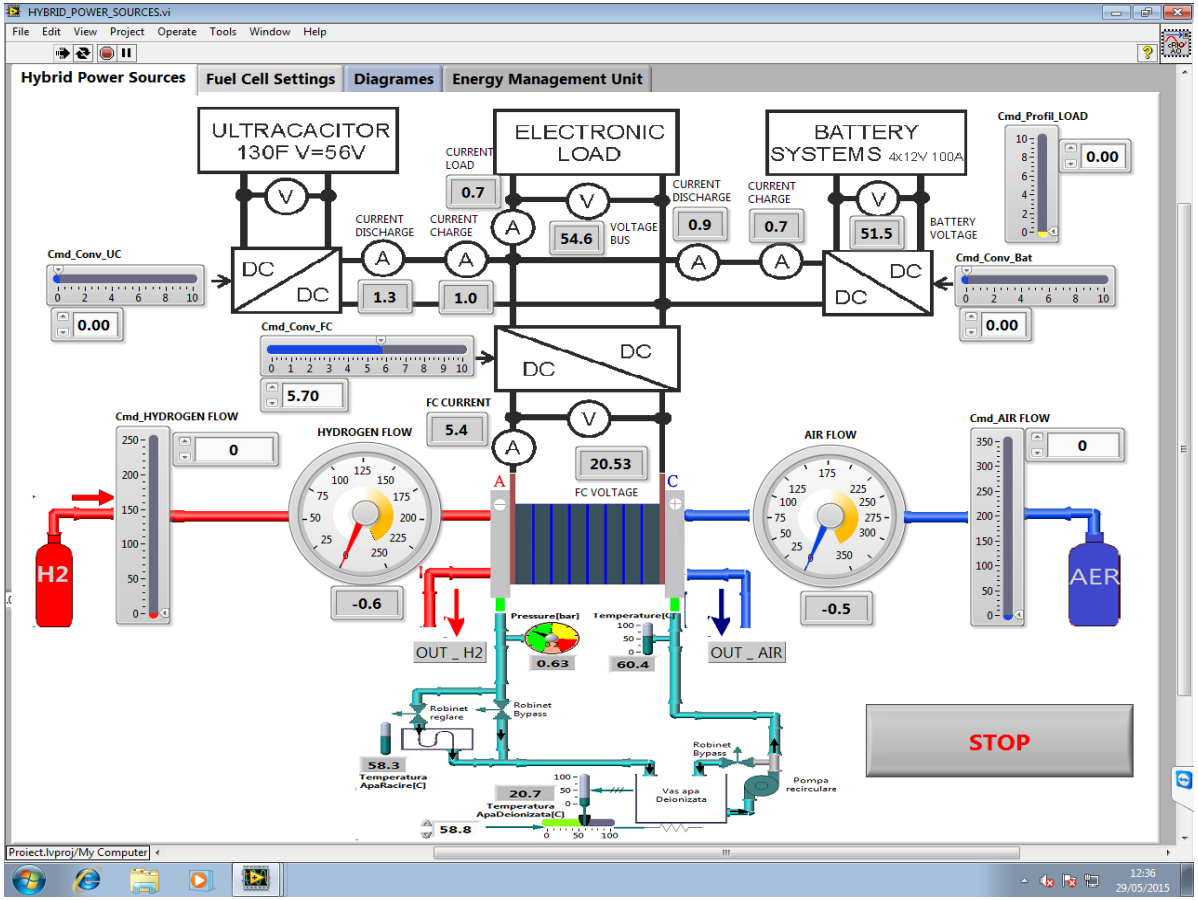

3. FC Hybrid Power Source (FC HPS) under test.

3.2. Wire diagram for the FC HPS.

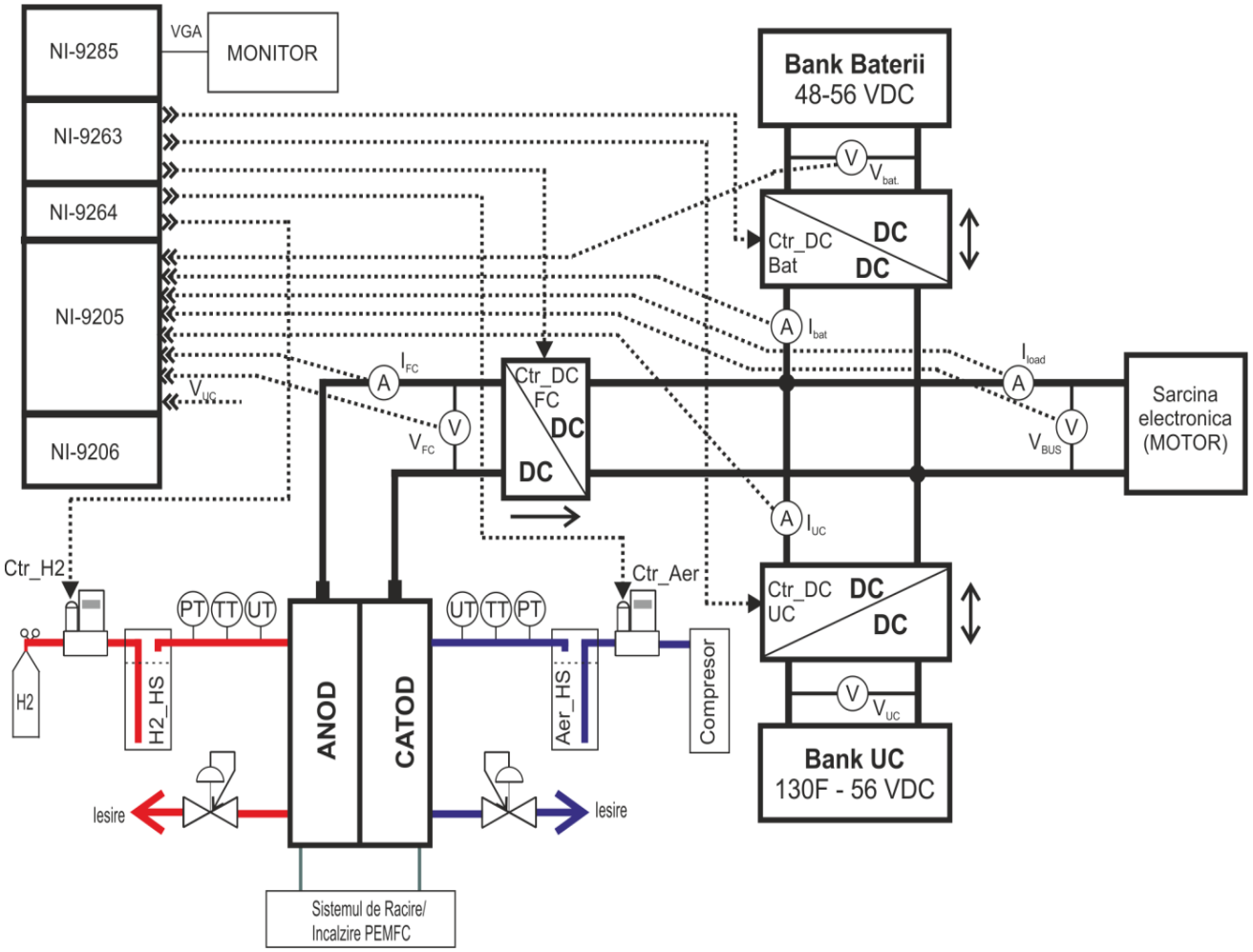

3. FC Hybrid Power Source (FC HPS) under test.

3.2. Energy Management Strategy (EMS) proposed for the FC HPS.

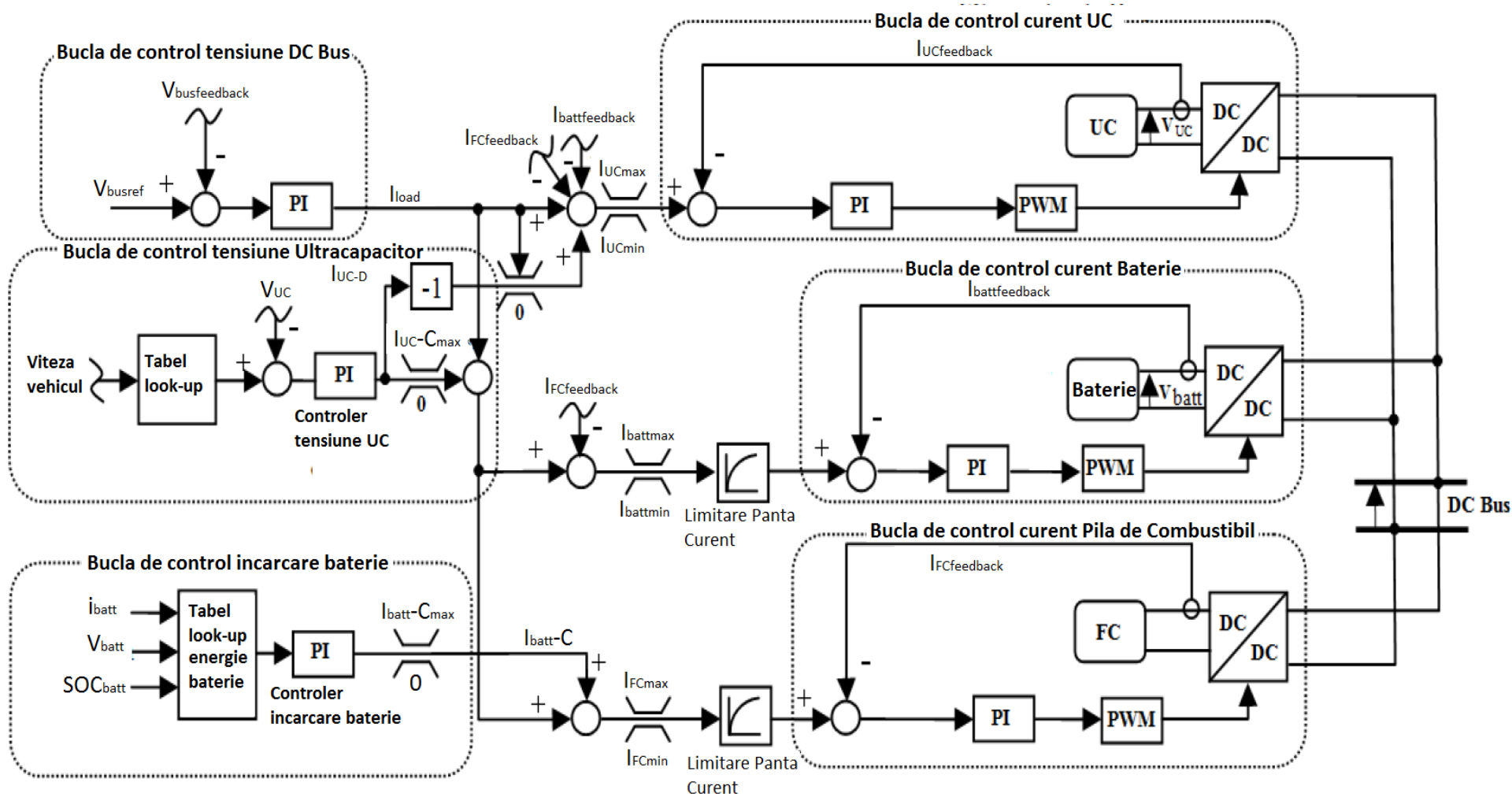

4. Preliminary experimental results.

Control of the fuel flows

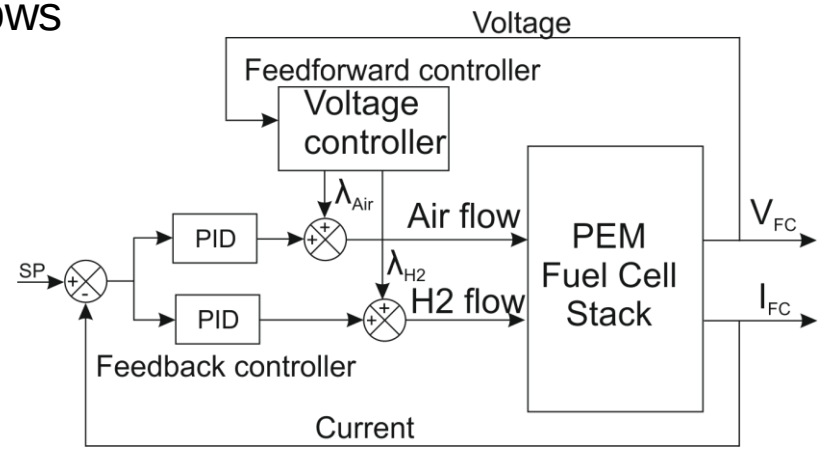

$$\dot{m}_{H2} = \frac{P_e \times \lambda_{H2} \times V_M \times 60}{n \times F \times V_c} = \\ = \frac{5000 \times 1.2 \times 22.4 \times 60}{2 \times F \times 0.5} = 83.5\, {}^{SL}/_{min} \qquad (1)$$

$$\dot{m}_{Air} = \frac{P_e \times \lambda_{Air} \times V_M \times 60}{0.21 \times n \times F \times V_c} = \\ = \frac{5000 \times 2.5 \times 22.4 \times 60}{0.21 \times 4 \times F \times 0.5} = 415\, {}^{SL}/_{min} \qquad (2)$$

4. Preliminary experimental results.

With fuel starvation

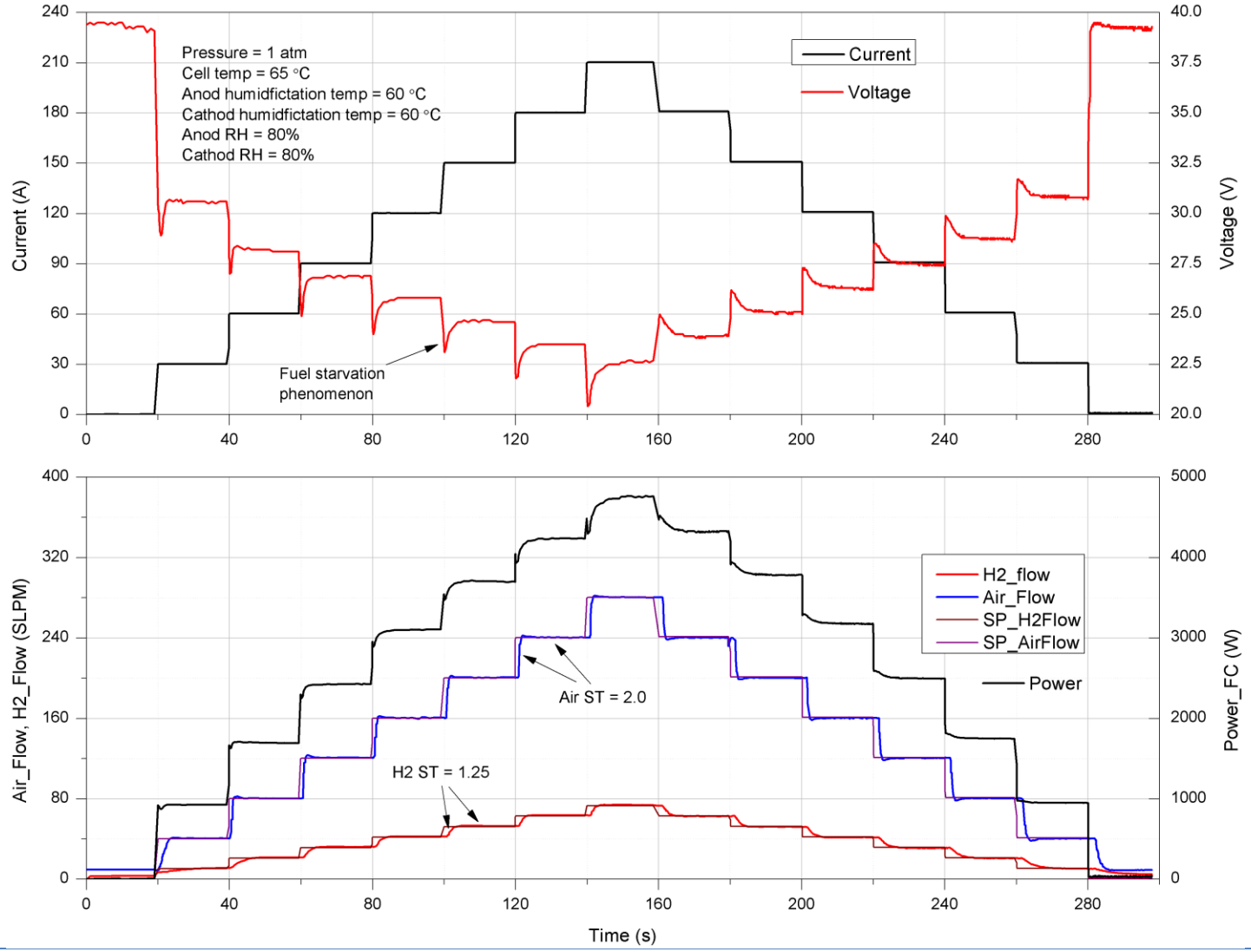

4. Preliminary experimental results.

Without fuel starvation

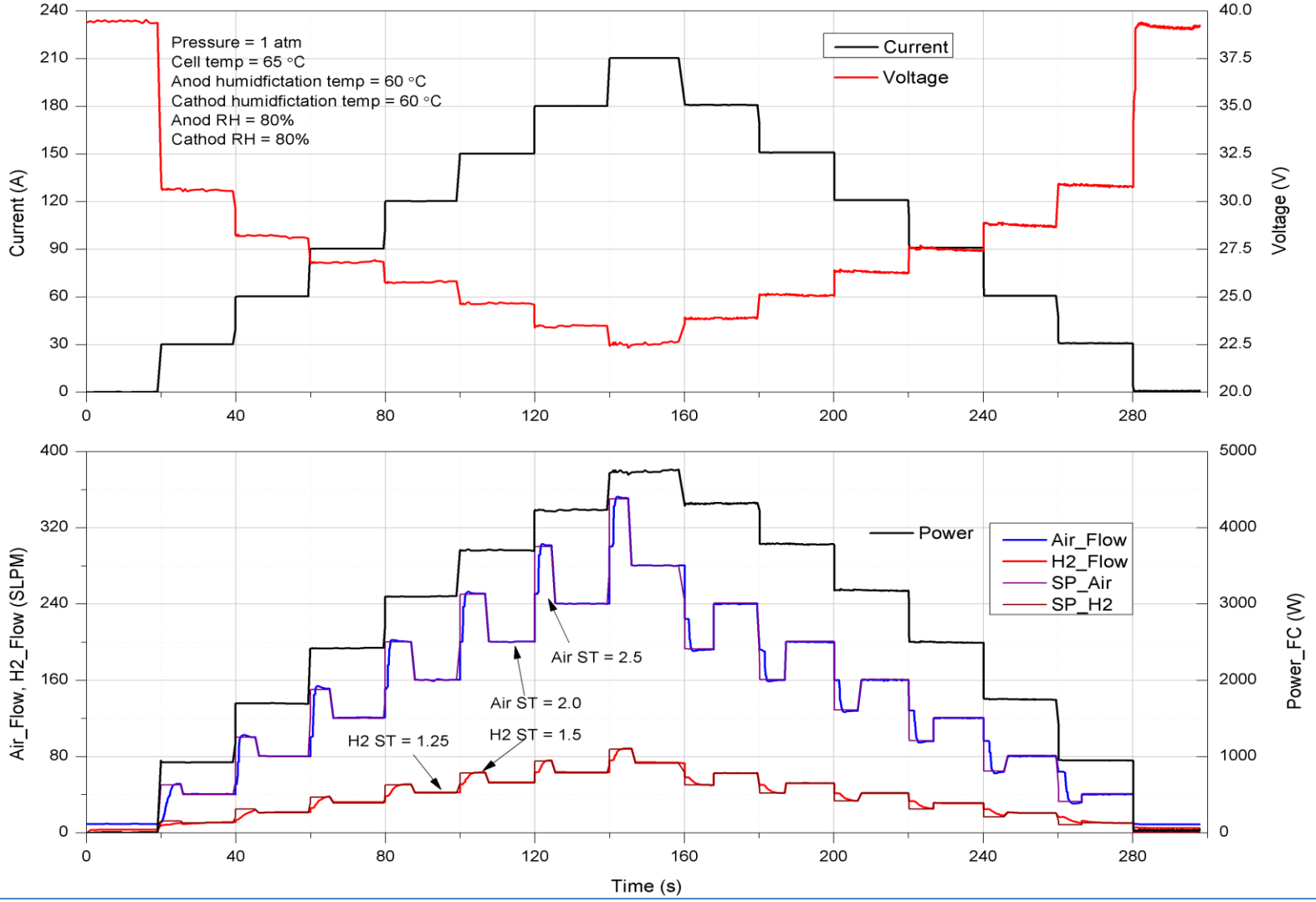

End of Part I
Thank you for your attention
Questions?
If not, we will go to Part II

Erasmus+ PROGRAMME,

KEY ACTION: Cooperation for innovation and the exchange of good practices,

ACTION: Strategic Partnerships

FIELD: Strategic Partnerships for higher education, CALL: 2015

INNOVATIVE EUROPEAN STUDIES ON RENEWABLE ENERGY SYSTEMS

2015-1-TR01-KA203-021342

Real-time optimization of the Renewable Energy Sources / Fuel Cell Hybrid Power Systems

Nicu BIZON
University of Pitesti, Pitesti, Romania

Summary of Part 2 – Energy efficiency of the FC HPS

1. Series (MPSs), parallel (MPCp) and Multiport Power Concerter (MPC) architectures of the FC Hybrid Power Source (FC HPS)
2. Energy efficiency of the MPCp, MPCs, and MPC FC HPS
3. FC Hybrid Power Source (FC HPS) under test.
4. Preliminary experimental results.
5. Conclusions.

1. Series, parallel and multiport architectures of the FC

1.1. Architecture of the FC HPS

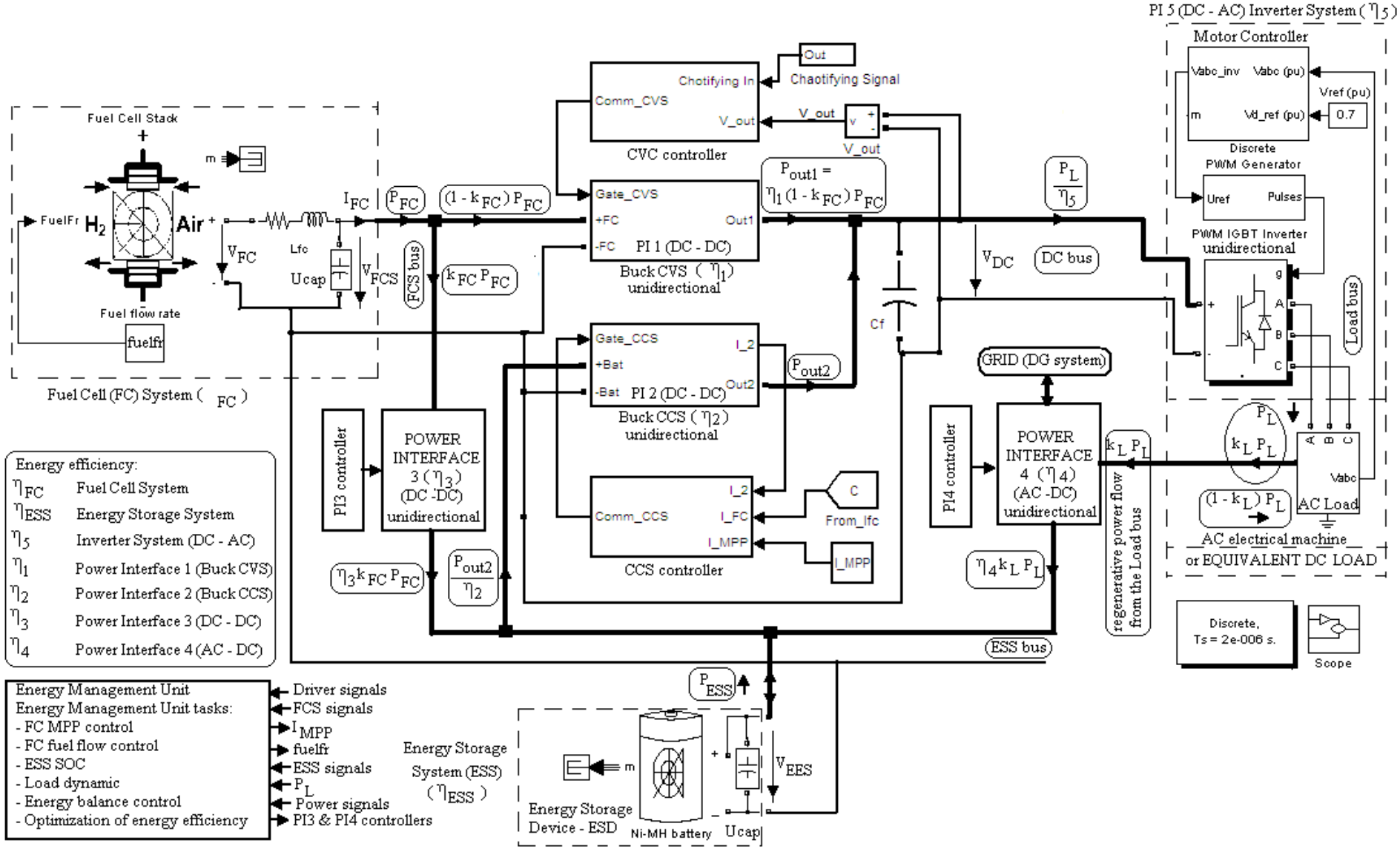

Figure 1.1. Diagram of FC HPS architecture

1. Series, parallel and multiport architectures of the FC HPS

1.2. Parallel FC HPS architecture

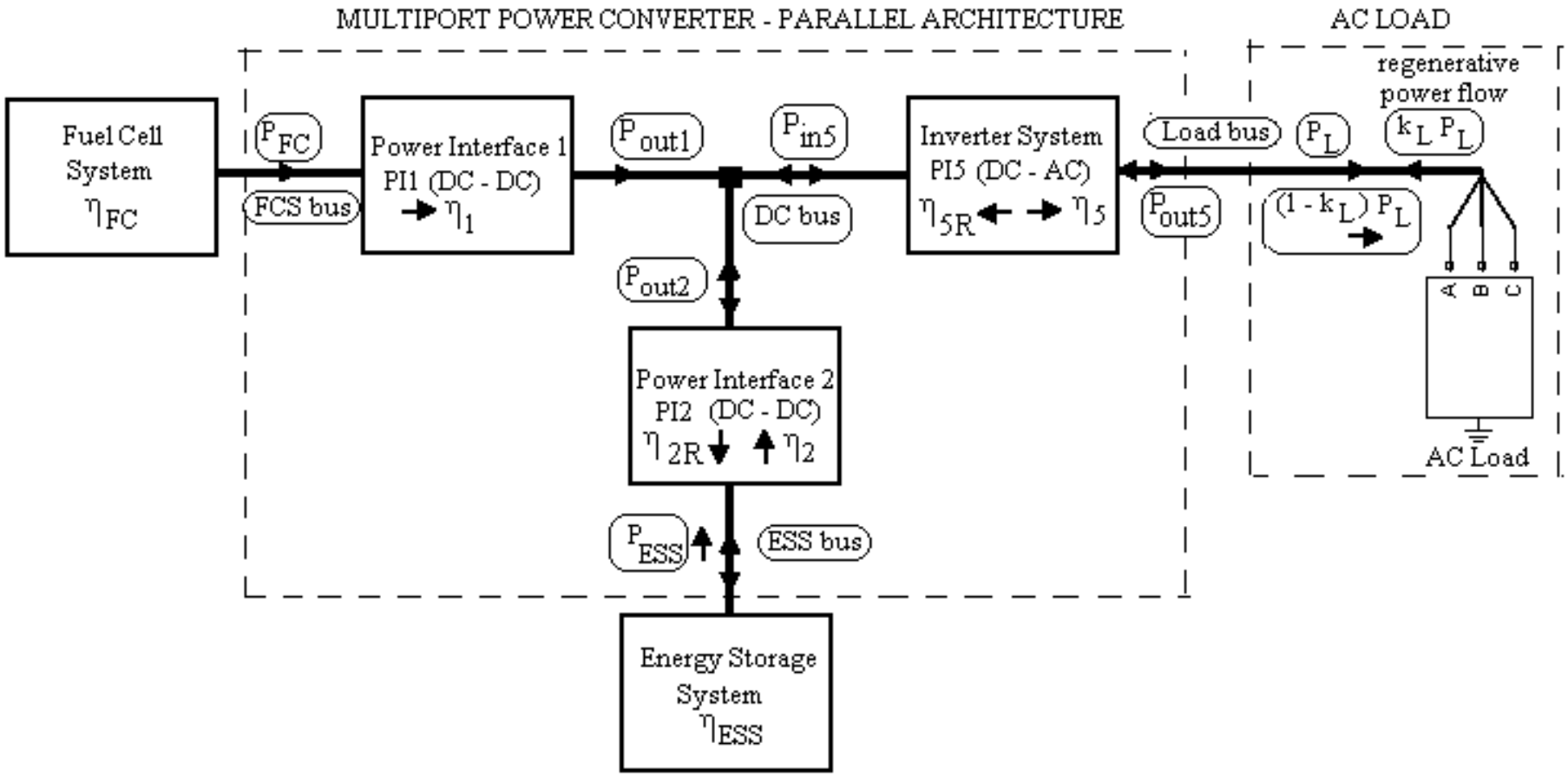

Figure 1.2. Diagram of the parallel FC HPS architecture

1. Series, parallel and multiport architectures of the FC HPS

1.3. Series FC HPS architecture

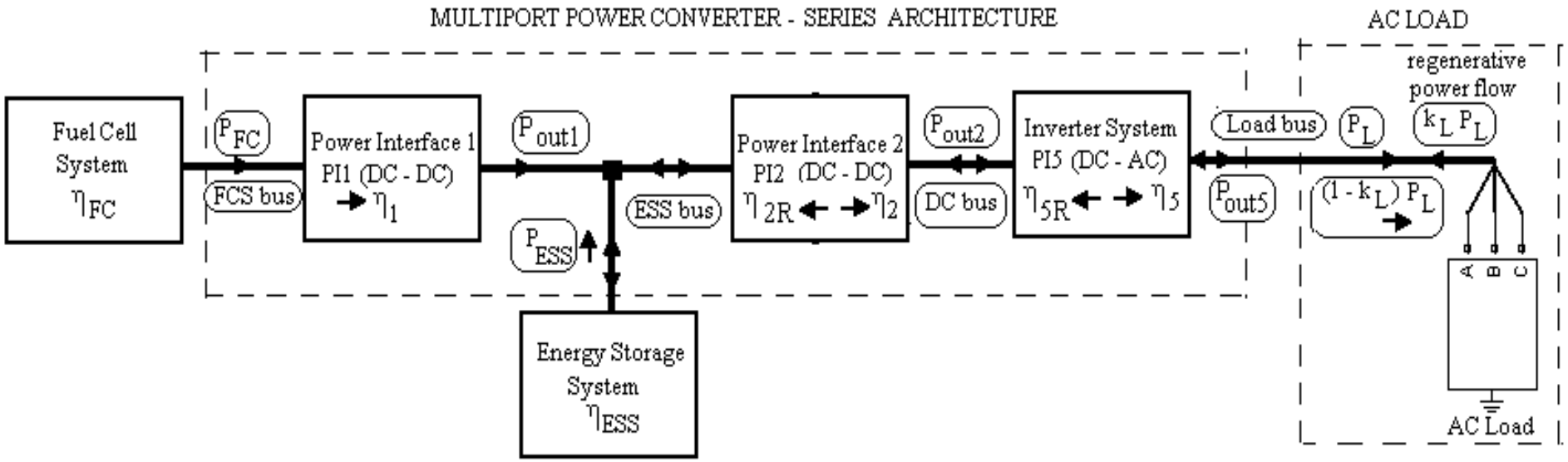

Figure 1.3. Diagram of the series FC HPS architecture

1. Series, parallel and multiport architectures of the FC HPS

1.4. Multiport Power Converter (MPC) interface for FC HPS architecture

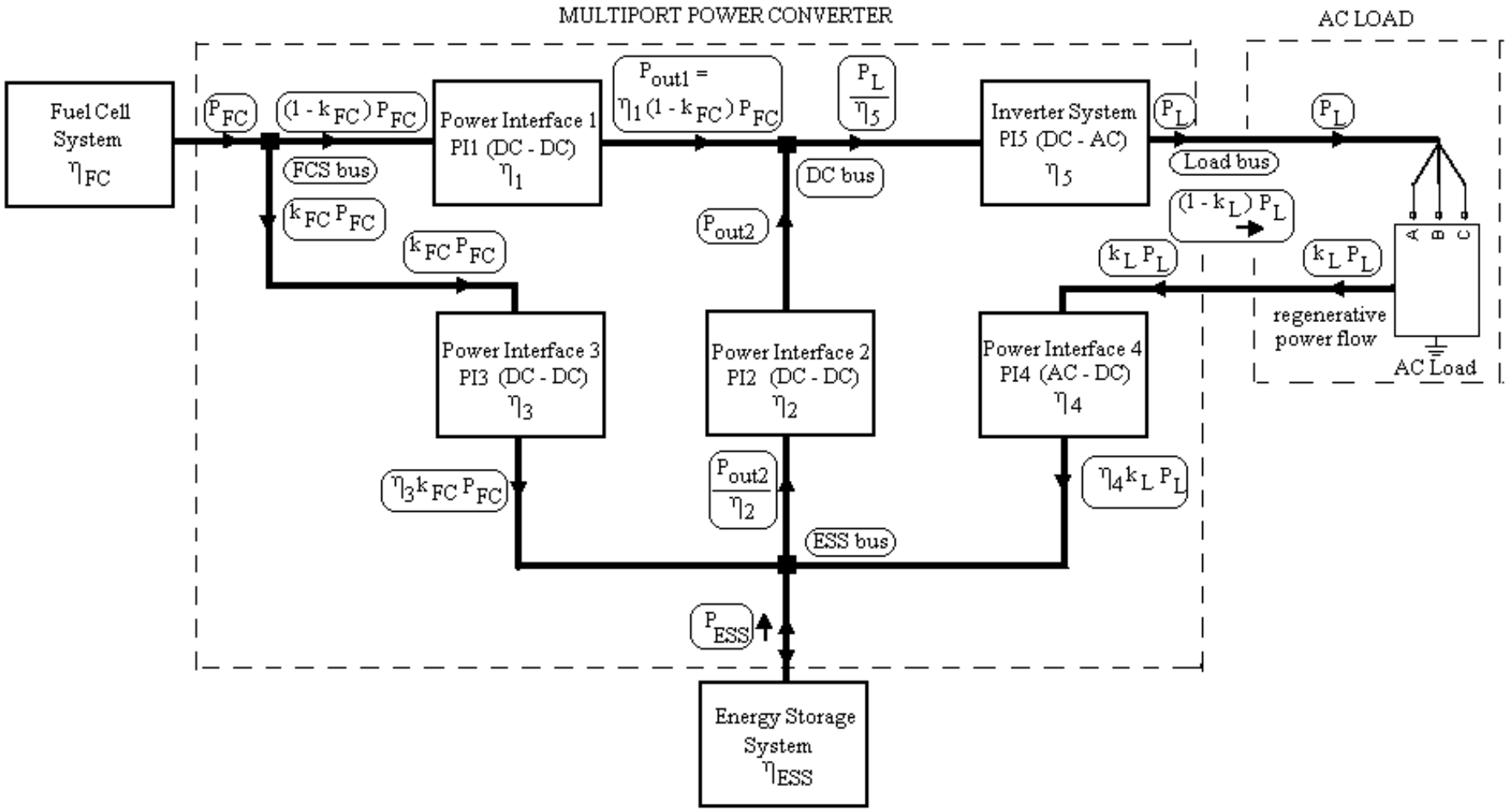

Figure 1.4. Diagram of the multiport FC HPS architecture

1. Series, parallel and multiport architectures of the FC HPS

1.5. Equivalent MPC of the parallel (MPCp) FC HPS architecture

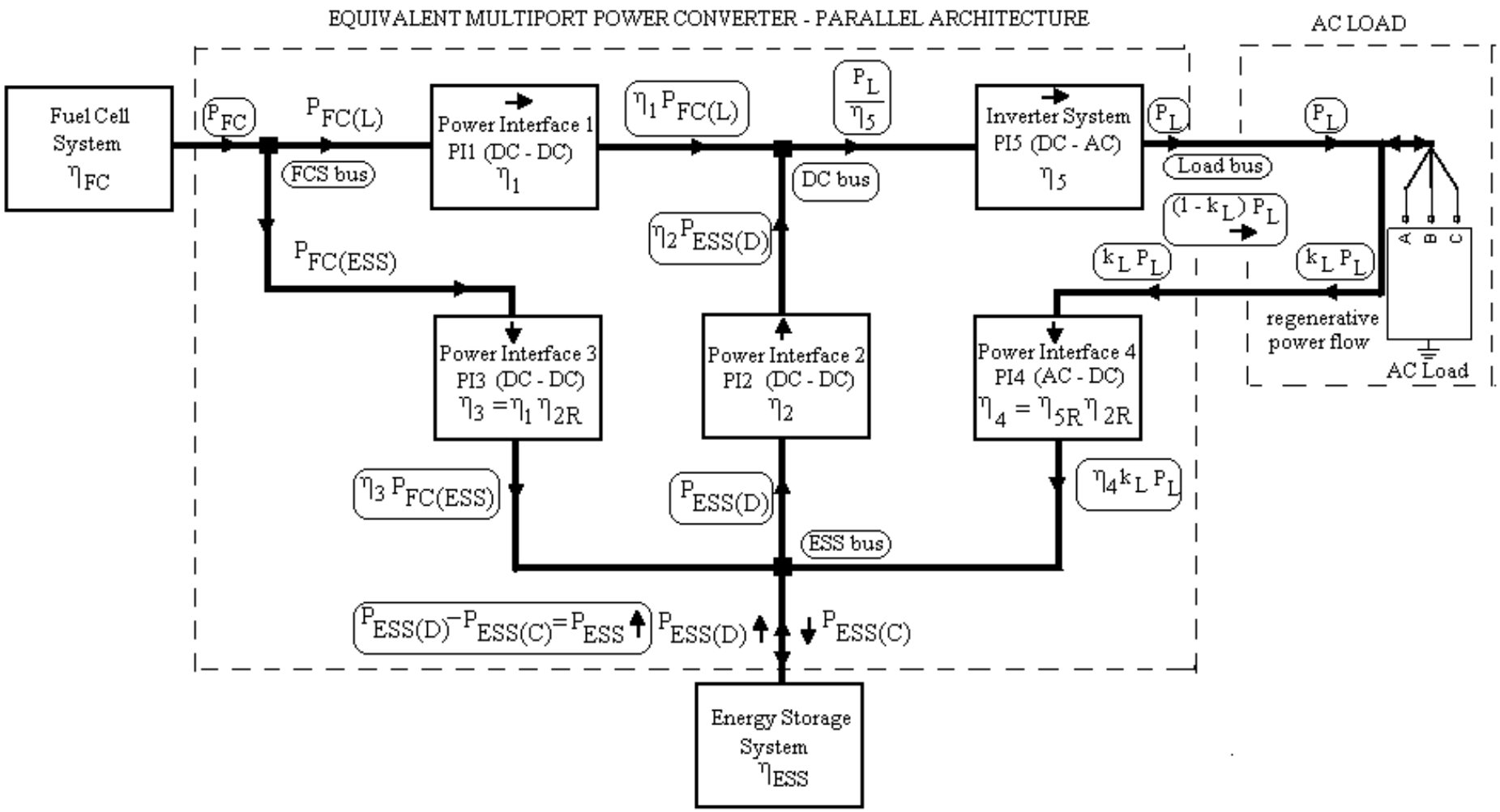

Figure 1.5. Diagram of the MPCp FC HPS architecture

1.6. Equivalent MPC of the series (MPCs) FC HPS architecture

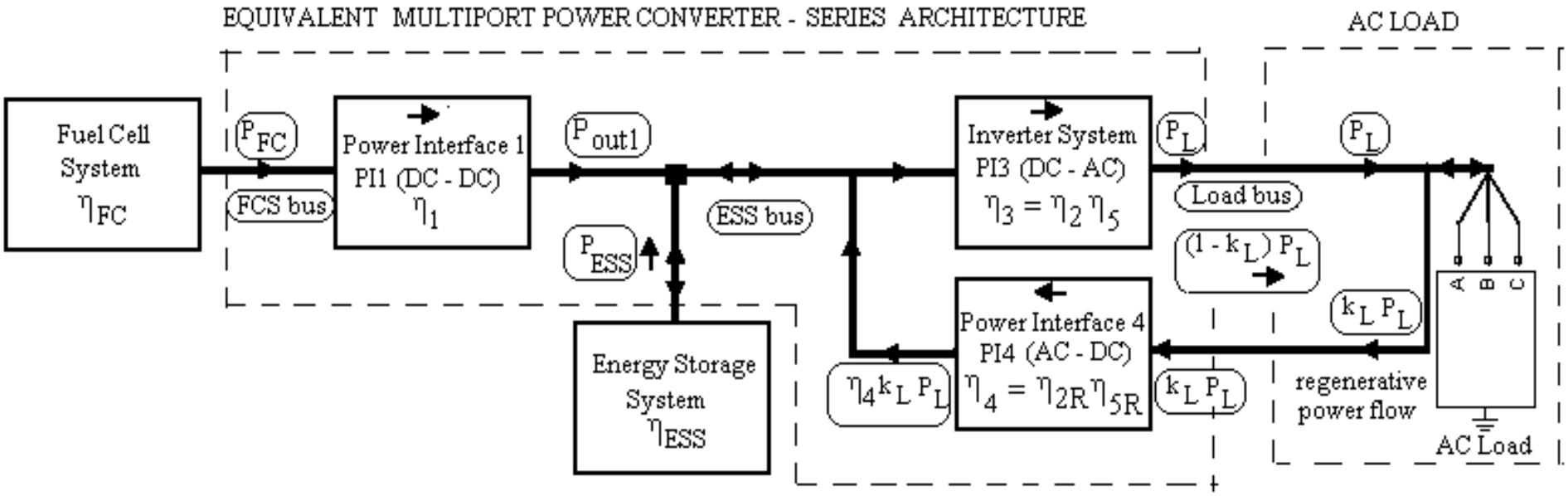

Figure 1.6. Diagram of the MPCs FC HPS architecture

2. Energy efficiency of the MPCp, MPCs, and MPC FC HPS

2.1. Energy efficiency of the MPCp FC HPS

The Energy Storage System (ESS) could operate in following regimes: (1) Charge-Sustaining (CS), (2) Charge-Depleting (CD), and (3) Charge-Increasing (CI).

$P_{ESS(C)}$ and $P_{ESS(D)}$ represent the average power exchanged by the ESS on CI and CD mode.

The FC system powers the load and ESS with $P_{FC(L)}$ and $P_{FC(ESS)}$

The power flow' balance on DC bus in CD mode is:

$$\eta_2 P_{ESS(D)} + \eta_1 P_{FC(L)} = P_L / \eta_5 \quad (1)$$

where the used notations are mentioned above.

The power flow' balance on ESS bus related to CI mode of ESS (which is charged in average with $P_{ESS(C)}$) is:

$$P_{ESS(C)} = \eta_3 P_{FC(ESS)} + \eta_4 k_L P_L = \eta_1 \eta_{2R} P_{FC(ESS)} + \eta_{2R} \eta_{5R} k_L P_L \quad (2)$$

The efficiency analysis will be performed considering as parameters the k_{ESS} and k_{CD} ratios: $k_{ESS(p)} = P_{ESS}/P_L$ and $k_{CD} = P_{ESS(C)}/P_{ESS(D)}$, respectively.

The energy efficiency for MPCp architecture is given by the relation:

$$\eta_p = \eta_{MPCp} = (1 - k_L) P_L / (P_{FC} + P_{ESS}) \quad (3)$$

2. Energy efficiency of the MPCp, MPCs, and MPC FC HPS

2.1. Energy efficiency of the MPCp FC HPS - continued

Relations (6) result by simple mathematical manipulations of (5) using the definitions for $k_{ESS(p)}$ and k_{CD} ratios:

$$P_{ESS(C)}=k_{ESS(p)}\, k_{CD}\, P_L / (1 - k_{CD}) \tag{6a}$$

$$P_{ESS(D)}=k_{ESS(p)}\, P_L / (1 - k_{CD}) \tag{6b}$$

If relations (6) will be used on relations (1) and (2), then relation (4) becomes:

$$P_{FC} = P_L \cdot \left(1/\eta_5 - \eta_{5R} k_L - k_{ESS(p)} \eta_{2m}\right) / \eta_1 \tag{7}$$

where

$$\eta_{2m} = (\eta_2 \eta_{2R} - k_{CD}) / [\eta_{2R} (1 - k_{CD})]\,,\; k_{CD} \neq 1 \tag{8}$$

It is obvious that:

$$k_{ESS(p)} \begin{matrix} < \\ = \\ > \end{matrix} 0 \Leftrightarrow P_{ESS(D)} \begin{matrix} < \\ = \\ > \end{matrix} P_{ESS(C)} \Leftrightarrow k_{CD} \begin{matrix} > \\ = \\ < \end{matrix} 1 \tag{9}$$

where the symbol used for comparison can be <, =, or >.

The case k_{CD}=1 ($k_{ESS(p)}$=0) was analyzed in [26]. Considering k_{CD}≠1, the energy efficiency for MPCp architecture is finally given by relation:

$$\eta_p = (1 - k_L)\eta_1 / [1/\eta_5 - \eta_{5R} k_L - k_{ESS(p)} (\eta_{2m} - \eta_1)] \tag{10}$$

2. Energy efficiency of the MPCp, MPCs, and MPC FC HPS

2.2. Energy efficiency of the MPCs FC HPS

The ESS bus is powered by the ESS and FC, directly and via PI1, respectively. Using the ratio of ESS power exchanged on ESS bus, $k_{ESS(s)} = P_{ESS}/P_L$, the power flows' balance on ESS bus is:

$$\eta_1 P_{FC} + P_{ESS} + \eta_{2R}\eta_{5R}k_L P_L = P_L/\eta_2\eta_5 \quad (11)$$

The same relation is obtained if the power flow balance on ESS bus is written in CI and CD mode of ESS, respectively:

$$P_{ESS(C)} = \eta_1 P_{FC(ESS)} + \eta_{2R}\eta_{5R}k_L P_L \quad (12a)$$

$$P_{ESS(D)} + \eta_1 P_{FC(L)} = P_L/\eta_2\eta_5 \quad (12b)$$

where the notations for the split power flow are the same.

In this case, the energy efficiency for MPCs architecture is given by (13):

$$\eta_s = \eta_{MPCs} = (1-k_L)P_L/(P_{FC}+P_{ESS}) \quad (13)$$

Using the $k_{ESS(s)}$ ratio, by simple mathematical manipulations of (11), results:

$$\eta_s = (1-k_L)\eta_1 / [1/(\eta_2\eta_5) - \eta_{2R}\eta_{5R}k_L - k_{ESS(s)}(1-\eta_1)] \quad (14)$$

2. Energy efficiency of the MPCp, MPCs, and MPC FC HPS

2.3. Energy efficiency of MPCp architecture vs. MPCs architecture

If both MPC architectures exchange the same ESS power (positive or negative), i.e. $k_{ESS(p)} = k_{ESS(s)} = k_{ESS}$, it is also important to know which ones operates more efficiently:

$$\eta_p \lessgtr \eta_s \tag{15}$$

Relation (15) is equivalent with (16) by using (10) and (14):

$$k_{ESS} \cdot (1-\eta_{2m}) \lessgtr [1-\eta_2 + k_L \eta_2 (1-\eta_{2R}) \eta_5 \eta_{5R}] / (\eta_2 \eta_5) \tag{16}$$

Using (8) will result (17):

$$1-\eta_{2m} = [\eta_{2R}(1-\eta_2) + k_{CD}(1-\eta_{2R})] / [\eta_{2R}(1-k_{CD})],\ k_{CD} \neq 1 \tag{17}$$

so (16) will become equivalent with (18):

$$\frac{k_{ESS}}{1-k_{CD}} \lessgtr \frac{\eta_{2R}}{\eta_2 \eta_5} \cdot \frac{1-\eta_2 + k_L \eta_2 (1-\eta_{2R}) \eta_5 \eta_{5R}}{\eta_{2R}(1-\eta_2) + k_{CD}(1-\eta_{2R})},\ k_{CD} \neq 1 \tag{18}$$

The following notation is made related to CS mode:

$$\frac{C_{\eta CD}}{1-k_{CD}} \triangleq \frac{\eta_{2R}}{\eta_2 \eta_5} \cdot \frac{1-\eta_2 + k_L \eta_2 (1-\eta_{2R}) \eta_5 \eta_{5R}}{\eta_{2R}(1-\eta_2) + k_{CD}(1-\eta_{2R})} > 0,\ k_{CD} \neq 1 \tag{19}$$

Finally, relation (15) will become equivalent with (20):

$$\frac{k_{ESS}}{1-k_{CD}} \lessgtr \frac{C_{\eta CD}}{1-k_{CD}},\ k_{CD} \neq 1 \tag{20}$$

2.3. Energy efficiency of MPCp architecture vs. MPCs architecture - continued

If $k_{ESS(p)} = k_{ESS(s)} = k_{ESS}$ then:

$$(|k_{ESS}| < |C_{\eta CD}| \Leftrightarrow \eta_p > \eta_s) \vee (|k_{ESS}| > |C_{\eta CD}| \Leftrightarrow \eta_p < \eta_s) \quad (22)$$

where the $\vee$ symbol is used for the logical OR operator.

Of course, if $k_{ESS(p)}=k_{ESS(s)}=C_{\eta CD}$, then both MPC architectures considered are equivalent in terms of energy efficiency, so $C_{\eta CD}$ is a border value.

If $k_{ESS(p)} \neq k_{ESS(s)}$, then η_p/η_s ratio of energy efficiency coefficients is computed in (23):

$$\frac{\eta_p}{\eta_s} = \frac{1/(\eta_2\eta_5) - \eta_{2R}\eta_{5R}k_L - k_{ESS(s)}(1-\eta_1)}{1/\eta_5 - \eta_{5R}k_L - k_{ESS(p)}(\eta_{2m}-\eta_1)} \quad (23)$$

Simulation results

If is not specifically mentioned, the energy efficiency coefficients of PIs are set in all simulations performed to η_1=0.9, η_2=0.9, η_{2R}=0.9, η_5=0.9, and η_{5R}=0.9. The used values for the charge-discharge parameter, k_{CD}, are 1/1.25 and 1.25 for CD and CI operating mode, respectively.

The dependence of energy efficiency for both MPC architectures, considering $k_{ESS(p)} = k_{ESS(s)} = k_{ESS}$, is given by (22) and (23), and is clearly shown in Figure 5 and 6, respectively.

2. Energy efficiency of the MPCp, MPCs, and MPC FC HPS

2.3. Energy efficiency of MPCp vs. MPCs architecture - continued

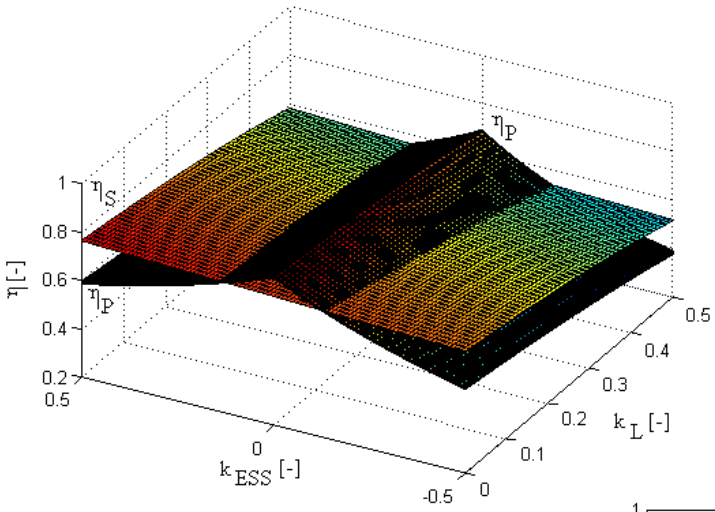

Figure 5. η_p & η_s for different k_{ESS} and k_L values

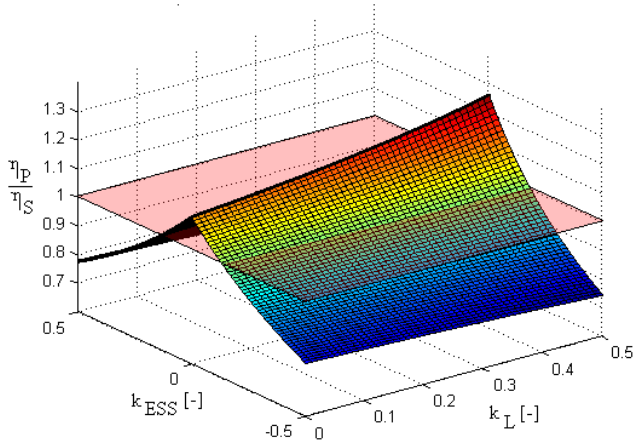

Figure 6. $\eta_p/\eta_s(k_{ESS}, k_L)$ surface, using k_{CD}=1/1.25 and k_{CD}=1.25 in regions where k_{ESS}>0 and k_{ESS}<0, respectively

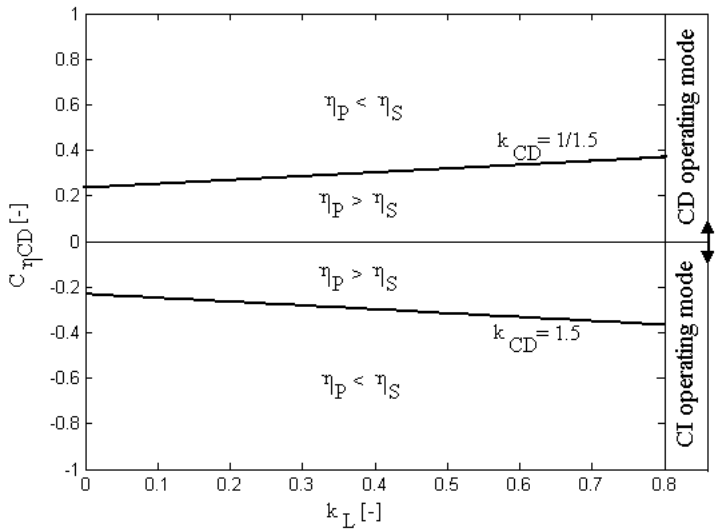

Fig. 7. Example of regions where MPCp or MPCs architectures may operate efficiently in CD or CI operating mode

2. Energy efficiency of the MPCp, MPCs, and MPC FC HPS

2.4. Energy efficiency of MPCp vs. MPCs in CS mode

In CS mode the average value of charge exchanged by ESS under a drive (load) cycle is zero, so:

$$k_{ESS} = 0 \Rightarrow P_{ESS0(D)} = P_{ESS0(C)} \tag{25}$$

The energy efficient coefficients given by (10) and (14) become as below:

$$\eta_{p0} = \eta_p\big|_{k_{ESS(p)}=0} = \frac{(1-k_L)\eta_1}{1/\eta_5 - \eta_{5R}k_L} \tag{10a}$$

$$\eta_{s0} = \eta_s\big|_{k_{ESS(s)}=0} = \frac{(1-k_L)\eta_1}{1/(\eta_2\eta_5) - \eta_{2R}\eta_{5R}k_L} \tag{14a}$$

where k_L is the regenerative braking factor.

The $k_{L\text{-}ESS0}$ coefficient is defined as a measure of load and ESS dynamic:

$$k_{L-ESS0} \overset{\Delta}{=} P_{ESS0(D)} / P_L \tag{26}$$

It is also important to know which ones operate more efficiently (for example, see Figure 13):

$$\eta_p \underset{>}{\overset{<}{=}} \eta_s \tag{27}$$

Relation (27) is equivalent with (28) by using (10a) and (14a):

$$k_{L-ESS0} \underset{>}{\overset{<}{=}} \frac{\eta_{2R}\left[1-\eta_2+k_L\eta_2\eta_{5R}(1-\eta_{2R})\right]}{\eta_2\eta_5(1-\eta_2\eta_{2R})} \overset{\Delta}{=} C_{\eta 0} > 0 \tag{28}$$

2. Energy efficiency of the MPCp, MPCs, and MPC FC HPS

2.4. Energy efficiency of MPCp vs. MPCs in CS mode - continued

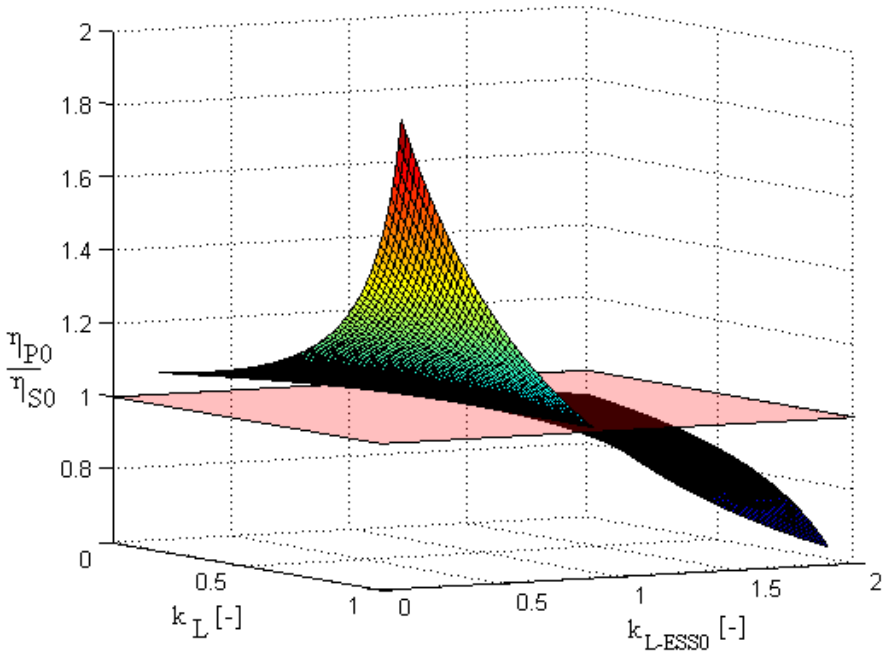

Figure 13. $\eta_p/\eta_s(k_L, k_{L\text{-}ESS0})$ surface for $\eta_1=\eta_2=\eta_{2R}=0.93$ and $\eta_5=\eta_{5R}=1$

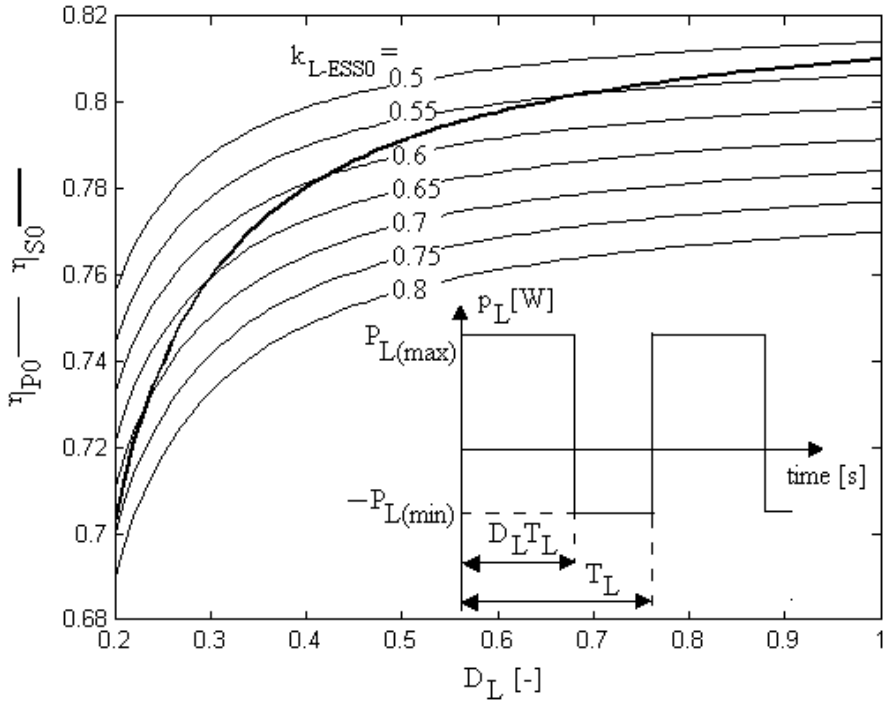

Figure 14. $\eta_s(D_L)$ - line width set to 2, and $\eta_p(D_L)$ - line width set to 1, for $\eta_1=\eta_2=\eta_{2R}=0.93$, $\eta_5=\eta_{5R}=1$, $C_L=9$ and different $k_{L\text{-}ESS0}$

The average (AV) and effective (RMS) value of load power are dependent by the duty cycle, D_L, the ratio of positive and negative amplitudes, $C_L = P_{L(max)} / P_{L(min)}$, and the regenerative braking factor, k_L, as in (29): $P_{L(AV)} = P_L k_L (D_L C_L - 1)$, $P_{L(RMS)} = P_L k_L \sqrt{D_L C_L^2 + 1 - D_L}$

2. Energy efficiency of the MPCp, MPCs, and MPC FC HPS

2.5. Energy efficiency of basic MPC (MPCb)

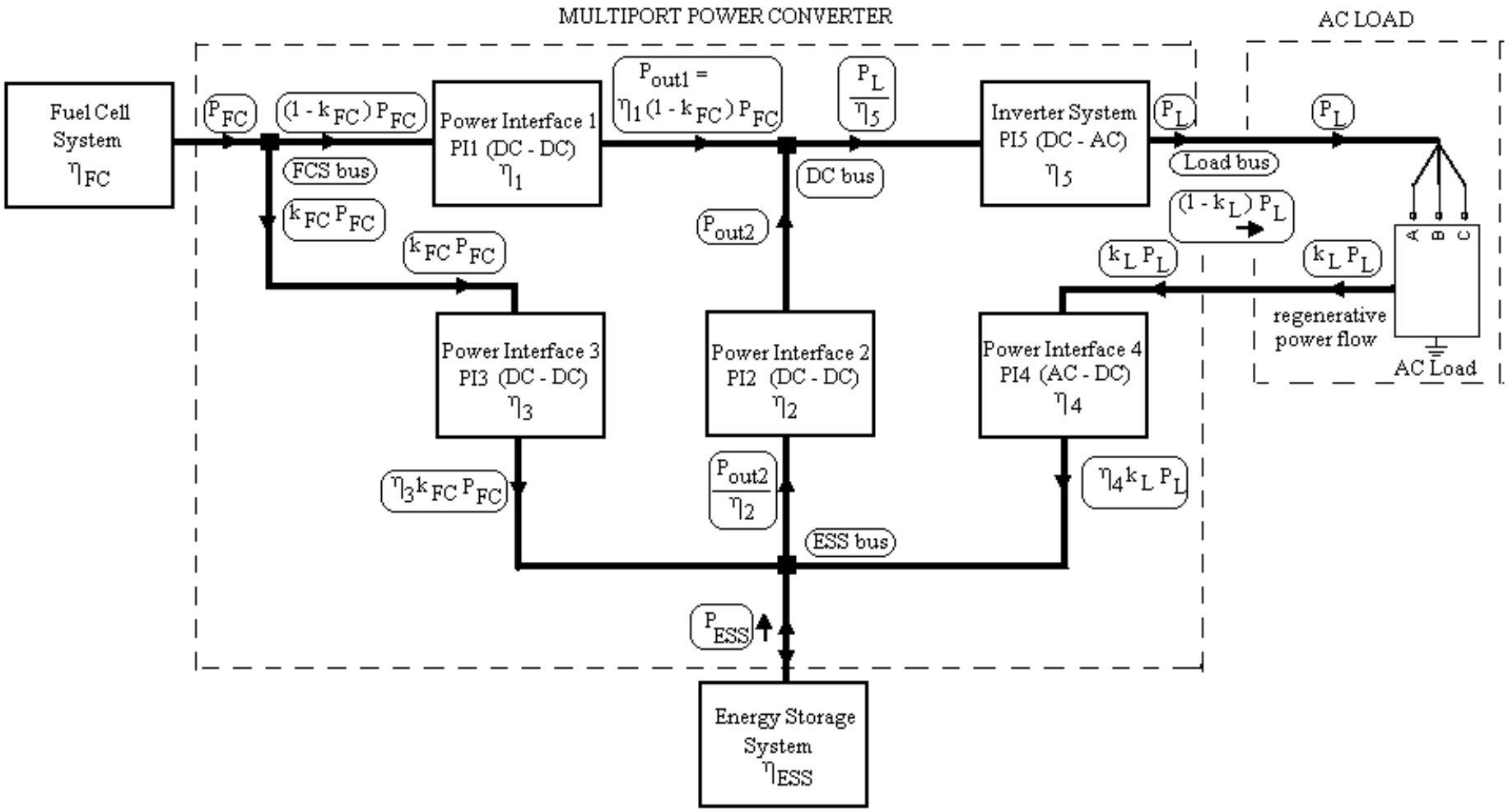

2. Energy efficiency of the MPCp, MPCs, and MPC FC HPS

2.5. Energy efficiency of basic MPC (MPCb) - continued

The power flows balance on DC bus is:

$$P_{DC}=P_{out1}+P_{out2} \tag{1}$$

The power balance on ESS bus is:

$$P_{ESS}+\eta_3 k_{FC} P_{FC}+\eta_4 k_L P_L=P_{out2}/\eta_2 \tag{2}$$

The energy efficiency for basic MPC architecture is given by relation:

$$\eta_{MPCb}=(1-k_L)P_L/(P_{FC}+P_{ESS}) \tag{3}$$

By simple mathematical manipulations of the first two relations, relation (3) became:

$$\eta_{MPCb}=(1-k_L)\cdot A / B_b \tag{4}$$

where:

$$A=\eta_1+k_{FC}(\eta_2\,\eta_3-\eta_1),$$

$$B=1/\eta_5-\eta_2\,\eta_4\,k_L-k_{ESS}\,[\eta_2-\eta_1-k_{FC}\,(\eta_2\,\eta_3-\eta_1)], \tag{5}$$

$$B_b=B\big|_{k_{ESS}=k_{ESSb}}=1/\eta_5-\eta_2\,\eta_4\,k_L-k_{ESSb}\,[\eta_2-\eta_1-k_{FC}\,(\eta_2\,\eta_3-\eta_1)]$$

2. Energy efficiency of the MPCp, MPCs, and MPC FC HPS

2.6. Energy efficiency of MPC without regenerative power flow (MPC1)

In this case, the energy efficiency for MPC1 is given by relation (4) considering $k_L=0$:

$$\eta_{MPC1}=A_1 / B_1 \tag{6}$$

where:

$$A_1 = A\big|_{k_L=0} = \eta_1 + k_{FC}(\eta_2 \eta_3 - \eta_1),$$

$$B_{b1} = B\big|_{k_{ESS}=k_{ESS1}} = 1/\eta_5 - \eta_2 \eta_4 k_L - k_{ESS1}\,[\eta_2 - \eta_1 - k_{FC}\,(\eta_2 \eta_3 - \eta_1)] \tag{7}$$

$$B_1 = B_{b1}\big|_{k_L=0} = 1/\eta_5 - k_{ESS1}\,[\eta_2 - \eta_1 - k_{FC}\,(\eta_2 \eta_3 - \eta_1)] = B_{b1} + \eta_2 \eta_4 k_L$$

If $k_{ESSb}= k_{ESS1}= k_{ESS(b1)}$, then it is important to know which ones operate more efficiently.

$$\eta_{MPCb} \lessgtr \eta_{MPC1} \Leftrightarrow k_{ESS(b1)} \cdot C_{FC} \lessgtr C_L \tag{8} \Leftrightarrow (9)$$

$$C_{FC} = \eta_2 - \eta_1 - k_{FC} \cdot (\eta_2 \eta_3 - \eta_1)$$

$$C_L = 1/\eta_5 - \eta_2 \eta_4 > 0 \tag{10}$$

So both MPC architectures could have the same efficiency for k_{ESS} given by relation (11):

$$k_{ESS(b1)} = C_L / C_{FC} \tag{11}$$

2. Energy efficiency of the MPCp, MPCs, and MPC FC HPS

2.6. Energy efficiency of MPC1 - continued

If value of k_{ESS} parameter is the same for both MPC architectures (but different to $k_{ESS(b1)}$ value), then energy efficiencies of considered MPC architectures are different, η_{MPCb} and η_{MPC1}, respectively (see Figure 5). From relations (8) and (9) it can be concluded that:

$$\left|k_{ESS}\right| < \left|C_L / C_{FC}\right| \Rightarrow \eta_{MPCb} < \eta_{MPC1}$$

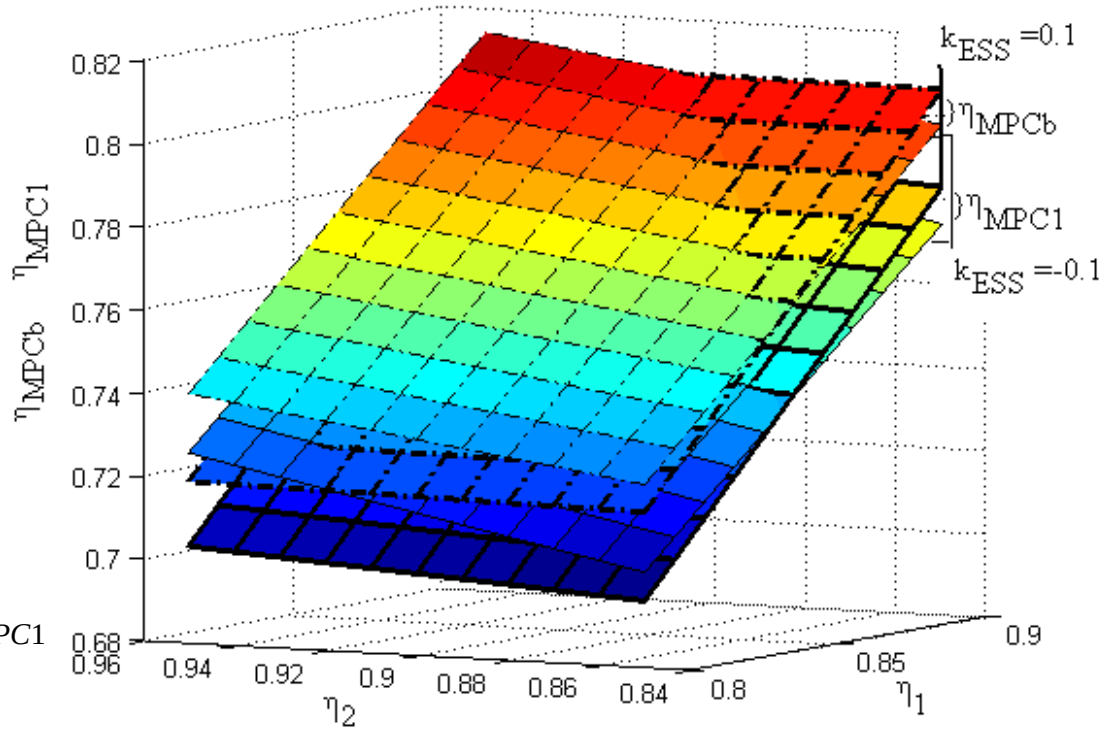

Figure 5. $\eta_{MPCb}(\eta_1, \eta_2)$ and $\eta_{MPC1}(\eta_1, \eta_2)$ for k_{FC}=0.1, k_L=0.1, η_3=0.95, η_4=0.95, and η_5=0.9

2. Energy efficiency of the MPCp, MPCs, and MPC FC HPS

2.7. Energy efficiency of MPC without charging power flow from the FC system (MPC2)

In this case, the energy efficiency for MPC is given by relation (4) considering $k_{FC}=0$:

$$\eta_{MPC2}=(1-k_L)\cdot A_2 / B_2 \tag{14}$$

where:

$$A_2 = A\big|_{k_{FC}=0} = \eta_1,$$

$$B_{b2} = B\big|_{k_{ESS}=k_{ESS2}} = 1/\eta_5 - \eta_2\,\eta_4\,k_L - k_{ESS2}\,[\eta_2 - \eta_1 - k_{FC}\,(\eta_2\,\eta_3 - \eta_1)] \tag{15}$$

$$B_2 = B_{b2}\big|_{k_{FC}=0} = 1/\eta_5 - \eta_2\,\eta_4\,k_L - k_{ESS2}\,(\eta_2 - \eta_1) = B_{b2} - k_{ESS2}\,k_{FC}\,(\eta_2\,\eta_3 - \eta_1)$$

If $k_{ESSb}= k_{ESS2}= k_{ESS(b2)}$, then it is important to know which ones operate more efficiently:

$$\eta_{MPCb} \underset{>}{\overset{<}{=}} \eta_{MPC2} \Leftrightarrow C_{kL}\cdot sign(\eta_2\cdot\eta_3-\eta_1) \underset{>}{\overset{<}{=}} k_{ESS(b2)}\cdot\eta_2\cdot sign(\eta_2\cdot\eta_3-\eta_1) \tag{16} \Leftrightarrow (17)$$

where:

$$C_{kL} = 1/\eta_5 - \eta_2\eta_4 k_L > 0 \tag{18}$$

Therefore, if $\eta_2\cdot\eta_3 \neq \eta_1$, then both MPC architectures have the same efficiency for k_{ESS} value given by relation:

$$k_{ESS(b2)} = C_{kL} / \eta_2 > 0 \tag{19}$$

2. Energy efficiency of the MPCp, MPCs, and MPC FC HPS

2.7. Energy efficiency of MPC2 - continued

If different values for k_{ESS} parameter are used in the operation of MPCb and MPC2 architectures (noted with k_{ESSb} and k_{ESS2}, respectively), then MPC architectures could have the same efficiency:

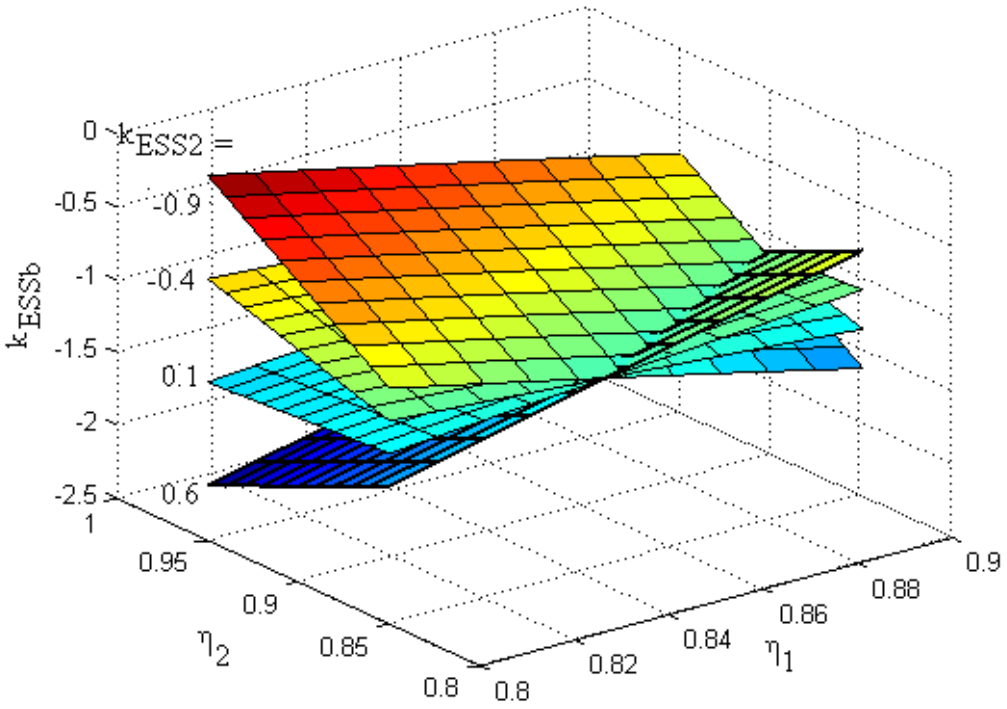

$$\eta_{MPCb} = \eta_{MPC2} \Rightarrow k_{ESSb} = -C_{kL} / \eta_1 + [C_{FC} / k_{FC} - (\eta_2 - \eta_1) / \eta_1] \cdot k_{ESS2}$$

The relation above for k_{FC}=0.1, k_L=0.1, η_3=0.95, η_4=0.95, η_5=0.9 and different k_{ESS2} values (negative and positive) is shown in Figure 8.

Figure 8. $k_{ESSb}(\eta_1, \eta_2)$ for k_{FC}=0.1, k_L=0.1, η_3=0.95, η_4=0.95, η_5=0.9 and different k_{ESS2} values

2. Energy efficiency of the MPCp, MPCs, and MPC FC HPS

2.8. Energy efficiency of MPC1, MPC2, and MPCb

$$\eta_{MPC1} = \eta_{MPC2} \Rightarrow \begin{cases} k_{ESS1}\{[k_{FC}(\eta_2\eta_3 - \eta_1) + \eta_1 k_L]\cdot[1/\eta_5 - \eta_2\eta_4 k_L + \eta_1 - \eta_2] + \eta_1 - \eta_2\} - \\ -k_{ESS2}[\eta_1 k_{FC}(1-k_L) + \eta_1 - \eta_2] = \eta_1\eta_2\eta_4 k_L(1-k_L) \end{cases}$$

$$\{[\eta_2\eta_3 > \eta_1] \vee [\eta_2 > \eta_1 > \eta_2\eta_3]\} \wedge \{k_{ESS} > C_L / C_{FC} > 0\} \Leftrightarrow \eta_{MPCb} > \eta_{MPC1}, \forall k_{FC} \in [0,1]$$

$$\{\eta_2 \le \eta_1\} \wedge \{0 \le (\eta_1 - \eta_2)/(\eta_1 - \eta_2\eta_3) < k_{FC} \le 1\} \wedge \{k_{ESS} > C_L / C_{FC} > 0\} \Leftrightarrow \eta_{MPCb} > \eta_{MPC1}$$

$$\{\eta_2 \le \eta_1\} \wedge \{0 \le k_{FC} \le (\eta_1 - \eta_2)/(\eta_1 - \eta_2\eta_3) \le 1\} \wedge \{k_{ESS} < C_L / C_{FC} < 0\} \Leftrightarrow \eta_{MPCb} > \eta_{MPC1}$$

$$\{\eta_2\eta_3 > \eta_1\} \wedge \{0 \le k_L < 1/\eta_2\eta_4\eta_5\} \wedge \{k_{ESS} > C_{kL} / \eta_2 > 0\} \Leftrightarrow \eta_{MPCb} > \eta_{MPC2}$$

$$\{\eta_2\eta_3 < \eta_1\} \wedge \{0 \le k_L < 1/\eta_2\eta_4\eta_5\} \wedge \{k_{ESS} < C_{kL} / \eta_2\} \Leftrightarrow \eta_{MPCb} > \eta_{MPC2}$$

So, basic MPC architecture may operate efficiently for all k_L values of regenerative braking factor in range, if proper EMU control of k_{FC} ratio is performed in all ESS operating modes.

4. Preliminary experimental results.

Energy Management Unit

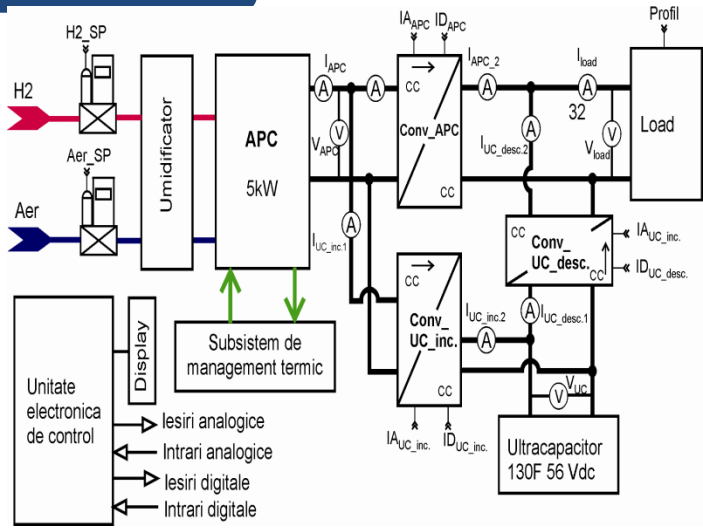

Efficiency of the FC stack

$$\varepsilon_{FC} = \frac{P_{FC}}{P_{H2}} = I_{APC} * \frac{V_{FC}}{M_{H2}} * m_{H2} * \Delta h$$

Efficiency of the FC HPS

$$\varepsilon_{sistem} = \frac{P_{sarcina}}{P_{H2}} = I_{sarcina} * \frac{V_{sarcina}}{M_{H2}} * m_{H2} * \Delta h$$

Zona	Eficiența maximă (%)	Consum Hidrogen (SLPM)	Consum Aer (SLPM)	Tensiune APC (V)	Curent APC (A)	Putere APC (W)
Zona 1	50	10.2	41.3	34.1	29.5	1005
Zona 2	63	21.5	84.2	30.3	61.1	1850
Zona 3	46	40.4	156.7	27.7	108	3000
Zona 4	42	56.7	217	26.5	151	4000
Zona 5	39	75.3	289	25	200	5000

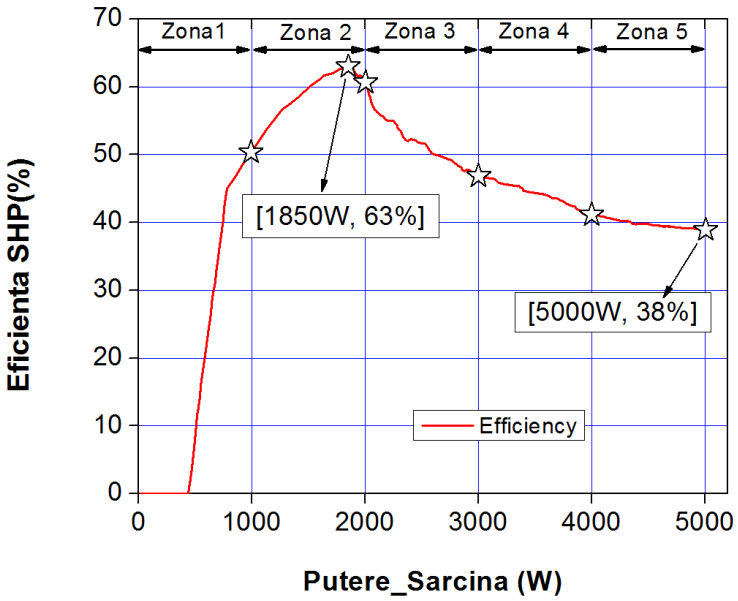

4. Preliminary experimental results.

Main diagram of the Energy Management Strategy

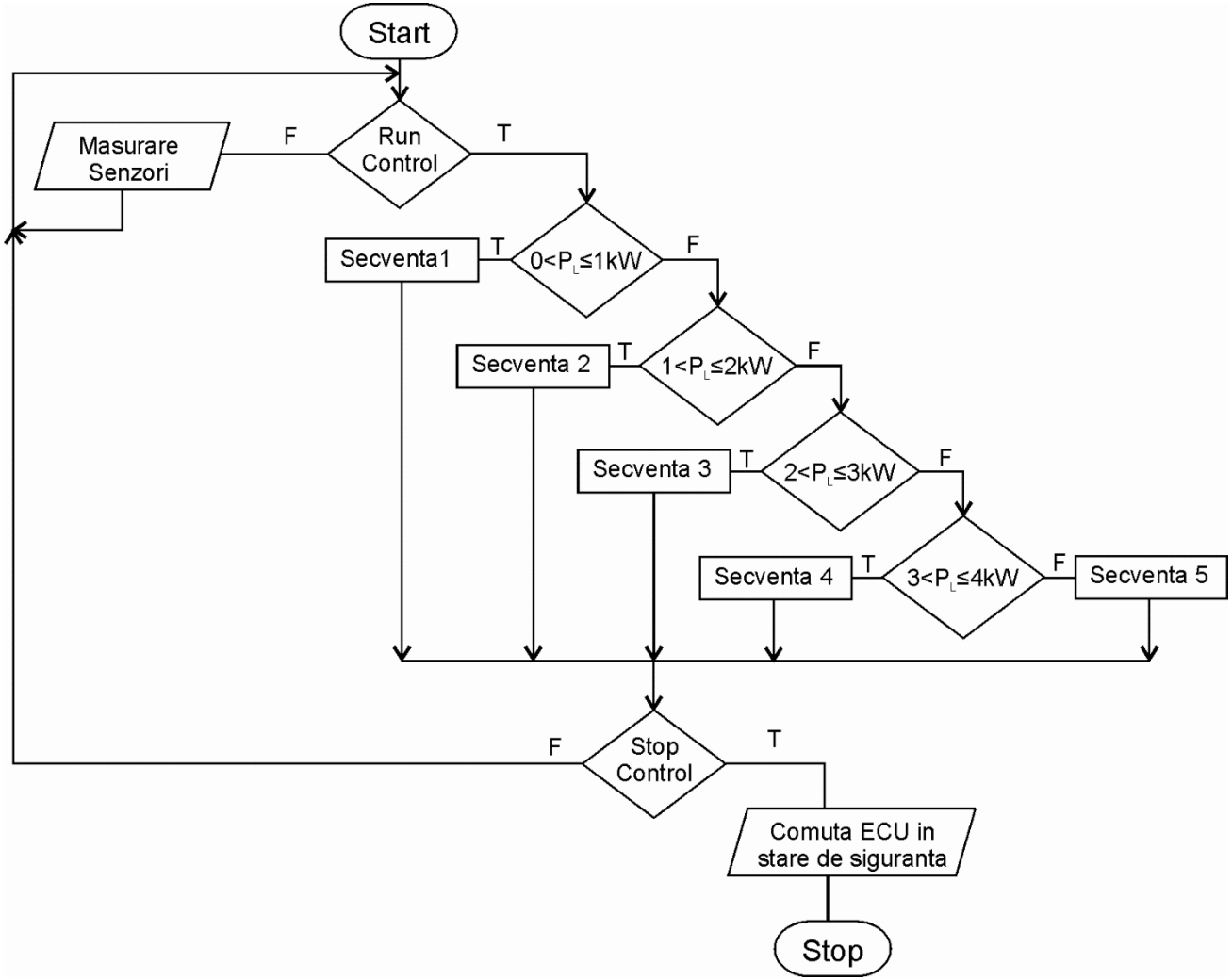

4. Preliminary experimental results.

Subroutine 2 of the EMS

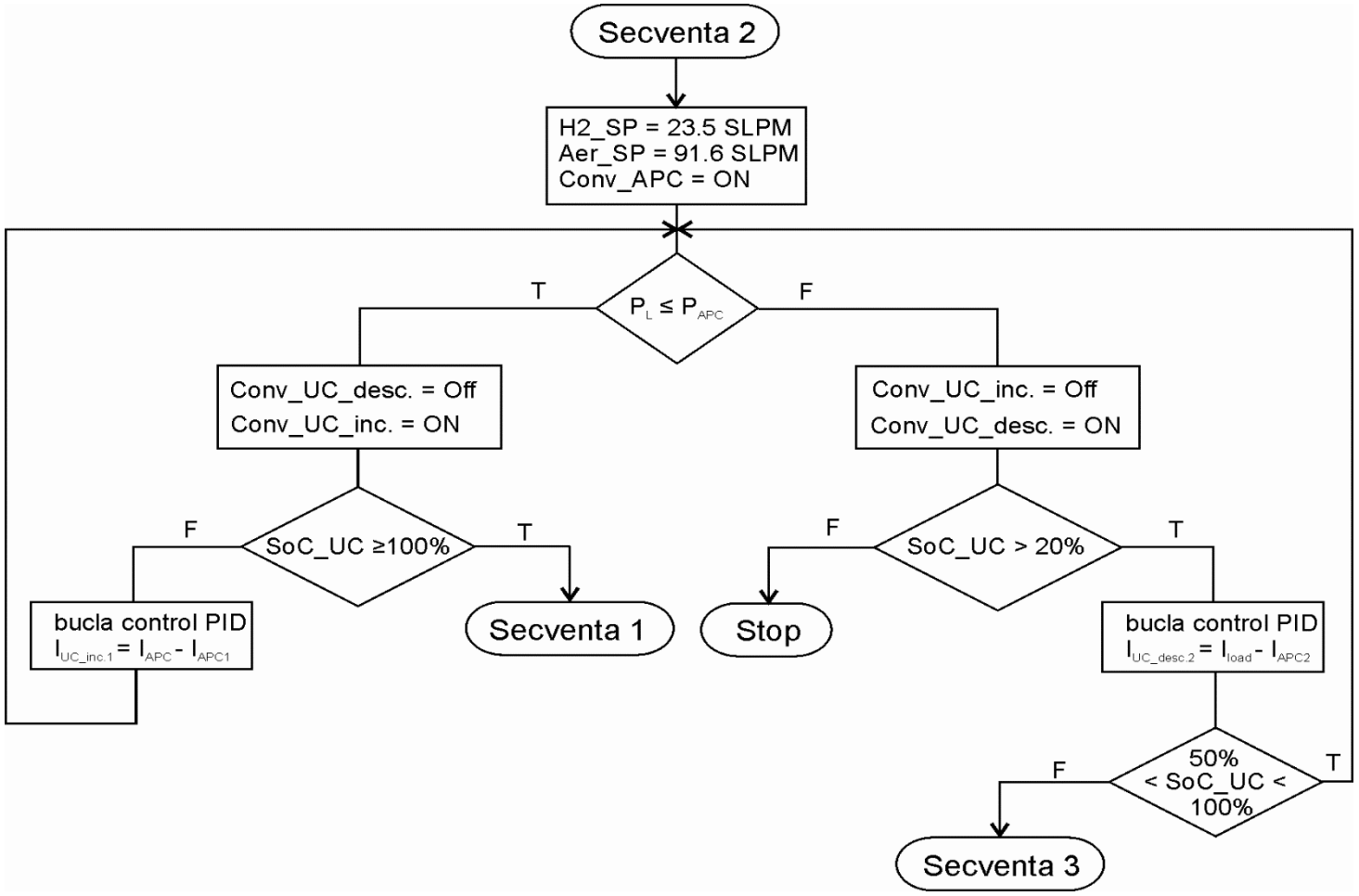

4. Preliminary experimental results.

EMS implementation

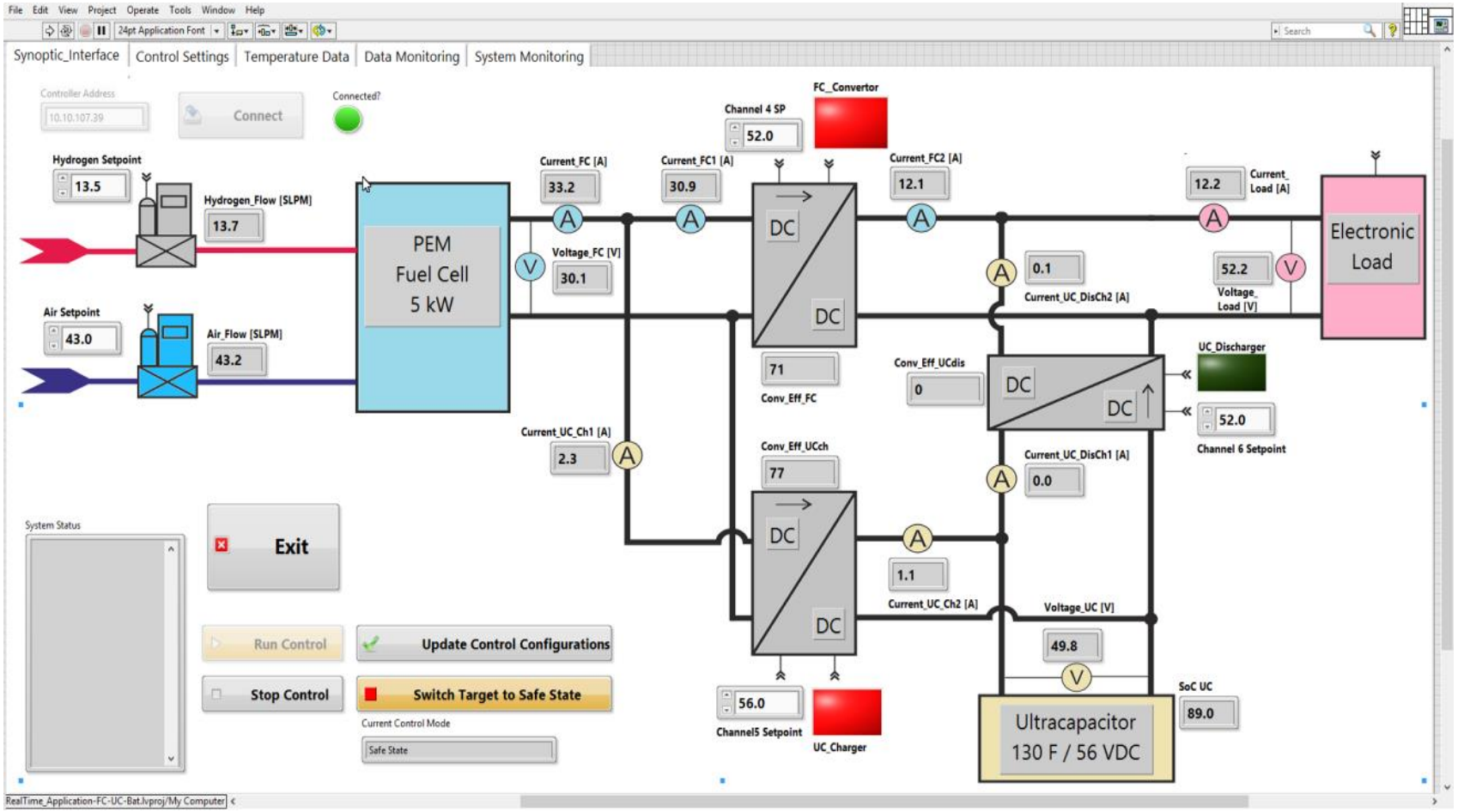

4. Preliminary experimental results.

EMS implementation

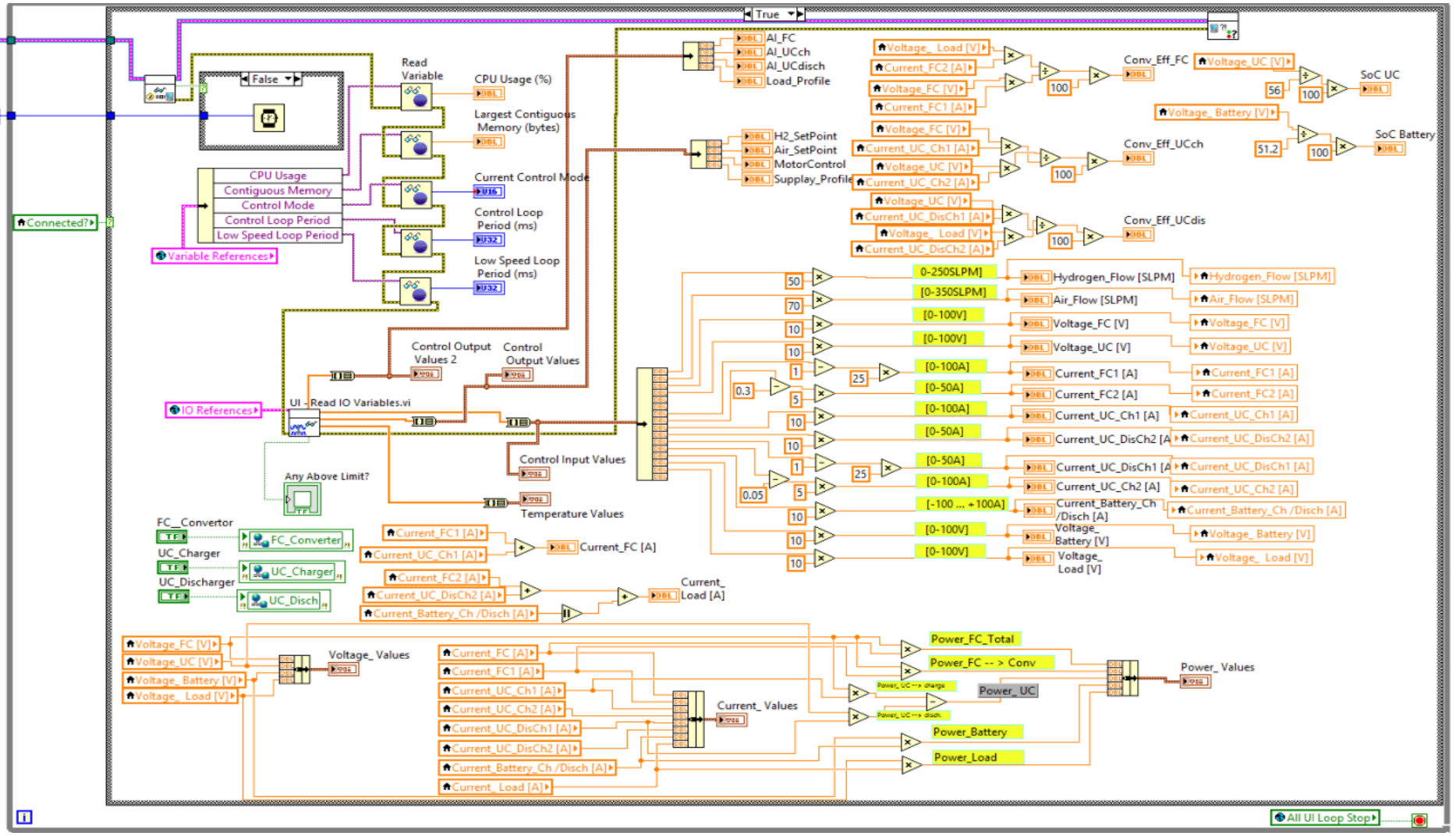

4. Preliminary experimental results.

EMS implementation

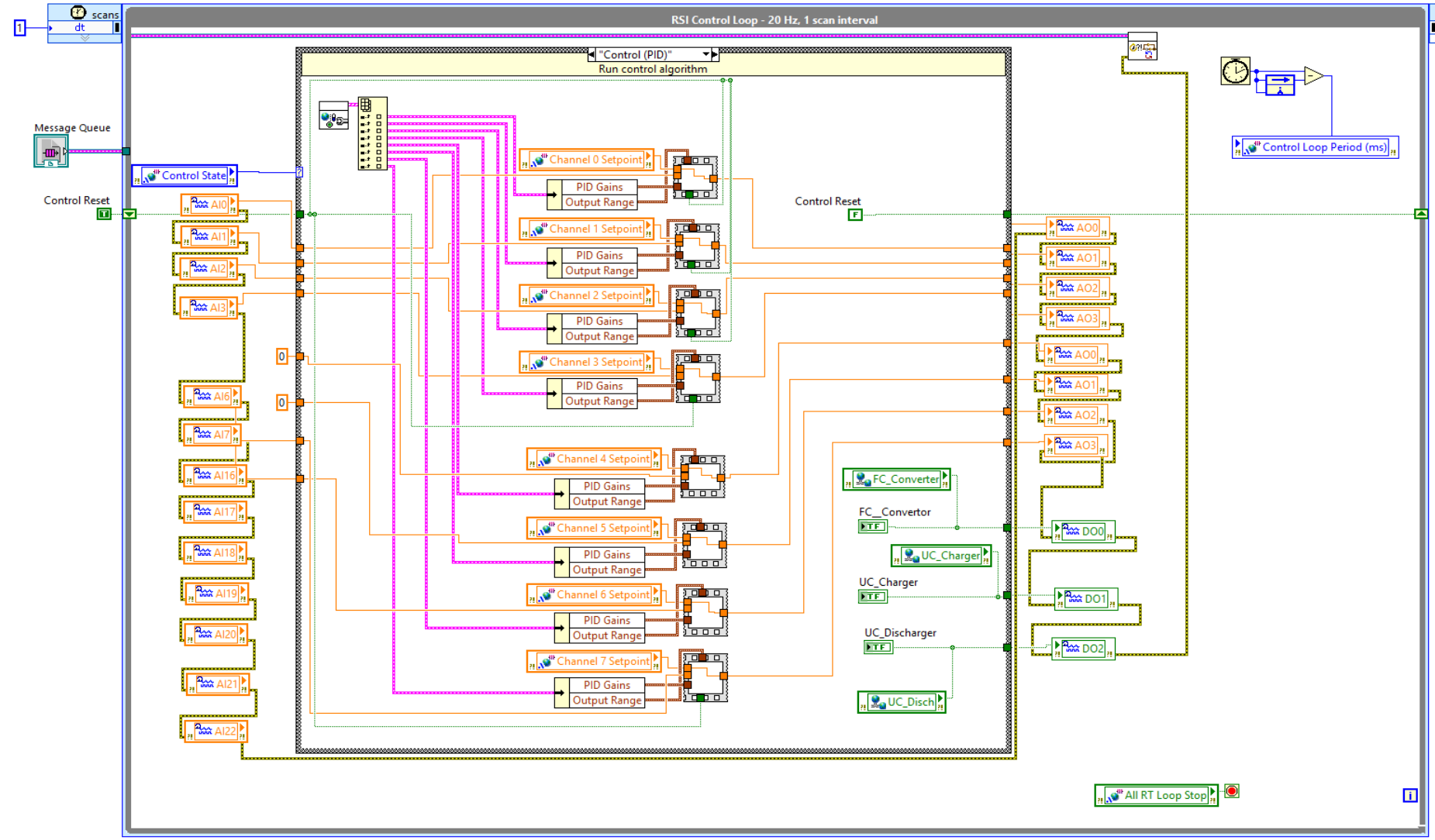

4. Preliminary experimental results.

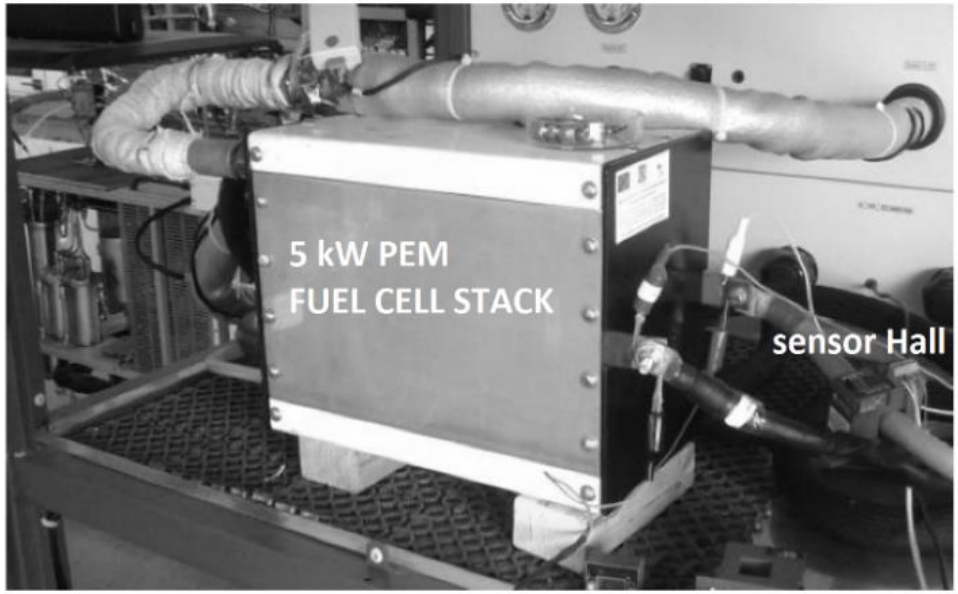

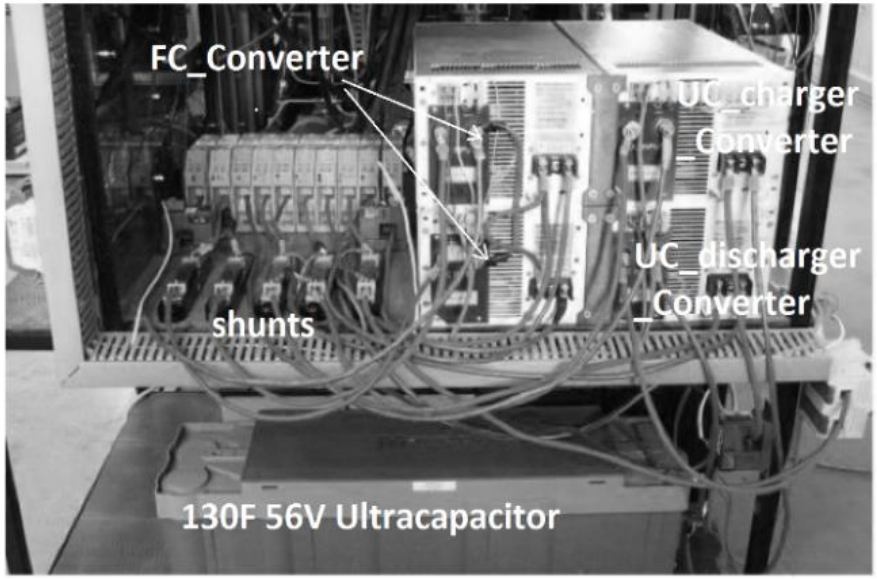

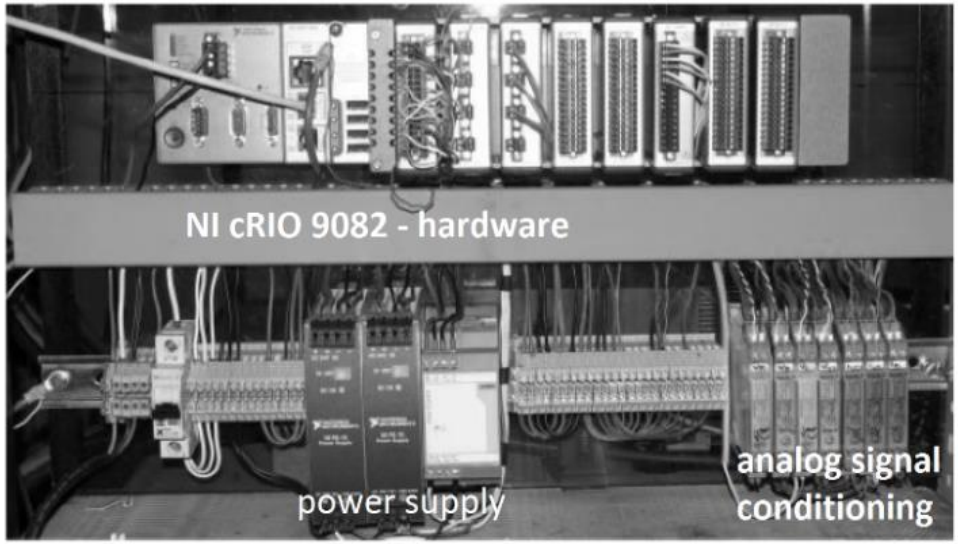

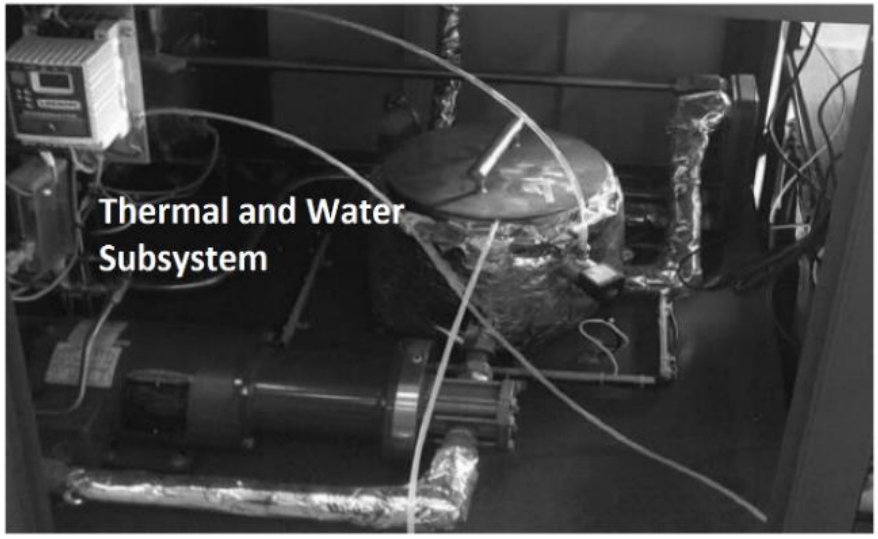

4. Preliminary experimental results.

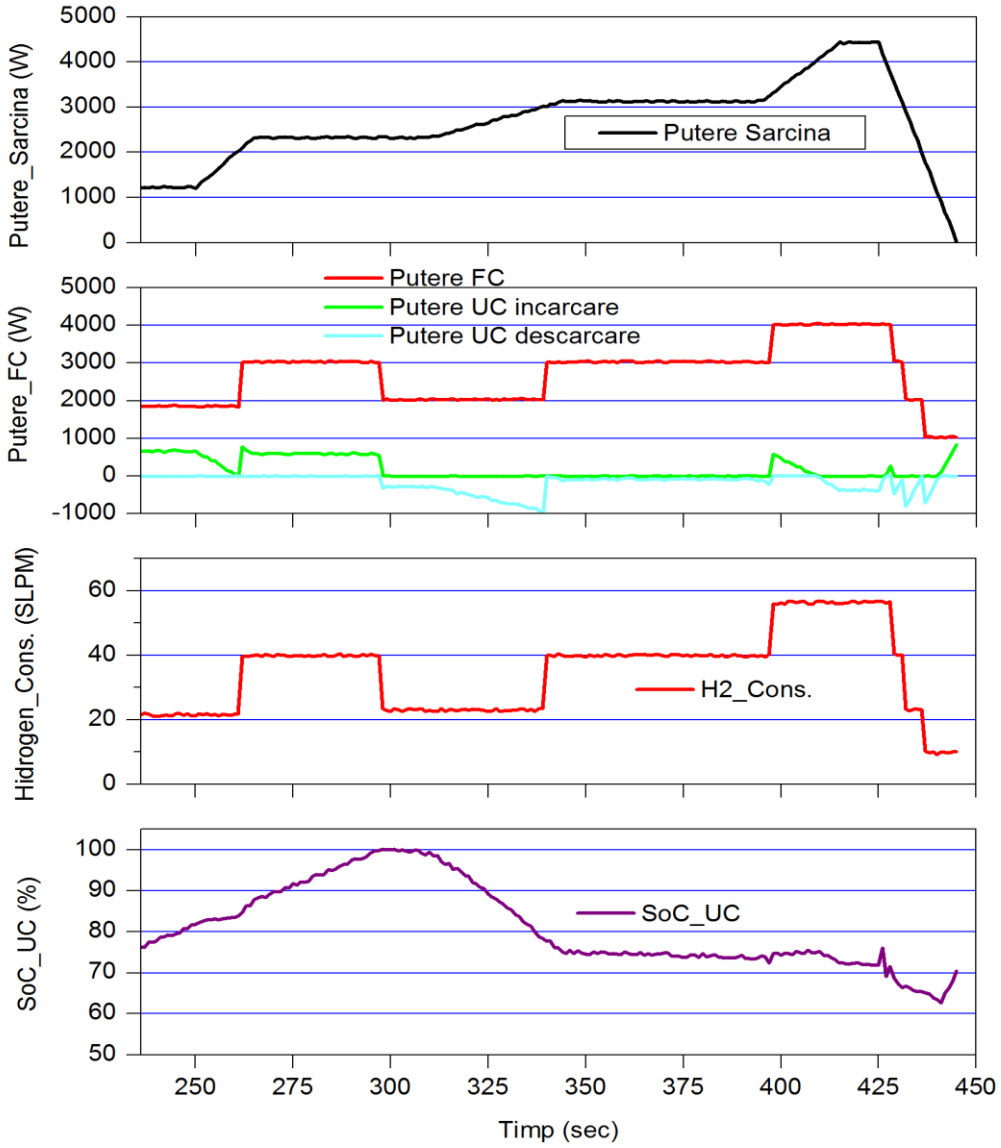

4. Preliminary experimental results.

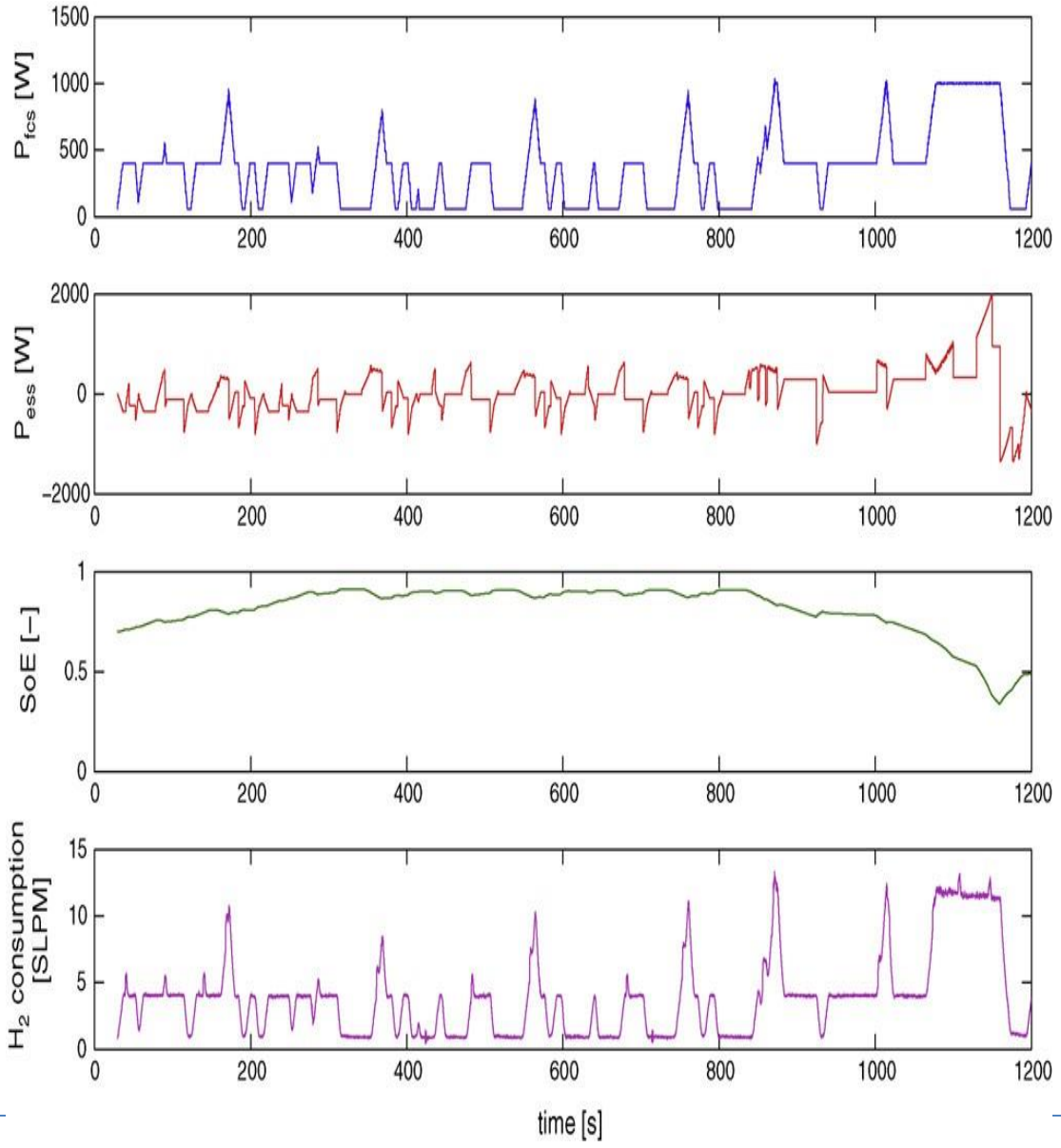

4. Preliminary experimental results.

Experimental study for a FC vehicle

An FC was developed at ICIT Rm. Valcea during a joint project. The project was awarded the Grand Prize at the Research Exposition in Bucharest in 2008.

e-WOLF GmbH
Ernst-Heinrich-Geist-Straße 5
50226 Frechen · Germany

e-WOLF

Mecro System
Mr. Radu PETRE
100 P, Timisoara Blvd
Bucharest-6, RO-061334
Roumanien

Dear Sir,

It is our pleasure to write this letter in support of the research activities developed by S.C. Mecro System S.R.L. in implementing PEM fuel cells in mass-produced electric vehicles.

We are proud that our e-WOLF vehicle, purchased by S.C. Mecro System S.R.L. in 2012, is a key element of the infrastructure involved in the research and development activities focused on assessing the potential of hydrogen technologies as part of the future of road transport.

As a company that integrates leading edge technology in the field of electric vehicles, we would like to express our interest in the outcomes of the R&D activity that could bring significant progress to the transport sector.

We would like to state our availability at any given time for a meeting concerning the technical aspects of innovative projects involving our products.

To conclude with, we completely support S.C. Mecro System S.R.L.'s efforts of developing new technologies that will allow more efficient and environmentally friendly transport solutions.

Sincerely,

Managing Director
Dipl. Kfm. Frank Maiworm

e-Wolf GmbH | Ernst-Heinrich-Geist-Str. 5 | 50226 Frechen
AG Köln HRB 71813 | UST-ID Nr. DE 263116666

4. Preliminary experimental results.

Experimental study for a FC vehicle

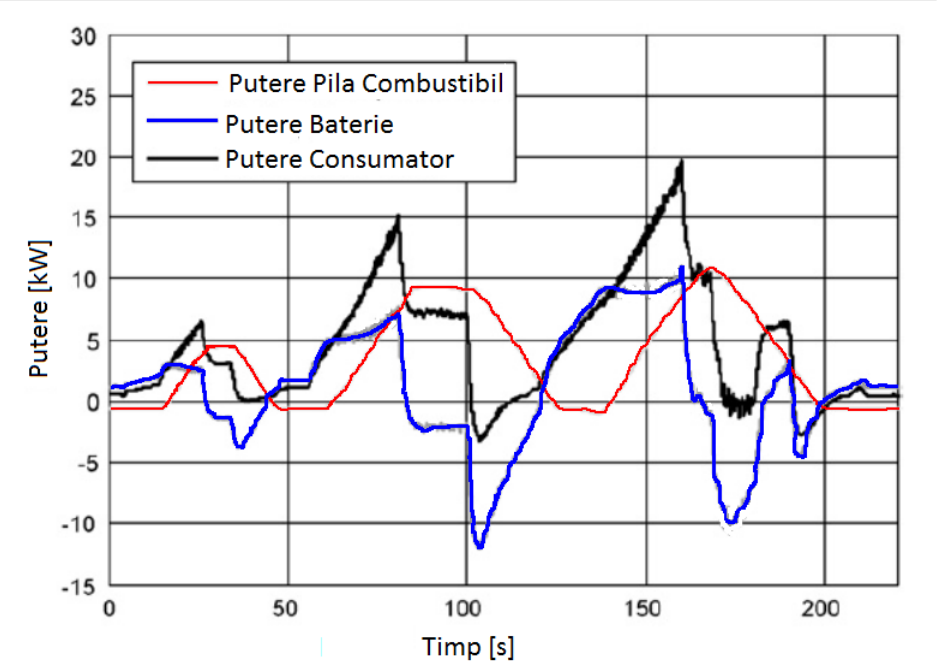

Figure a. Power flow for the FC system, electrical motor and bateries stack with FC current rate limited 5A/sec

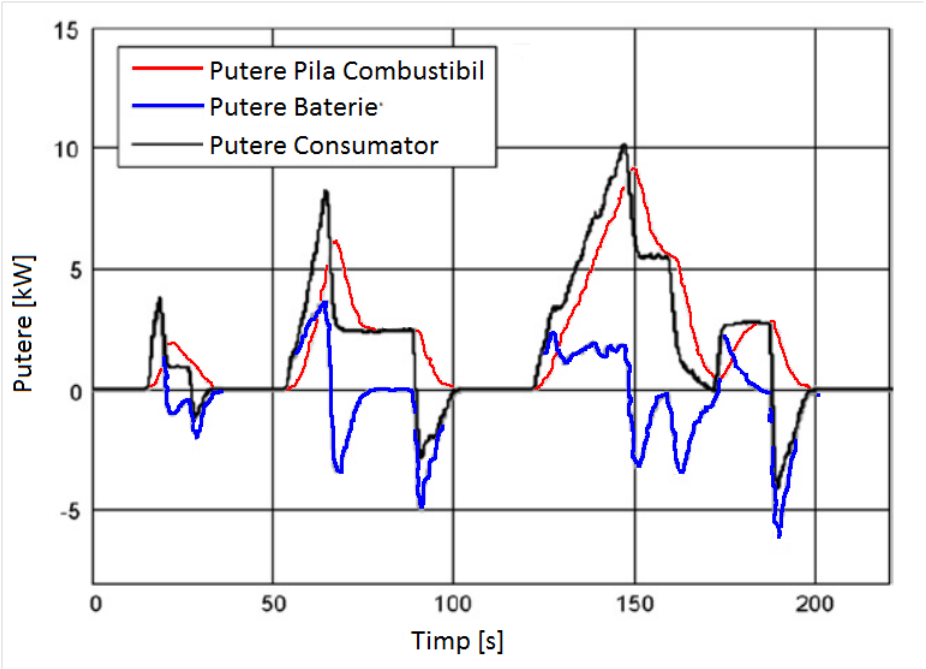

Figura b. Power flow for the FC system, electrical motor and bateries stack with FC current rate limited 10A/sec

5. Conclusions of Part 2.

Hybrid architectures for the interconnection of Fuel Cell (FC) system and Energy Storage Devices (ESD) are briefly shown here.

Energy management strategies of the Hybrid Power Source (HPS) are introduced here.

The components of the FC Hybrid Power Source (FC HPS) under test are shown.

Energy Management Strategy (EMS) based on Proportional-Integral control was analyzed the FC HPS.

Some preliminary experimental results are presented.

The advantages of this new FC HPS topologies are:
- increasing the life of FC stack by running efficiently at constant power inside of one zone;
- protecting the ultracapacitors' stack (UCs) to be discharged below 20% SOC;
- **a reduction in hydrogen consumption by 11.8% compared to a FC HPS without UCs.**

These results will be the reference for other EMSs proposed.

N. Bizon, FC energy harvesting using the MPP tracking based on advanced extremum seeking control, International Journal of Hydrogen Energy 38(4) (12 February 2013),1952-1966. http://dx.doi.org/10.1016/j.ijhydene.2012.10.112 WOS:000314860600023

N. Bizon, Energy efficiency for the multiport power converters architectures of series and parallel hybrid power source type used in plug-in/V2G fuel cell vehicles. Applied Energy 102 (12 February 2013), 726-734. http://dx.doi.org/10.1016/j.apenergy.2012.08.021 WOS:000314190800078

Mircea RACEANU, Comparative analysis regarding the fuel flow control depending on load for power efficiency and high reliability of the Hybrid Power Source, PhD report 4, 2015

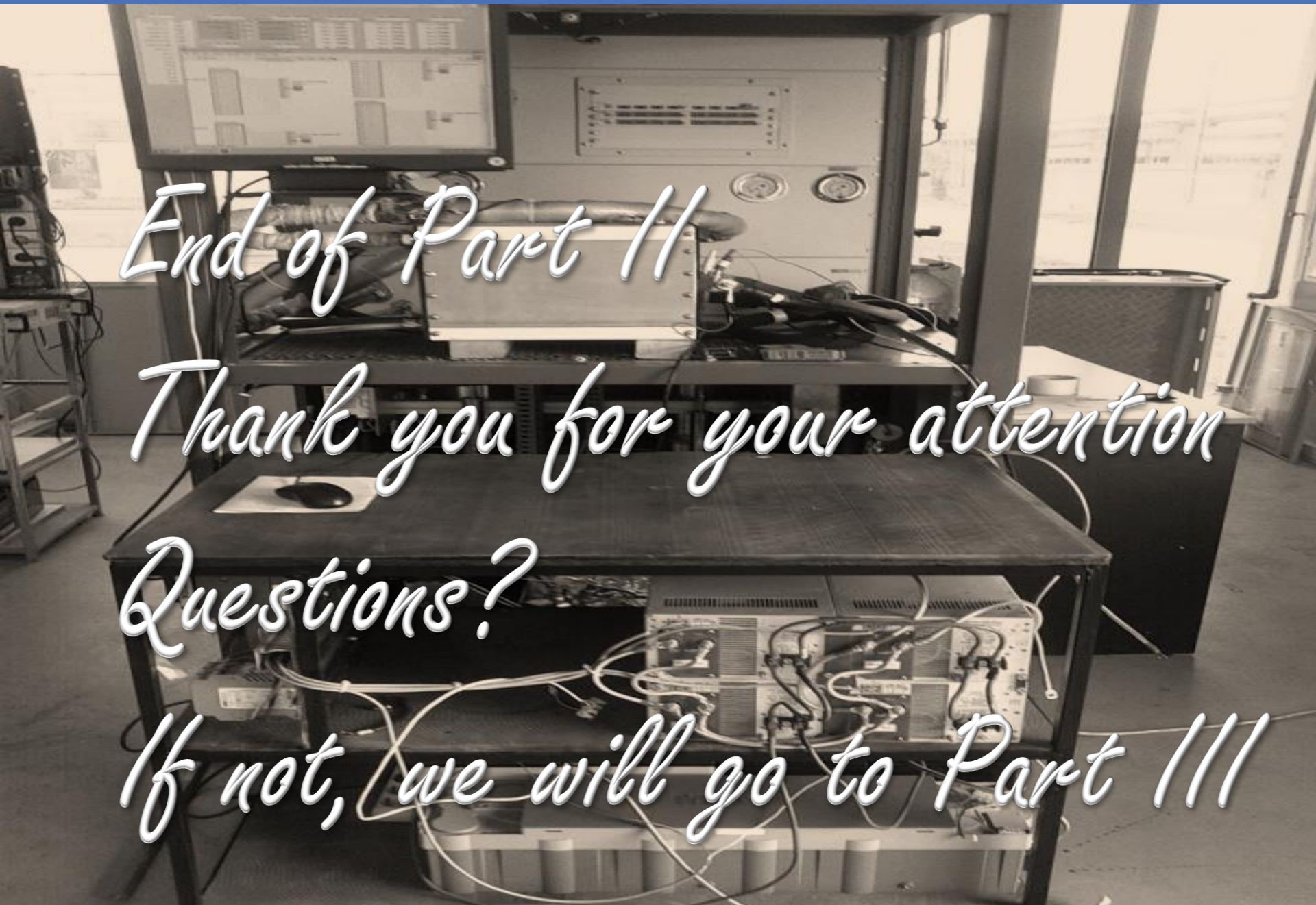
End of Part II
Thank you for your attention
Questions?
If not, we will go to Part III

Erasmus+ PROGRAMME,

KEY ACTION: Cooperation for innovation and the exchange of good practices,

ACTION: Strategic Partnerships

FIELD: Strategic Partnerships for higher education, CALL: 2015

INNOVATIVE EUROPEAN STUDIES ON RENEWABLE ENERGY SYSTEMS

2015-1-TR01-KA203-021342

Real-time optimization of the Renewable Energy Sources / Fuel Cell Hybrid Power Systems

Nicu BIZON
University of Pitesti, Pitesti, Romania

Summary of Part 3 –
Energy management strategies for FC vehicle

1. Powertrain architecture of the FC vehicle (FCV)
2. FC hybrid power source (FC HPS) model
3. Energy management strategies for FC HPS
4. Results
5. Conclusion

1. Powertrain architecture of the FC vehicle (FCV)

1.1. Drive cycle

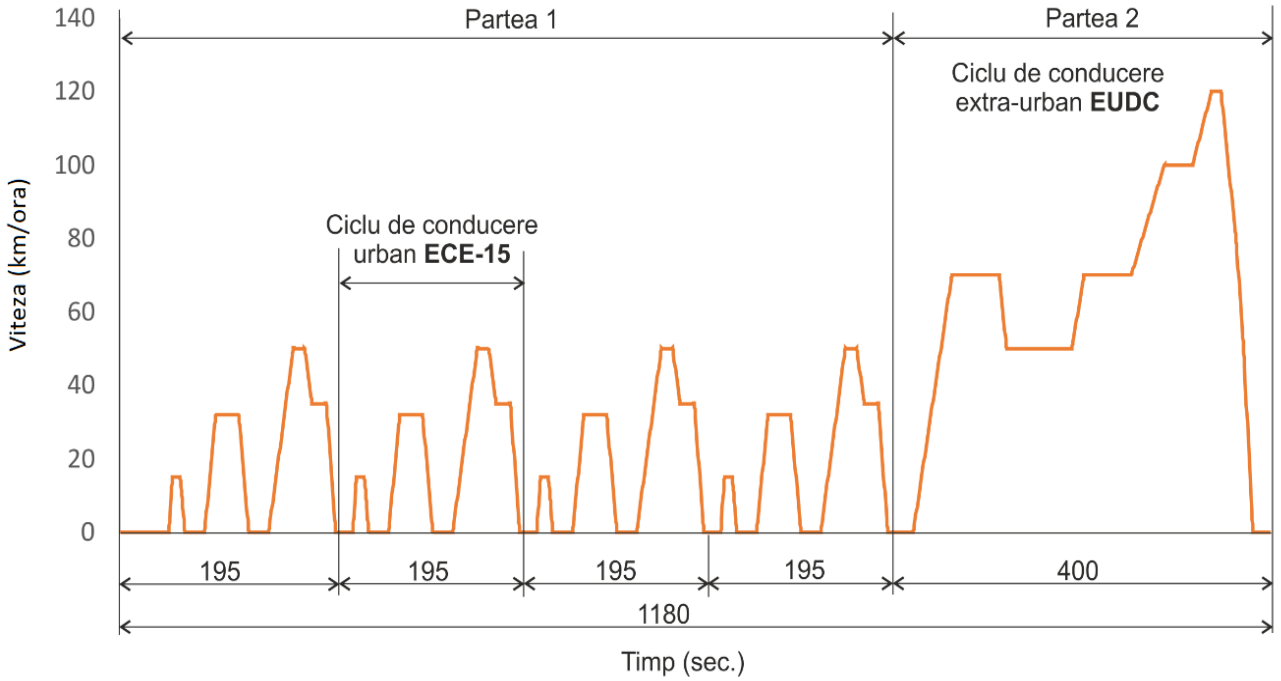

Figure 1.1. Drive cycle **NEDC**

.

Tabel 2.1 Parameters for ECE and EUDC drive cycles

Parameter	ECE-15	EUDC	NEDC
Distance (m)	4 X 994 = 3.976	6.956	10.932
Time (s)	4 x 195 = 780	400	1180
Average speed (km/h)	18.7	62.6	33.6
Maximum speed (km/h)	50	120	120

1. Powertrain architecture of the FC vehicle (FCV)

1.2. Determinarea profilului de putere

Table 2.2. FCV parameters

Parameter	Value
Vehicle weight	1540 kg
Efficiency of the transmission (electric motor \ inverter)	90%
Rolling radius of the wheel	0.25 m
Vehicle frontal area (A)	2.05 m^2
The air drag coefficient (C_W)	0.3
The coefficient of rolling resistance (C_r)	0.01
Air density	1.23 kg/m^3

1. Powertrain architecture of the FC vehicle (FCV)

1.2. Modeling of the FCV

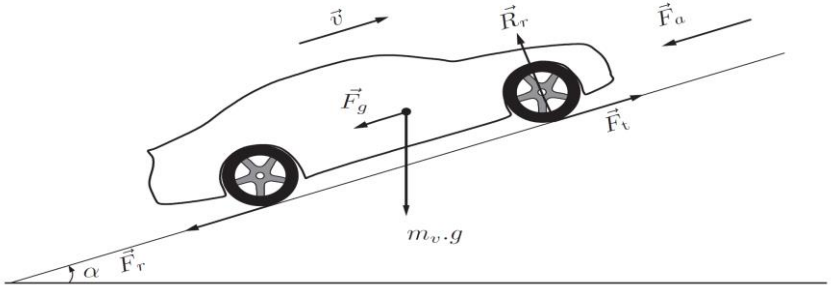

The traction force (F_t) is

$$F_t(t) = m_v(t)\frac{d}{dx}(v(t)) + F_a(t) + F_r(t) + F_g(t)$$

where, F_a is the air resistance force, F_r is the rolling resistance, F_g is the gravity force:

$$F_a = 0.5 * \rho * c_W * A * \vartheta^2$$

$$F_r = C_r * m_v(t) * g\cos(\alpha)$$

$$F_g = m_v(t) \cdot g \cdot \sin(\alpha)$$

1. Powertrain architecture of the FC vehicle (FCV)

1.2. Design of the FC HPS for the FCV

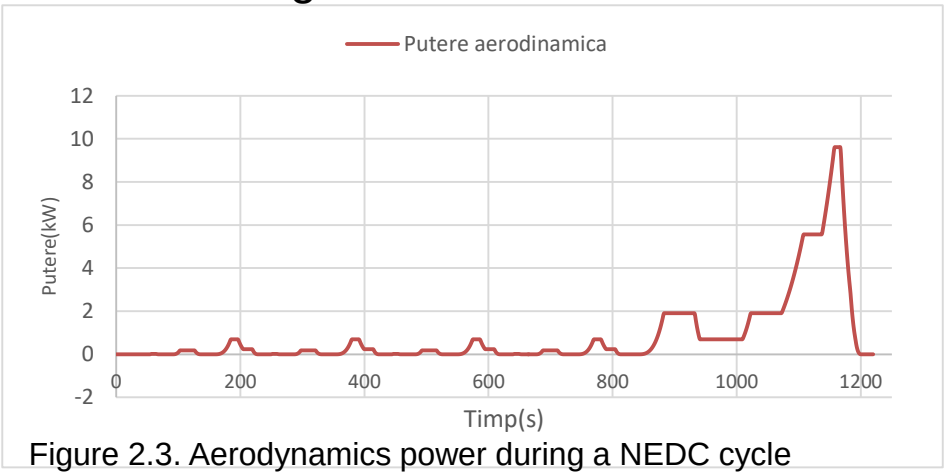

Figure 2.3. Aerodynamics power during a NEDC cycle

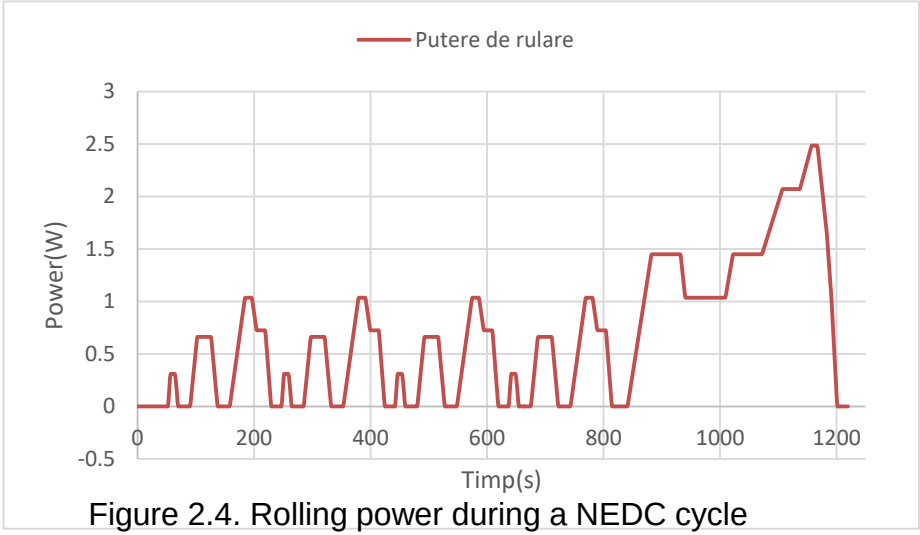

Figure 2.4. Rolling power during a NEDC cycle

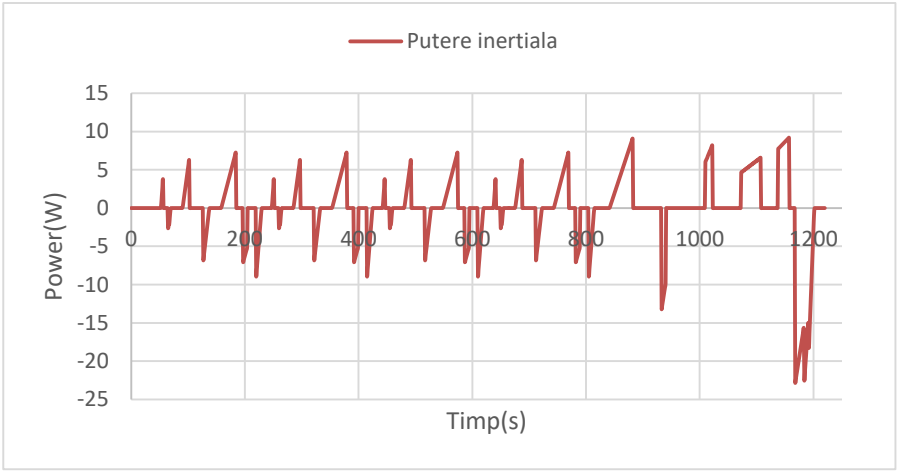

Figure 2.5. Inertial power during a NEDC cycle

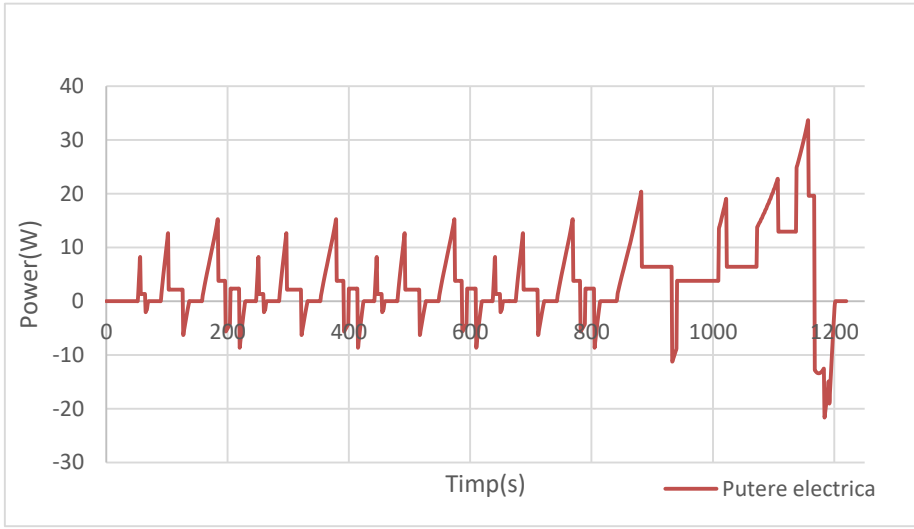

Figure 2.6. Traction power during a NEDC cycle

1. Powertrain architecture of the FC vehicle (FCV)

1.2. Design of the FC HPS for the FCV

Net power of the FC stack	**33 kW**
Litiu-ion stack (16 bateries 12.8V - 160Ah)	32,768 kWh
Ultracapacitors (UC) stack (8 Ucs of 12,6F)	57Wh
Power converter efficiency (100% -10% of rated load)	85-92%
Electric motor	75kW

Tabelul 2.3. The FC HPS components

1. Powertrain architecture of the FC vehicle (FCV)

1.3. FCV powertrain architecture

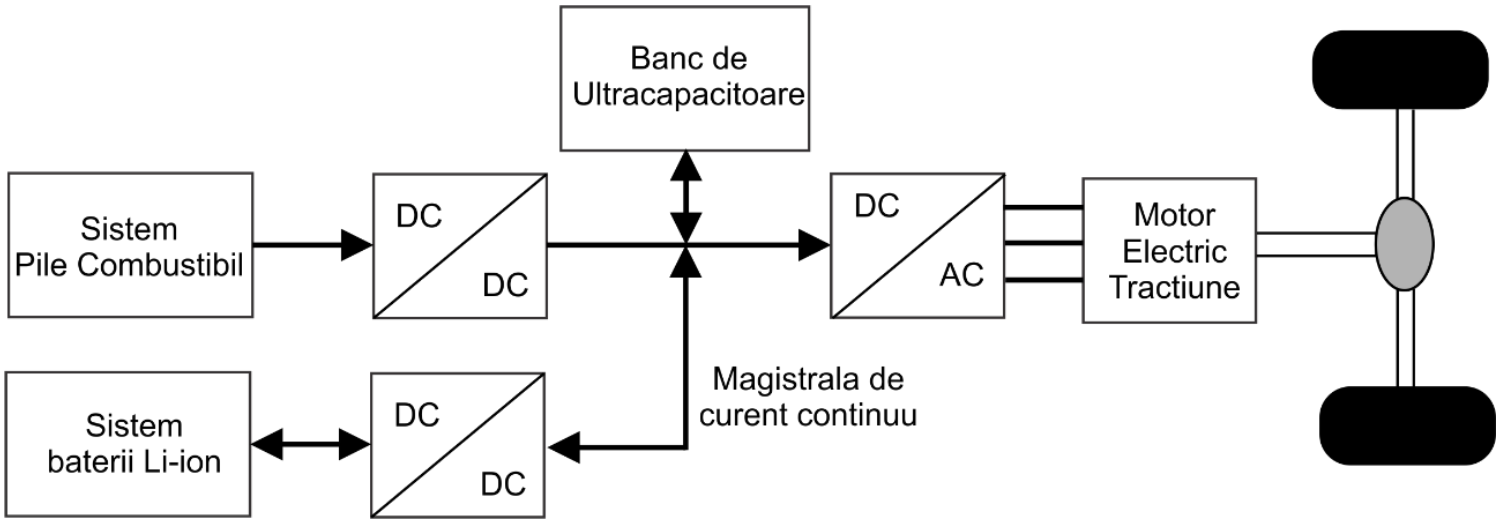

Figure 2.7. **FCV powertrain architecture**

2. FC hybrid power source (FC HPS) model

2.1. FC system

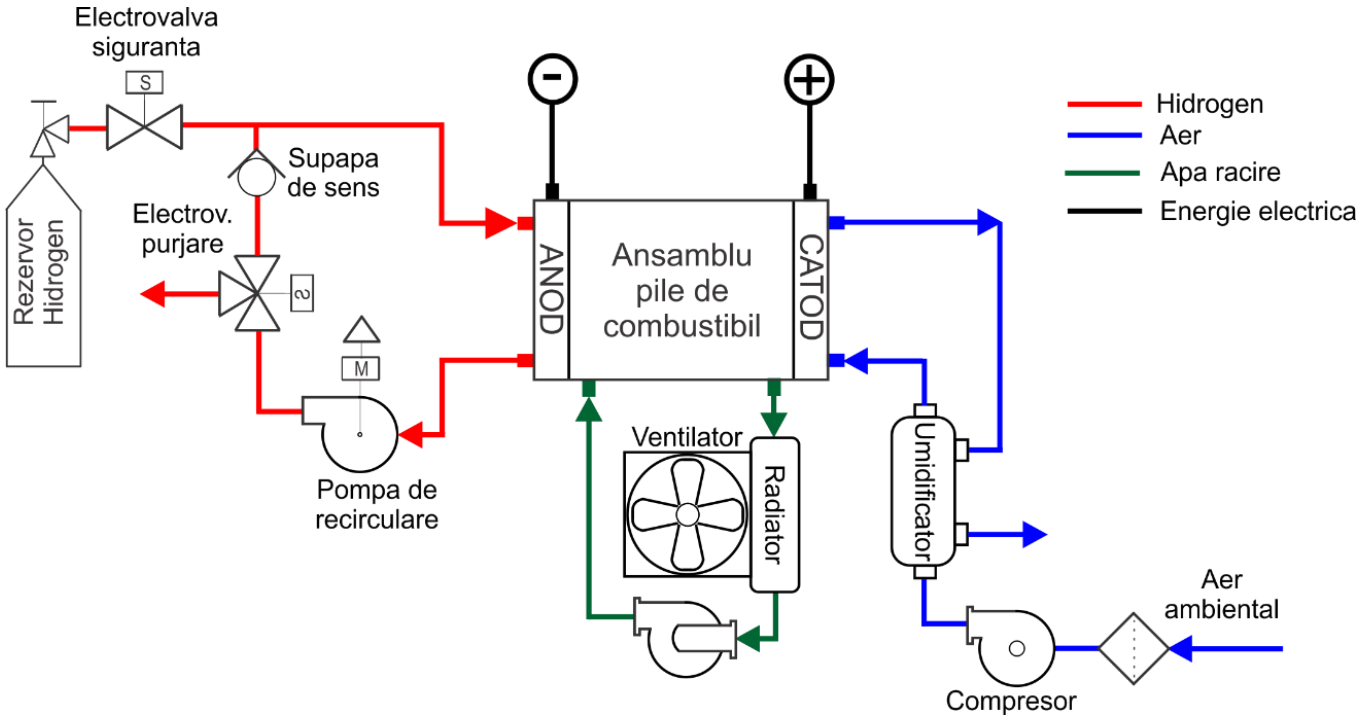

Figura 3.2. FC system

2. FC hybrid power source (FC HPS) model

2.2. Purge algorithm for FC stack operating in blocking anode

$$V_p - V_{FC} \geq 2V \qquad (3.1)$$

$$\frac{\Delta V_{FC}}{\Delta t} \leq -0{,}05\ V\ s^{-1} \qquad (3.2)$$

$$\frac{\left|\,|V_N - V_{N-1}|\,\right|}{V_{N-1}} \geq 10\% \qquad (3.3)$$

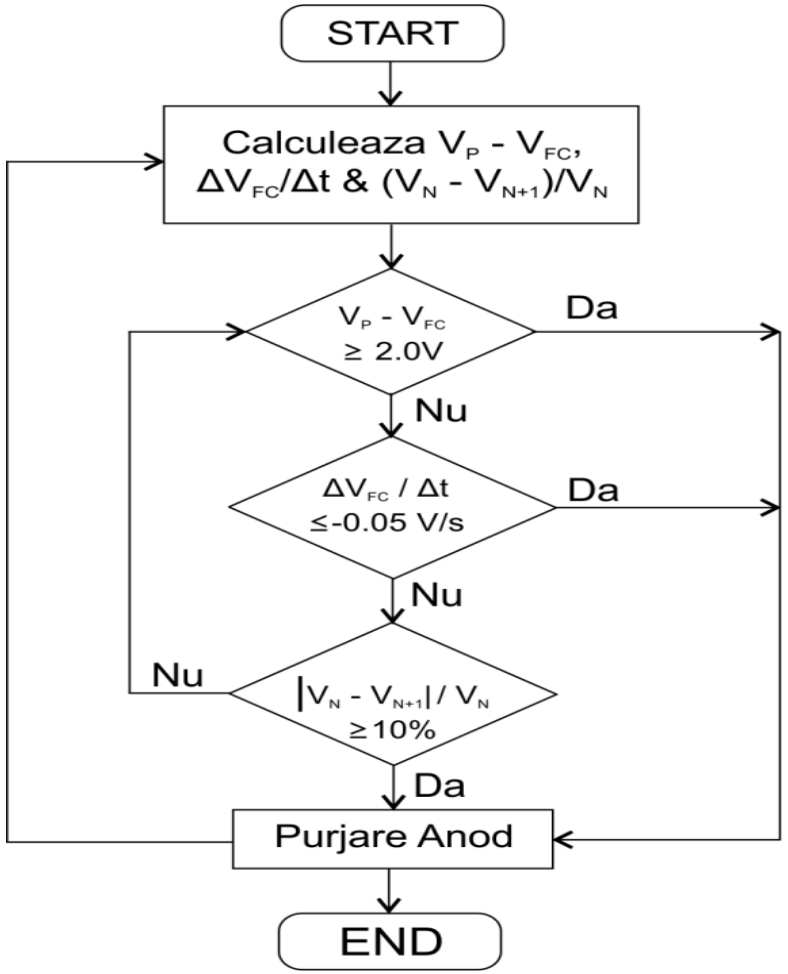

2. FC hybrid power source (FC HPS) model

2.3. Fuel flow regulators

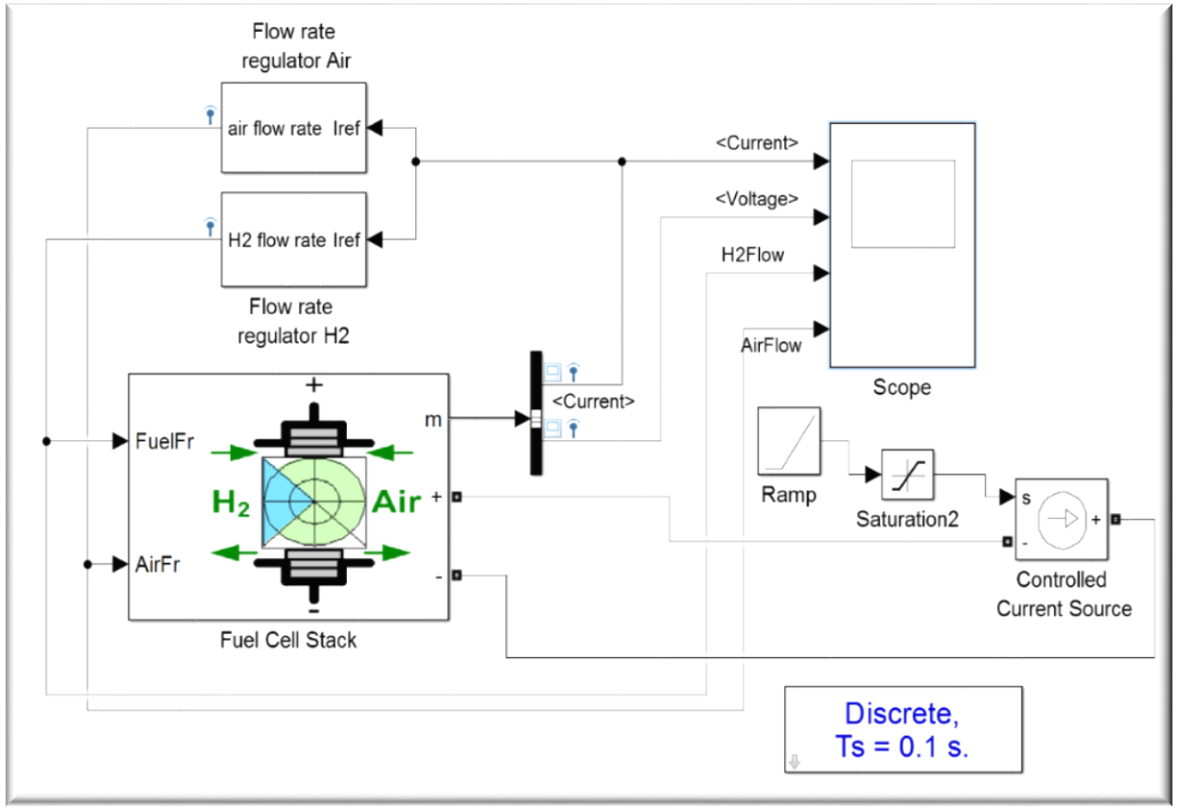

Figura 3.5. Test diagram

$$U\,f_{H_2} = \frac{60000\,R\,T\,i_{fc}}{2\,F\,P_{fuel}\,V_{fuel}\,x\%}$$

$$U\,f_{air} = \frac{60000\,R\,T\,i_{fc}}{4\,F\,P_{air}\,V_{air}\,y\%}$$

$$P_{H_2} = \left(1 - U\,f_{H_2}\right) x\%\; P_{fuel}$$

$$P_{O_2} = \left(1 - U\,f_{O_2}\right) y\%\; P_{air}$$

2. FC hybrid power source (FC HPS) model

2.3. FC system parameters

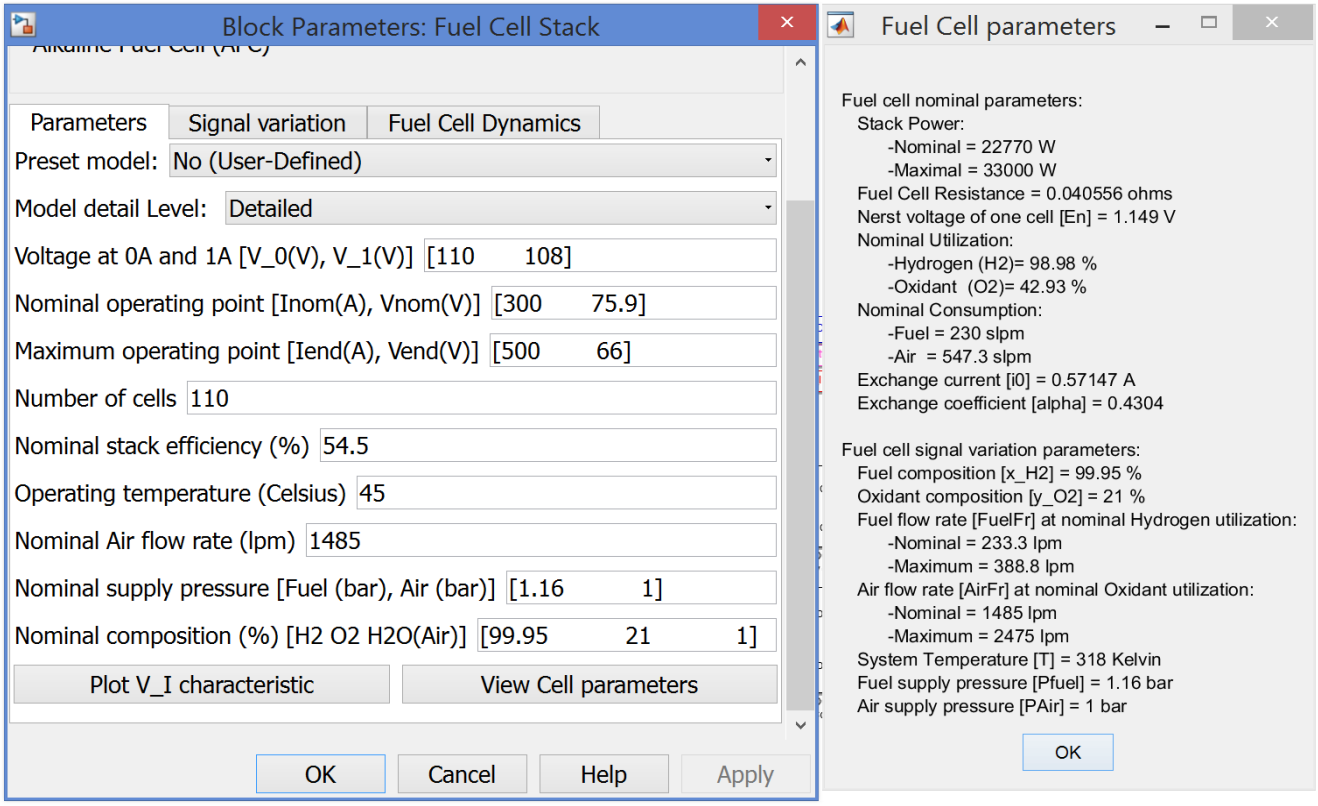

Figura 3.6. FC system parameters

2. FC hybrid power source (FC HPS) model

2.3. FC characteristics

Rated power	**33 kW**
Current	0 – 500A
Voltage	60 – 120 Vdc
Maximum energy efficiency (MEE)	55%
Response time	< 5 s from off to idle < 3 s from idle to rated power
Fuel	dry hydrogen > 99.98% purity
Oxidant	Ambiental air
Cooling agent	Deionized water
Comunication	CAN V2.oA

Table 3.1 Data sheet for FC type HD 33

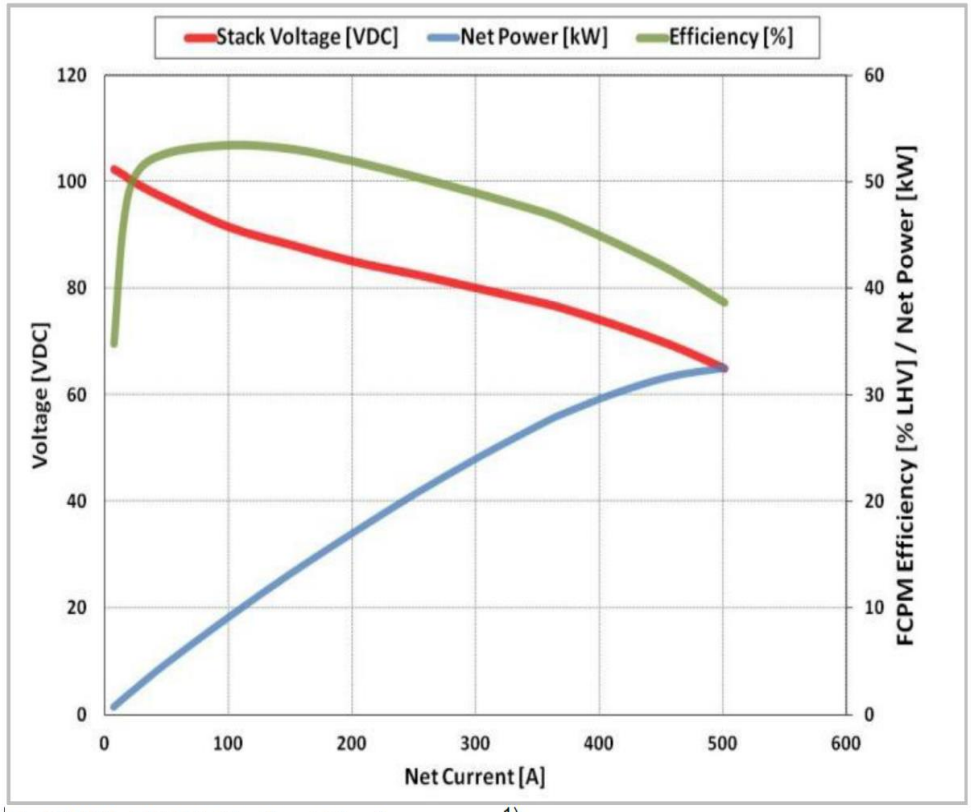

HyPM™ HD30 Typical Performance[1)]

Figura 3.4. Characteristics of HD-33 FC

2. FC hybrid power source (FC HPS) model

2.4. Battery model

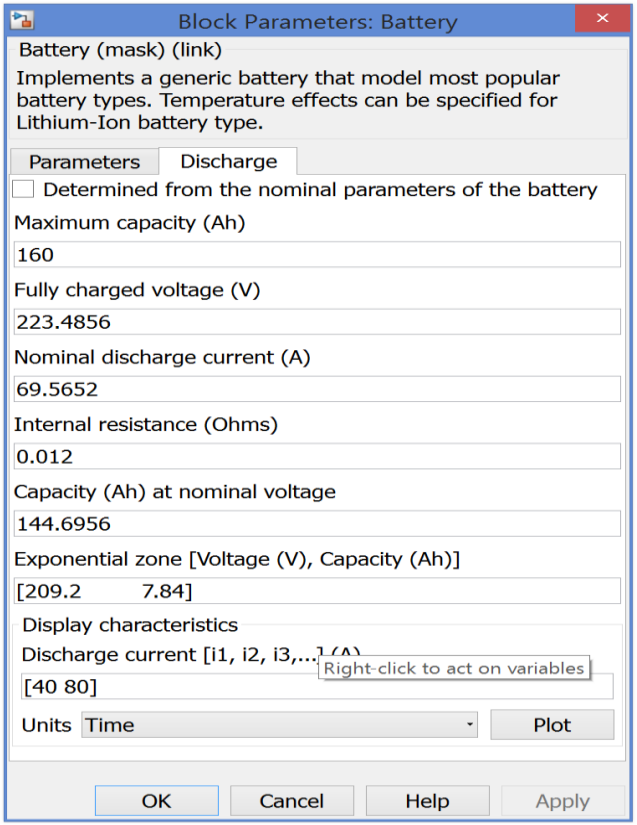

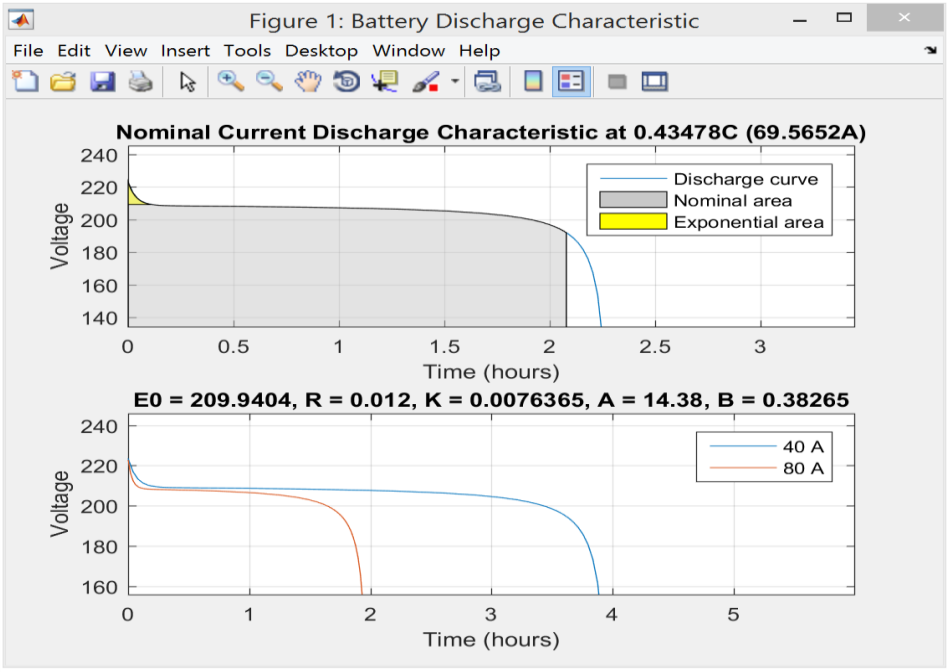

$$v_{batt} = E_0 k \frac{Q}{Q-it} \cdot it - R_b \cdot i + A_b \exp(-B \cdot it) - K \frac{Q}{Q-it} \cdot i^*$$

Figure 3.7. Parameters and characteristics of the batteries' stack

2. FC hybrid power source (FC HPS) model

2.5. Ultracapacitors' (UCs) stack model is based on Stern model that combines the Helmholtz and Gouy-Chapman models

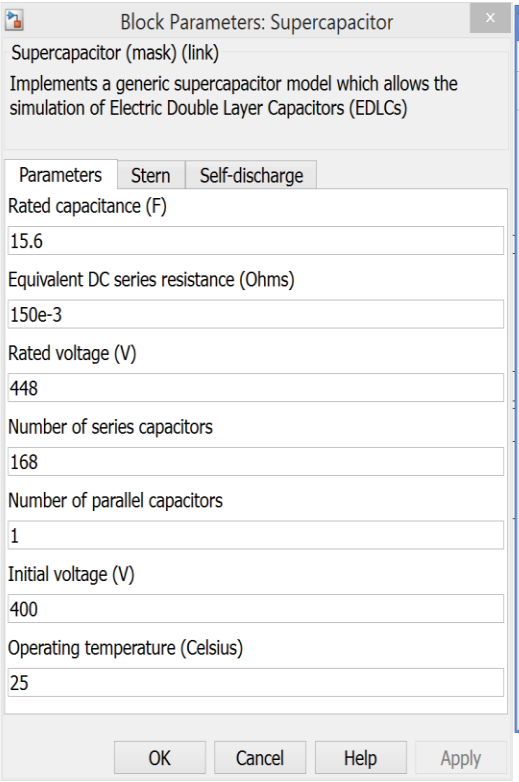

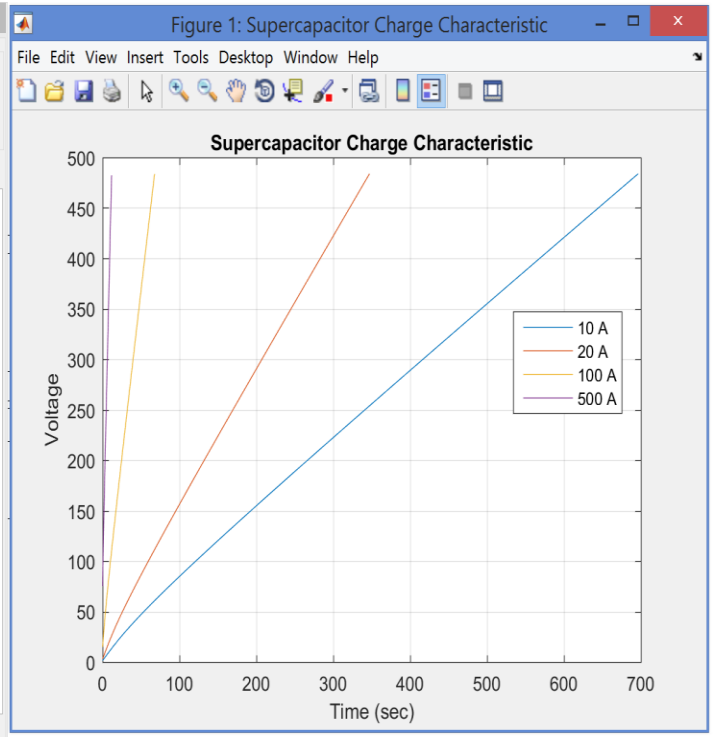

$$C = \left[\frac{1}{C_H} + \frac{1}{C_{GC}}\right]^{-1}$$

$$C_H = \frac{N_e \in_r \in_0 A_i}{d}$$

$$C_{GC} = \frac{FQ_c}{2N_c RT} sinh\left(\frac{Q_c}{N_c^2 A_i \sqrt{8RT \in_r \in_0 c}}\right)$$

Figure 3.8. UC parameters and characteristics

2. FC hybrid power source (FC HPS) model

2.6 Modeling and control of the DC-DC boost converter

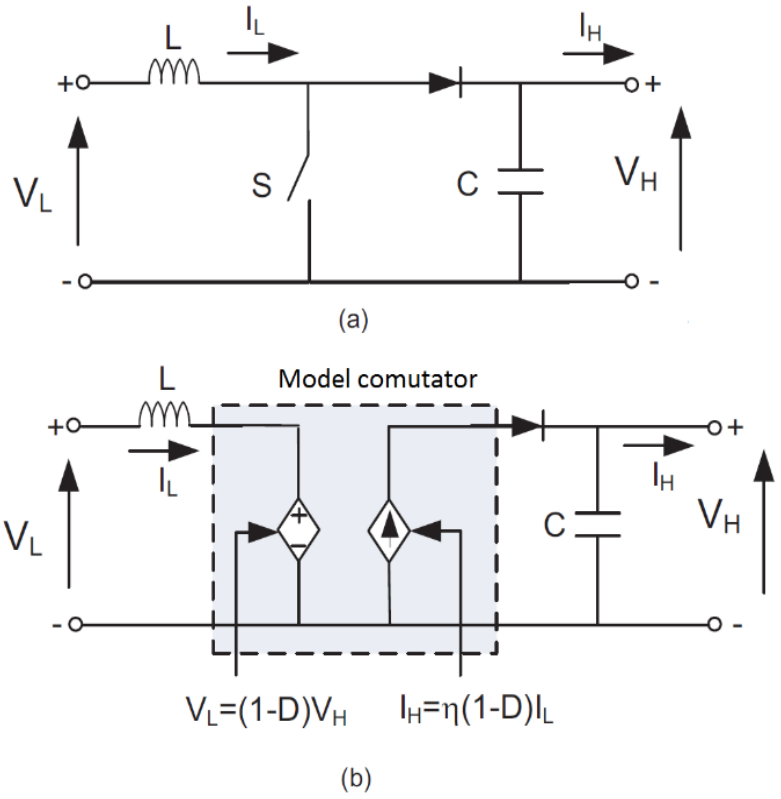

Figure 3.9. DC-DC boost converter:
(a) Electrical circuit;
(b) Average model

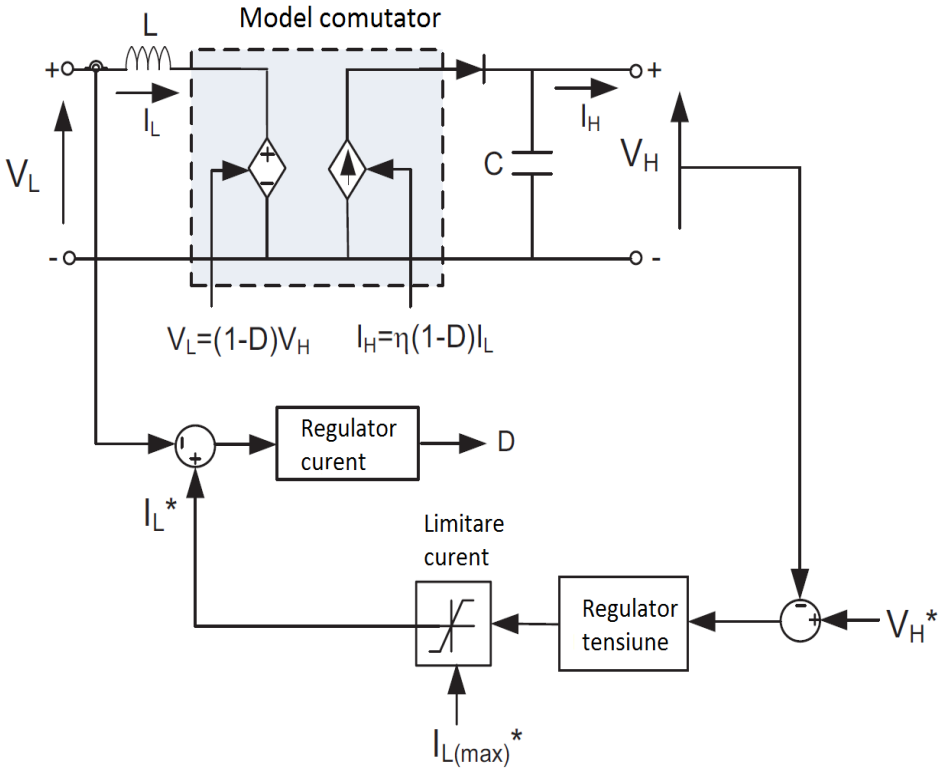

Figure 3.10. Control of the DC-DC boost converter

2. FC hybrid power source (FC HPS) model

2.6 Control of the DC-DC boost converter

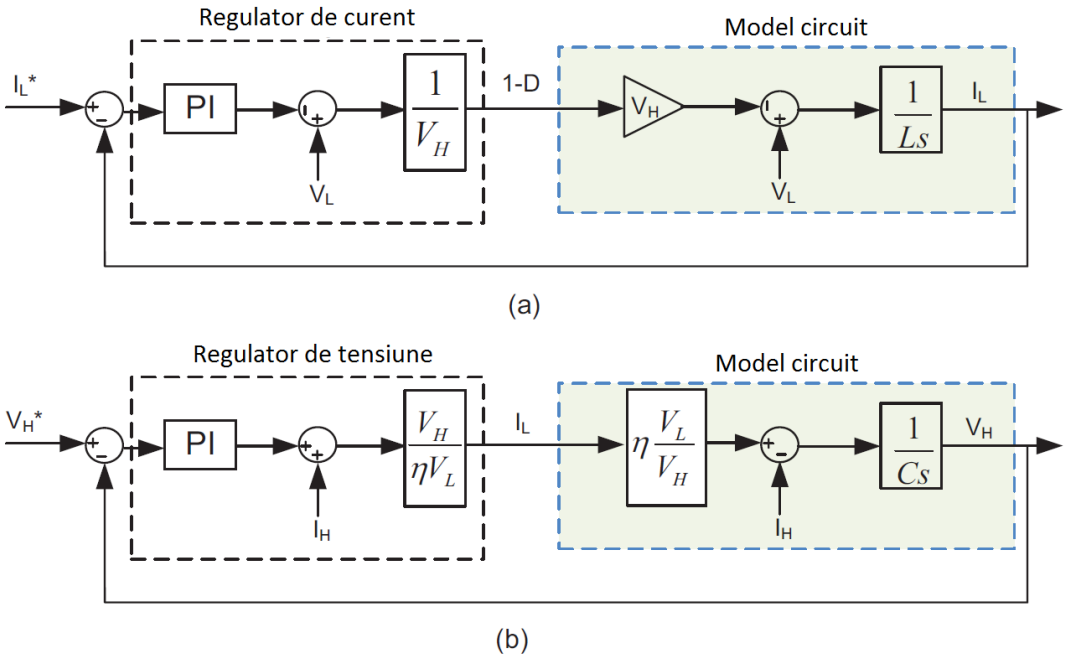

$$V_L = (1 - D) \cdot V_H$$

$$I_H = \eta \cdot (1 - D) \cdot I_L$$

$$\eta = a \cdot I_H + b$$

Figure 3.11. (a) current regulator, (b) voltage regulator

Parameter	
Maximum Current [A]	85
Eficiency @ 100% and 10% rated load [a, b]	[85, 90]
Response time (s)	0.1
Filtering capacity (F)	15.6

Table 3.3. Parameters of the DC-DC boost converter

2. FC hybrid power source (FC HPS) model

2.6 Modeling and control of the DC-DC buck converter

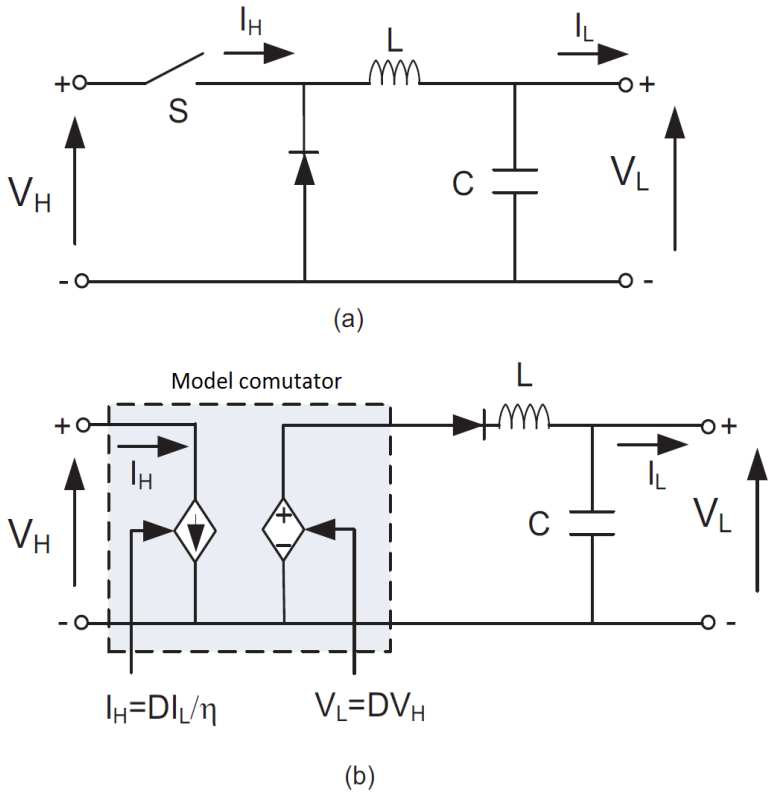

Figure 3.12. DC-DC buck converter:
(a) Electrical circuit;
(b) Average model

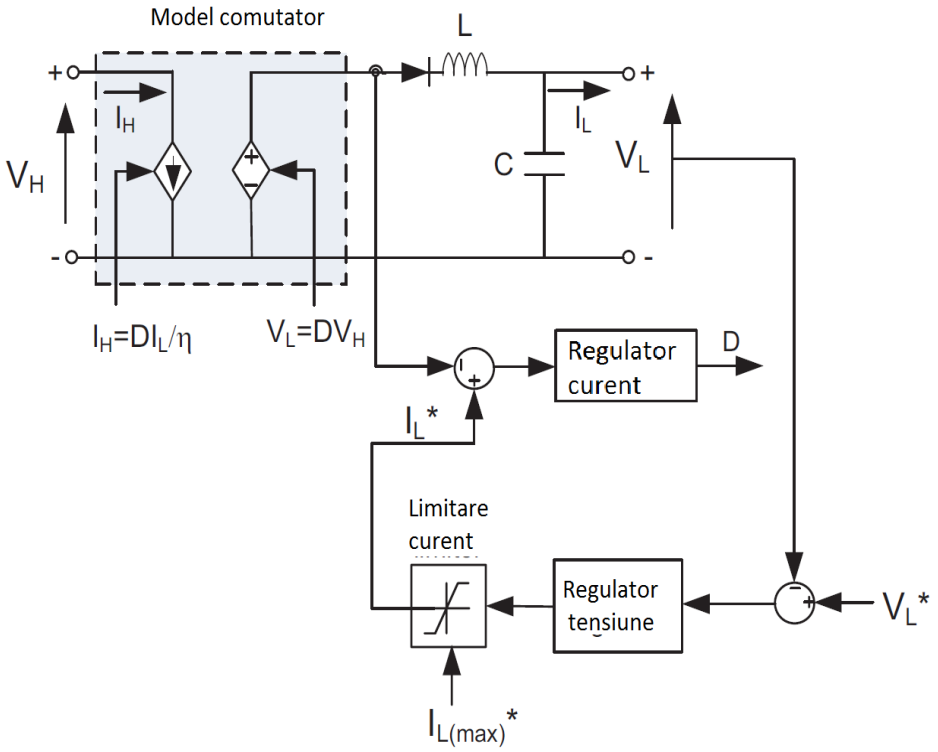

Figure 3.13. Control of the DC-DC buck converter

2. FC hybrid power source (FC HPS) model

2.6 Control of the DC-DC buck converter

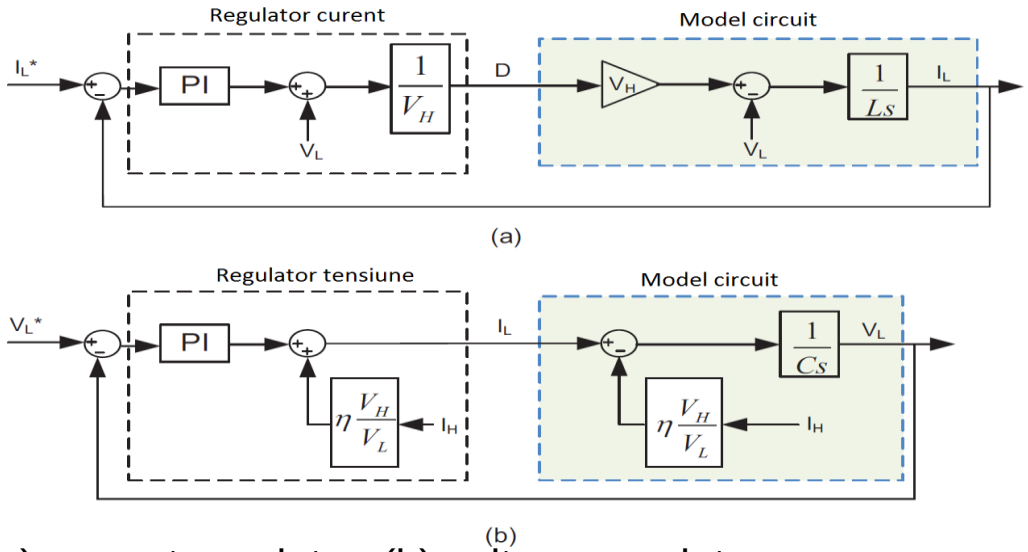

Figure 3.14. a) current regulator, (b) voltage regulator

$$V_L = D \cdot V_H$$

$$I_H = \frac{D \cdot I_L}{\eta}$$

$$\eta = a \cdot I_H + b$$

Table 3.3. Parameters of the DC-DC buck converter

Parametrii de intrarea ai modelului de convertor coborâtor pentru baterie	
Maximum Current [A]	20
Eficiency @ 100% and 10% rated load [a, b]	[80, 88]
Response time (s)	0.1
Filtering capacity (F)	0.1

3. Energy management strategies (EMS) for FC HPS

2.6 Objectives for the EMS unit

- Assuring the load demand
- Operating the FC stack at high efficiency
- Minimizing the fuel consumption
- Protecting the FC stack to fuel starvation
- Protecting the batteries' stack to deep discharge by monitoring the State-Of-Charge (SOC)

The EMS can be mainly classified into rule-based energy management strategy and optimization-based energy management strategy.
Several energy management control strategies have been already proposed for FC vehicle, such as heuristic strategies, equivalent consumption minimization strategy (ECMS) and strategies based on optimal control theory.
Not all objectives mentioned above can be optimized simultaneously.

Below, the following two EMS types will be evaluated:

- Strategies using the control diagram based on the operating states designed;
- PI controllers-based strategies;

3. Energy management strategies (EMS) for FC HPS

2.6 EMS based on PI regulator

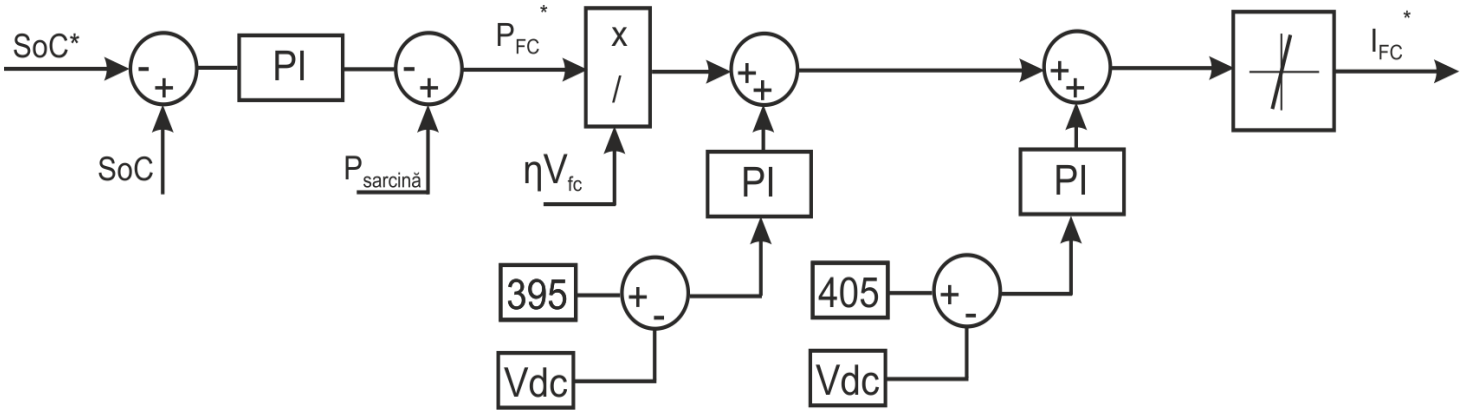

Figure 4.1. b. Diagram of the EMS based on PI regulator

3. Energy management strategies for FC HPS

2.6 Matlab-Simulink diagram of the EMS based on PI regulator

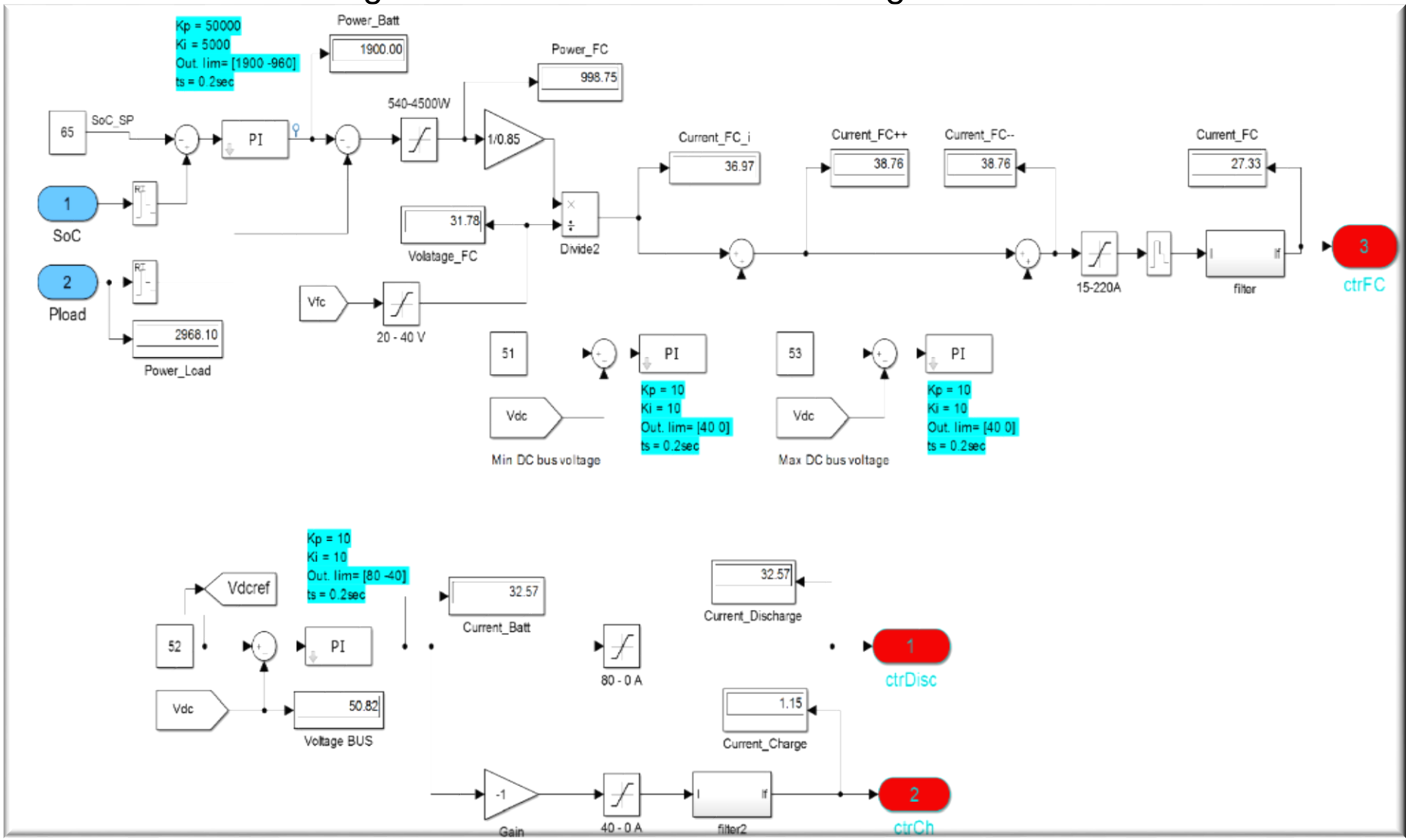

3. Energy management strategies for FC HPS

2.6 Strategies using the control diagram based on the designed operating states

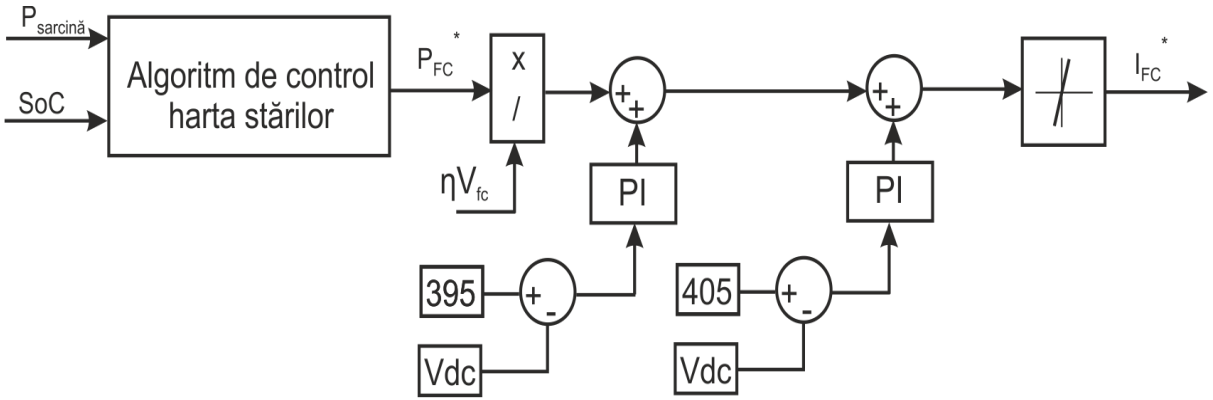

IF $SOC > 90$ & $P_{\mathbf{load}} < Pfc_{min}$	$State = 1$	$Pfc^* = Pfc_{min}$
IF $SOC > 90$ & $P_{\mathbf{load}} \in [Pfc_{min}, Pfc_{max}]$	$State = 2$	$Pfc^* = Pfc_{\mathrm{load}}$
IF $SOC > 90$ & $P_{\mathbf{load}} \geq Pfc_{max}$	$State = 3$	$Pfc^* = Pfc_{max}$
IF $SOC \in [65, 85]$ & $P_{\mathbf{load}} < Pfc_{opt}$	$State = 4$	$Pfc^* = Pfc_{opt}$
IF $SOC \in [65, 85]$ & $P_{\mathbf{load}} \in [Pfc_{opt}, Pfc_{max}]$	$State = 5$	$Pfc^* = Pfc_{\mathrm{load}}$
IF $SOC \in [65, 85]$ & $P_{\mathbf{load}} \geq Pfc_{max}$	$State = 6$	$Pfc^* = Pfc_{max}$
IF $SOC < 60$ & $P_{\mathbf{load}} < Pfc_{max}$	$State = 7$	$Pfc^* = Pfc_{\mathrm{load}} + P_{charge}$
IF $SOC < 60$ & $P_{\mathbf{load}} \geq Pfc_{max}$	$State = 8$	$Pfc^* = Pfc_{max}$

3. Energy management strategies for FC HPS

2.6 Matlab-Simulink diagram of the EMS based states' diagram

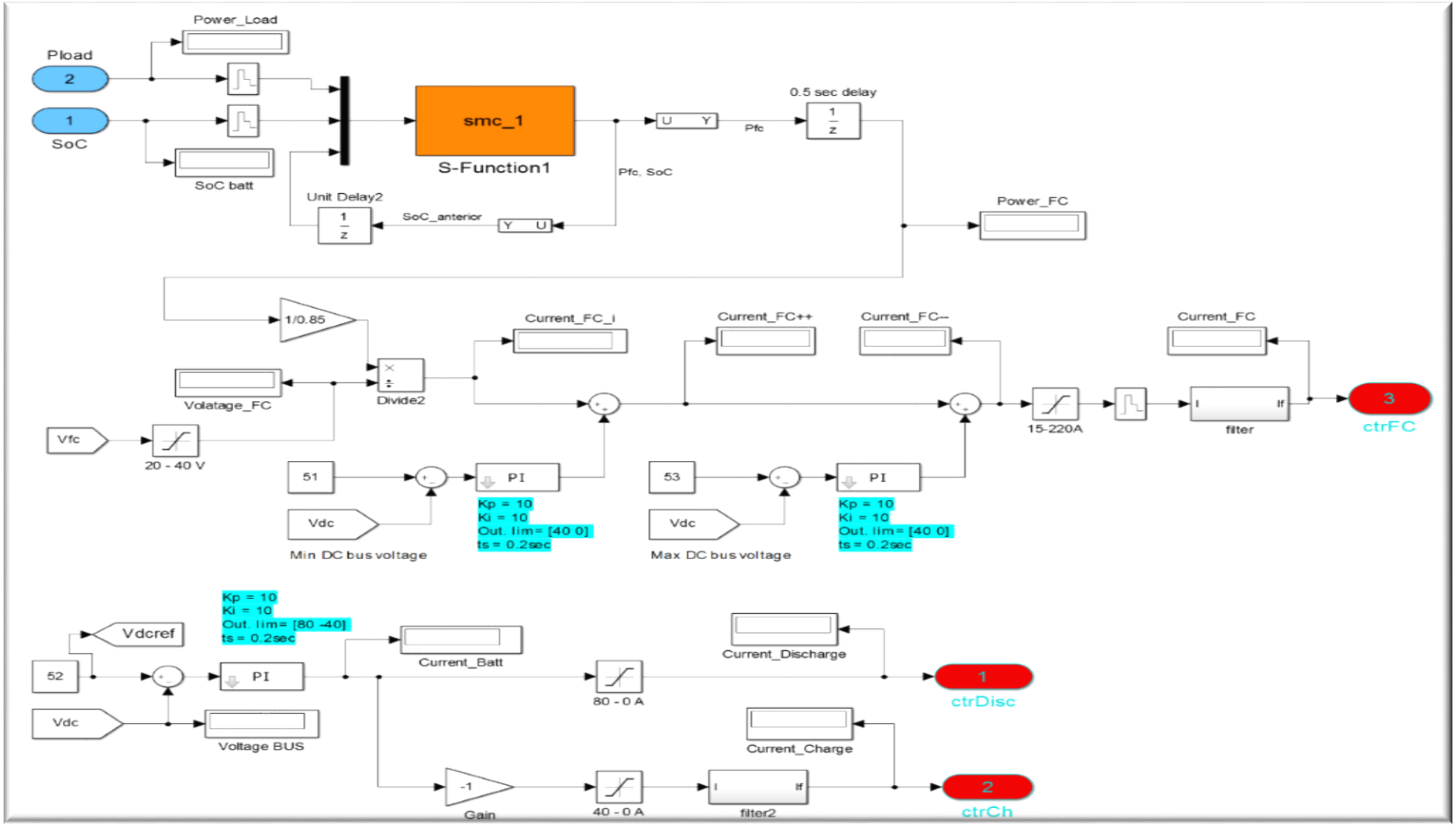

4. Results

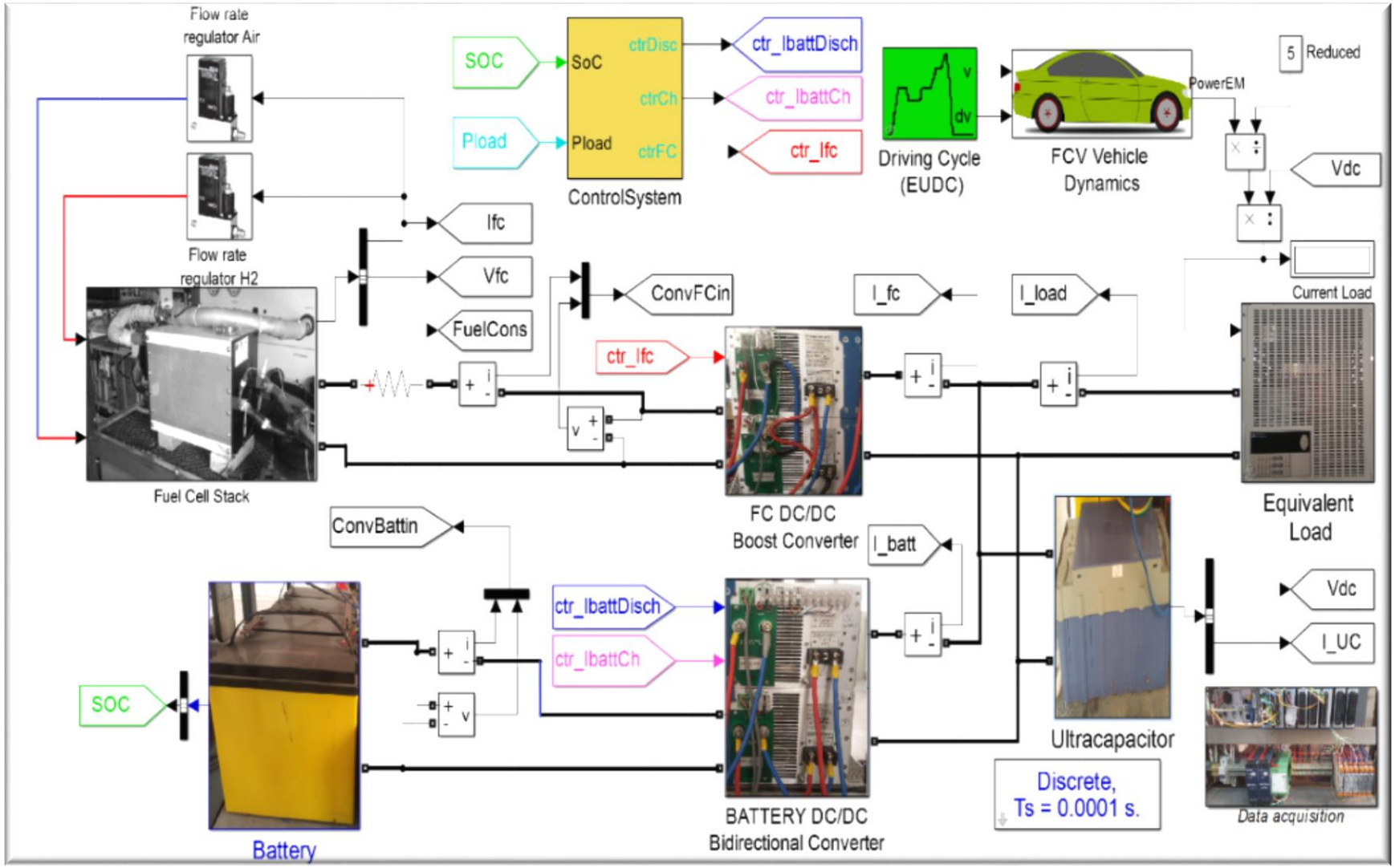

Figure 5.1. Matlab-Simulink diagram of the FCV

4. Results

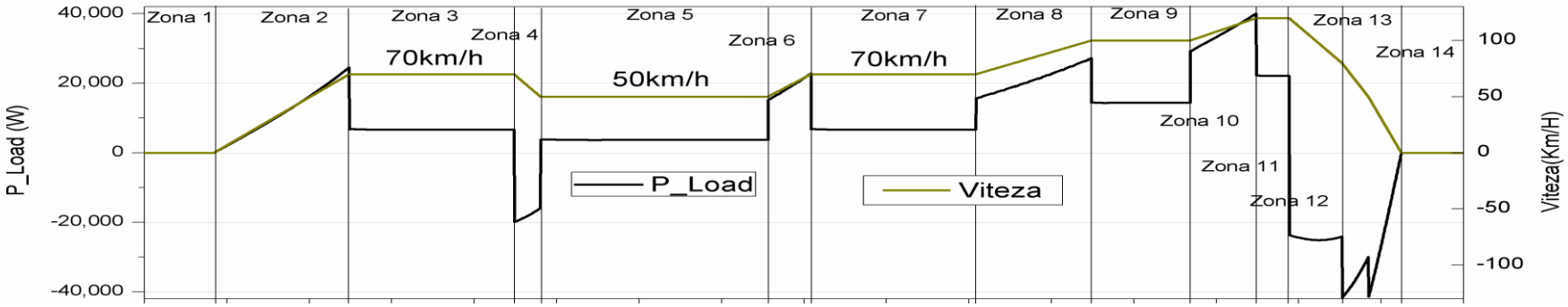

The EUDC driving cycle is divided into 14 areas, which are shown in next Figures.
Zone 1: At first the vehicle is stopped for a period of 20 seconds; in this zone 1 the fuel cell operates at minimum output of 3910W; this power is used to charge the battery system.
Zone 2: the vehicle accelerates slightly to 70 km / h in 41 seconds (simulated vehicle gearbox is automatic). Depending on EMS implemented, the power flows are different.
Zone 3: the vehicle is moving at a speed of 70 km / h for 50 seconds.
Zone 4: the vehicle decelerates to 50 km / h in 8 seconds and then travels at 50 km / h for a period of 69 seconds (zone 5).
Then, the vehicle accelerates slightly to 70 km / h in 13 seconds (zone 6), by moving at a constant speed of 70 km / h for 50 seconds (zone 7).
In zone 8 vehicle reaches 100 km / h in 35 seconds and then keep the cruising speed for 30 seconds (zone 9).
Further, the vehicle accelerates to 120 km / h for 20 seconds (zone 10), followed by a cruising speed of 120 km / h for 10 seconds (zone 11).
Finally, in zones 12 and 13 vehicle brakes in two steps: in step 1, 16 seconds up to 70 km / h and in step 2 the vehicle is stopped in 18 seconds.
In the last zone (zone 14), the vehicle is stopped for 20 seconds.
The total duration of EUDC driving cycle is 400 seconds and distance covered with an average speed of 62.6 km / h is of 6956 meters.

4. Results for EMS based on states' diagram

4.1. Load power & vehicle speed, FC power, battery power, and UC power

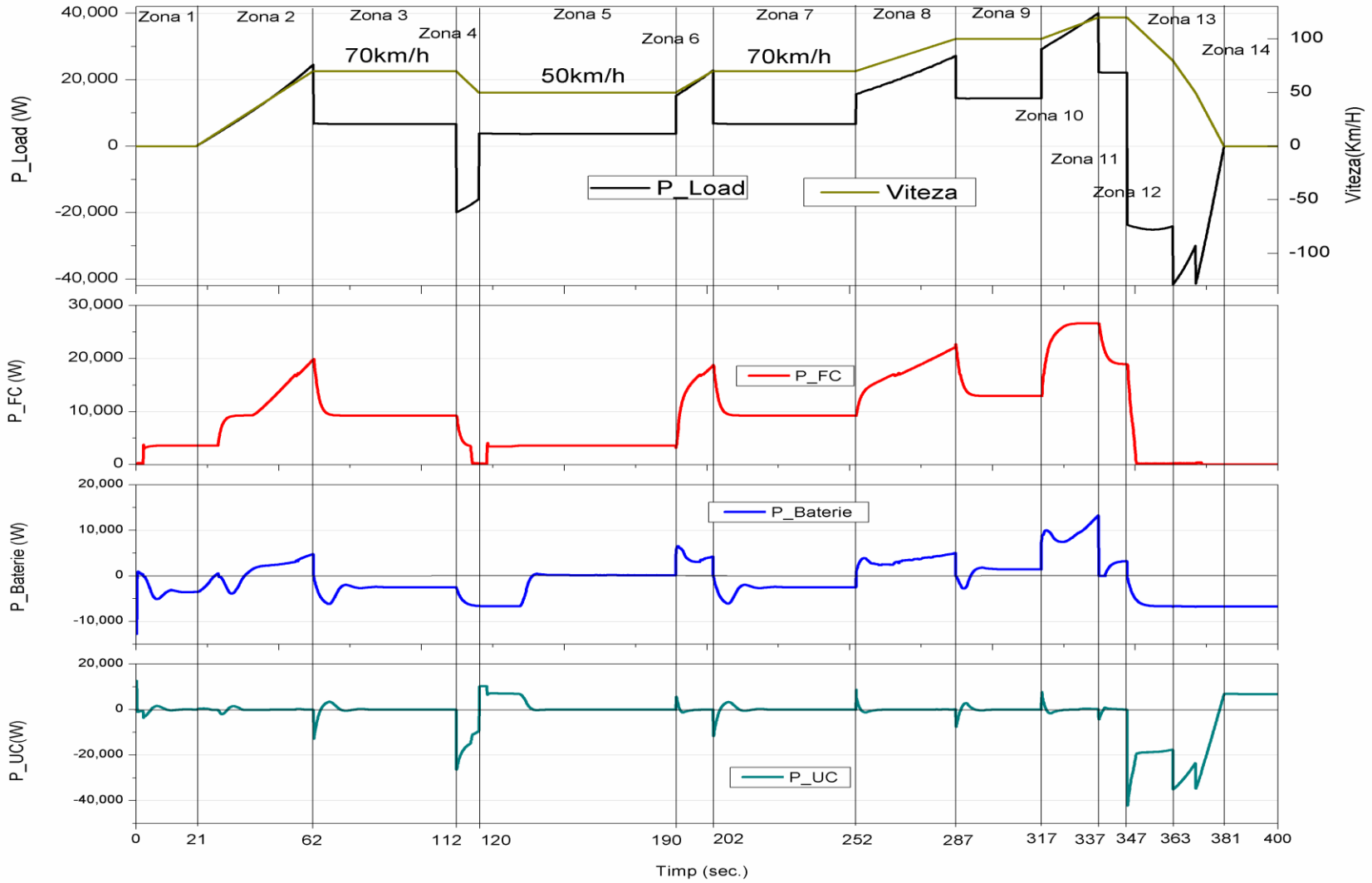

Figure 5.2. Power flows for EMS based on states' diagram

4. Results for EMS based on PI regulators

4.1. Load power & vehicle speed, FC power, battery power, and UC power

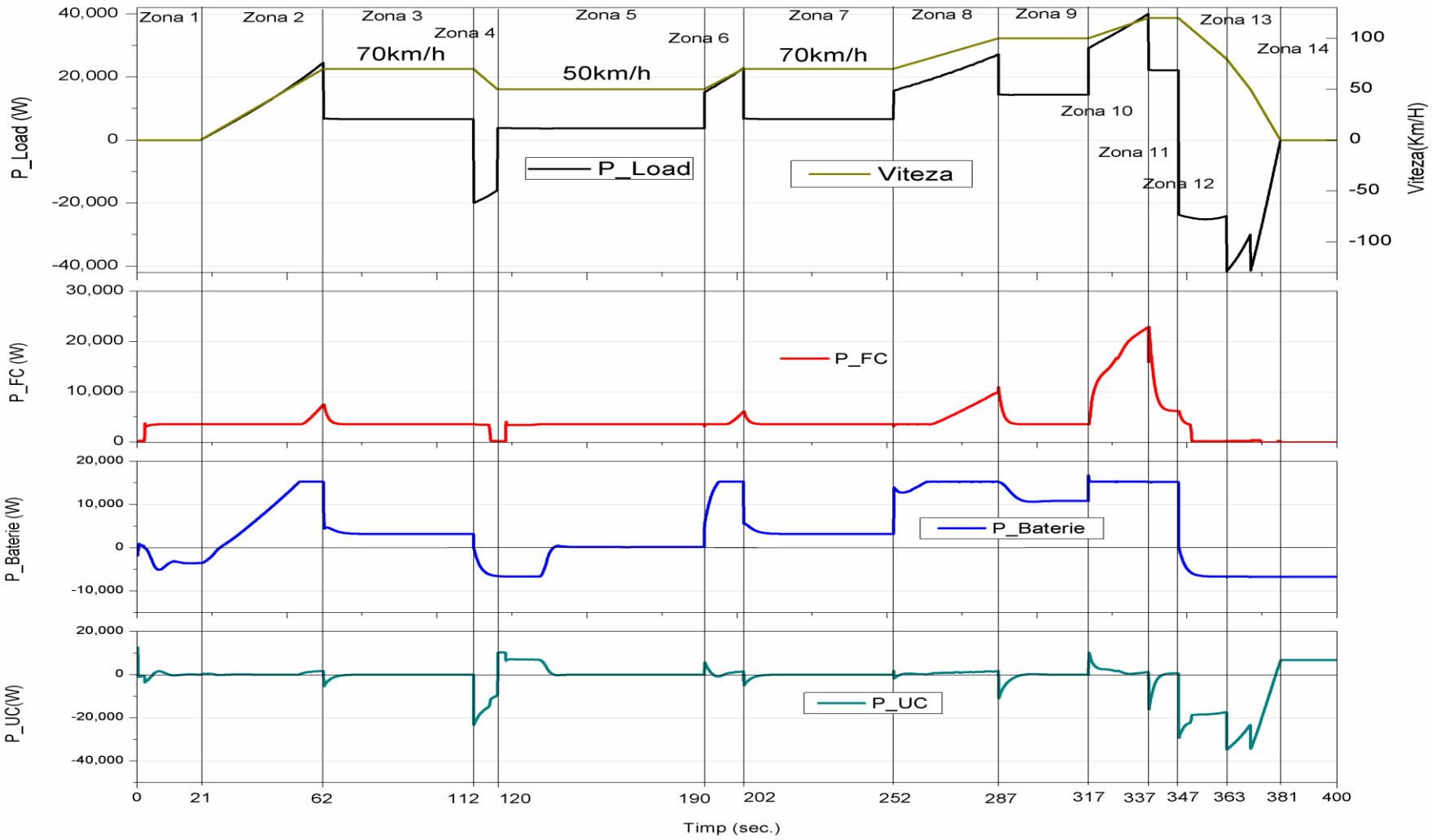

Figure 5.3. Power flows for EMS based on PI regulators

4. Results for EMS based on PI regulators

4.1. H2 consumption, efficiency of H2 consumption, FC/HPS energy efficiency

efficiency of H2 consumption

$$eff_{H2} = \frac{100 * P_{FC}^{out}}{LHV * H2_{cons}}$$

FC energy efficiency

$$eff_{FC} = \frac{100 * P_{FCnet}}{P_{FCout}}$$

HPS energy efficiency

$$eff_{HPS} = \frac{P_{load}}{P_{FC}^{out} + P_{Bat}^{out} + P_{UC}^{out}}$$

H2 consumption

$$H2_{cons} = \frac{N}{F}\int_{0}^{420} i_{FC}dt$$

Figure 5.3. Power flows for EMS based on PI regulators

4. Results

Power, voltage & current, H2 & air flows, H2 consumption, efficiency of H2 consumption & FC energy efficiency

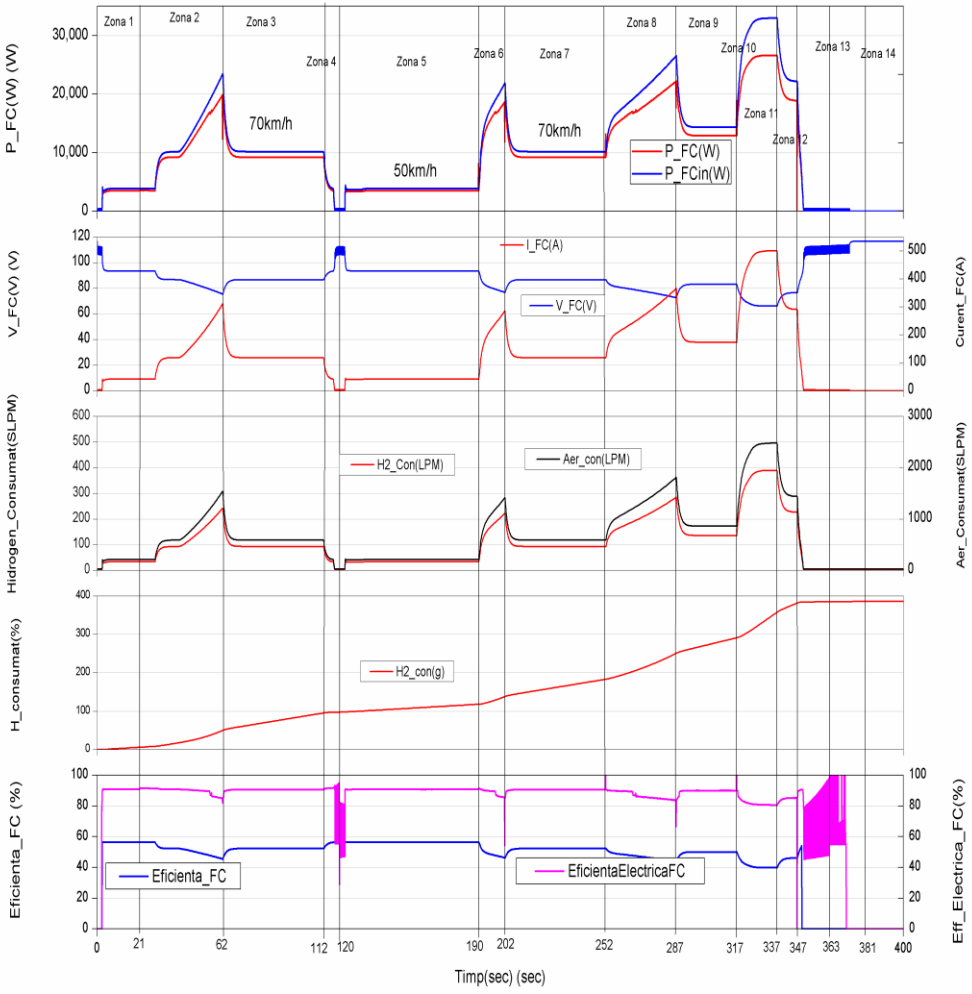

Figure 5.4. EMS based on states' diagram

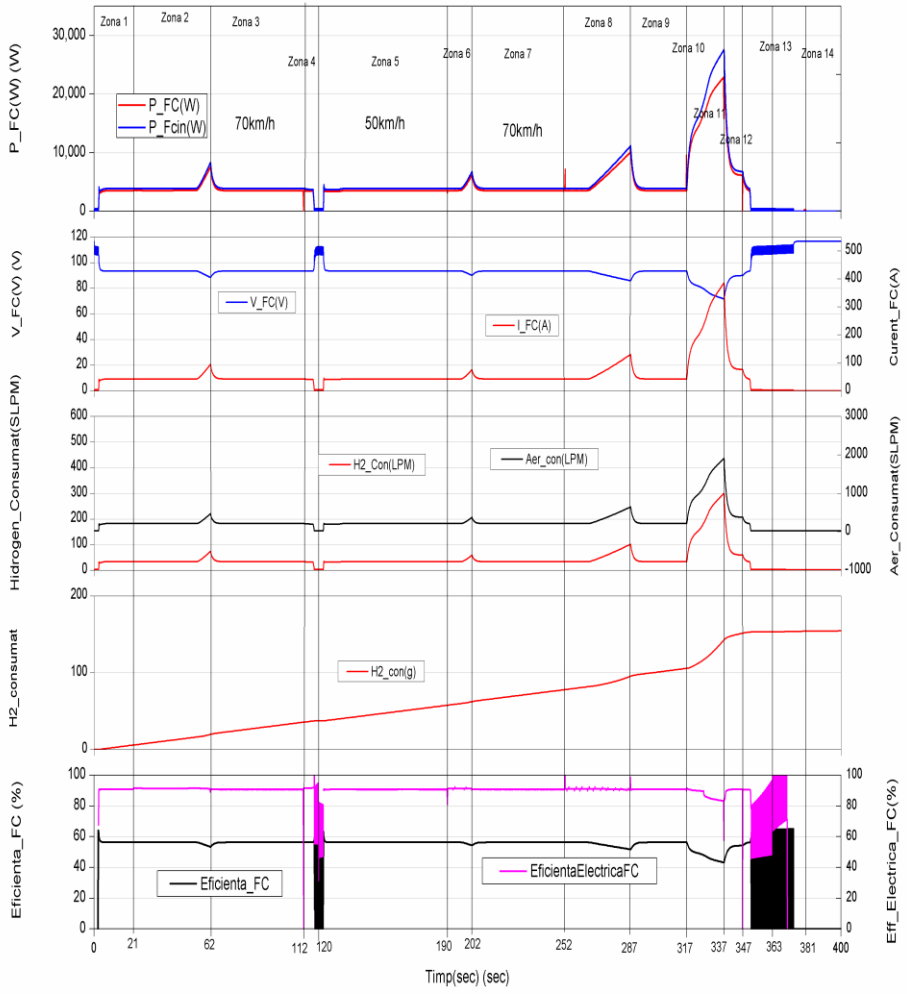

Figure 5.4. EMS based on PI regulators

4. Results

Power, voltage, current and SOC for batteries stack

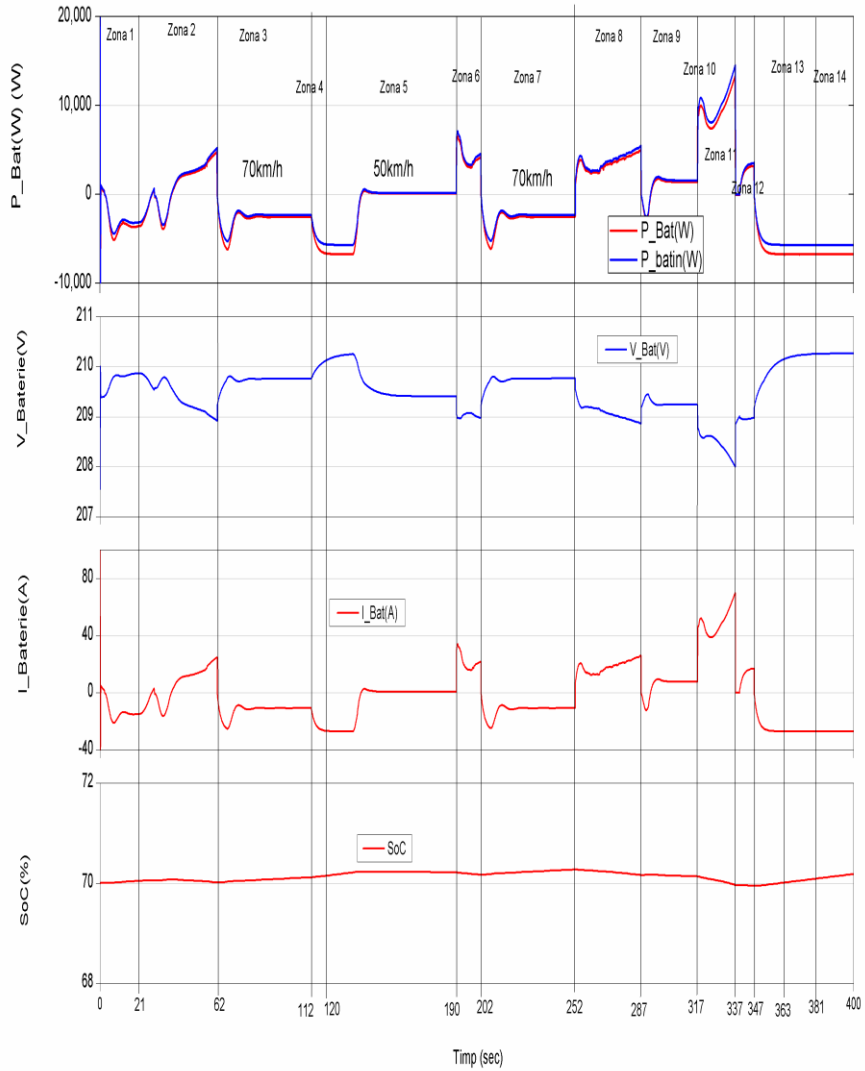

Figure 5.6. EMS based on states' diagram

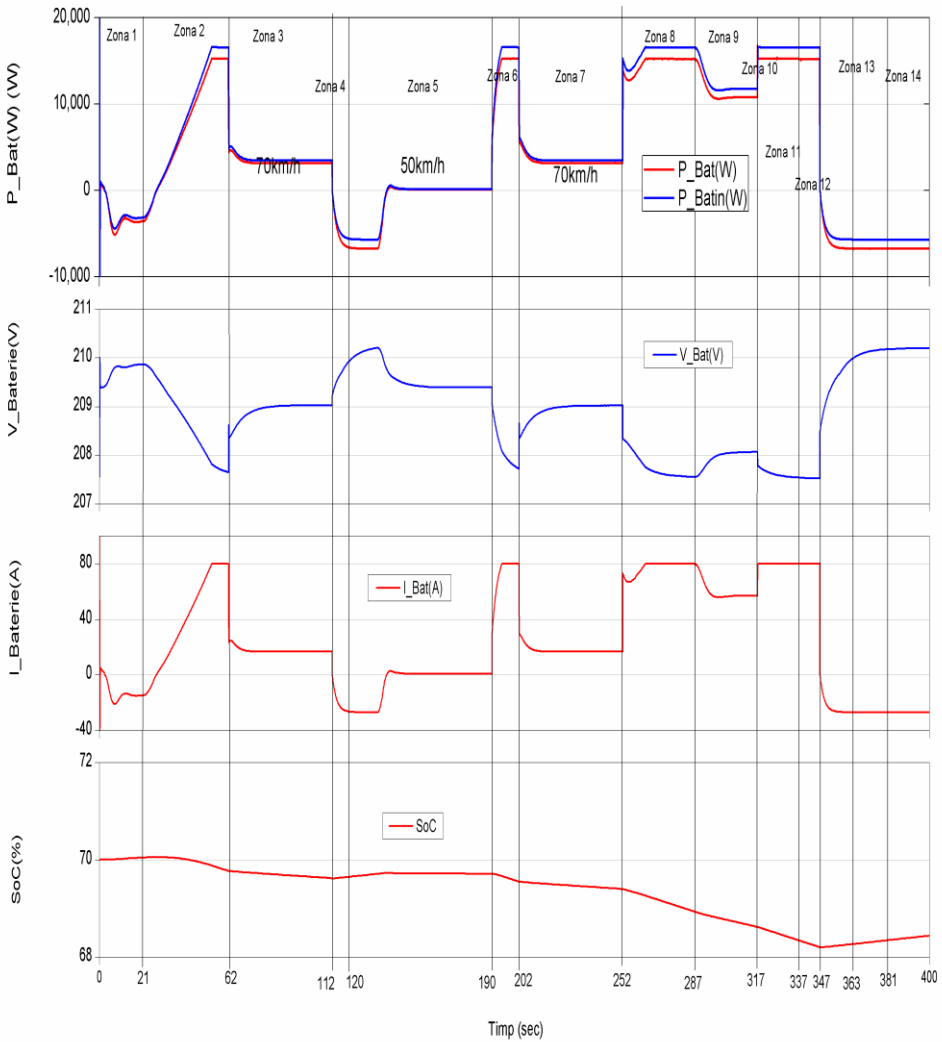

Figure 5.7. EMS based on PI regulators

4. Results

UC power, UC voltage, and UC current

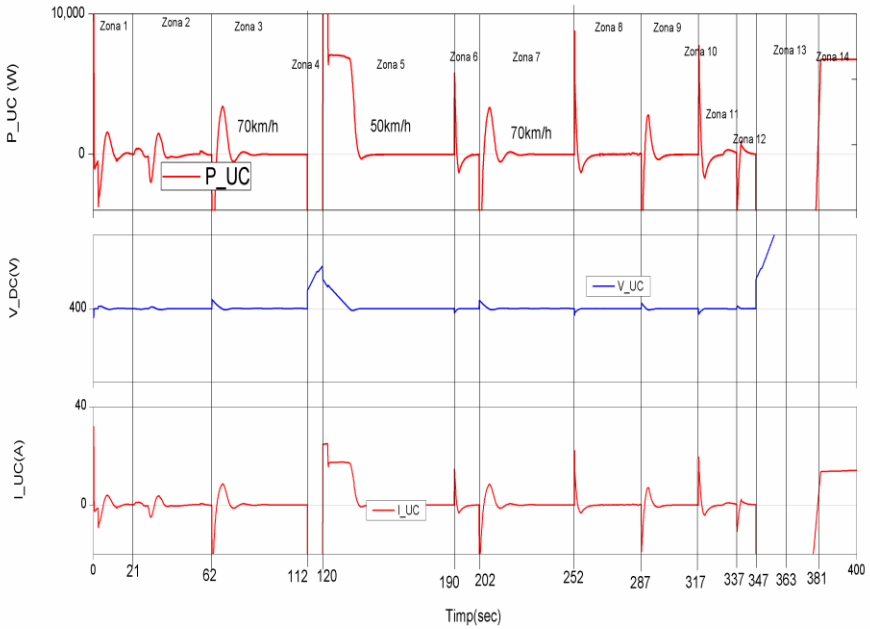

Figure 5.8. EMS based on states' diagram

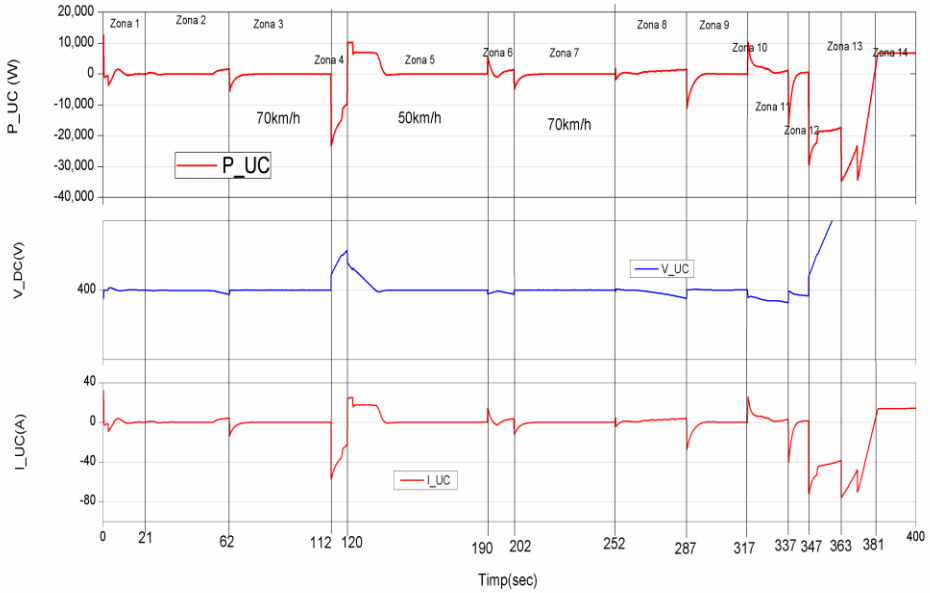

Figure 5.9. EMS based on PI regulators

4. Results

HPS energy efficiency

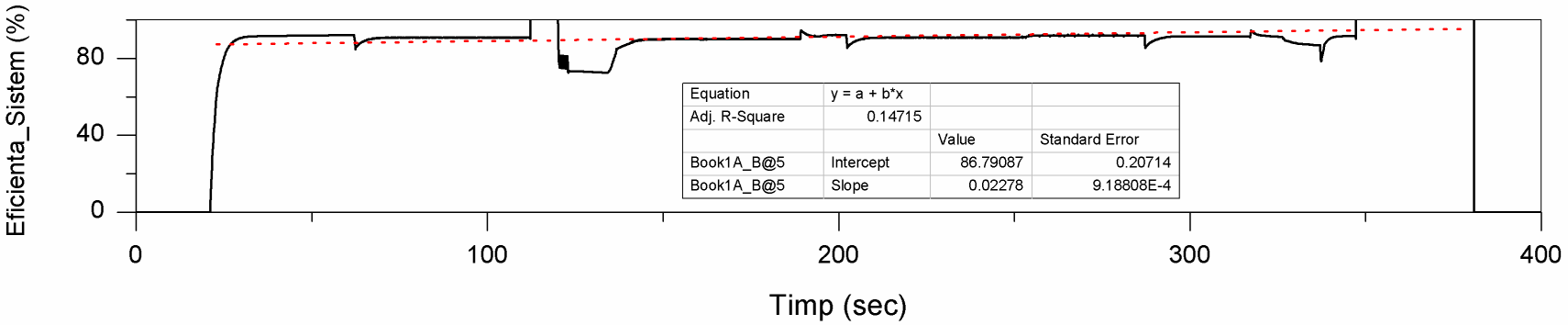

Figure 5.10. EMS based on states' diagram

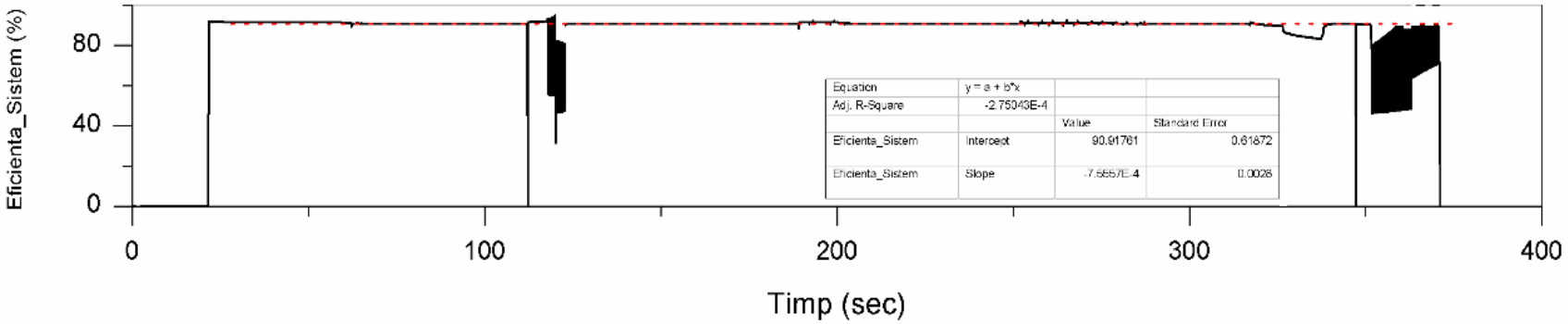

Figure 5.11. EMS based on PI regulators

5. Conclusion

Performance indicator	States' diagram	PI regulators
Battery SoC	70,2%	68,4%
H2 consumption	385 g	155 g
HPS energy efficiency	86,8%	90,9%

Table 5.1. Performance obtained

The EMS based on PI regulators performed better in terms of efficiency, highlighting an overall electrical efficiency with 4% greater in comparison with that obtained with EMS based on states' diagrams, but note that the battery SOC is with 2% lower due to high use (in discharge mode) in the last part of the driving cycle.

The EMS based on PI regulators has achieved but hydrogen consumption noticeably reduced by approx. 40% in comparison with that obtained with EMS based on states' diagrams.

The three criteria adopted for performance comparison of the two control strategies do not allow their hierarchy, because, as has been shown, both strategies shows both advantages and disadvantages during a driving cycle.

4. Possible solutions for advanced EMS

Suwat Sikkabut, Pongsiri Mungporn, Chainarin Ekkaravarodome, Nicu Bizon, et all. Control of High-Energy High-Power Densities Storage Devices by Li-ion Battery and Supercapacitor for Fuel Cell/Photovoltaic Hybrid Power Plant for Autonomous System Applications. IEEE Transactions on Industry Applications 52(5) (2016):4395-4407, WOS:000384659900078

N. Bizon M. Radut, M. Oproescu, Energy control strategies for the Fuel Cell Hybrid Power Source under unknown load profile, Energy 86 (15 June 2015) 31-41 http://dx.doi.org/10.1016/j.energy.2015.03.118 WOS:000356986300004

N. Bizon, M. Oproescu, M. Raceanu, Efficient Energy Control Strategies for a Standalone Renewable/Fuel Cell Hybrid Power Source, Energy Conversion Management 77 (15 January 2015), 768-772. doi:10.1016/j.enconman.2014.11.002 WOS:000348886800010

N. Bizon, Improving the PEMFC energy efficiency by optimizing the fuelling rates based on extremum seeking algorithm, International Journal of Hydrogen Energy 39(20) (3 July 2014), 10641–10654. http://dx.doi.org/10.1016/j.ijhydene.2014.04.194 WOS:000338388200032

N. Bizon, Tracking the maximum efficiency point for the FC system based on extremum seeking scheme to control the air flow, Applied Energy 129 (15 September 2014) 147–157. http://dx.doi.org/10.1016/j.apenergy.2014.05.002 WOS:000339775400016

N. Bizon, Load-following Mode Control of a Standalone Renewable/Fuel Cell Hybrid Power Source, Energy Conversion Management 77 (January 2014) 763–772. http://dx.doi.org/10.1016/j.enconman.2013.10.035 WOS:000330494600080

N. Bizon, Energy harvesting from the PV Hybrid Power Source, Energy 52 (1 April 2013): 297–307. http://dx.doi.org/10.1016/j.energy.2013.02.006 WOS:000317941000031

N. Bizon, Energy harvesting from the FC stack that operates using the MPP tracking based on modified extremum seeking control, Applied Energy 104 (1 April 2013) 326-336. http://dx.doi.org/10.1016/j.apenergy.2012.11.011 WOS:000316152700033

N. Bizon, FC energy harvesting using the MPP tracking based on advanced extremum seeking control, International Journal of Hydrogen Energy 38(4) (12 February 2013),1952-1966. http://dx.doi.org/10.1016/j.ijhydene.2012.10.112 WOS:000314860600023

4. Possible solutions for advanced EMS

N. Bizon, N. M. Tabatabaei, Frede Blaabjerg, and Erol Kurt (Ed.), Energy Harvesting and Energy Efficiency: Technology, Methods and Applications, Springer Verlag London Limited, 2016; eBook ISBN: 978-3-319-49875-1; DOI 10.1007/978-3-319-49875-1; Hardcover ISBN 978-3-319-49874-4; Series ISSN 2195-1284
http://www.springer.com/us/book/9783319498744
N. M. Tabatabaei, N. Bizon, A. J. Aghbolaghi, and Frede Blaabjerg (Ed.), Fundamentals and Contemporary Issues of Reactive Power Control in AC Power Systems, Springer Verlag London Limited, 2016; eBook ISBN: 978-3-319-51118-4, Hardcover ISBN: 978-3-319-51117-7; Series ISSN: 1612-1287
http://www.springer.com/us/book/9783319511177#otherversion=9783319511184
N. Bizon, L. Dascalescu, and N. M. Tabatabaei (Ed.), Autonomous Vehicles: Intelligent Transport Systems and Smart Technologies, Nova Science Publishers Inc., USA, 2014, ISBN: 978-1-63321-324-1
https://www.novapublishers.com/catalog/product_info.php?products_id=50365&osCsid=756a848447737596b96d62aa86a64cba
N. Bizon, N. M. Tabatabaei and Hossein Shayeghi (Ed.), Analysis, Control and Optimal Operations in Hybrid Power Systems - Advanced Techniques and Applications for Linear and Nonlinear Systems, Springer Verlag London Limited, London, UK, 2013. 978-1-4471-5538-6, 978-1-4471-5537-9 ;
http://dx.doi.org/10.1007/978-1-4471-5538-6
http://www.springer.com/engineering/control/book/978-1-4471-5537-9
N. Bizon and N. M. Tabatabaei (Ed.), Advances in Energy Research: Energy and Power Engineering, Nova Science Publishers Inc., USA, 2013 978-1-62257-534-3 (hardcover), 978-1-62257-546-6 (ebook).
https://www.novapublishers.com/catalog/product_info.php?products_id=36315&osCsid=cce0dd5ced12df6ba9340d8c9d71142b
N. Bizon (Ed.), Advances in Energy Research: Distributed Generation systems integrating Renewable Energy Resources, 3 chapters by N. Bizon, Nova Science Publishers Inc., USA, 2012, 978-1-61209-991-0 (hardcover), 978-1-61209-991-2 (ebook).
https://www.novapublishers.com/catalog/product_info.php?products_id=22516

5. Future trends of energy management strategy for FCVs

The latest reviews in field of FCVs' energy management strategy reveals that there are still some issues to be solved and others that must to be improved.

Firstly, the performances of all EMSs are dependent by driving cycle. Therefore, the intelligent-based EMS that will include a driving cycle recognition or driving cycle prediction could be a viable solution to improve the FCV performance. Anyway, these recognition or prediction technologies will increase computation time and the intelligent-based EMSs will be difficult to be implemented as the real-time algorithms. So, the EMS based on load-following technique could be an feasible alternative, being independent by driving cycle.

Secondly, multi-objective EMSs, which integrate into a optimization function the fuel economy, the FC energy efficiency, the safety of FCV, and comfort (drivability), are challenges for high-performance FCVs. Most of proposed EMSs only consider fuel economy of HEV, the FC energy efficiency or both, and few EMSs take into account the last two performance as penalty term in the optimization function.

Thirdly, the compromise between system complexity, level of computation needed and optimization performance of EMSs continue to be an open issue.

Finally, every eEMS has its own advantages and disadvantages. Thus, a standard to make a accurate and convincing evaluation of EMS will be helpful to design a suitable EMS for FCV with specific performance objectives.

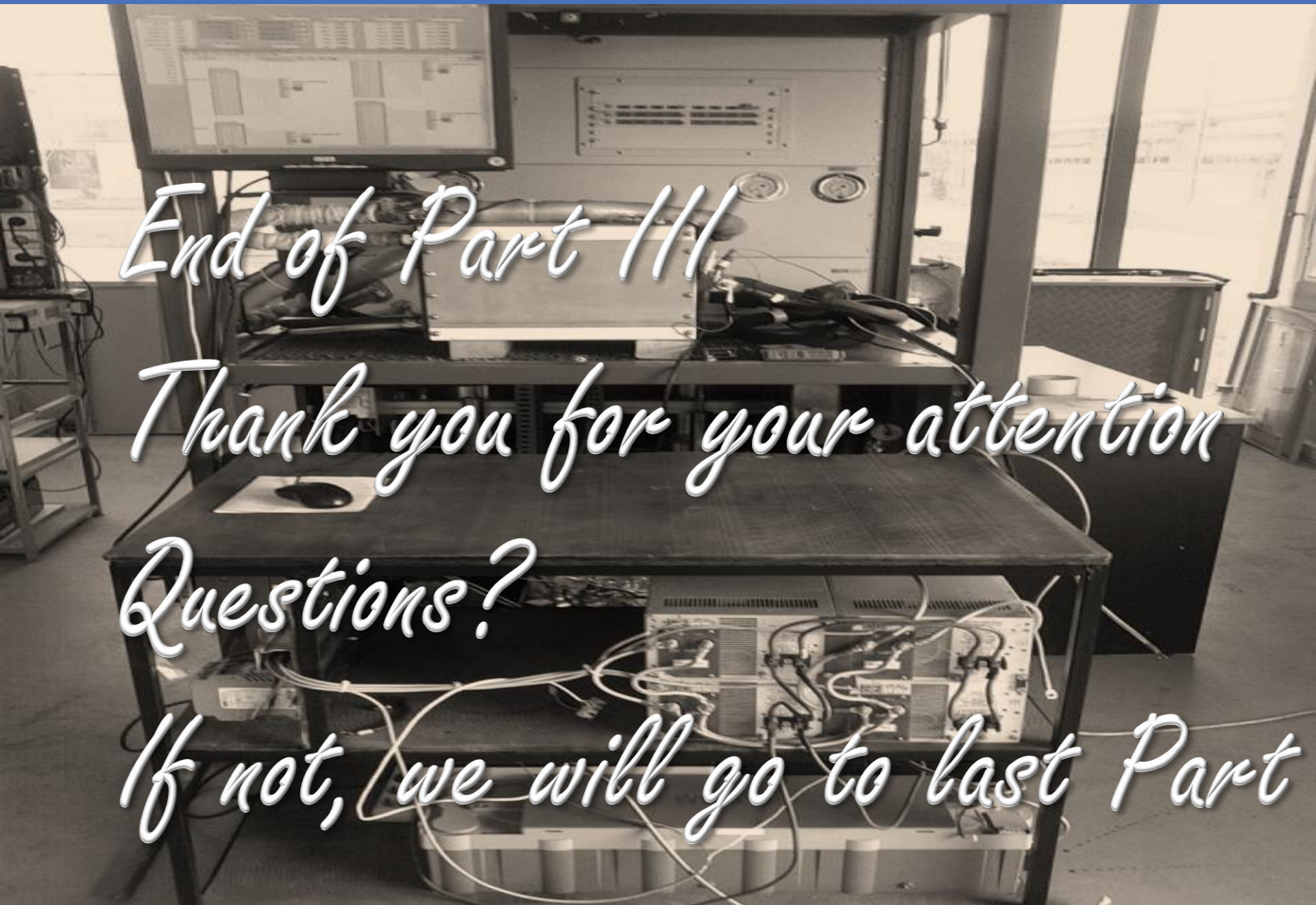
End of Part III
Thank you for your attention
Questions?
If not, we will go to last Part

Erasmus+ PROGRAMME,

KEY ACTION: Cooperation for innovation and the exchange of good practices,

ACTION: Strategic Partnerships

FIELD: Strategic Partnerships for higher education, CALL: 2015

INNOVATIVE EUROPEAN STUDIES ON RENEWABLE ENERGY SYSTEMS

2015-1-TR01-KA203-021342

Real-time optimization of the Renewable Energy Sources / Fuel Cell Hybrid Power Systems

Nicu BIZON
University of Pitesti, Pitesti, Romania

Summary of Part 4 – Advanced EMS for FC / Renewable HPS

1. Load-following Mode Control of a Standalone Renewable/Fuel Cell Hybrid Power Source (FC RES HPS)
2. Improving the PEMFC energy efficiency by optimizing the fuelling rates based on extremum seeking algorithm
3. Efficient Energy Control Strategies for a Standalone Renewable/Fuel Cell Hybrid Power Source
4. Global Maximum Power Point Tracking algorithms for Photovoltaic arrays under Partially Shaded Conditions
5. Conclusions

1. Load-following Mode Control of a FC RES HPS

1.1. Architecture of the FC RES HPS

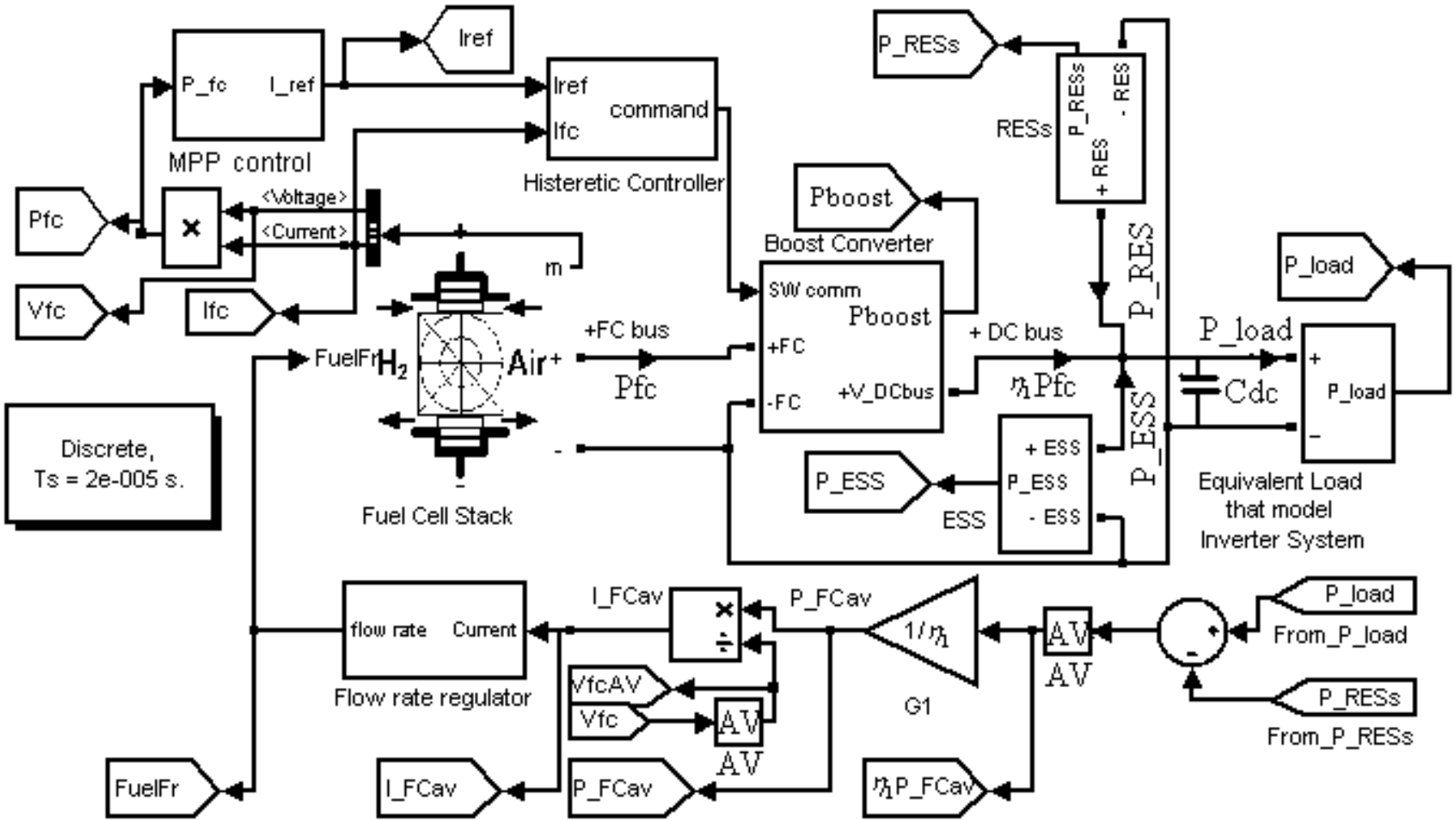

Figure 1. Diagram of FC RES HPS architecture

1. Load-following Mode Control of a FC RES HPS

1.2. Features of the load-following strategy

The load-following strategy has the following features:

- assures the grid active power based on power balancing strategy for the backup power source, which is the FC system;
- optimizes the energy efficiency of the FC system and each RES based on energy harvesting technique of MPP tracking type;
- compensates the energy gap between the load demand and the output power from the RESs and FC based on minimal batteries stack;
- mitigates the impact of HF perturbation on the load power due to the fluctuations of the electric utility grid and RES power based on controlled power flow exchanged with the ultracapacitors stack.

Figure 1. Diagram of FC RES HPS architecture

1. Load-following Mode Control of a FC RES HPS

1.3. FC Maximum Power Point (MPP) tracking control

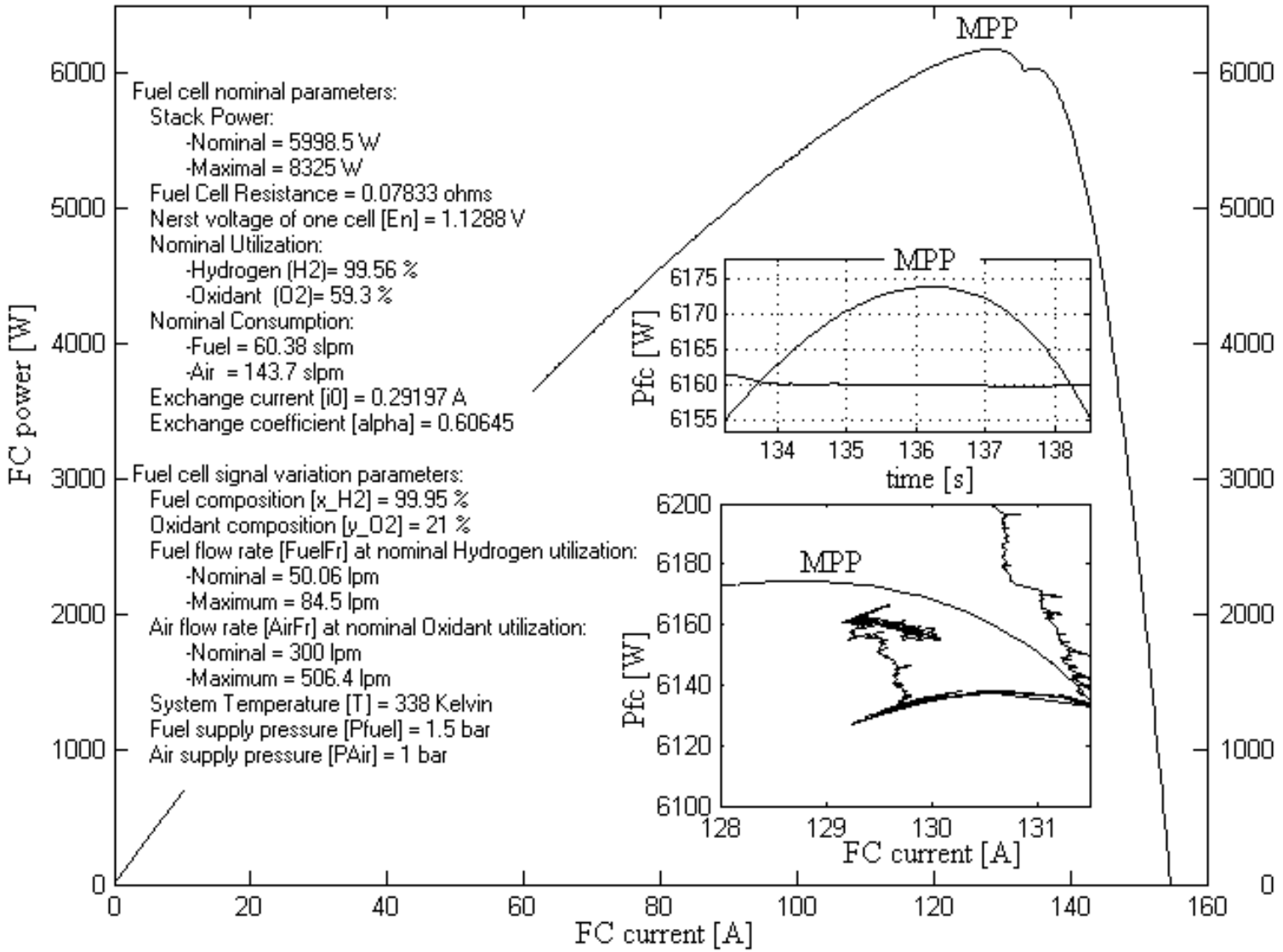

Figure 2. The FC parameters, P-I characteristic, and MPP tracking (zooms)

1. Load-following Mode Control of a FC RES HPS

1.4. Tracking Accuracy

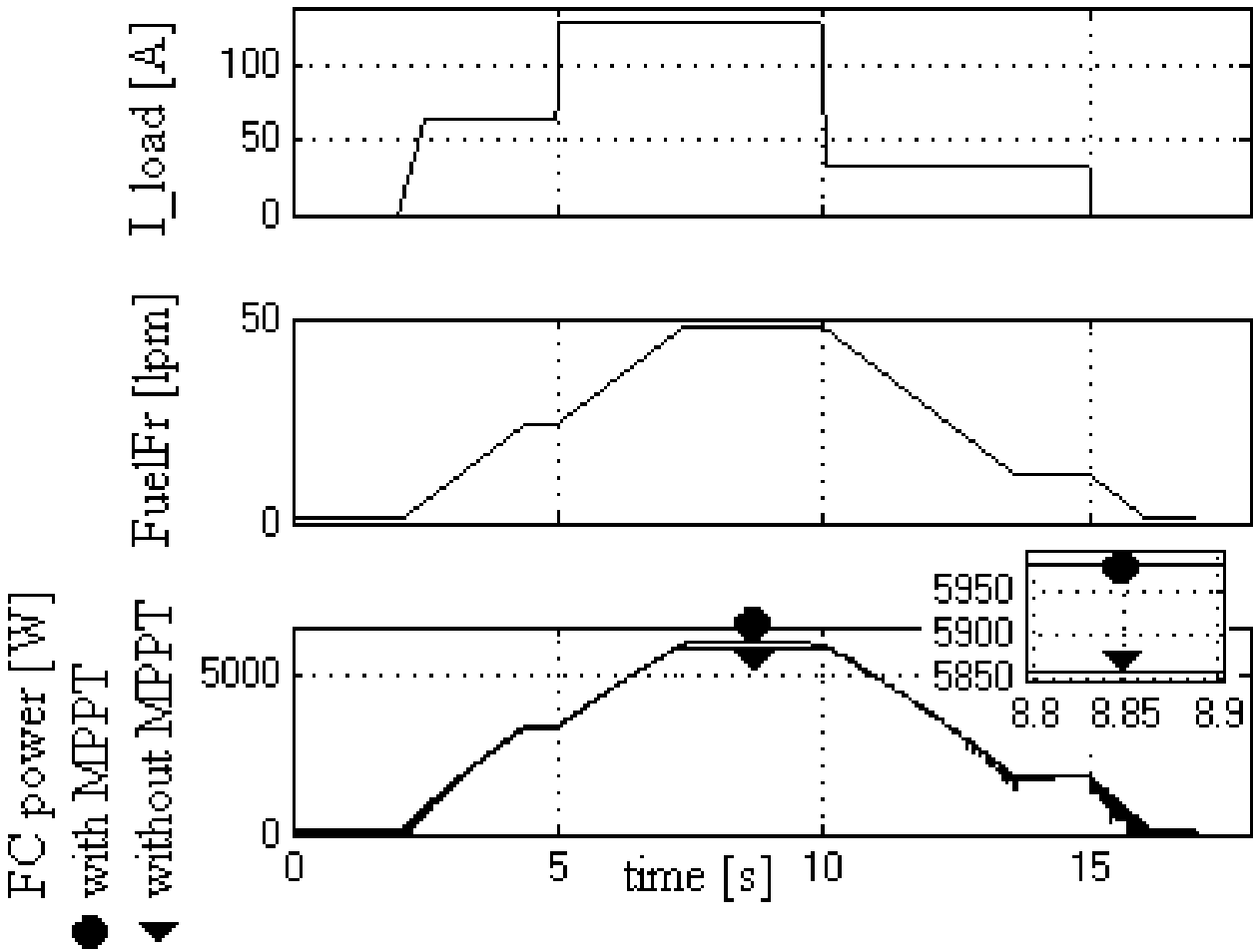

POWER FLOW BALANCE

$$p_{dc}=dE_{dc}/dt=C_{dc}u_{dc}du_{dc}/dt= p_{RES}+p_{ESS}+\eta_1 p_{FC}-p_L$$

Figure 3. The load power profile to evaluate the FC energy harvested

1. Load-following Mode Control of a FC RES HPS

1.5. Results

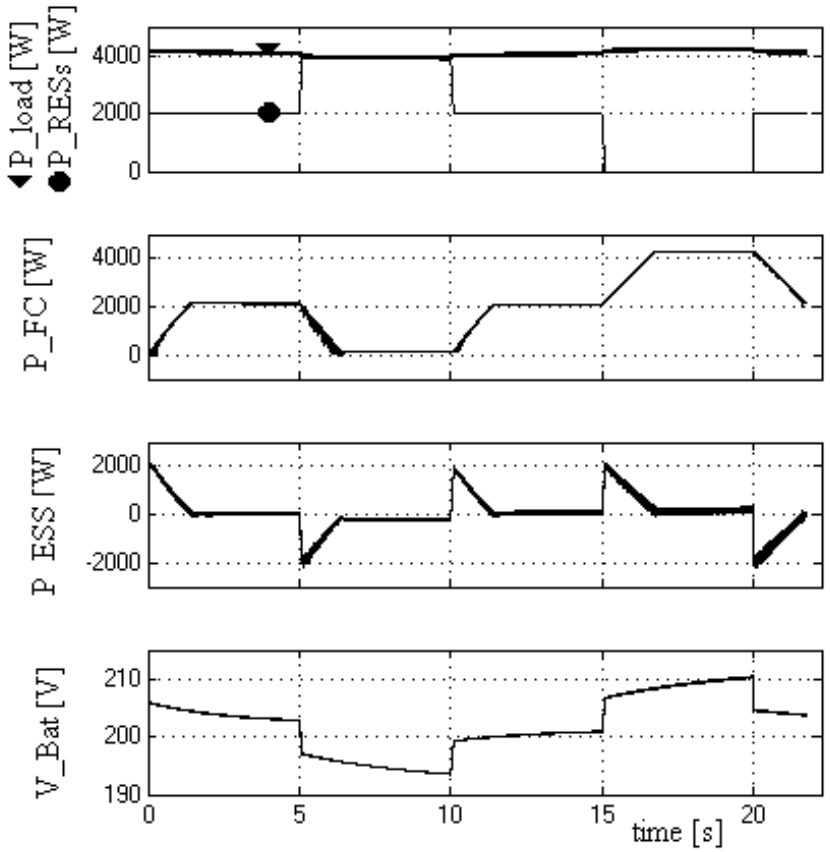

under constant load

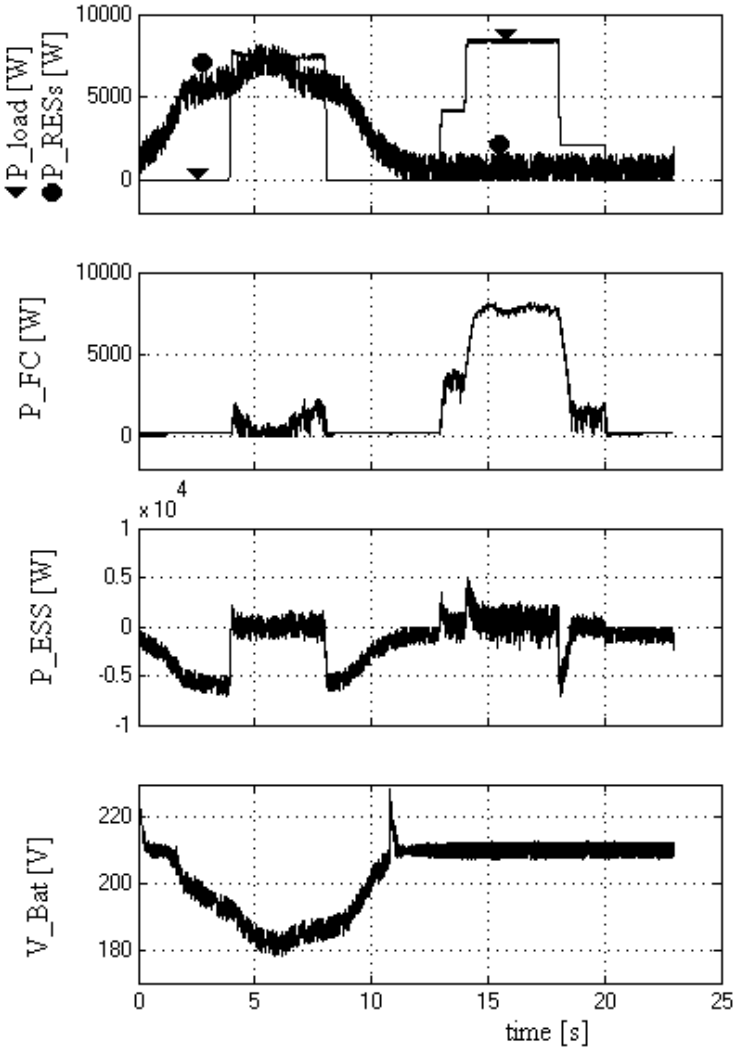

under variable load

Figure 4. The simulation results for the FC/RES/ESS HPS

2. Improving the PEMFC energy efficiency

2.1. PEMFC system

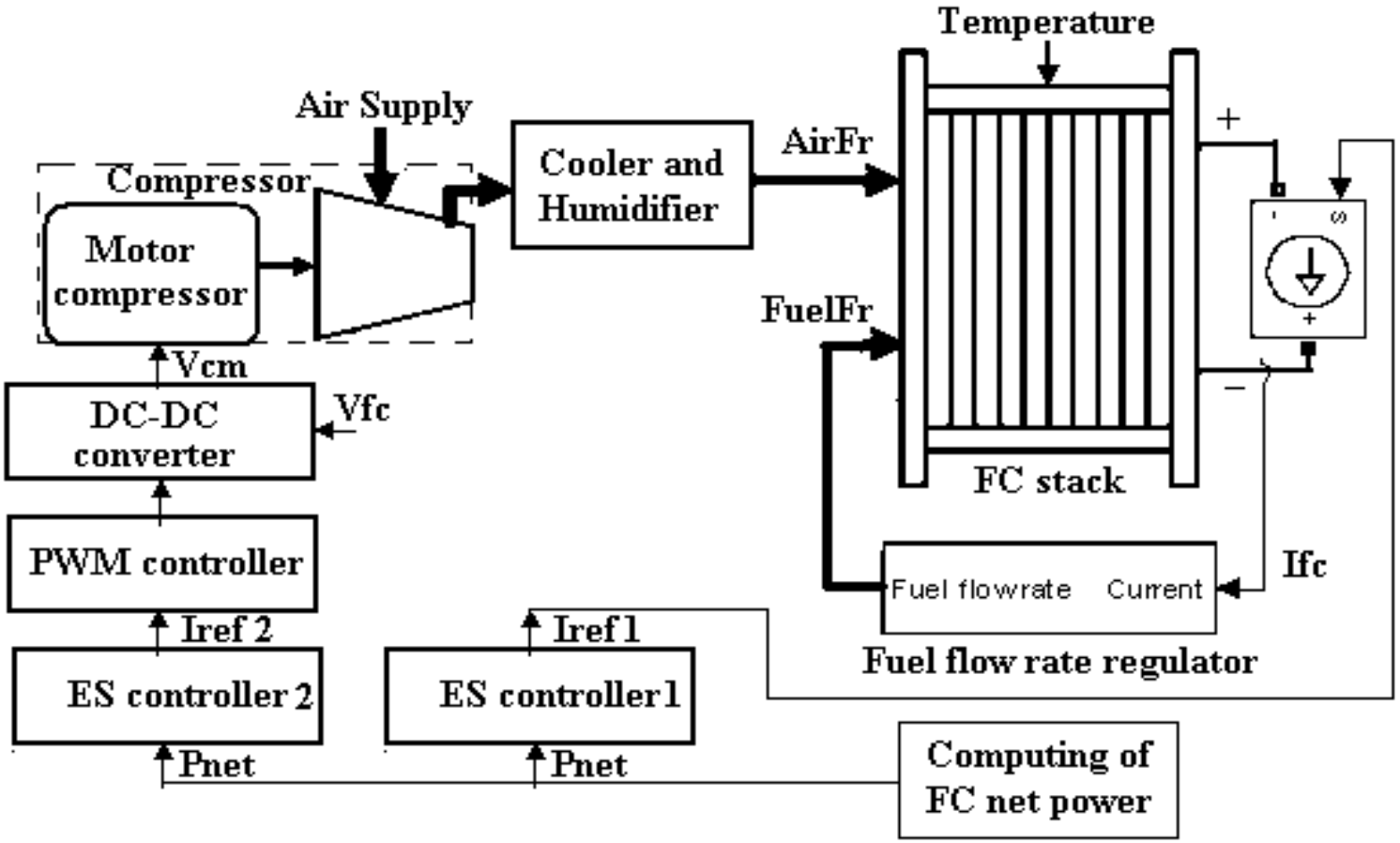

Figure 5. The Proton Exchange Membrane Fuel Cell (PEMFC) system

2. Improving the PEMFC energy efficiency

2.1. PEMFC system

$$P_{net} = V_{FC} \cdot I_{net} \qquad P_{net} = P_{FC} - P_{aux}$$

$$P_{cm} = (a_2 \cdot AirFr^2 + a_1 \cdot AirF + a_0) \cdot (b_1 \cdot I_{FC} + b_0) \cdot k_{cm}$$

$$G_{d(cm)} = \frac{\omega_{cm}^2}{s^2 + 2\xi_{cm}\omega_{cm} \cdot s + \omega_{cm}^2}$$

$$\eta_{sys} = P_{net} / P_{FC}$$

$$p_{O2} = \frac{1/k_{O2}}{1 + t_{O2} \cdot s}(AirFr \cdot y_{O2} - \frac{N_c}{4FU_{O2}} I_{FC}), t_{O2} = \frac{V_{catode}}{R \cdot (273 + \theta) \cdot k_{O2}}$$

$$p_{H2} = \frac{1/k_{H2}}{1 + t_{H2} \cdot s}(FuelFr \cdot y_{H2} - 2\frac{N_c}{4FU_{H2}} I_{FC}), t_{H2} = \frac{V_{anode}}{R \cdot (273 + \theta) \cdot k_{H2}}$$

$$AirFr = \frac{60000 \cdot R \cdot (273 + \theta) \cdot N_C \cdot i_{FC}}{4F \cdot (101325 \cdot P_{f(O2)}) \cdot (U_{f(O2)} / 100) \cdot (y_{O2} / 100)}$$

$$FuelFr = \frac{60000 \cdot R \cdot (273 + \theta) \cdot N_C \cdot i_{FC}}{2F \cdot (101325 \cdot P_{f(H2)}) \cdot (U_{f(H2)} / 100) \cdot (x_{H2} / 100)}$$

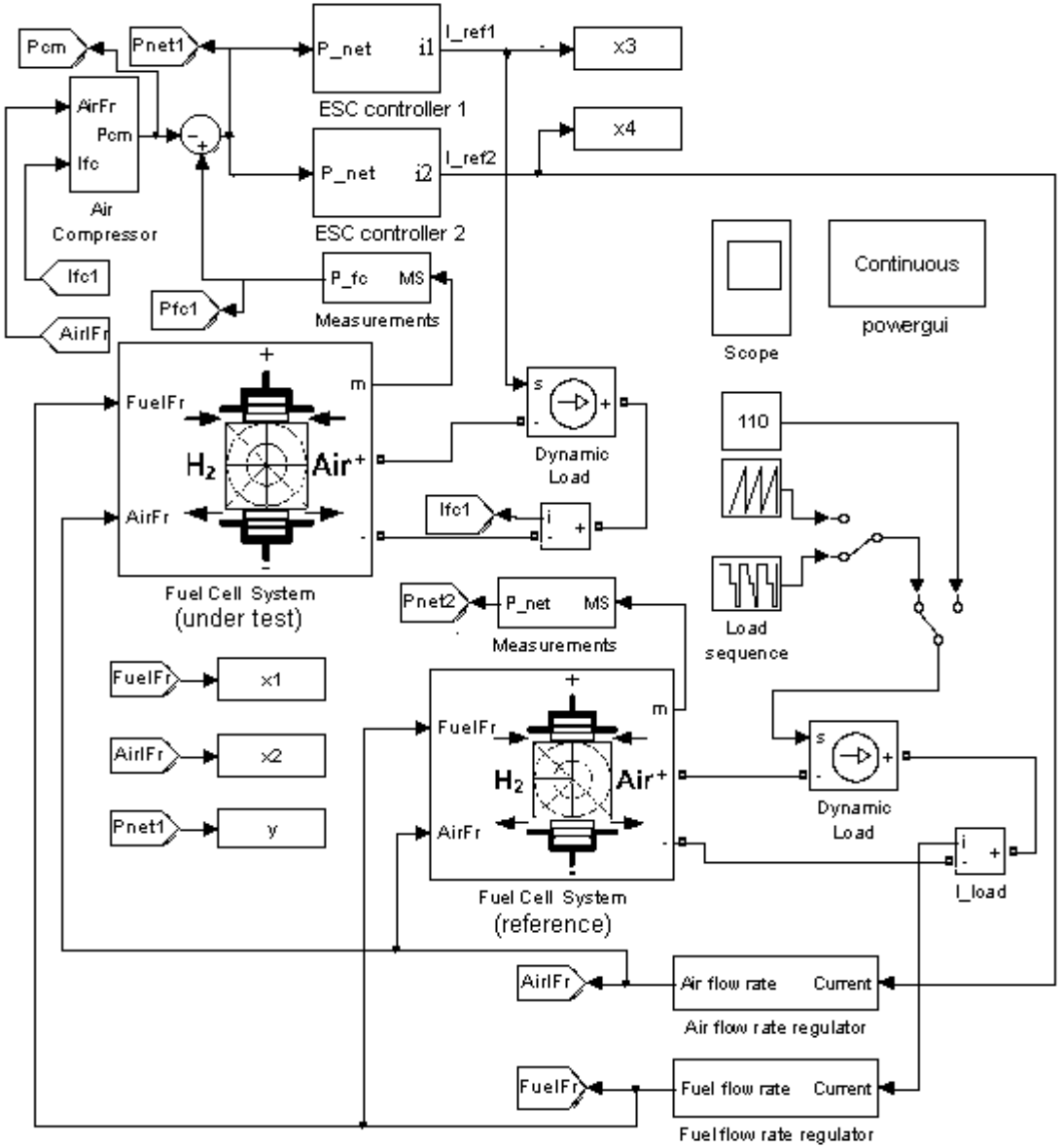

Figure 6. The simulation diagram

2. Improving the PEMFC energy efficiency

2.1. PEMFC characteristics

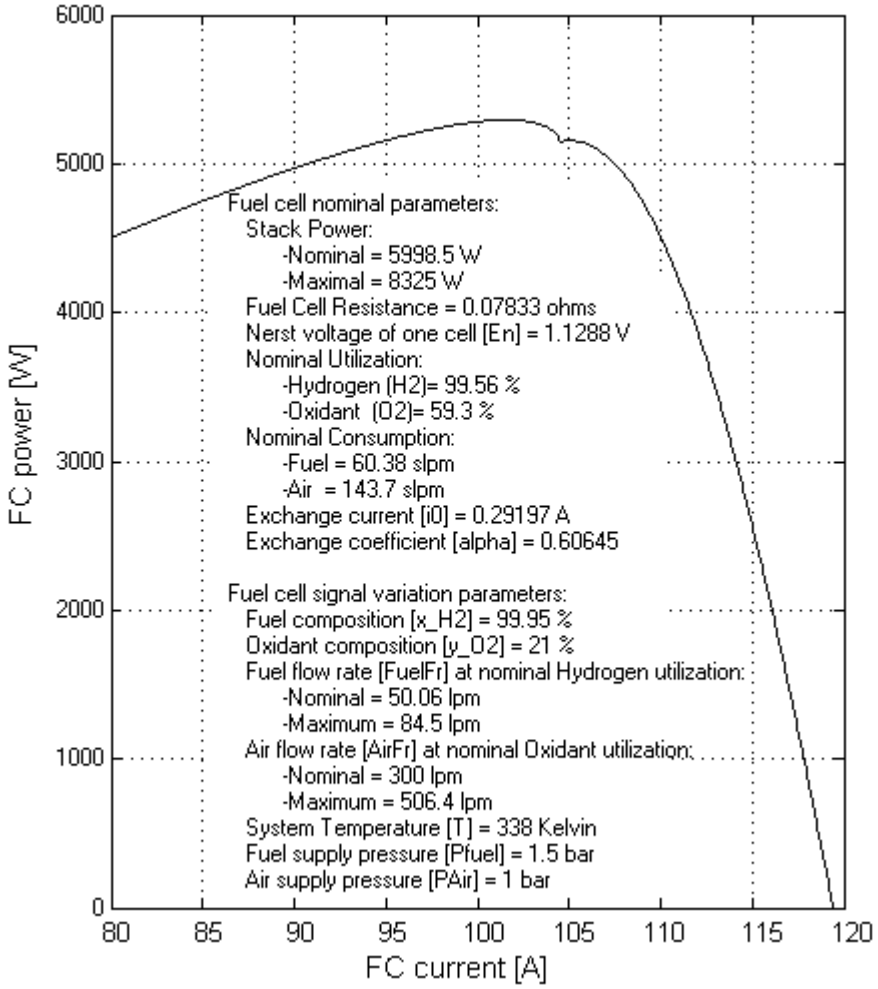

Figure 7. The FC parameters and the P-I characteristic for FuelFr and AirFr of 40.69 lpm and 245.3 lpm

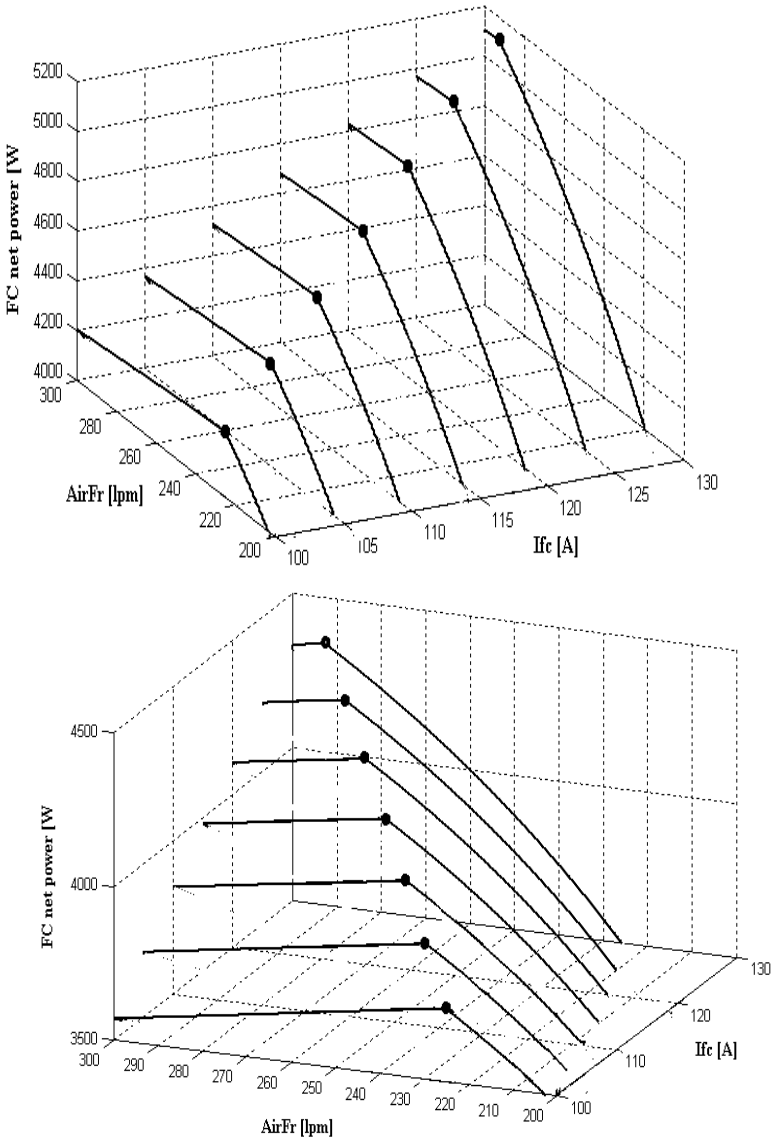

Figure 8. The FC net power surface for two compressors types

2. Improving the PEMFC energy efficiency

2.1. PEMFC characteristics

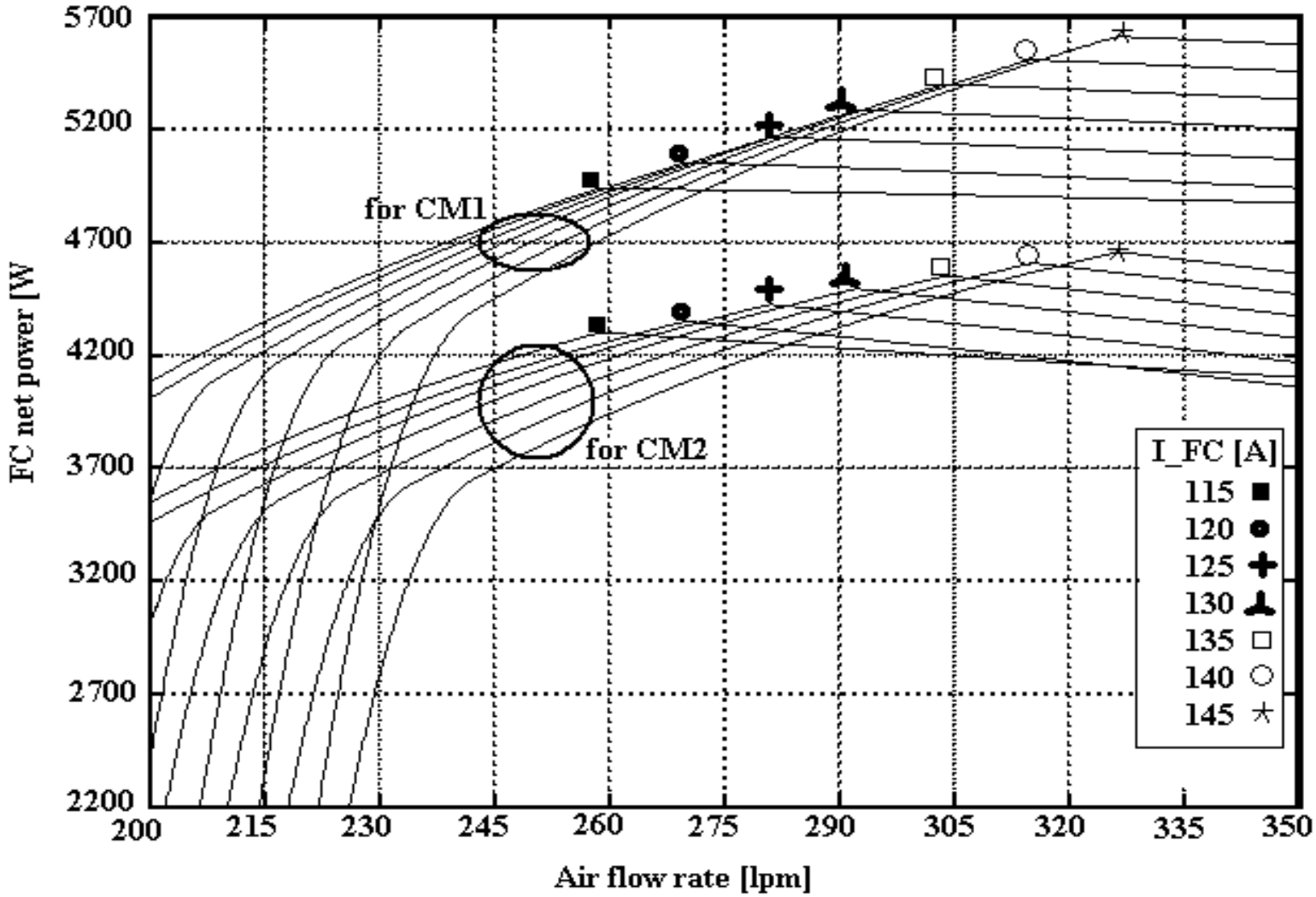

Figure 9. The net power characteristics of the 6 kW PEMFC stack under different load power levels (the air supplied by the compressor 1 and 2)

2.2. The single-input dual-output Extremum Seeking (SIDOES) control scheme

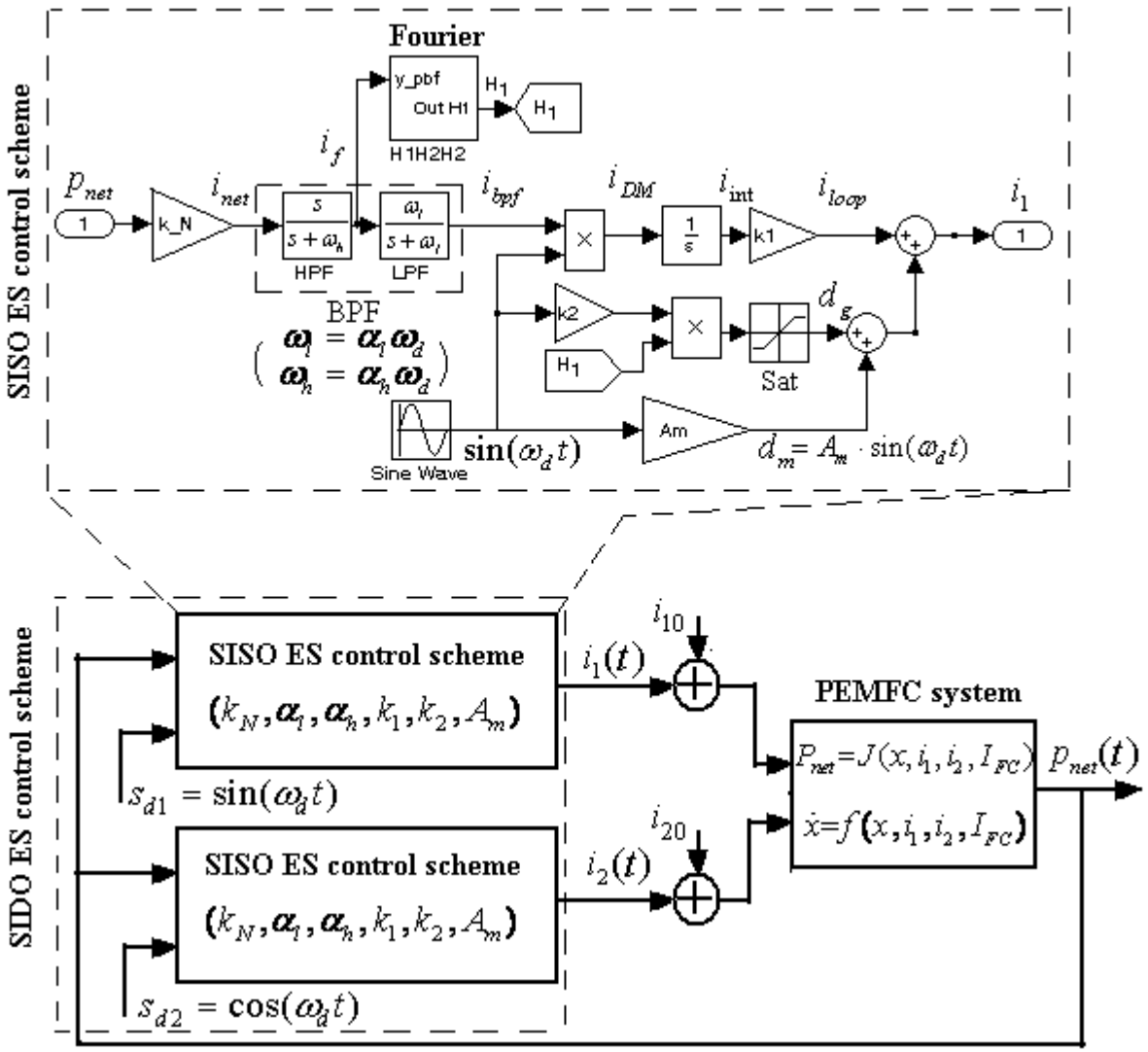

Figure 10. The SIDOES control scheme

2.3. The static feed-forward (sFF) control technique

The static feed-forward (sFF) control technique will be used as reference to report the improvements on FC net power.

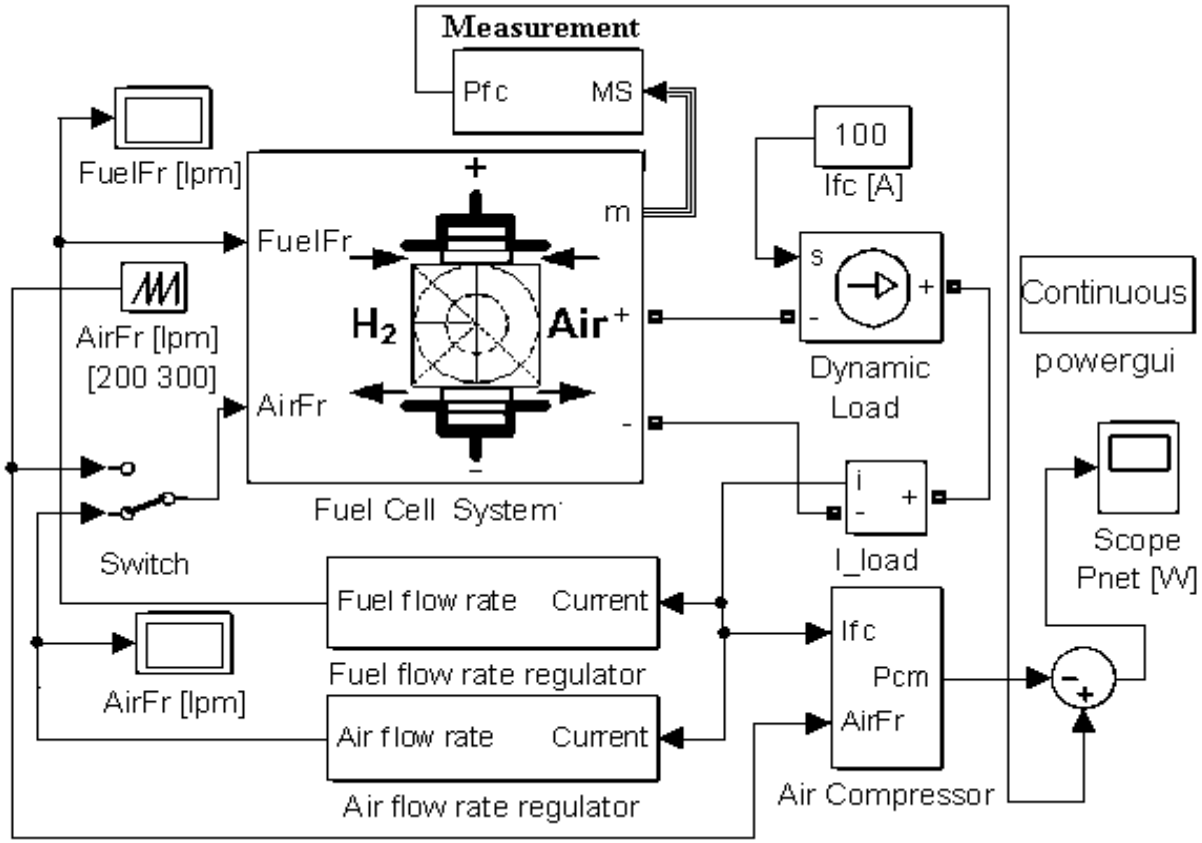

Figure 11. The diagram to compute the FC net power under sFF control

2. Improving the PEMFC energy efficiency

2.3. The static feed-forward (sFF) control technique

I_{FC} [A]	$FuelFr_{sFF}$ [lpm]	$AirFr_{sFF}$ [lpm]	P_{net1} [W]	P_{cm1} [W]	P_{net2} [W]	P_{cm2} [W]	P_{FC} [W]	η_{sys1} [%]	η_{sys2} [%]
115	43.19	258.8	4730	636.2	4094	1272	5366	88.1	76.3
120	45	270.1	4870	675	4194	1350	5545	87.8	75.6
125	46.94	281.3	5004	714.7	4289	1429	5719	87.5	75.0
130	48.82	300.7	5134	754.7	4379	1509	5889	87.2	74.4
135	50.7	303.8	5259	795.1	4463	1590	6054	86.9	73.7
140	52.58	315.1	5380	825.9	4544	1672	6216	86.6	73.1
145	54.45	326.3	5498	877	4619	1754	6373	86.3	72.5

Table 1. The FC net power under sFF control for airFR and FuelFr of the 6 kW FC stack supplied by CM1 and CM2

2. Improving the PEMFC energy efficiency

2.4. sFF control for the FuelFr and ES control for the AirFr

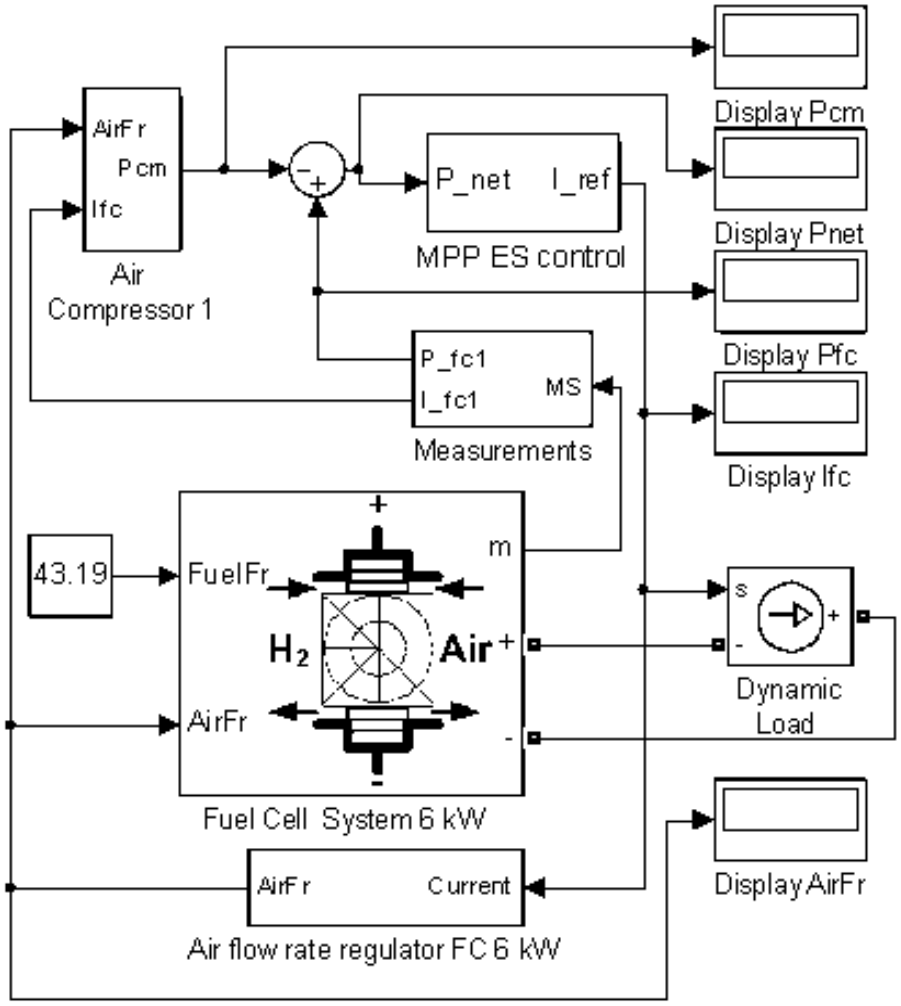

Figure 12. The diagram to compute the FC net power under sFF control for the FuelFr and ES control for the AirFr

2. Improving the PEMFC energy efficiency

2.4. sFF control for the FuelFr and ES control for the AirFr

$FuelFr_{sFF}$ [lpm]	I_{FC1a} [A]	$AirFrM_{1a}$ [lpm]	P_{net1a} [W]	P_{cm1a} [W]	P_{FC1a} [W]	η_{sys1a} [%]
43.19	113.1	254.6	4866	621	5487	88.7
45	117.8	266.2	5009	657	5666	88.4
46.94	122.8	276.5	5158	697	5855	88.1
48.82	127.7	287.4	5298	735	6034	87.8
50.7	132.6	298.3	5434	774	6208	87.5
52.58	137.4	309.3	5566	813	6379	87.3
54.45	142.2	320.1	5693	853	6546	87.0

Table 2. The FC net power under aES control for AirFr of the 6 kW FC stack supplied by CM1

$FuelFr_{sFF}$ [lpm]	I_{FC2a} [A]	$AirFrM_{2a}$ [lpm]	P_{net2a} [W]	P_{cm2a} [W]	P_{FC2a} [W]	η_{sys2a} [%]
43.19	113.1	254.6	4245	1243	5487	77.4
45	117.8	266.2	4353	1314	5666	76.8
46.94	122.8	276.5	4463	1392	5855	76.2
48.82	127.7	287.4	4564	1470	6034	75.6
50.7	132.6	298.3	4661	1548	6208	75.1
52.58	137.4	309.3	4753	1626	6379	74.5
54.45	142.2	320.1	4840	1706	6546	73.9

Table 3. The FC net power under aES control for AirFr of the 6 kW FC stack supplied by CM2

2. Improving the PEMFC energy efficiency

2.5. sFF control for the AirFr and ES control for the FuelFr

$AirFrM_{sFF}$ [lpm]	I_{FC1f} [A]	$FuelFr_{1f}$ [lpm]	P_{net1f} [W]	P_{cm1f} [W]	P_{FC1f} [W]	η_{sys1f} [%]
258.8	128.3	48.18	5214	192	5406	96.4
270.1	132.4	49.74	5376	201	5577	96.4
281.3	136.4	51.25	5533	210	5743	96.3
300.7	143.2	53.79	5797	225	6022	96.3
303.8	144.3	54.19	5838	228	6066	96.2
315.1	148.1	55.62	5986	237	6223	96.2
326.3	151.8	57.01	6129	247	6376	96.1

Table 4. The FC net power under aES control for FuelFr of the 6 kW FC stack supplied by CM1

$AirFrM_{sFF}$ [lpm]	I_{FC2f} [A]	$FuelFr_{2f}$ [lpm]	P_{net2f} [W]	P_{cm2f} [W]	P_{FC2f} [W]	η_{sys2f} [%]
258.8	128.3	48.18	5022	384	5406	92.9
270.1	132.4	49.74	5175	402	5577	92.8
281.3	136.4	51.25	5323	420	5743	92.7
300.7	143.2	53.79	5572	450	6022	92.5
303.8	144.3	54.19	5610	456	6066	92.5
315.1	148.1	55.62	5749	474	6223	92.4
326.3	151.8	57.01	5882	494	6376	92.3

Table 5. The FC net power under aES control for FuelFr of the 6 kW FC stack supplied by CM2

2.6. ES control for FuelFr and ES search of the optimum AirFr based on FC current

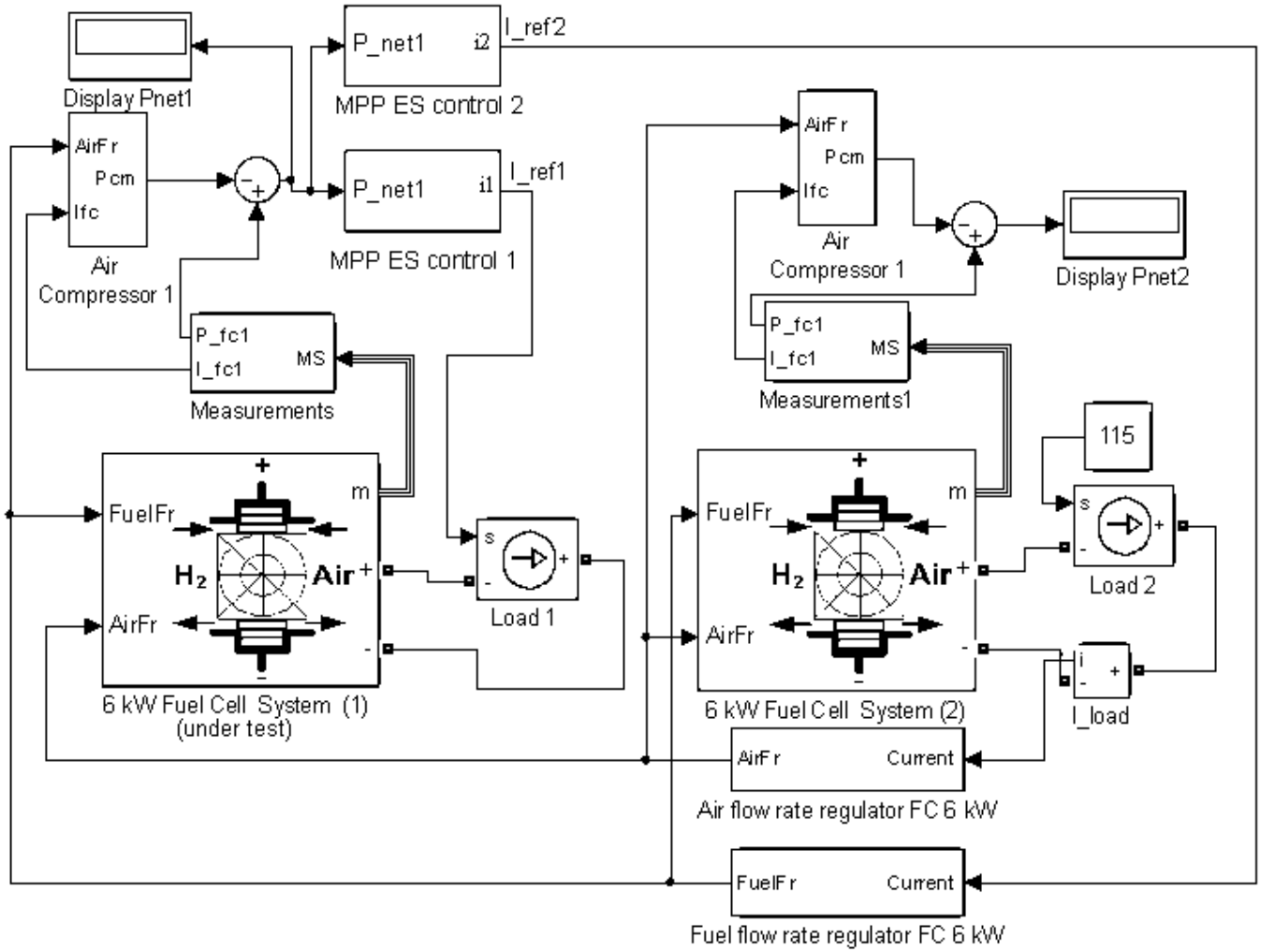

Figure 13. The diagram to evaluate the improvement in the FC net power considering the ES control for FuelFr and ES search of the optimum AirFr based on FC current

2. Improving the PEMFC energy efficiency

2.7. ES control for AirFr and ES search of the optimum FuelFr based on FC current

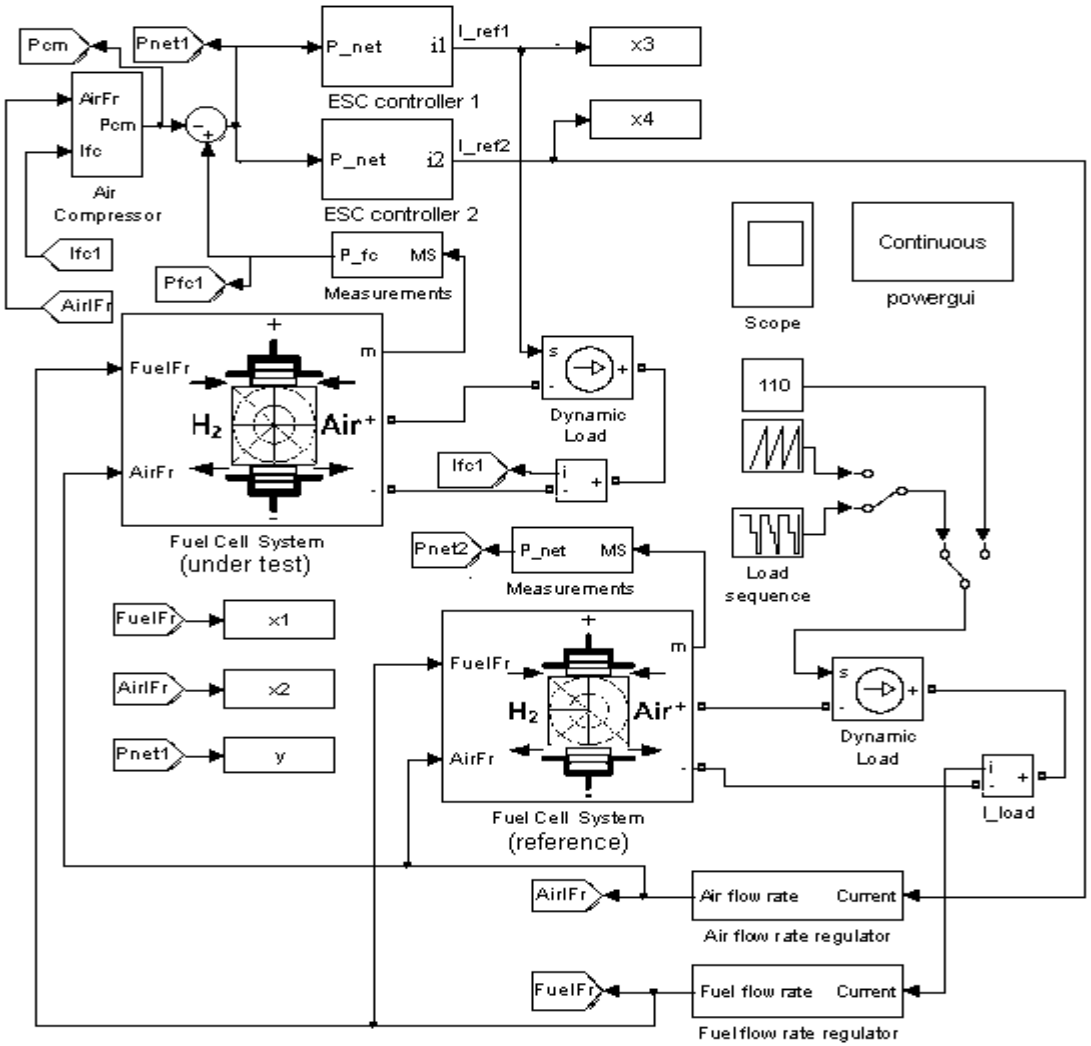

Figure 14. The diagram to evaluate the improvement in the FC net power considering the ES control for AirFr and ES search of the optimum FuelFr based on FC current

2. Improving the PEMFC energy efficiency

2.6. The improvements in the FC net power

I_{FC} [A]	$\Delta P_{net(1fa)}$ [W]	$\Delta P_{net(2fa)}$ [W]	$\Delta P_{net(1af)}$ [W]	$\Delta P_{net(2af)}$ [W]
115	333	516	111	121
120	337	539	118	129
125	342	563	126	137
130	348	589	134	146
135	355	616	142	155
140	363	645	150	164
145	373	675	159	173

Table 6. The improvements in the FC net power using simulation diagram from Figure 13 ($\Delta P_{net(1fa)}$ and $\Delta P_{net(2fa)}$) and Figure 14 ($\Delta P_{net(1af)}$ and $\Delta P_{net(2af)}$) for both compressors (CM1 and CM2)

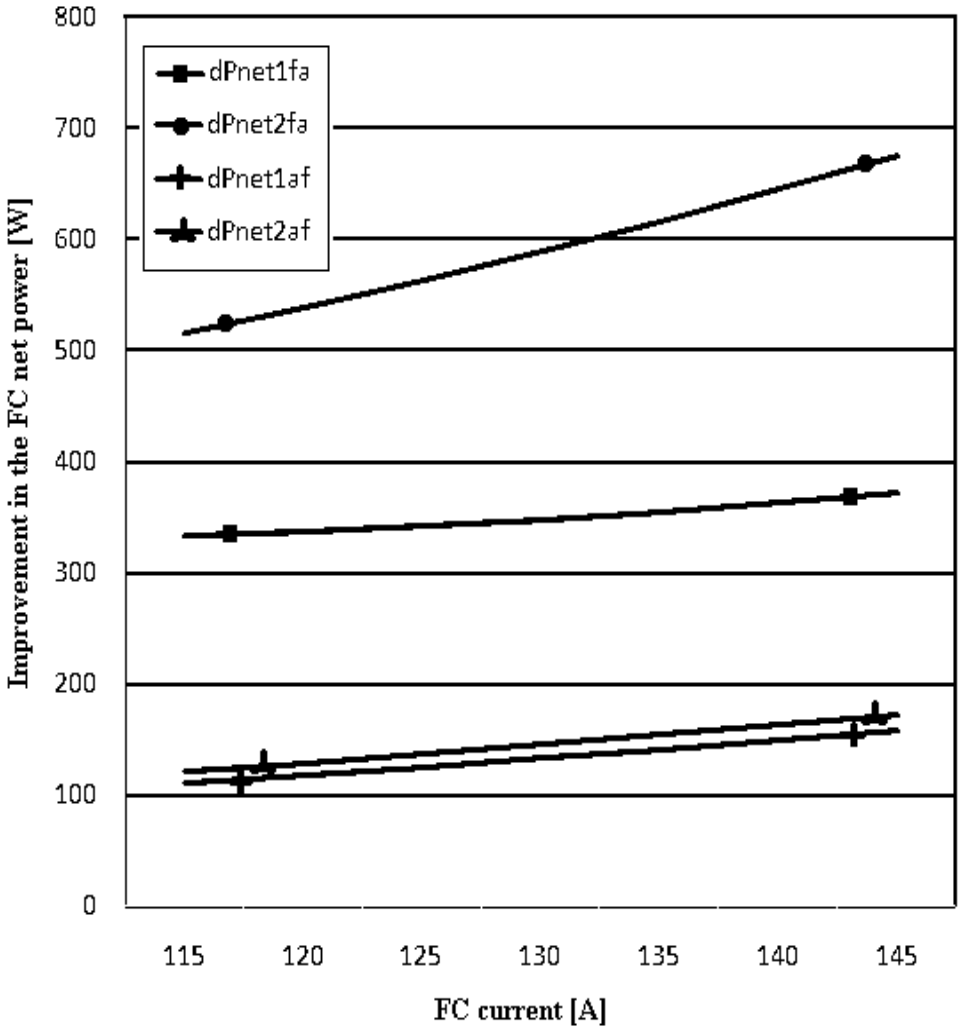

Figure 15. The improvement in the FC net power

2.7. Conclusion

ES control for FuelFr and ES search of the optimum AirFr based on FC current:

- the improvement in the net power $\Delta P_{net(1fa)}$ increases with a rate of 1.3 W/A ;
- the improvement in the net power $\Delta P_{net(2fa)}$ increases with a rate of 5.3 W/A
- the relative improvement in the FC net power, $\Delta P_{net(2fa)}/ \Delta P_{net(1fa)}$, has values in range 1.5 to 1.8.

This means that the PEMFC system must to be mandatory operated close to the MEP if the power losses are high, otherwise the energy efficiency decreases dramatically.

ES control for AirFr and ES search of the optimum FuelFr based on FC current:

- the improvement in the net power $\Delta P_{net(1af)}$ increases with a rate of 1.6 W/A ;
- the improvement in the net power $\Delta P_{net(2af)}$ increases with a rate of 1.73 W/A
- the relative improvement in the FC net power, $\Delta P_{net(2af)}/ \Delta P_{net(1af)}$, has values about of 1.09.

This means that in this case the improvements in FC net power are less sensitive to power losses and load level.

This also sustains that the improvement in the FC net power is less sensitive to power losses if the optimum AirFr is set by the ES controller.

The MEP is more sensitive to FuelFr changes than the changes in AirFr. So, under dynamic load, it is recommended a load following control of the FuelFr and an optimal control of the AirFr based on appropriate strategy that can maximize the energy efficiency.

3. Efficient Energy Control Strategies for FC RES HPS

2.7. Energy Management Unit (EMU) for FC RES HPS

The objectives of this section are:

(1) To apply the load-following (LF) control based on the MEP tracking (MEPT) control scheme in order to ensure the load demand;

(2) To improve the fuel consumption and fuel efficiency that are both used as performances indicators based on control of both fuel flow rates;

(3) To find a methodology to compare the four EMU control topologies based on the performances indicators proposed;

(4) To shown the advantage of the LF control that operates the ESS in CS mode under any load demand, with direct implications in the size and cost of the RES/FC HPS;

(5) To shown the advantage of the MEPT control that operates efficiently the FC stack considering the variability of RES and load power profiles, with direct implications in efficiency of the whole RES/FC HPS.

3. Efficient Energy Control Strategies for FC RES HPS

2.7. Energy Management Unit (EMU) for FC RES HPS

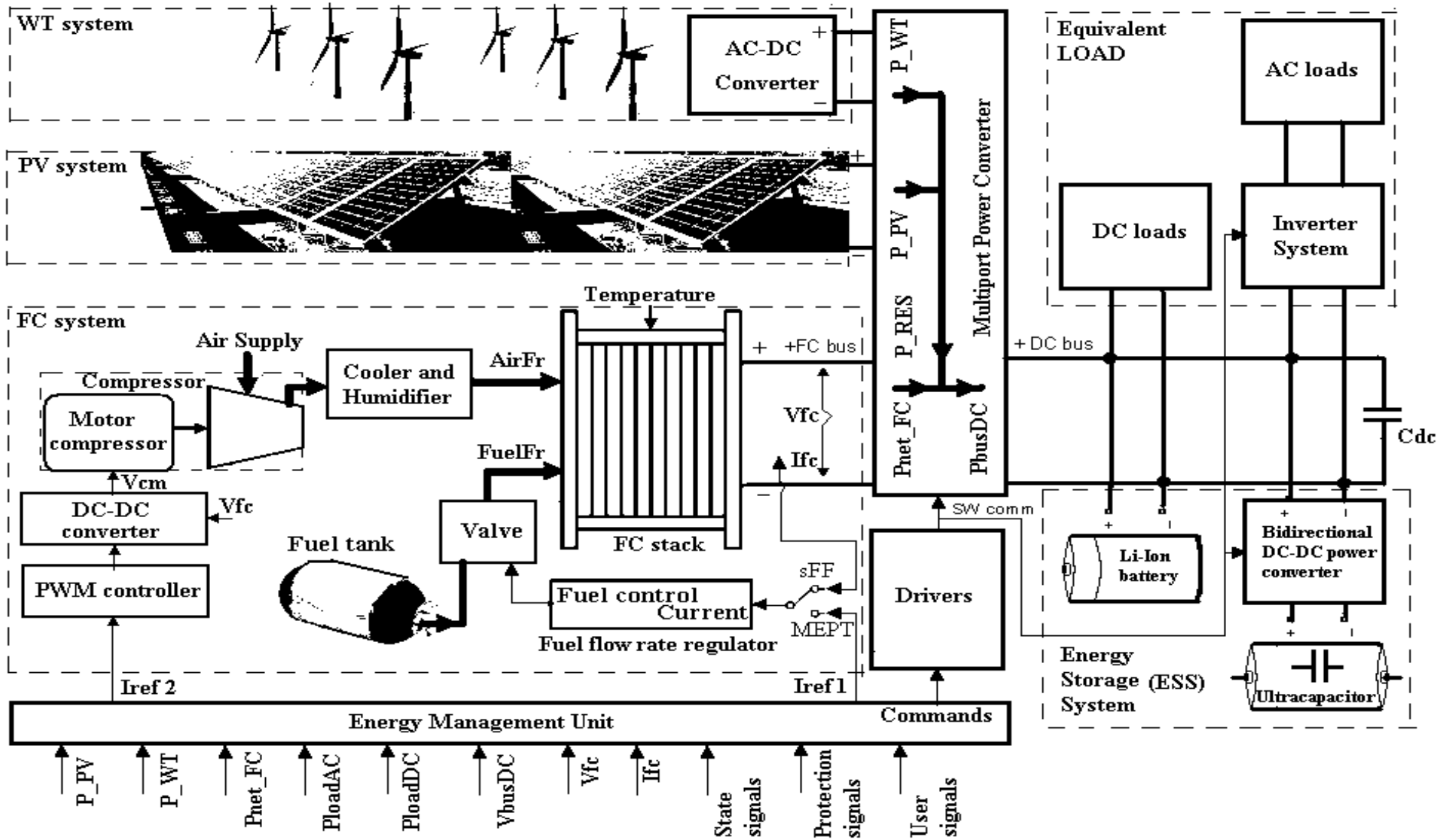

Figure 16. The standalone Renewable/Fuel Cell Hybrid Power Source system

3. Efficient Energy Control Strategies for FC RES HPS

3.1. Energy Management Unit (EMU) for FC RES HPS

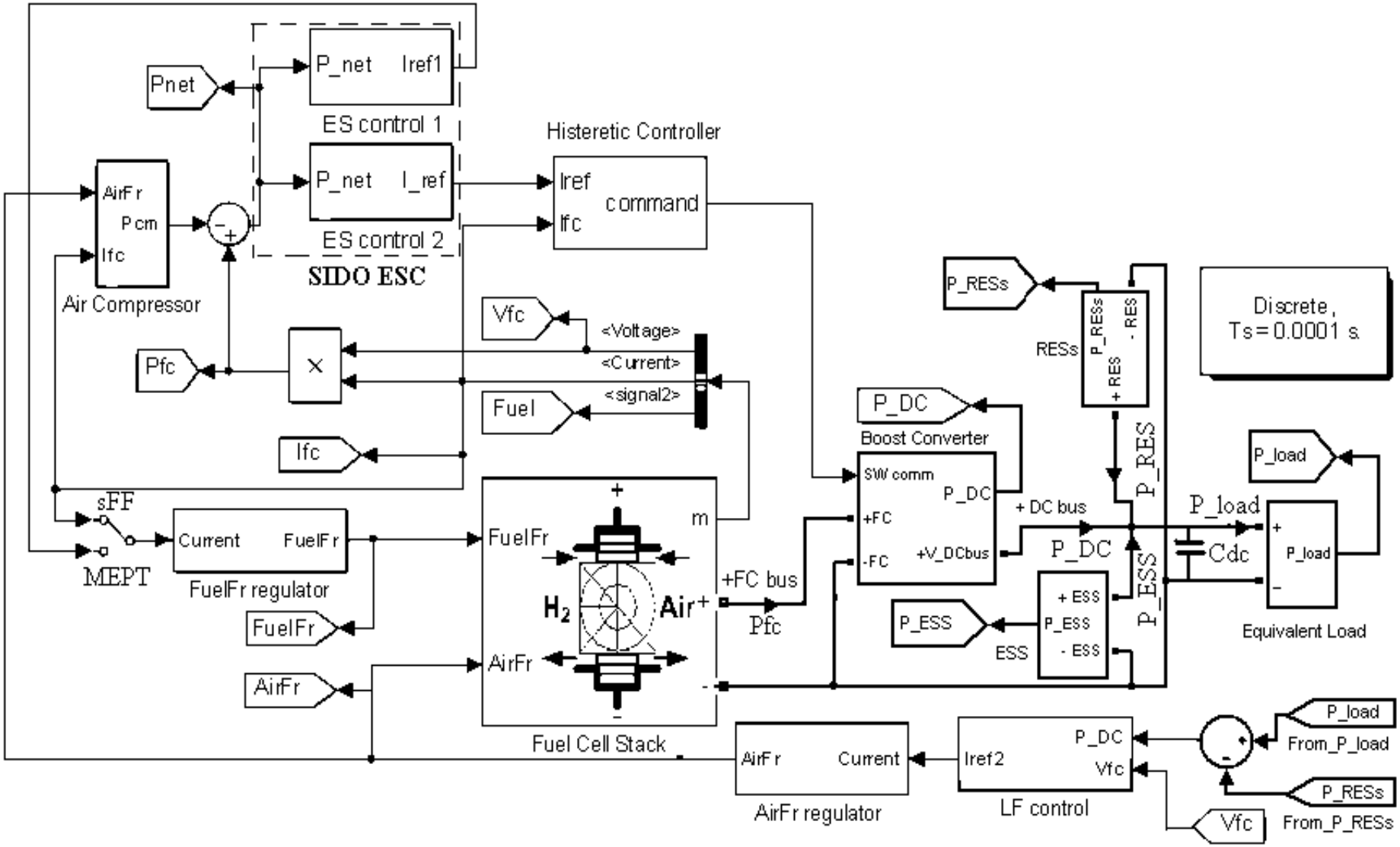

Figure 17. The simulation diagram for Air-LF/Fuel-ESC and Air-LF/Fuel-sFF cases

3. Efficient Energy Control Strategies for FC RES HPS

3.1. Energy Management Unit (EMU) for FC RES HPS

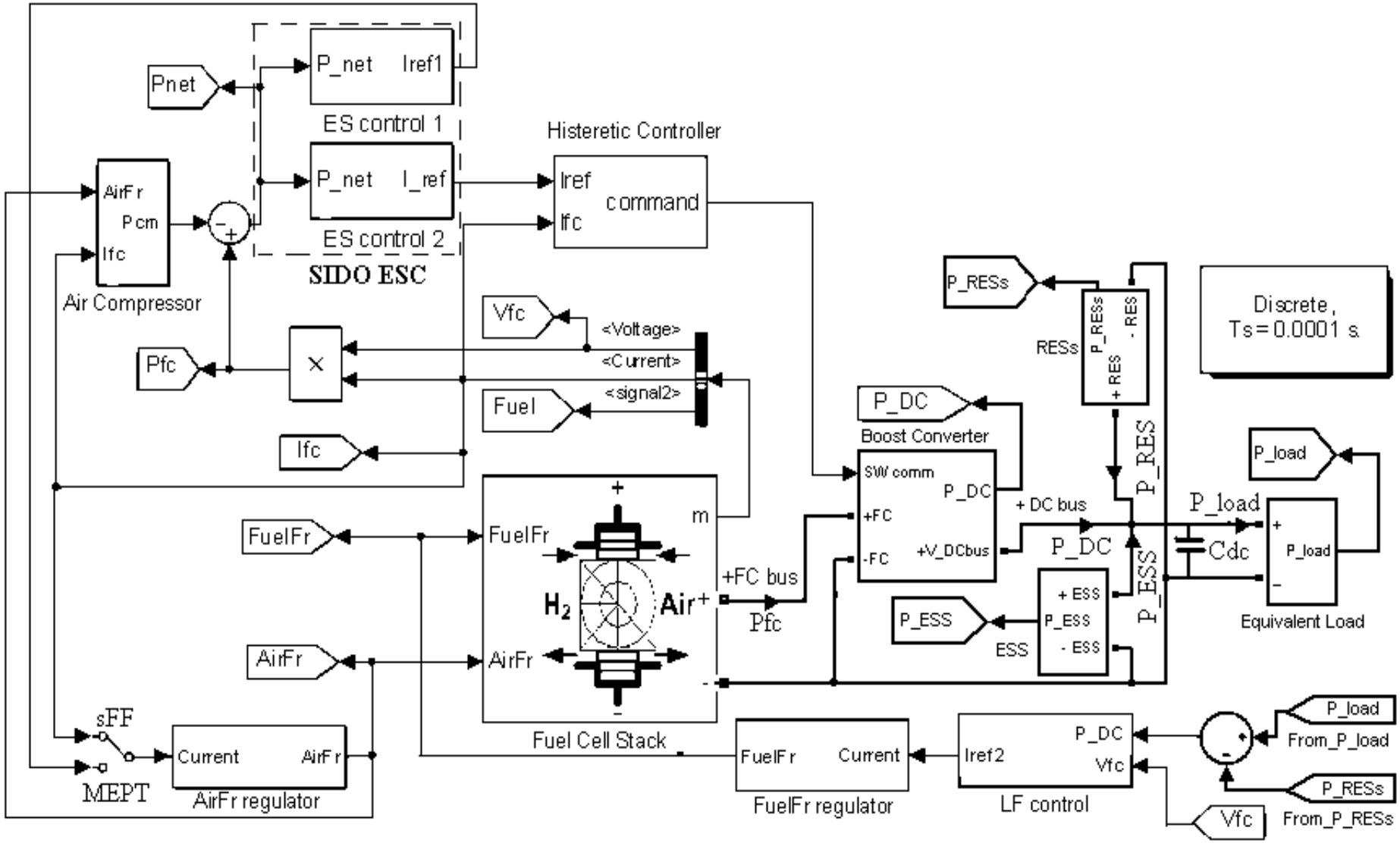

Figure 18. The simulation diagram for Air-ESC/Fuel-LF and Air-sFF/Fuel-LF cases

3.2. The FC net power characteristics

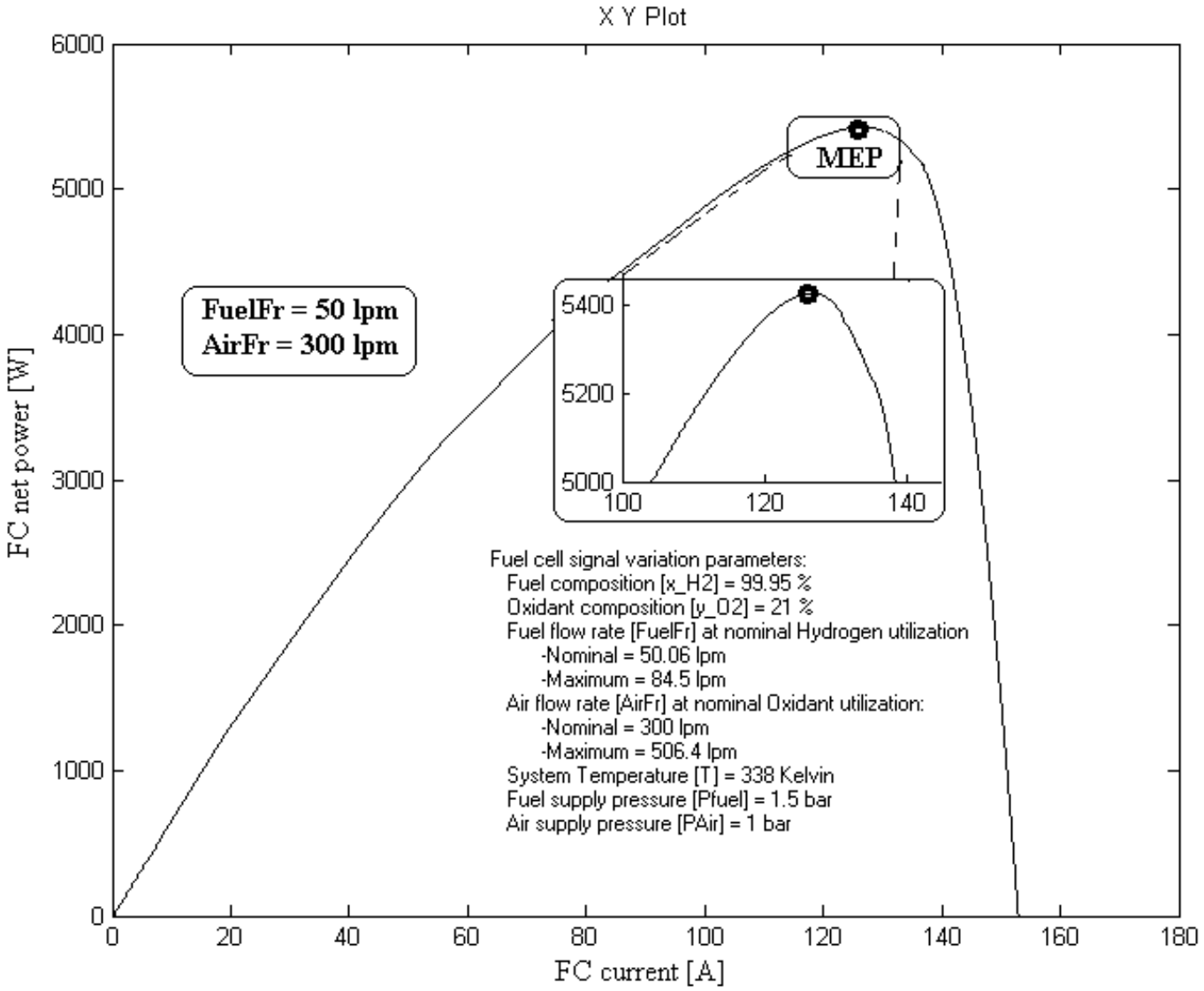

Figure 19. The FC net power characteristic for the nominal values of fueling rates

3.2. The FC net power characteristics

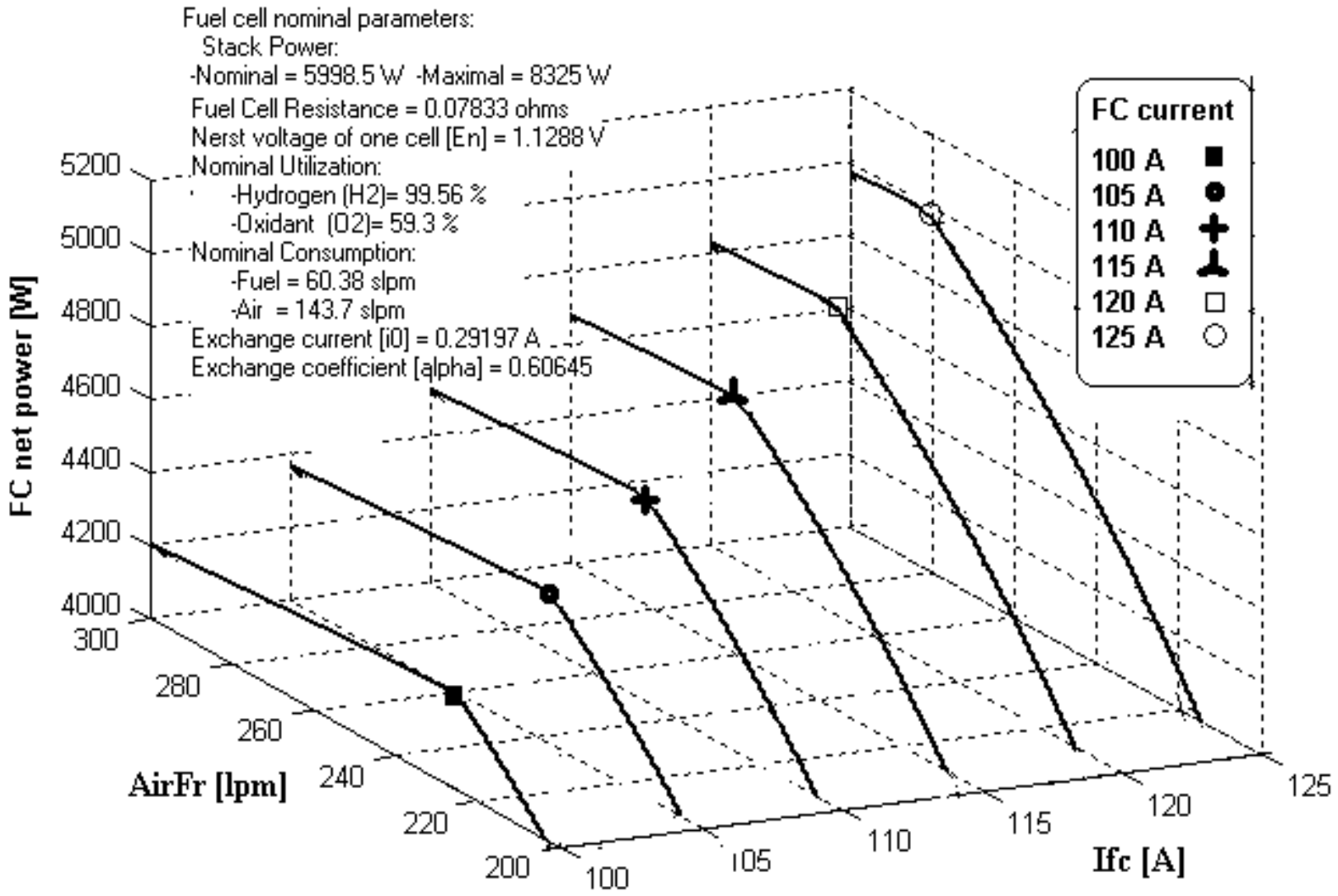

Figure 20. The FC net power surface

3.3. The RES and load power characteristics

Figure 21. The diagram and power profile of the RES

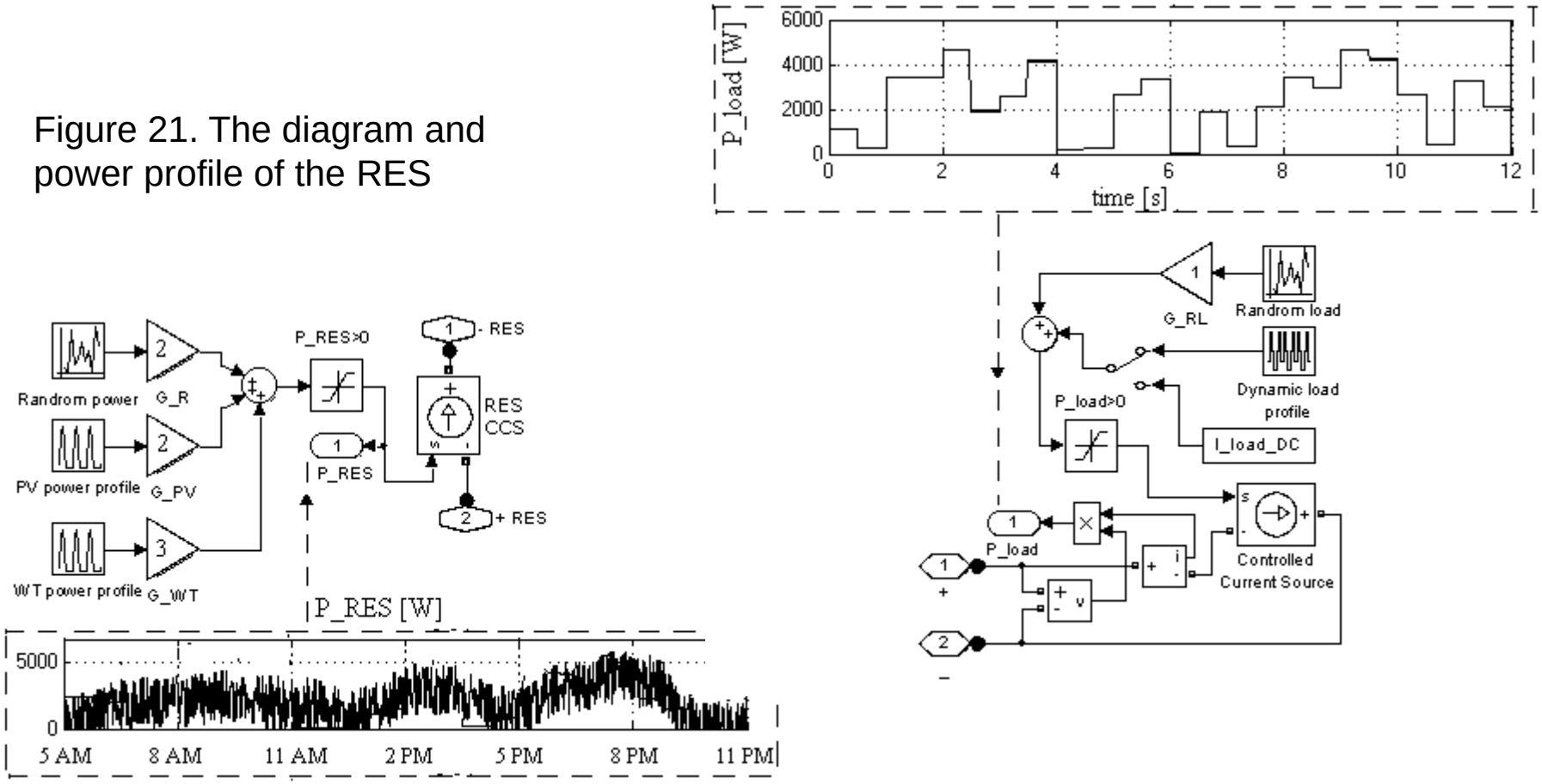

Figure 22. The diagram and power profile of the dynamic load

3.4. Energy Management Unit (EMU) for FC RES HPS

All HPS topologies proposed are based on an MEPT and LF control loops that generate the reference currents:
I_{ref}, for the boost controller,
and I_{ref1} and I_{ref2}, for the FuelFr and AirFr regulators, respectively.

If I_{FC} current is used to control the FuelFr regulator or the AirFr regulator, instead of the I_{ref1} current, then other two fueling control configurations will be obtained based on the sFF control scheme.

$$P_{RES} + \eta_{boost} P_{FCnet} + P_{ESS} - P_{Load} = 0$$

P_{ESS}=0 during a drive cycle

$$I_{ref2} = I_{FC(AV)} = (P_{Load} - P_{RES})/(V_{FC}\eta_{boost})$$

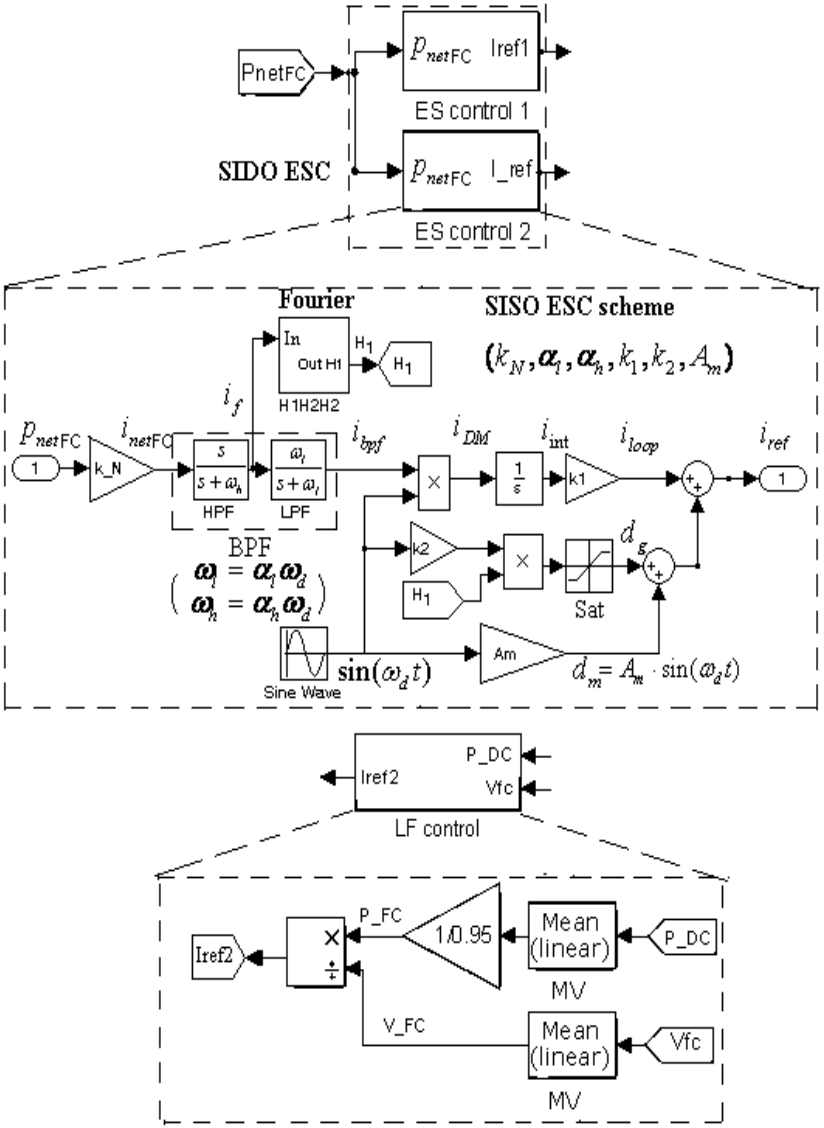

Figure 23. The diagrams of the EMU controllers

3.5. Results

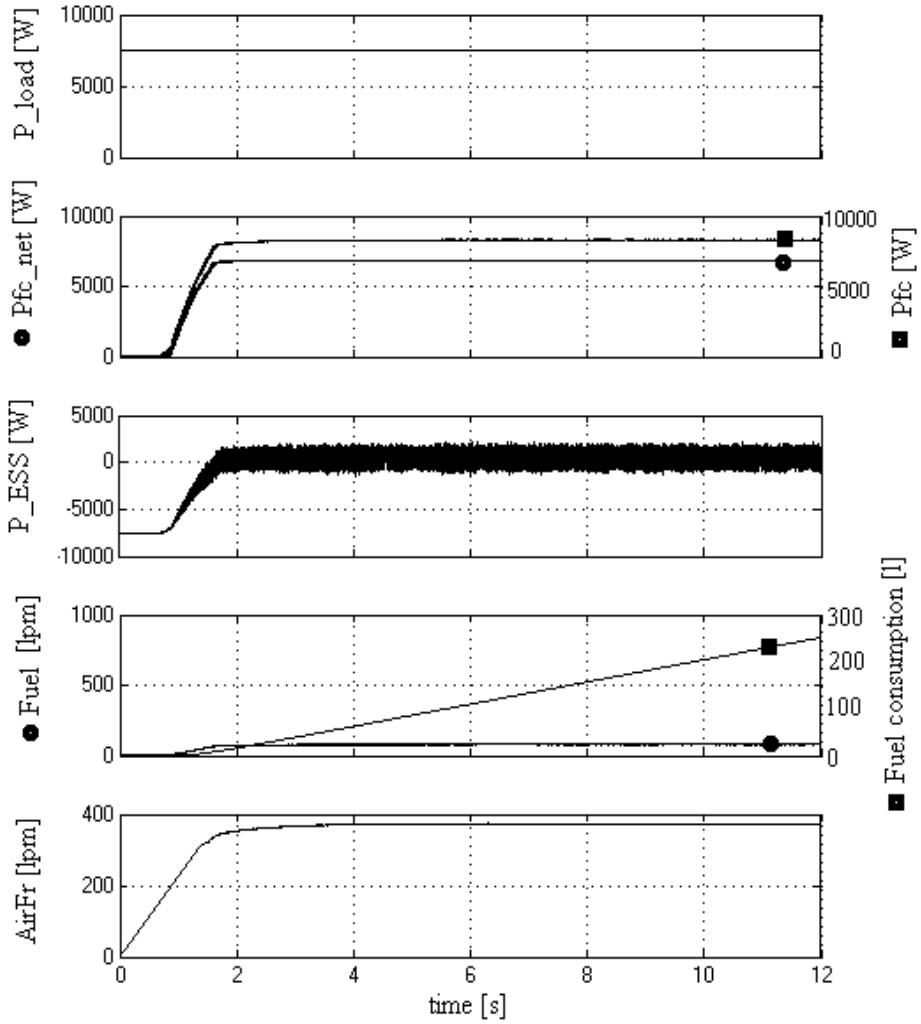

Figure 24. The results for Air-LF/Fuel-ESC EMU

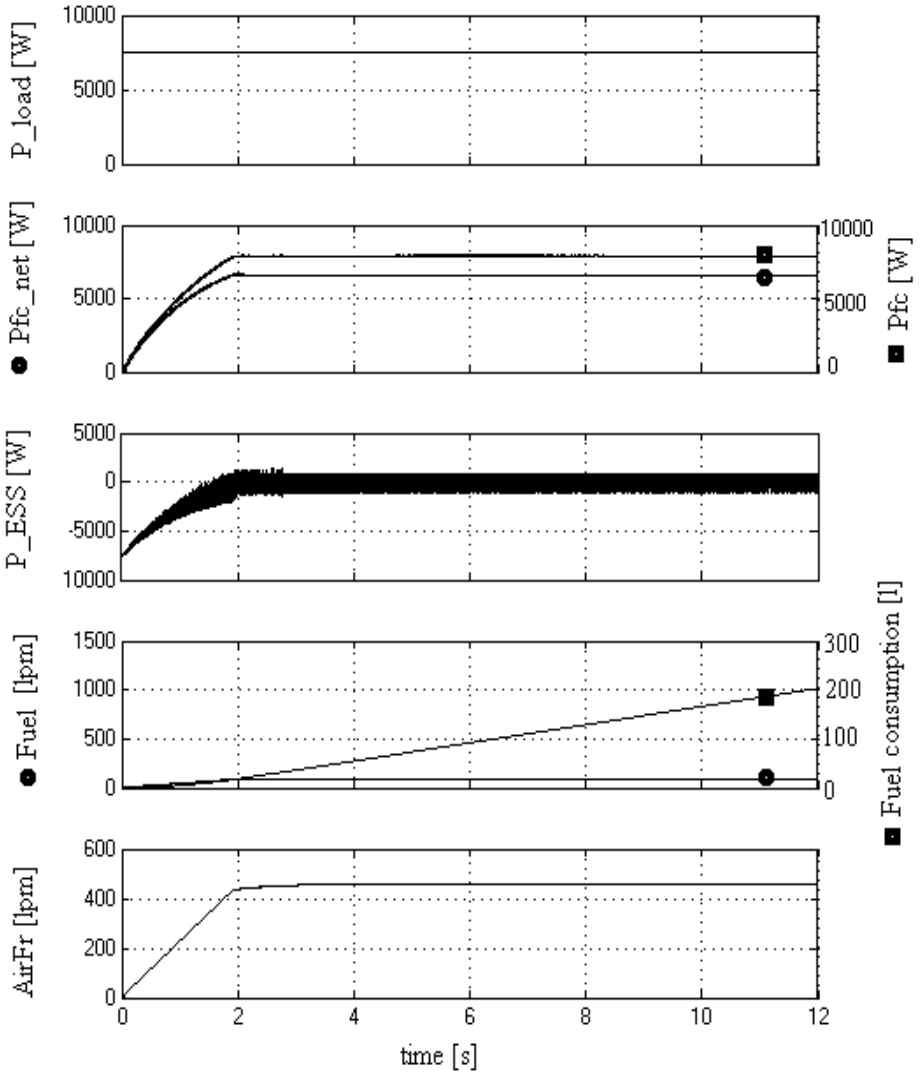

Figure 25. The results for Air-LF/Fuel-sFF EMU

3.5. Results

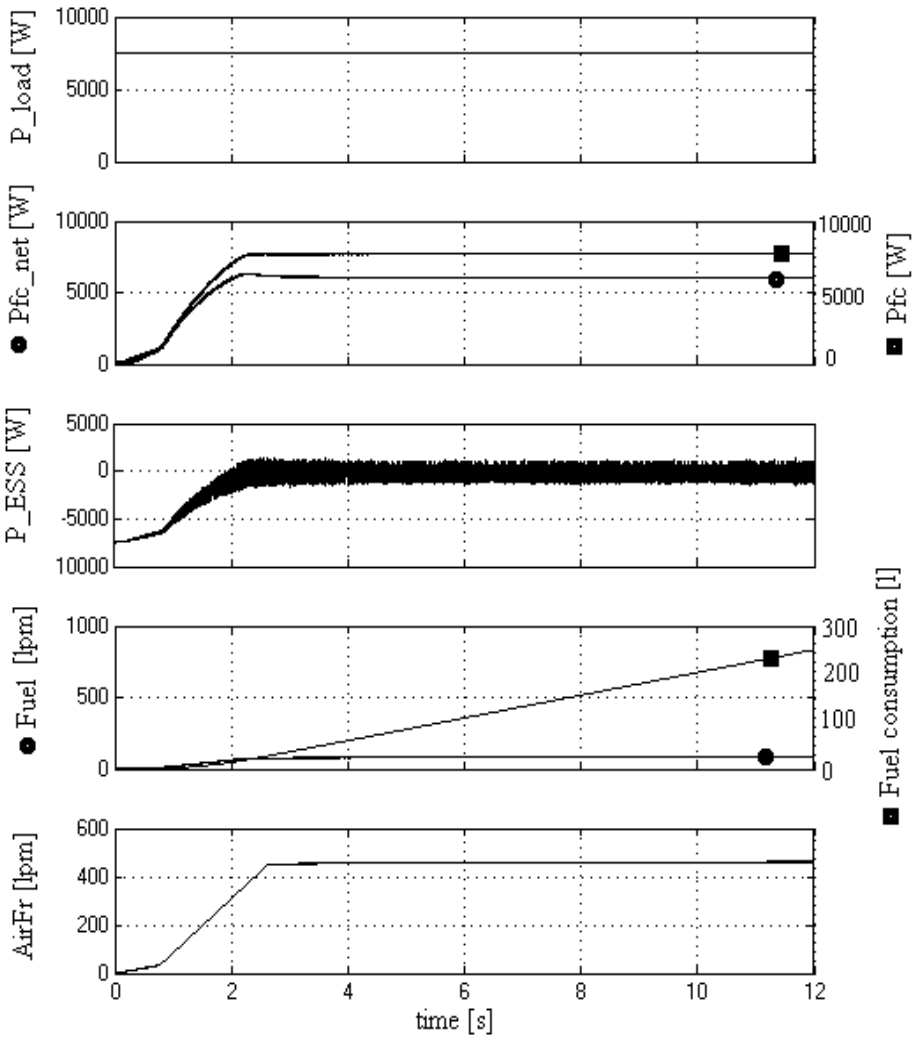

Figure 26. The results for Air-ESC/Fuel-LF EMU

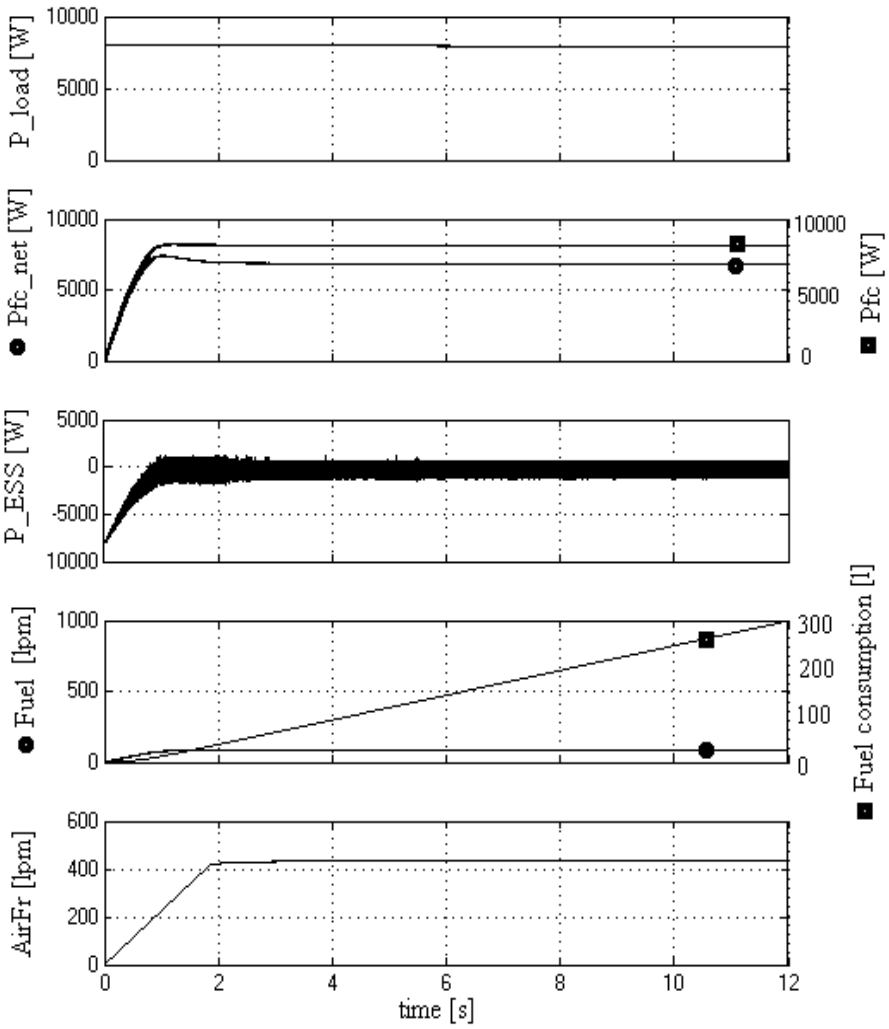

Figure 27. The results for Air-sFF/Fuel-LF EMU

Air-sFF/ Fuel-LF	Air-LF/ Fuel-sFF	Air-ESC/ Fuel-LF	Air-LF/ Fuel-ESC	Diagram I_{load} [A]	
1306	1588	793.6	1613	5	FC net power, P_{netFC} [W]
2553	2925	2003	3131	10	
3699	3989	3205	4309	15	
5442	4874	4152	5318	20	
5886	5674	5157	6131	25	
6836	6639	6064	6850	30	
25.5	39.22	22.71	32.54	5	Fuel consumption, F [l]
54.66	75.84	47.66	70	10	
83.86	105.44	73	99.68	15	
117.44	130.78	100.56	125.34	20	
155.5	156.68	130.48	144.08	25	
199	203	166.56	167.62	30	
596.5	480.35	467.6	558.5	5	Fuel efficiency [J/l]
556.5	453.3	509.5	497.45	10	
526.5	440.45	499.45	474.25	15	
487.75	430.05	467.2	461.6	20	
446.5	413.95	432.35	450.6	25	
403.6	363.8	396.1	440.9	30	

3.5. Results

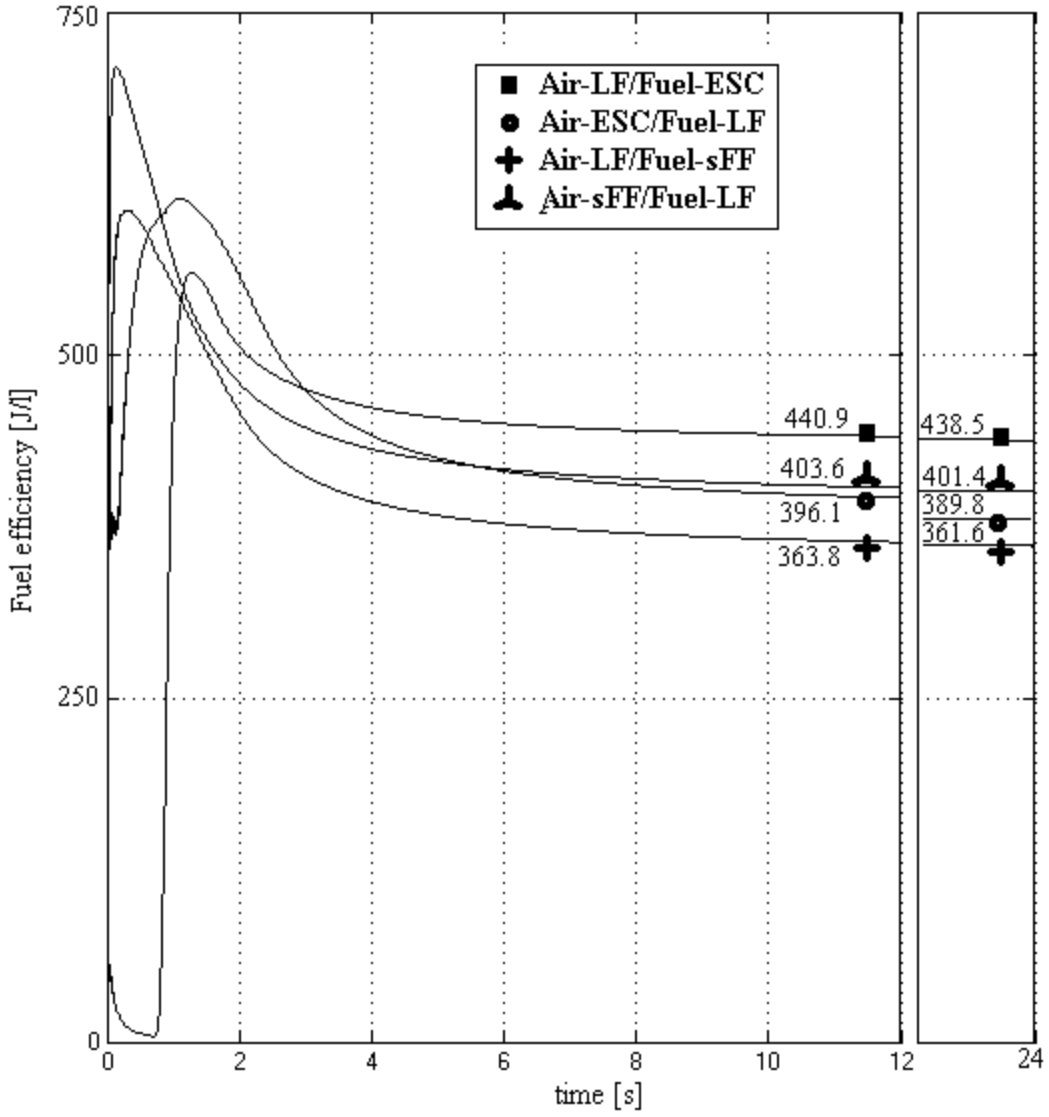

Figure 28. Fuel efficiency indicators for a load current of 30 A

3. Efficient Energy Control Strategies for FC RES HPS

3.5. Results

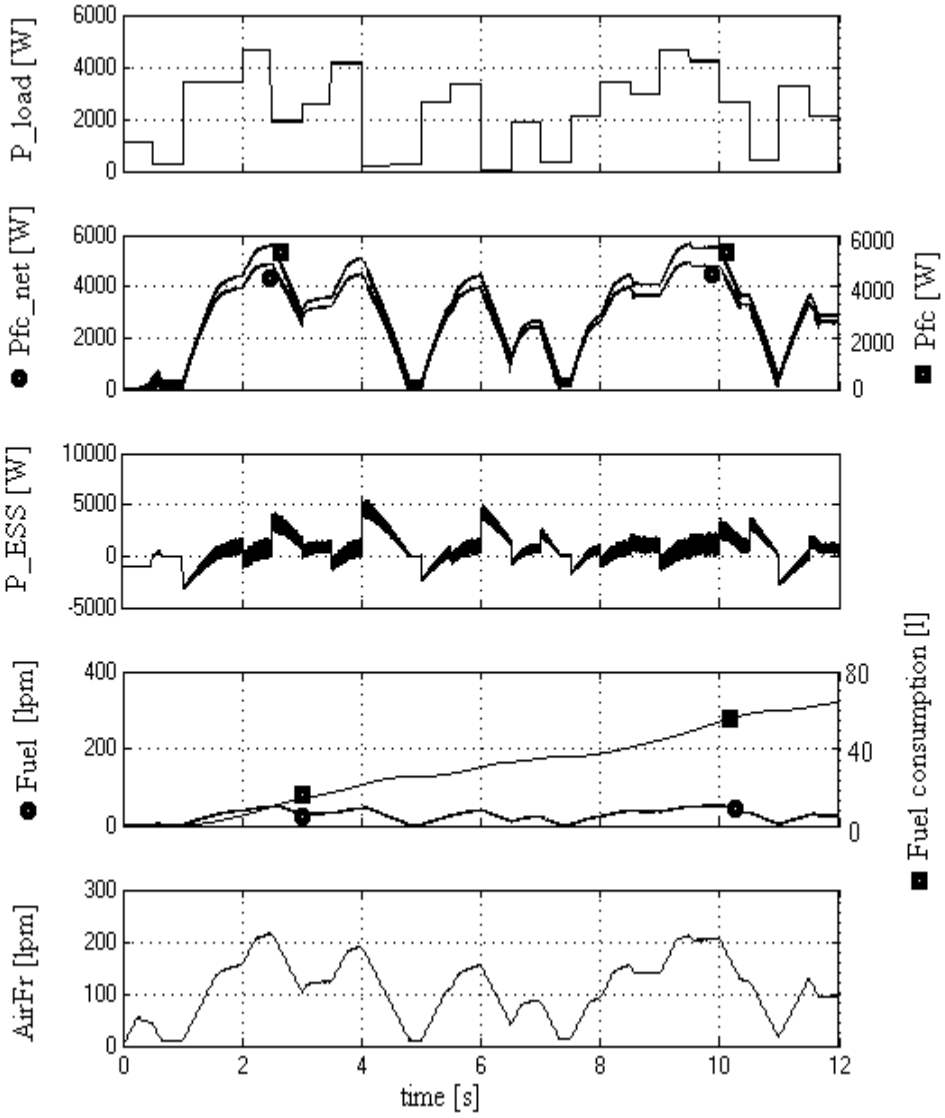

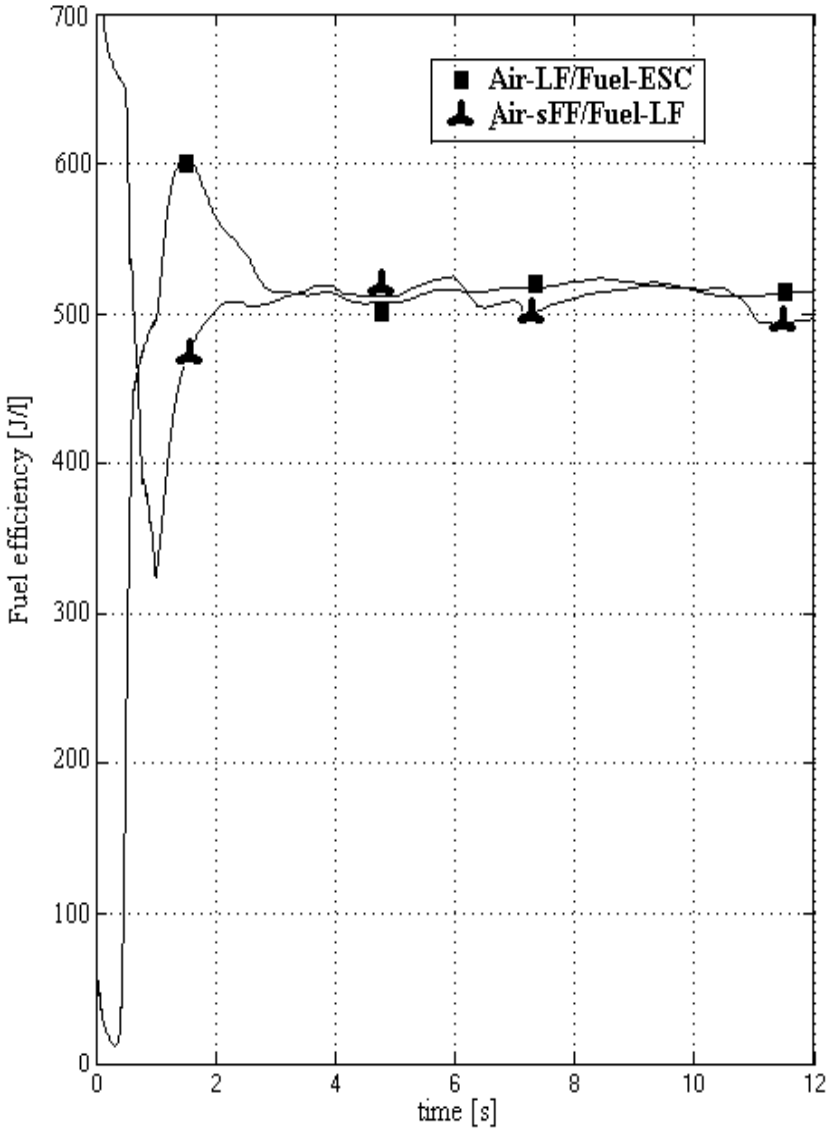

Fig 29. The FC response for Air-LF/ Fuel-ESC EMU and fuel efficiency under random load

3. Efficient Energy Control Strategies for FC RES HPS

3.5. Results

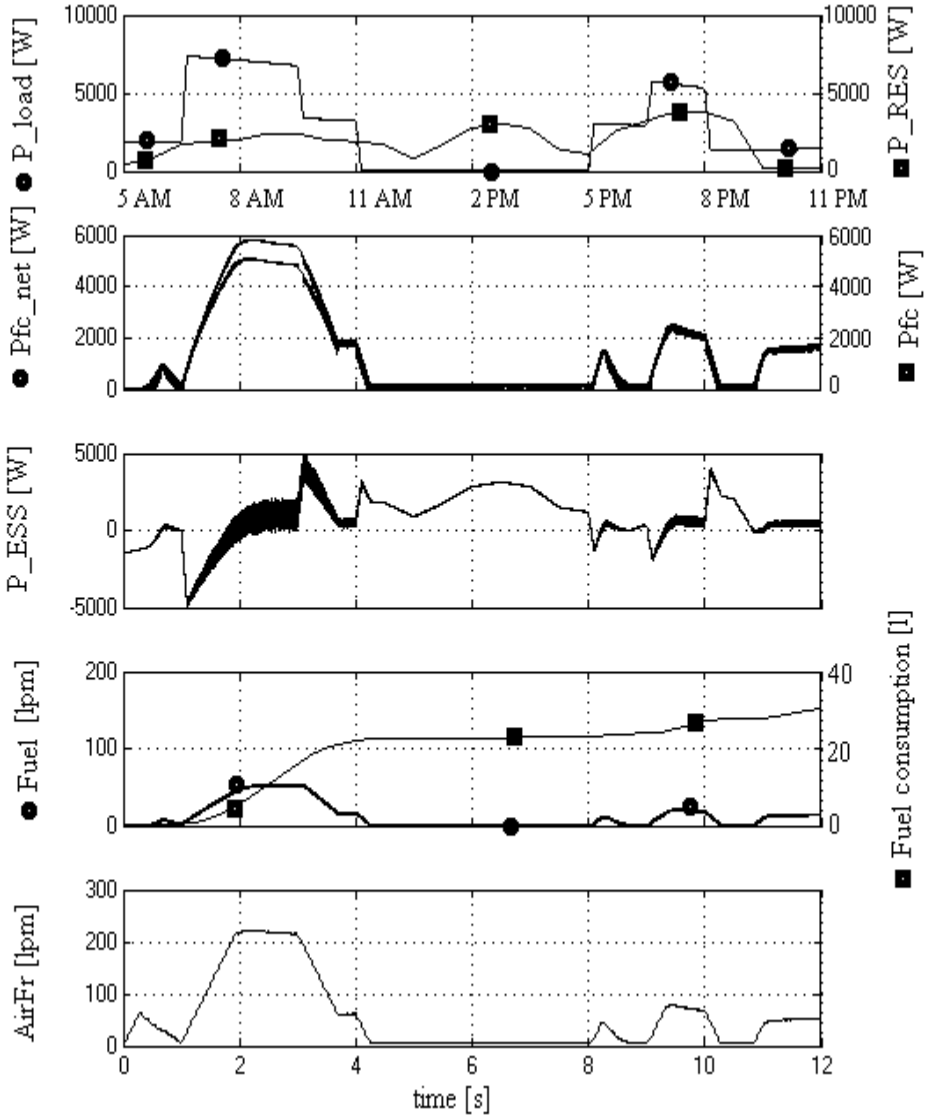

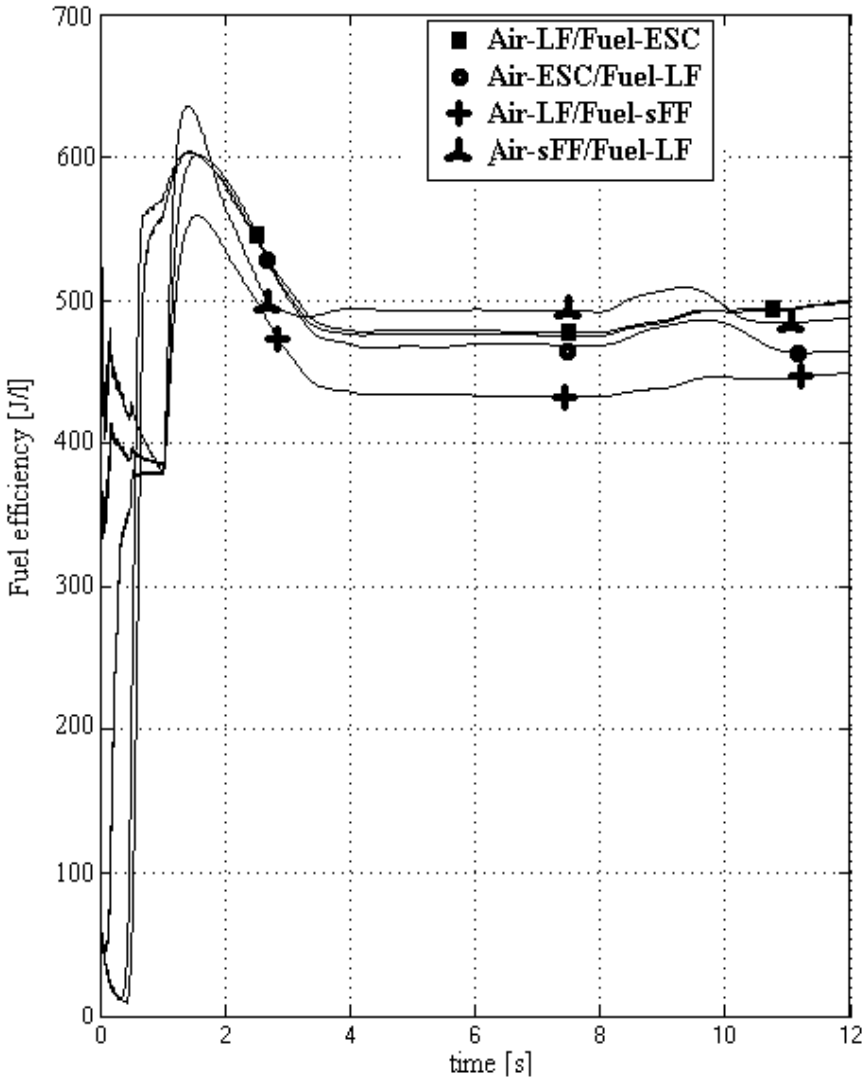

Fig. 30. The FC response for Air-LF/ Fuel-ESC EMU and fuel efficiency under variable load & RES

3. Efficient Energy Control Strategies for FC RES HPS

3.5. Results

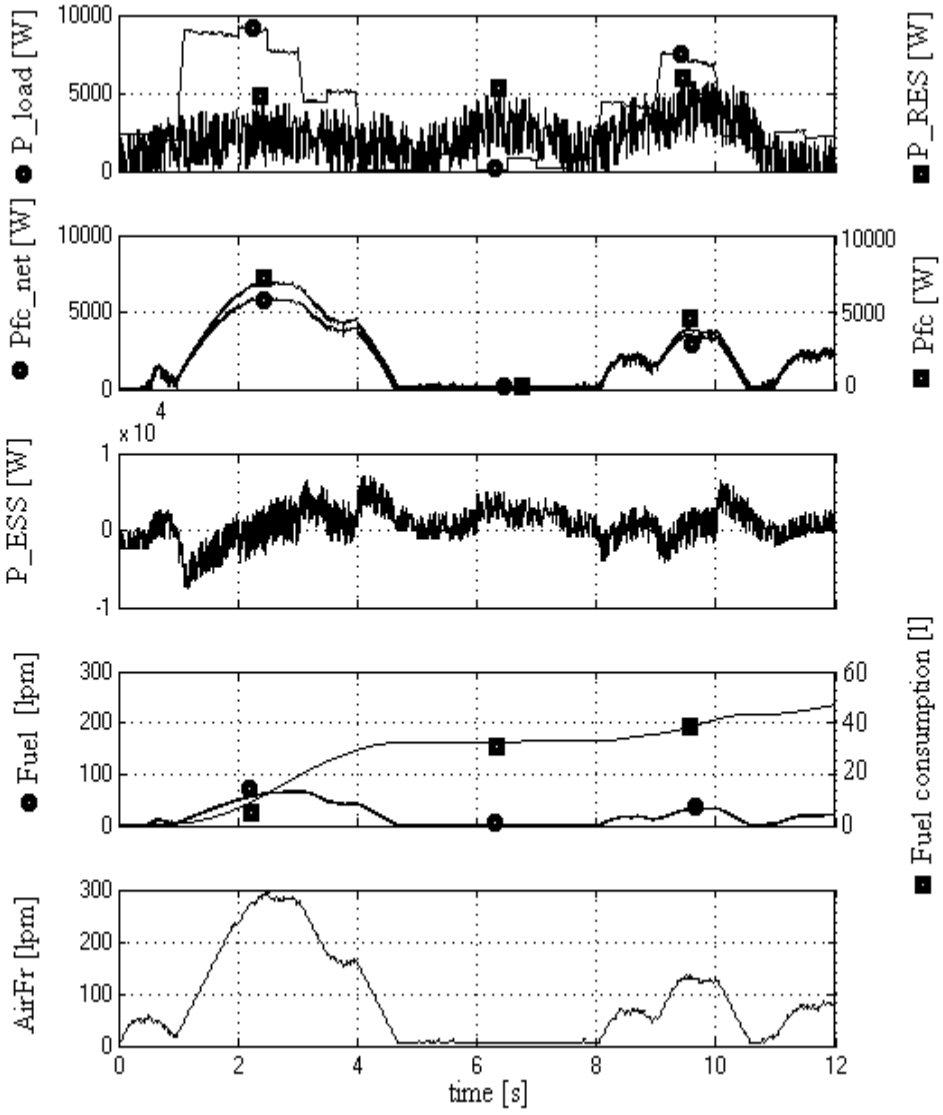

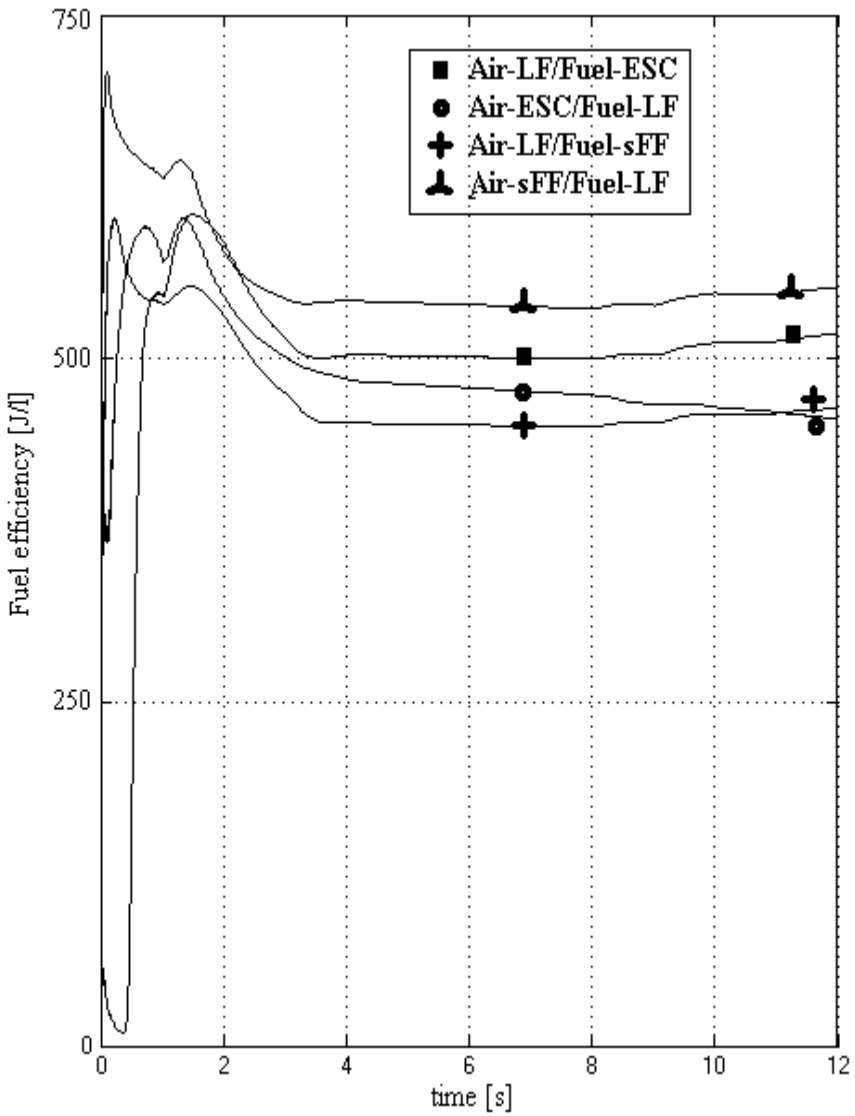

Fig. 31. The FC response for Air-LF/ Fuel-ESC EMU and fuel efficiency under variable load & RES

3. Efficient Energy Control Strategies for FC RES HPS

3.5. Results

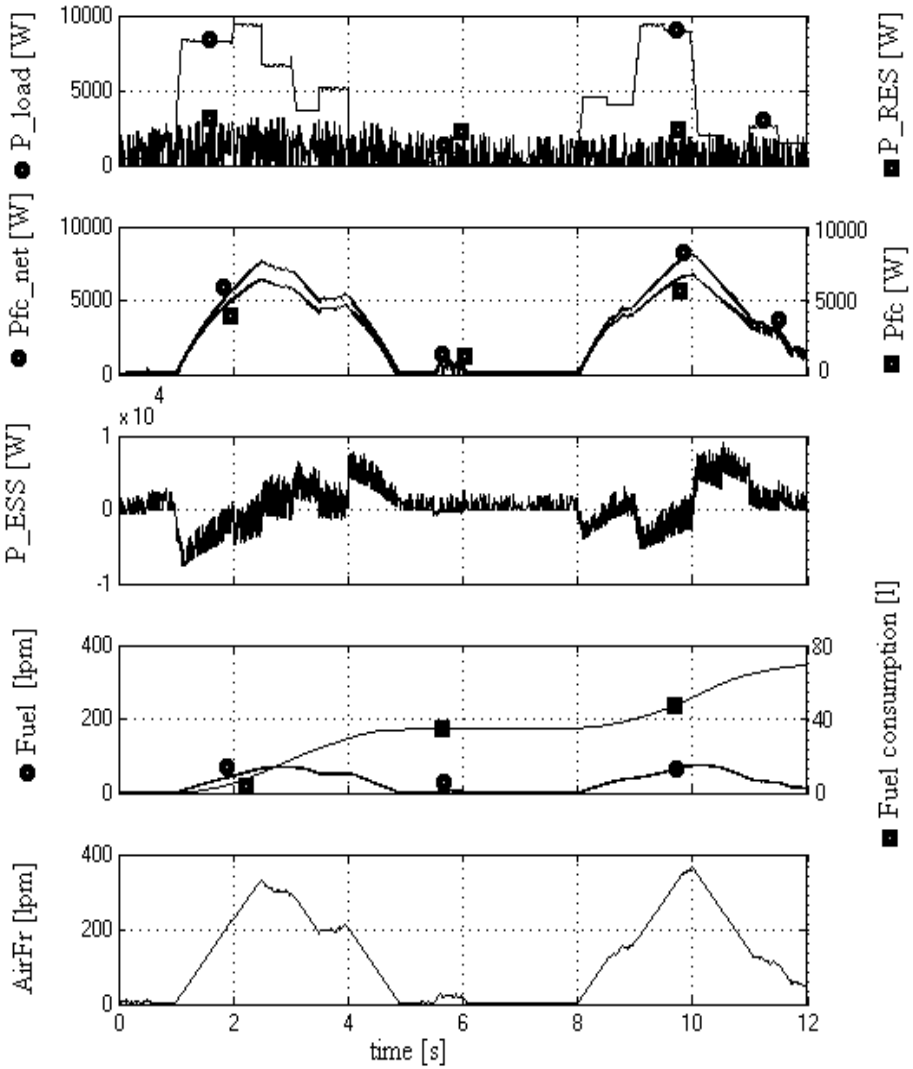

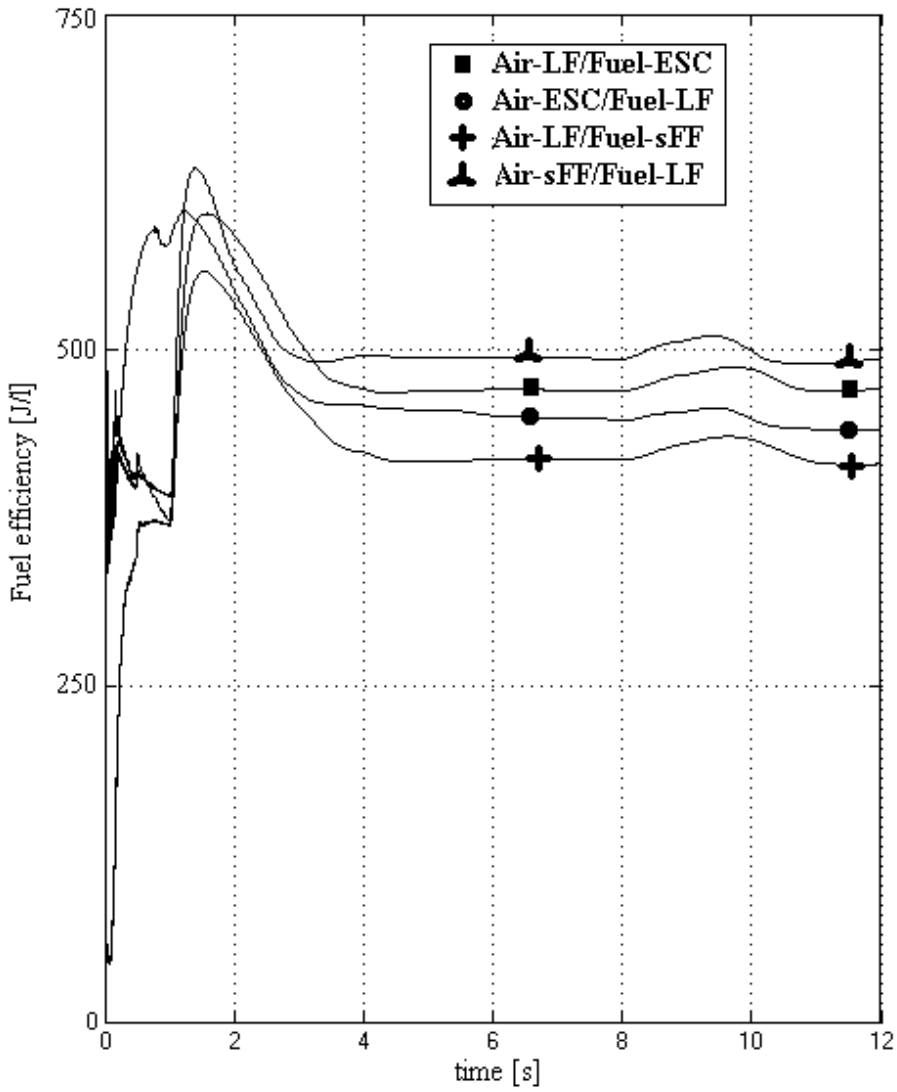

Fig. 32. The FC response for Air-LF/ Fuel-ESC EMU and fuel efficiency under variable load & RES

3.6. Conclusion

The main contributions of the analysis made in this section are the following:

(1) the Air-sFF/Fuel-LF control topology is more efficient that others control topologies analyzed under different load and RES power profiles (an increase of 3-5% of fuel efficiency indicator was observed in comparison with the Air-LF/Fuel-ESC control topology, which is the next control topology that ensure a high value of the fuel efficiency indicator);

(2) the fuel consumption is minimum for the Air-ESC/Fuel-LF control topology (the reduction of the fuel consumption value for the Air-ESC/ Fuel-LF control diagram in comparison with the minimum value obtained with other control diagrams depends by the load, being in range of 5-75%);

(3) both Air-LF/Fuel-ESC and Air-sFF/Fuel-LF control topologies are efficient for the FC HPS under pulsed loads;

(4) the Air-LF/Fuel-ESC control topology is efficient at FC rated power (an increase of 6.7% of fuel efficiency indicator was observed in comparison with the Air-sFF/Fuel-LF control topology, which is the next control topology that ensure a high value of the fuel efficiency indicator)

Finally, it may be concluded that the performances of the EMU strategy depend by the availability of the RES power, and level and dynamics of the load.

4. Global Maximum Power Point Tracking algorithms

4.1. Global Maximum Power Point (GMPP) algorithms

- The main objective of this section is to present an overview in the Global Maximum Power Point (GMPP) algorithms applied on power generated by the Photovoltaic (PV) arrays.
- Besides this survey on the GMPP algorithms proposed in last decade, the Perturbed-based Extremum Seeking Control (PESC) methods and their applications in PV arrays under Partially Shaded Conditions (PSCs) are investigated as well.
- The PESC schemes proposed to seek and track the GMPP of the PV power will be analyzed as performance obtained for the following indicators:
- the searching resolution,
- tracking accuracy,
- tracking efficiency,
- tracking speed,
- and percent of the hit count.

4. Global Maximum Power Point Tracking algorithms

4.1. Performance indicators

The searching resolution (R_S) is defined by:

$$R_S = \frac{\min_i \left| y_{GMPP} - y_{LMPPi} \right|}{y_{GMPP}} \cdot 100[\%]$$

The tracking accuracy (T_{acc}) is defined by:

$$T_{acc} = \frac{y_{PV}}{y_{GMPP}} \cdot 100[\%]$$

where y_{PV} is the PV power that is theoretically available and y_{GMPP} is the power extracted by the GMPP algorithm.

The number of iterations to locate the GMPP is a measure of the tracking speed. An iteration for the PESC-based GMPPT algorithms means a dither period (which is a step of scanning). Iteration can be defined for all GMPPT algorithms and it refers to the number of times the specific function of the algorithm is calculated, and this is related only to the method

4. Global Maximum Power Point Tracking algorithms

4.1. Performance indicators

The tracking efficiency (T_{eff}) is given by:

$$T_{eff} = \frac{\int_0^t y_{PV}\,dt}{\int_0^t y_{GMPP}\,dt} \cdot 100[\%]$$

The percent of the hit count (PHC) is defined by:

$$PHC = \frac{\text{number of positive results in finding the GMPP}}{\text{number of tests performed}} \cdot 100[\%]$$

The results obtained will be shown and commented as well. The performance of the PESC-based GMPPT algorithms will be compared with that of other GMPP algorithms proposed in the literature. Different PV and nonlinear multimodal patterns will be used to test the PESC-based GMPPT schemes. The results obtained under different PSCs simulated have shown a very good performance related to search speed and tracking accuracy of the PESC-based GMPPT algorithms.

4. Global Maximum Power Point Tracking algorithms

4.2. Asymptotic Perturbed Extremum Seeking Control (aPESC) scheme

- The first Asymptotic Perturbed Extremum Seeking Control (aPESC) scheme was proposed in [41] for GMPP search based on Scalar PESC (PESCs) scheme. The PESCs scheme and its Asymptotic variant (aPESCs) are shown in Figure 1 for switch in position (1) and (2).
- [41] Tan Y, Nešic D, Mareels I, Astolfi A. On global extremum seeking in the presence of local extrema. Automatica

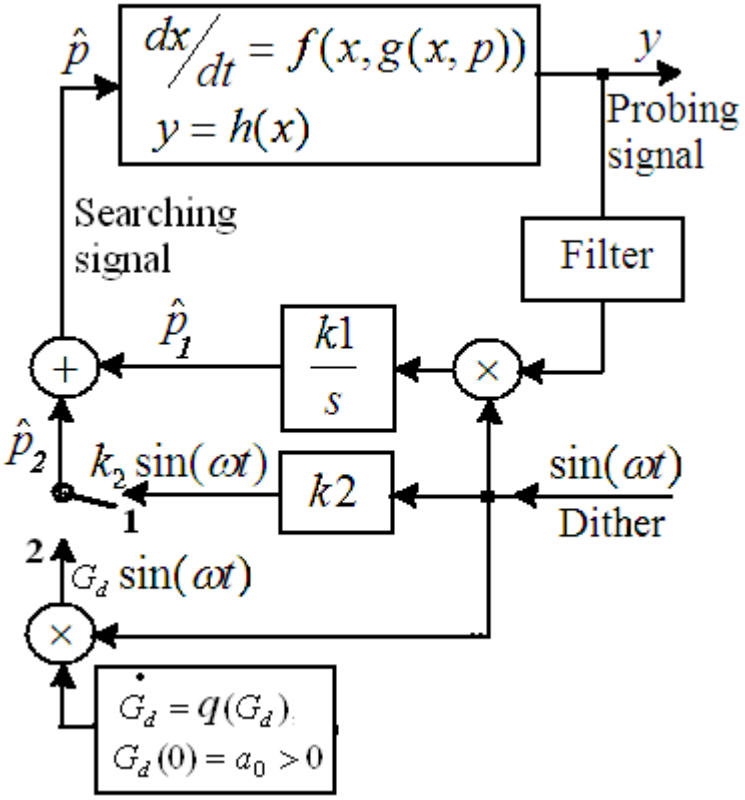

- Figure 1. The scalar PESC (PESCs) scheme and its asymptotic variant (aPESCs)

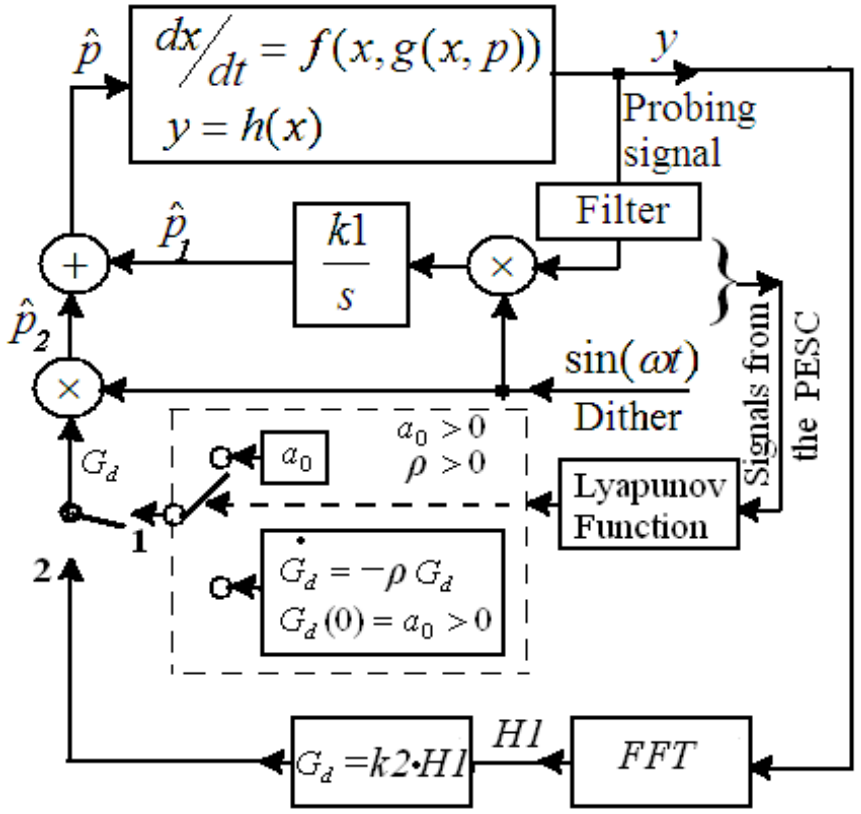

- Figure 2. The aPESC schemes based on (1) the Lyapunov function (aPESCLy) and (2) the H1 harmonic (aPESCH1)

4. Global Maximum Power Point Tracking algorithms

4.2. Asymptotic Perturbed Extremum Seeking Control (aPESC) scheme

- The tracking loop is the same for all aPESC schemes proposed in the literature and contains the following signal processing blocks of the process output ($y=y_{CC}+y_{AC}$): the filtering (of the CC value, y_{CC}), demodulation (product of the AC value, y_{AC}, with the dither signal), integration (of the demodulated signal), and amplification (with k_1). The filter can be of High-Pass Filter (HPF) type or Band-Pass Filter (BPF) type. The average value of the gradient for the tracking signal is given by:

$$\frac{d\overline{p}_1}{dt} = \frac{A^2 \cdot k_1}{2} \cdot \frac{dy}{dx} \overset{A=1}{\Rightarrow} \frac{d\overline{p}_1}{dt} = \frac{k_1}{2} \cdot \frac{dy}{dx}$$

- The sweeping signal (p2) can have different expressions depending on the asymptotic function chosen to modulate the dither:
- - The asymptotic function is based on an exponential implementation [41];
- - The asymptotic function is obtained through commutation between constant and exponential amplitude of dither based on the Lyapunov switching function [44];
- - The asymptotic function is based on the magnitude of first harmonic (H1) of the process output, which is obtained with Fast Fourier Transform (FFT)

- [44] Moura SJ, Chang YA. Lyapunov-based switched extremum seeking for photovoltaic power maximization. Control Eng Pract 2013;21(7):971–80.

4. Global Maximum Power Point Tracking algorithms

4.3. Proposed Global aPESC schemes

The H1 magnitude of the process output can be approximated by a using a BPF2 centered on the first harmonic, a derivative operator, or the BPF1 (see Figure 3). Thus the following variants of the aPESCH1 scheme can be obtained in order to be tested for GMPP search:

- (1) the GaPESC scheme based on the BPF1,
- (2) the GaPESCbpf scheme based on the BPF2,
- (3) the GaPESCH1 scheme based on the H1 magnitude computed with the FFT, and
- (4) the GaPESCd scheme based on the derivative operator.

- If the BPF2 is designed to approximate the H1 magnitude, then the behavior of both GaPESCbpf and GaPESCH1 schemes are almost the same. So, only GaPESCH1 scheme will be considered below.

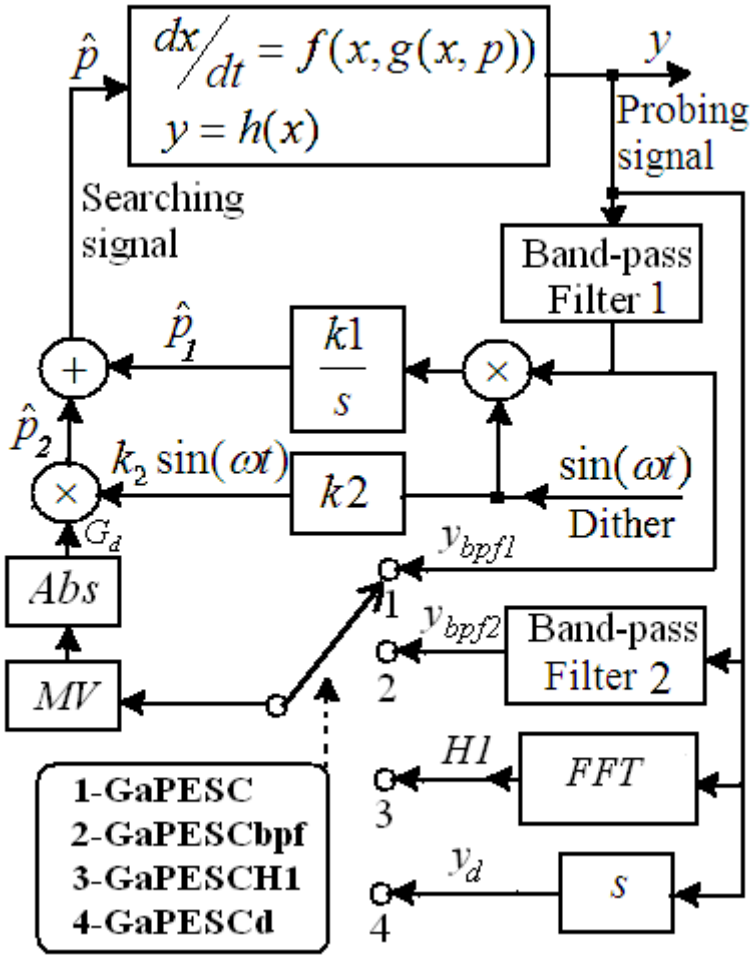

- Figure 3. The aPESC schemes

4. Global Maximum Power Point Tracking algorithms

4.4. GaPESC scheme

Figure 4. The diagram of the GaPESC scheme

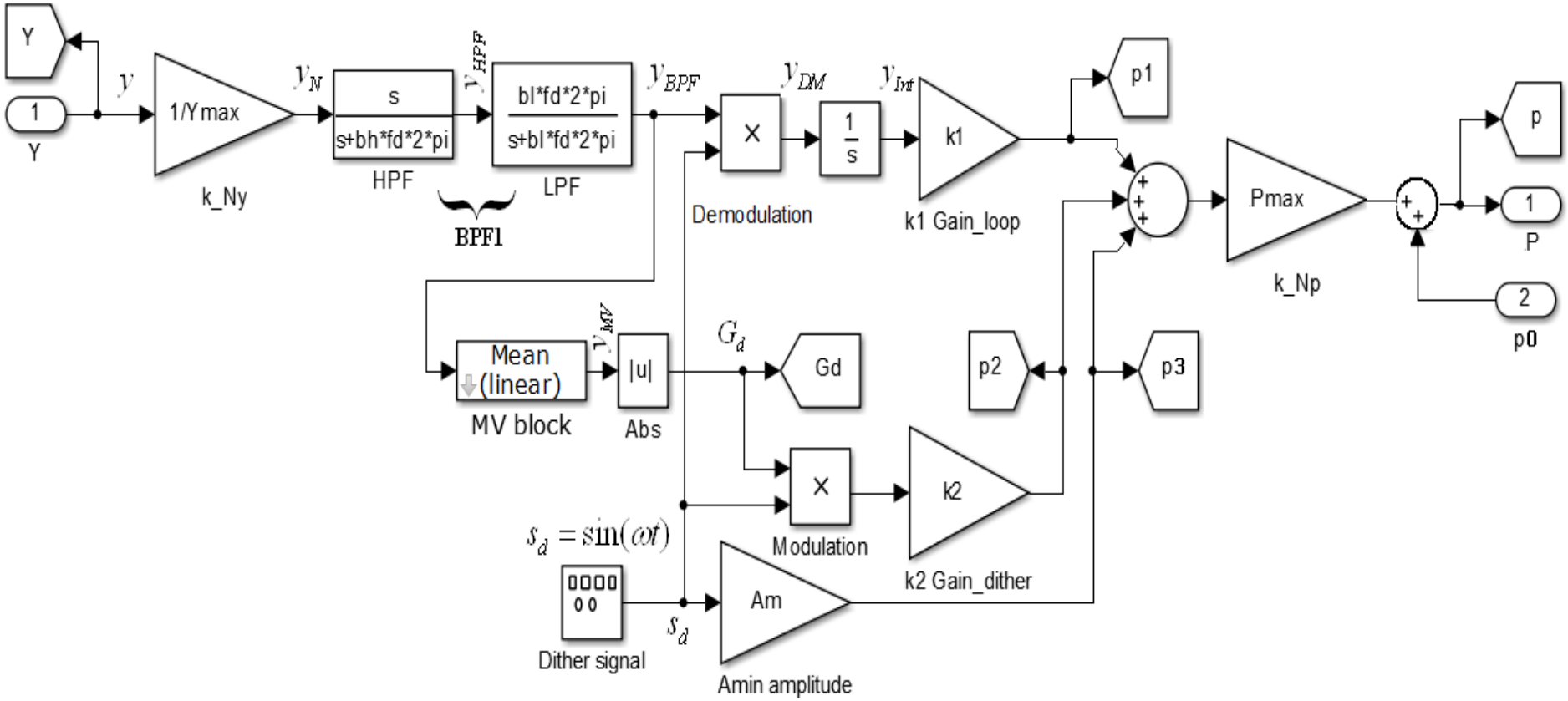

Request permission from the copyright holder for the use of any part from this presentation

4. Global Maximum Power Point Tracking algorithms

4.4. GaPESC scheme parameters

The parameters used in simulation are the following:

- the dither frequency is $f_d=1/T_d=\omega/2\pi=100$ Hz;
- the dither amplitude is set to 1;
- the cut-off frequency of the HPF1, $f_{h1}=\beta_{h1}\cdot f_d$, where $\beta_{h1}=0.1$;
- the cut-off frequency of the LPF1, $f_{l1}=\beta_{l1}\cdot f_d$, where $\beta_{l1}=1.9$ in order to approximate the H1 amplitude [40];
- the cut-off frequency of the HPF2, $f_{h2}=\beta_{h2}\cdot f_d$, where $\beta_{h2}=0.5$;
- the cut-off frequency of the LPF2, $f_{l2}=\beta_{l2}\cdot f_d$, where $\beta_{l2}=5.5$ in order to increase the dither persistence on the control loop [46];
- the minimum amplitude of dither, A_m, is set to 0.001, but can be smaller that this value in order to obtain a very low ripple on the probing signal during the stationary phases;
- the normalization gains, $k_{Ny}\cong 1/y_N$ and $k_{Np}\cong p_N$, where the p_N value sets the initial amplitude of the dither and the y_N value is chosen in the range of maximum and maximum values estimated for the GMPP on the nonlinear map, $y=h(p)$; $k_{Ny}=k_{Np}=1$ for the nonlinear map (6); note that '$\cong$' means in a large range around the mentioned value;
- the gain of the dither amplitude, $k_2\cong\Delta p$, where $\Delta p=|p_{GMPP}-p_0|$, and p_0 is the initial value for starting the search of the p_{GMPP}; $k_2=3$ for the nonlinear map (6);
- the loop gain, $k_1=\gamma_{sd}\cdot\omega$, where $\gamma_{sd}=1.5$ was set based on the dynamic performance analysis shown below.

4. Global Maximum Power Point Tracking algorithms

4.5. GMPP search based on the GaPESC scheme

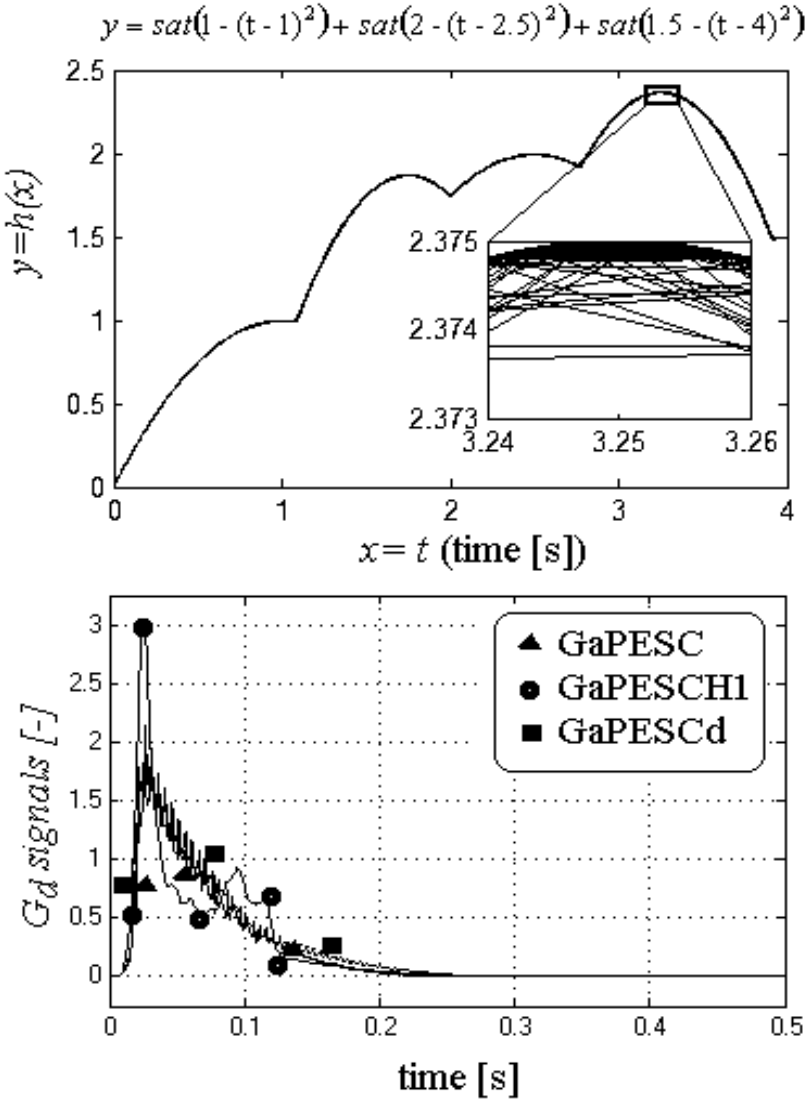

Figure 4. The G_d signals during the GMPP search based on the GaPESC scheme

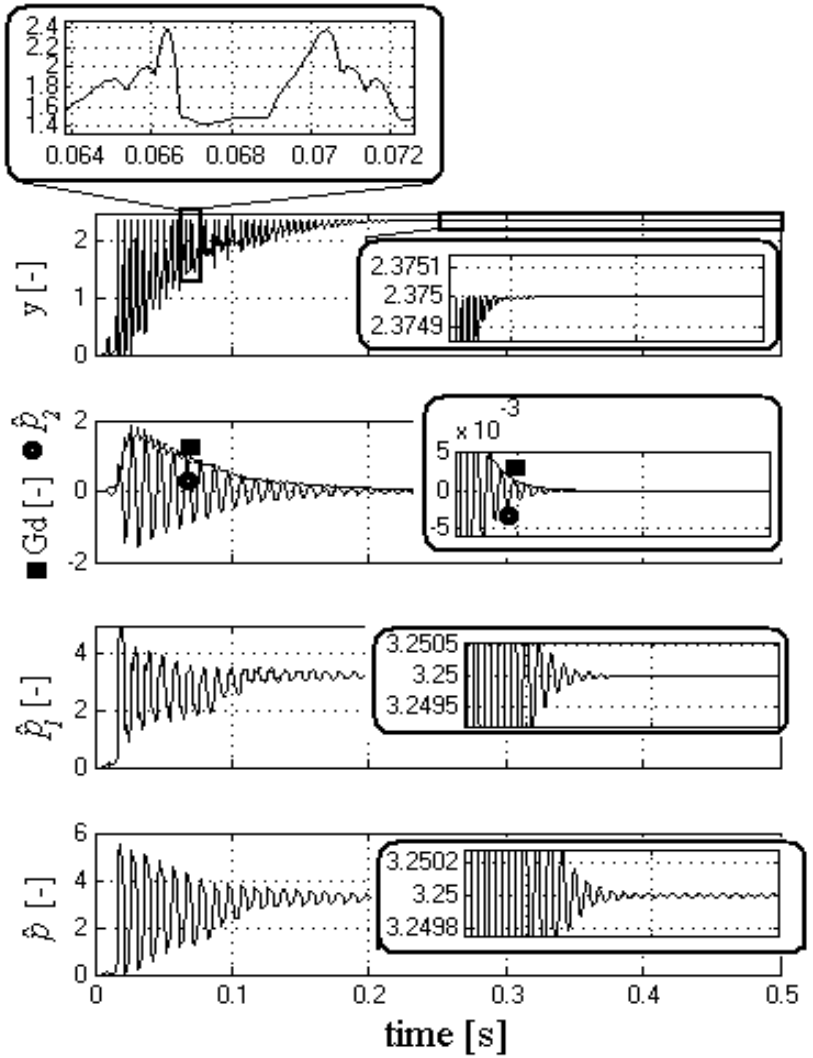

Figure 5. The GMPP search based on the GaPESC scheme

4. Global Maximum Power Point Tracking algorithms

4.6. The PV characteristics for PV arrays under Partial Shading Condition (PSC)

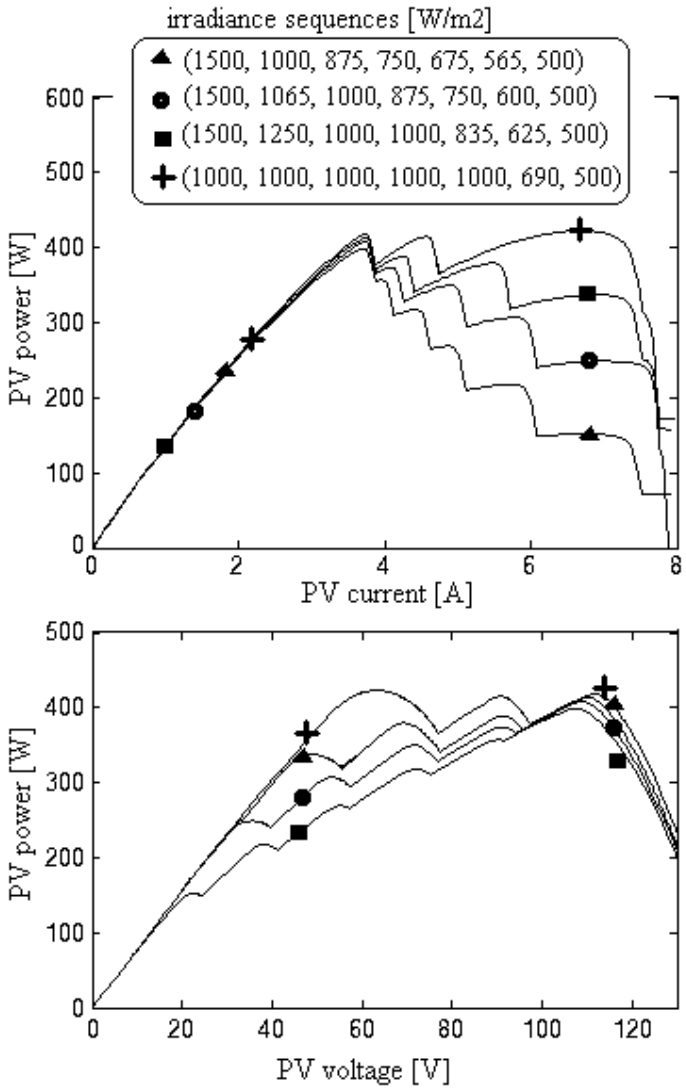

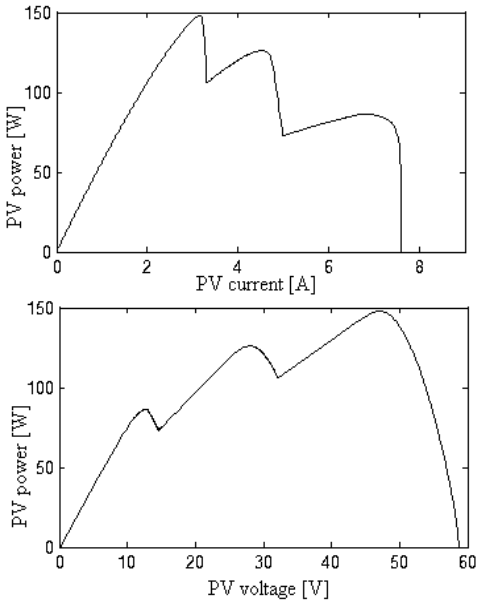

- PV characteristics for the 1Px3S PV array

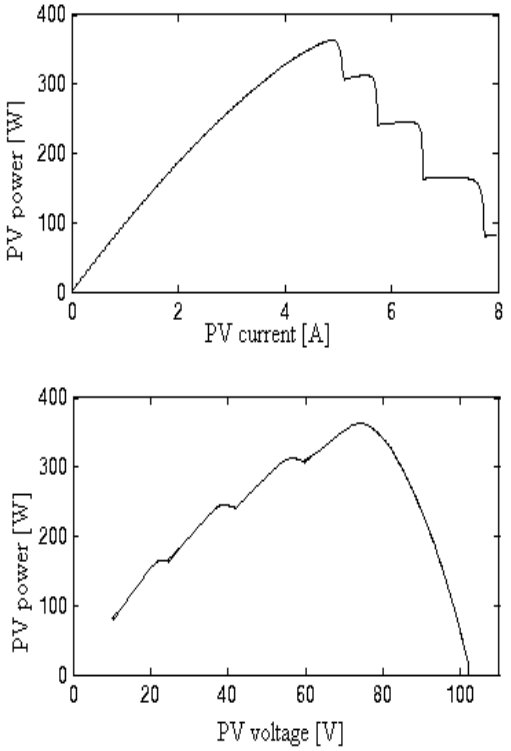

- PV characteristics for the 1Px5S PV array

Figure 6. The PV characteristics for the 1Px7S PV array under different irradiance sequences

4. Global Maximum Power Point Tracking algorithms

4.7. GMPP search under PSC based on the GaPESC scheme

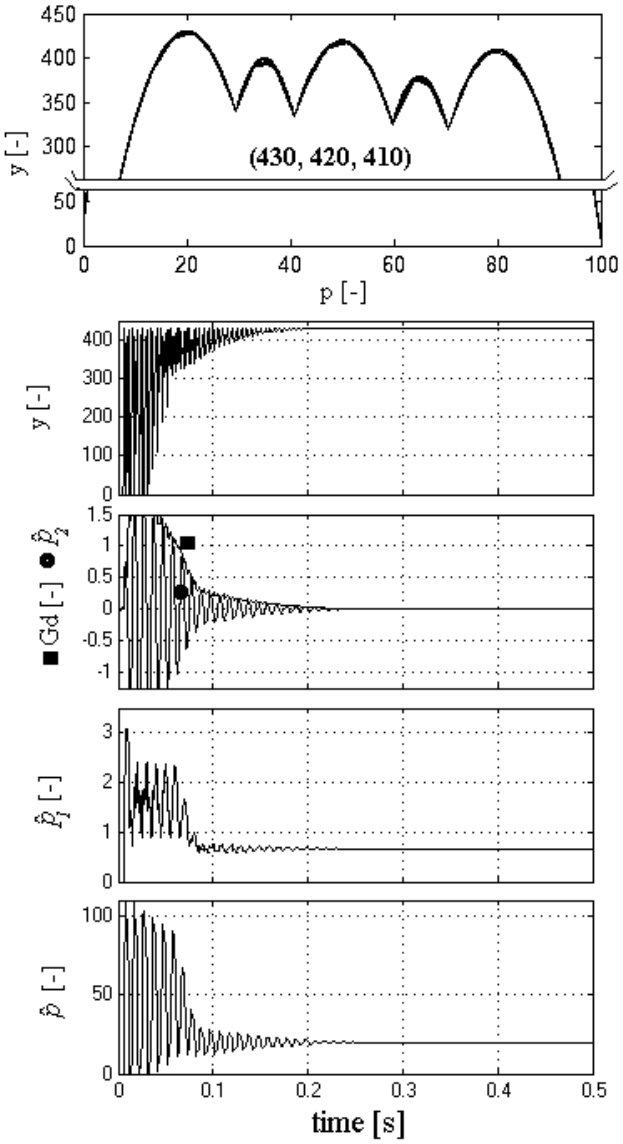

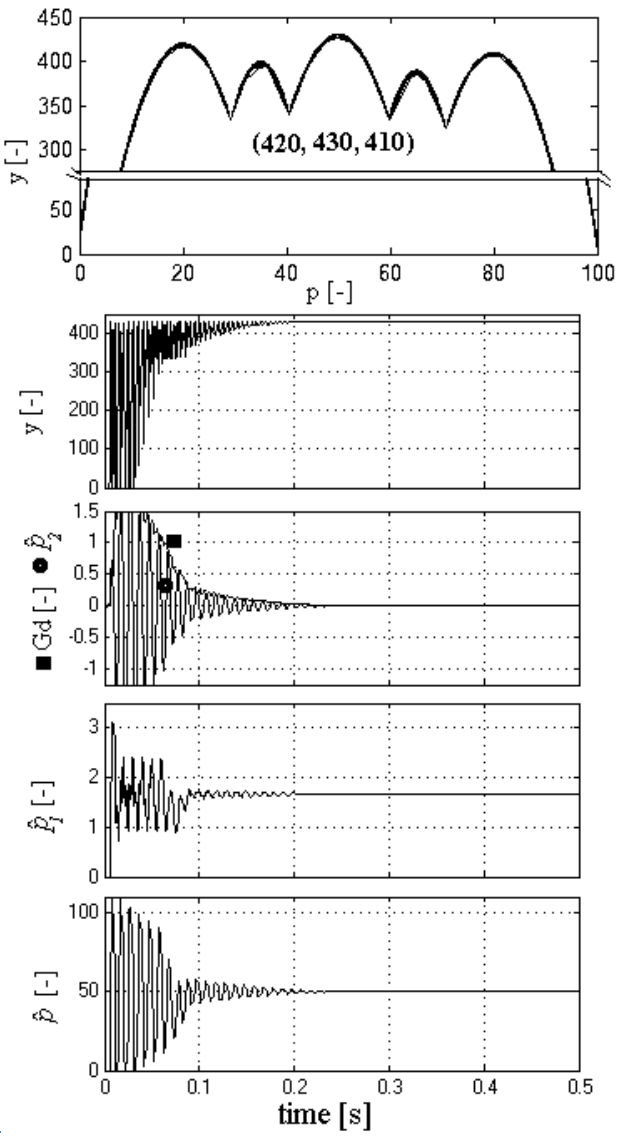

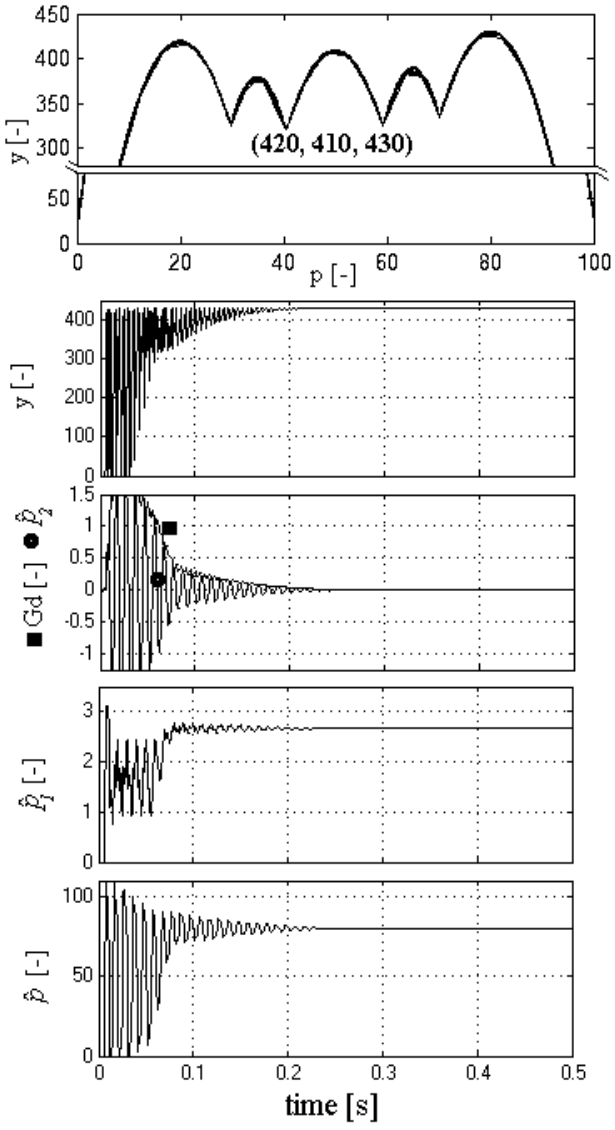

Request permission from the copyright holder for the use of any part from this presentation

4. Global Maximum Power Point Tracking algorithms

4.8. The resolution of GMPP searching

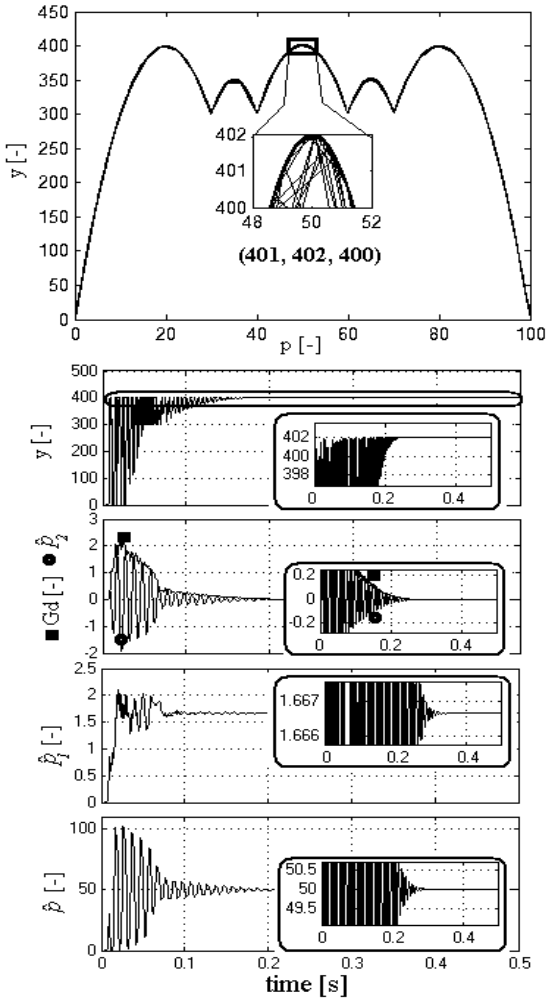

GaPESC scheme

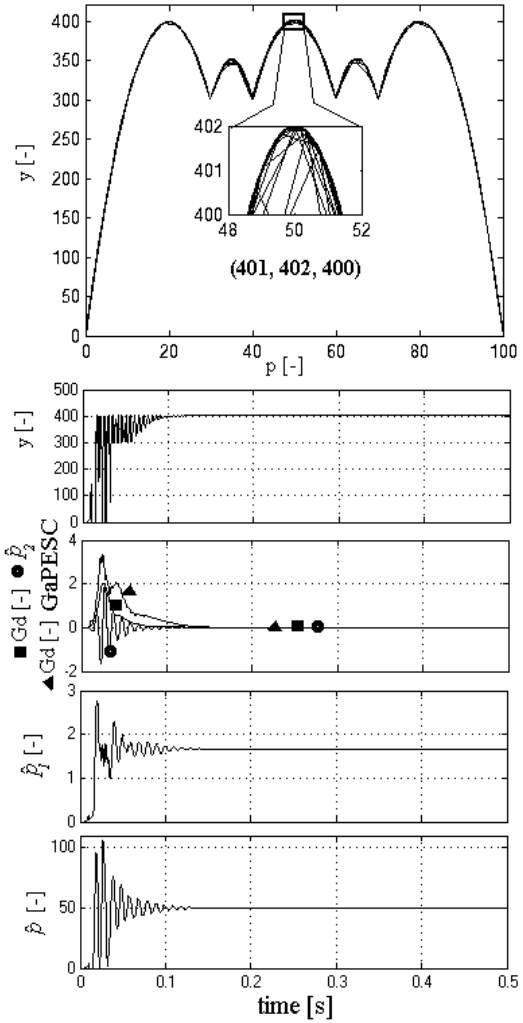

GaPESCH1 scheme

Request permission from the copyright holder for the use of any part from this presentation

4. Global Maximum Power Point Tracking algorithms

4.9. GMPP search under dynamic PSC based on the GaPESC scheme

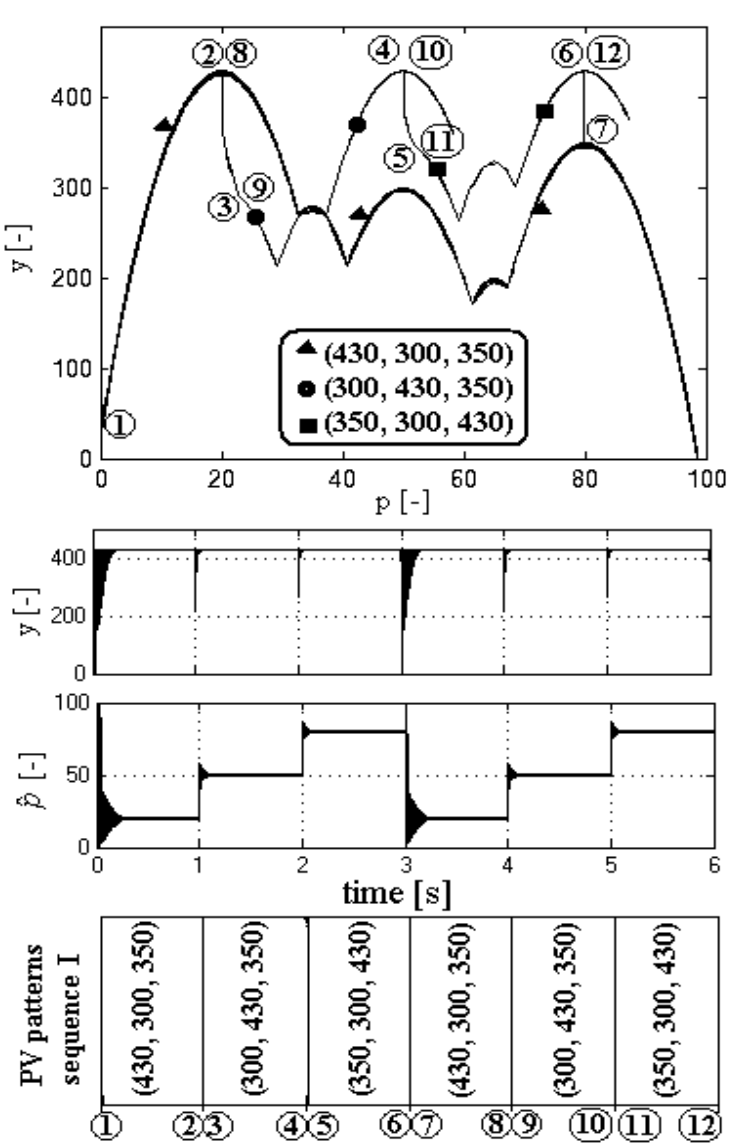

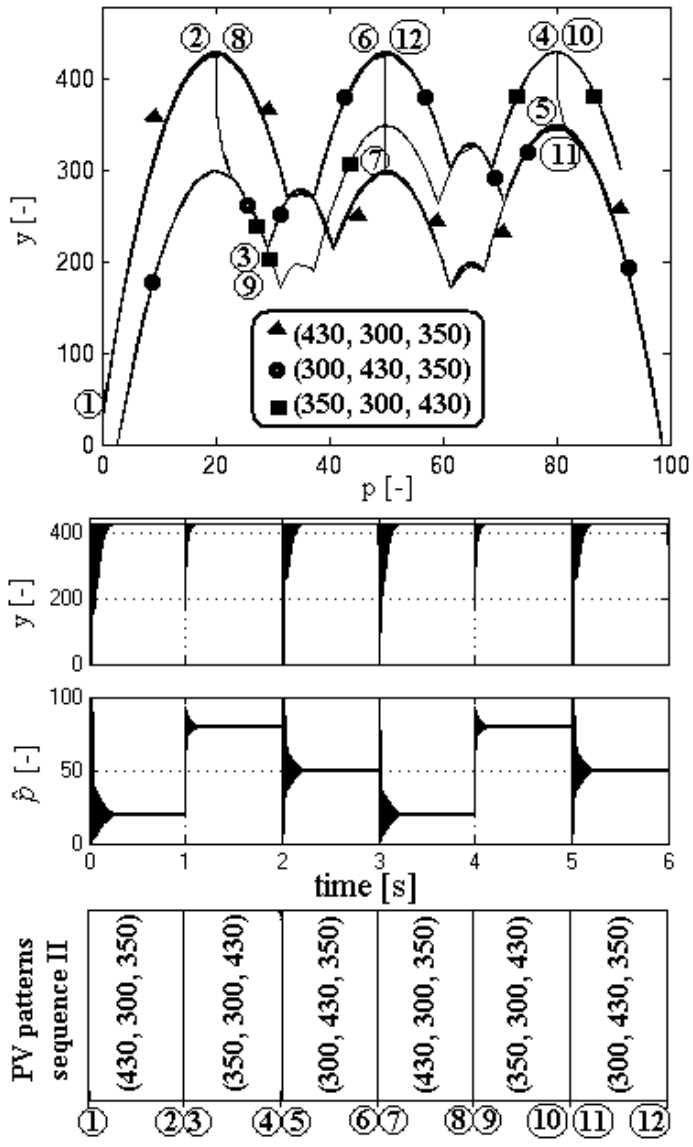

4. Global Maximum Power Point Tracking algorithms

4.10. GMPP search under noisy PSC based on the GaPESC scheme

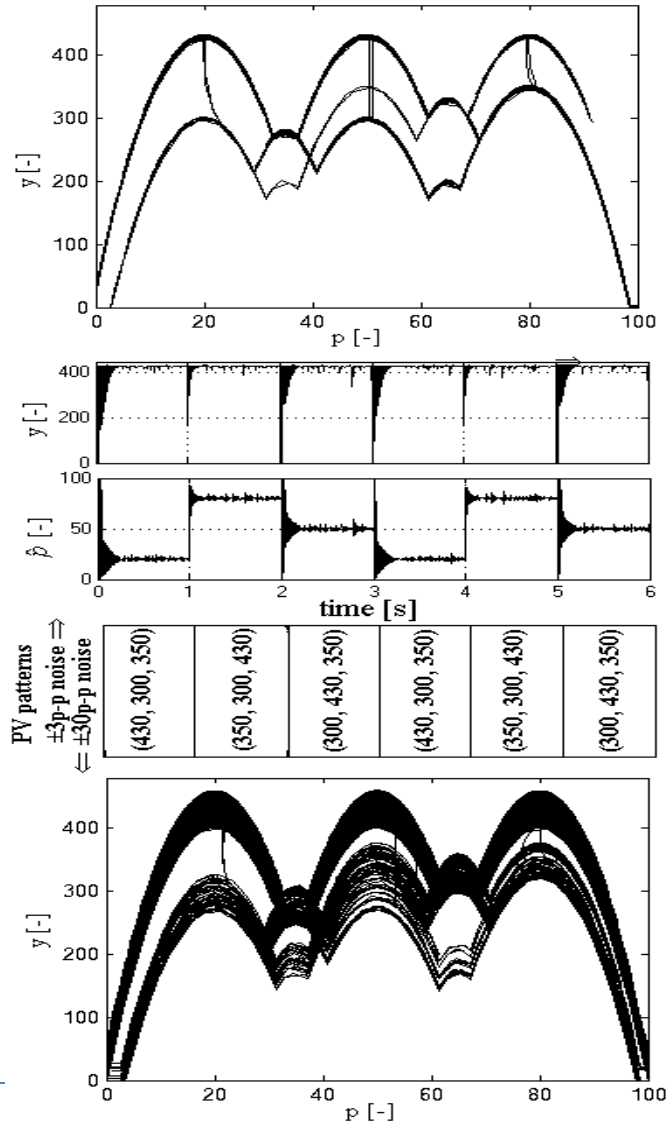

4. Global Maximum Power Point Tracking algorithms

4.11. Conclusions

- The maximum, minimum and average value of the tracking accuracy reported for GaPESC scheme is of 99.99%, 99.95% and 99.97%
- The tracking efficiency of 99.97%
- The resolution of all schemes is lower than 0.25% (≅1/402).
- The robustness of the GMPP searching was tested for two PV patterns' sequences
- Each time the GMPP of the PV pattern from the noiselessly sequence was accurately tracked.
- The level of GMPP of the PV pattern from the noisy sequence is changed randomly at each 10 milliseconds. Therefore, the GaPESC scheme searches continuously the current GMPP.
- Based on the performance shown and its simplicity of implementation, the GaPESC scheme is competitive with similar techniques to scan the GMPP or other advanced GMPP algorithms proposed.
- Furthermore, the tuning ranges for the design parameters are relatively large because the GaPESC scheme is based on adaptive control of ESC type.

4. Global Maximum Power Point Tracking algorithms

References

1. N. Bizon, E. Kurt. Performance Analysis Of The Tracking Of The Global Extreme On Multimodal Patterns using the Asymptotic Perturbed Extremum Seeking Control Scheme, International Journal of Hydrogen Energy 2017; 42(28):17645-54, Impact Factor: 3.205
2. N. Bizon, P. Thounthong, M. Raducu, L.M. Constantinescu. Designing and Modelling of the Asymptotic Perturbed Extremum Seeking Control Scheme for Tracking the Global Extreme. International Journal of Hydrogen Energy 2017 42(28):17632-44.
3. N. Bizon, Global Maximum Power Point Tracking (GMPPT) of Photovoltaic array using the Extremum Seeking Control (ESC): A review and a new GMPPT ESC scheme, Renewable & Sustainable Energy Reviews 57 (may 2016), 524–539, WOS:000370456000041, Impact Factor: 5.901; doi:10.1016/j.rser.2015.12.221
5. N. Bizon, Global Extremum Seeking Control of the Power Generated by a Photovoltaic Array under Partially Shaded Conditions, Energy Conversion and Management 109 71-85 (2016), Impact Factor: 4.380 WOS:000369453600007 http://dx.doi.org/10.1016/j.enconman.2015.11.046
6. N. Bizon, Global Maximum Power Point Tracking based on new Extremum Seeking Control scheme, Progress in Photovoltaics: Research and Applications 2016;24(5):600-22. DOI: 10.1002/pip.2700, Impact Factor: 7.584; http://onlinelibrary.wiley.com/doi/10.1002/pip.2700/full WOS:000373624100002

Summarizing, the research directions in field of the RES/FC HPS that are approached in the studies mentioned above are the following:

• The RES need advanced control techniques to harvest all power available, operating the RES close to MPP. This control is mandatory due to poor efficiency of solar PV, which is the main impediment in encouraging its use until the PV technology will be improved.

• The power losses in power interfaces have been substantially reduced using advanced topologies, switches and appropriate control scheme, eventually integrated in multiport power converter structure. In general, the energy efficiency of power converters used in HPS is higher than 95%.

• The hybrid batteries/ultracapacitors ESS is used in HPS to ensure the power flow balance on the DC bus, but their life-cycle need to be improved through innovative technologies, too. The CS mode proposed here for the ESS can improve the life-cycle of the batteries stack, besides other advantages such as reduced size and low costs of the ESS.

• The cost reduction could be an incentive for the producers of HPS to implement such systems that will ensure decreasing of the payback time for the capital invested.

Summarizing,

• The hydrogen technology (to generate and store hydrogen) is still a costly and unsafe technology. So, alternative technologies based on fuel reformers are developed at low cost. Furthermore, the PEMFC system must be operated at the MEP to increase the energy efficiency of the entire RES/FC HPS, as it is proposed here.

• These standalone RES/FC HPSs based on EMU strategies must to predict the RES power available or be adaptable to RES power fluctuations to sustain any unpredictable load demand. The LF control proposed here could be o solution, because it is very simple to be implemented in the commercial RES/FC HPS, requesting only software upgrade and few circuits reconfiguration.

• The protection issue, especially for use of PEMFC system and batteries stack from the ESS, are identified and implemented in EMU of the commercial RES/FC HPS. The proposed protection measures are also implemented in simulation diagram shown here, but this issue was not extensively studied, being outside of the scope of this presentation.

Thank you for your attention
Questions...

Erasmus+ PROGRAMME,

KEY ACTION: Cooperation for innovation and the exchange of good practices,

ACTION: Strategic Partnerships

FIELD: Strategic Partnerships for higher education, CALL: 2015

INNOVATIVE EUROPEAN STUDIES ON RENEWABLE ENERGY SYSTEMS

2015-1-TR01-KA203-021342

Real-time optimization of the Renewable Energy Sources / Fuel Cell Hybrid Power Systems

Nicu BIZON
University of Pitesti, Pitesti, Romania

Summary of Part 5 – Real-time Optimization of FC / Renewable HPS

1. REAL-TIME OPTIMIZATION (RTO) based on EXTREMUM SEEKING (ES) CONTROL algorithm
2. RTO Strategy for Fuel Cell Hybrid Power Sources with Load-Following (LF) control of the Fuel or Air Flow Rates
3. RTO Strategy for Fuel Cell Hybrid Power Sources with ES control and LF control of the Fuel and Air Flow Rates
4. RTO Strategy for Fuel Cell / Wind Turbine Hybrid Power System under Turbulent Wind Gusts and Variable Load
5. RTO Strategy for Fuel Cell Hybrid Power Sources with ES control of the both Fuel and Air Flow Rates
6. Conclusions

Real-time Optimization of FC / Renewable HPS

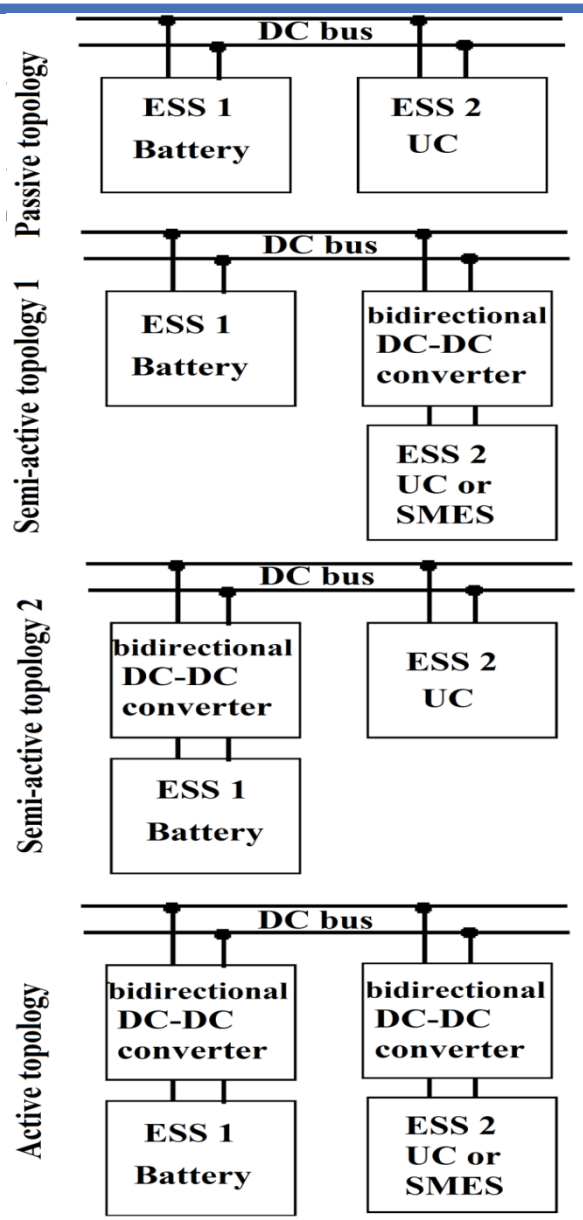

ESS topologies

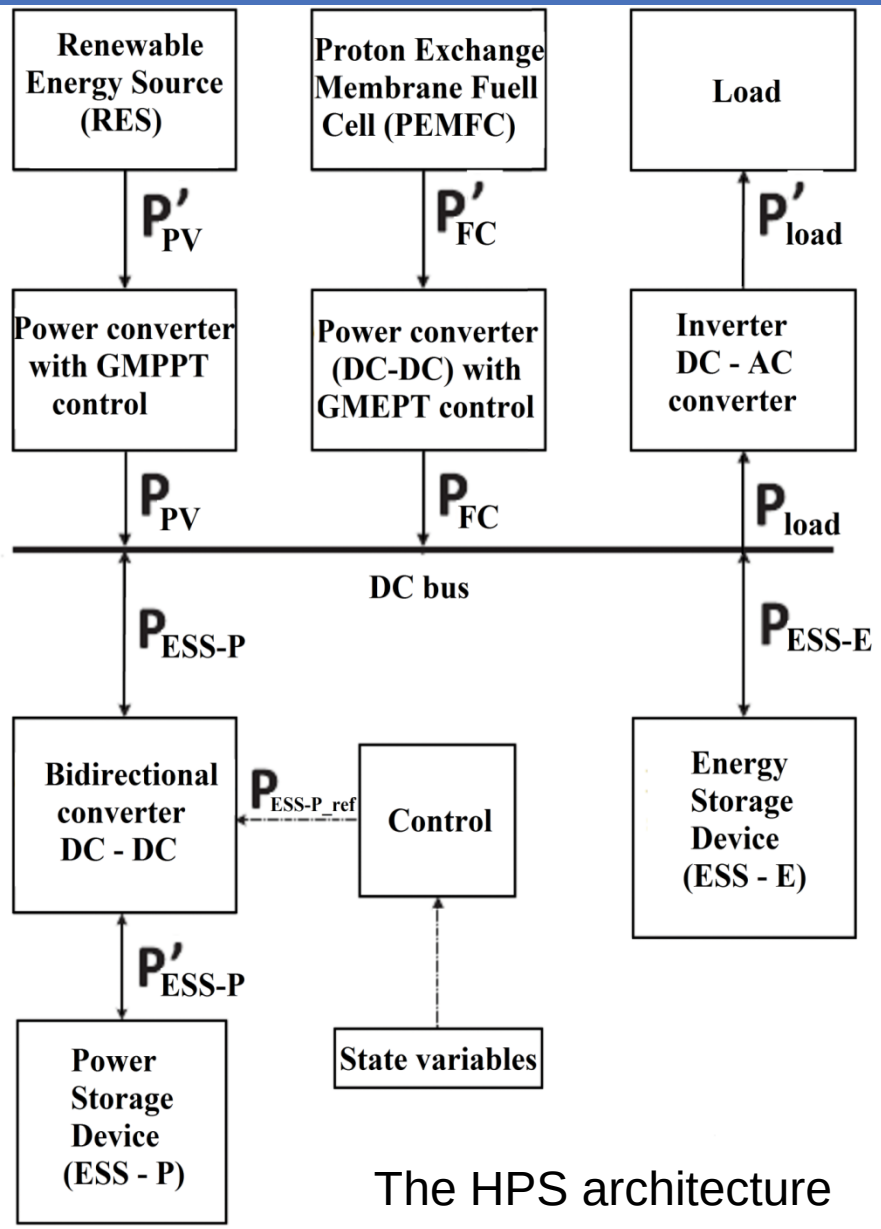

The HPS architecture

with semi-active ESS topology 1

Real-time Optimization of FC / Renewable HPS

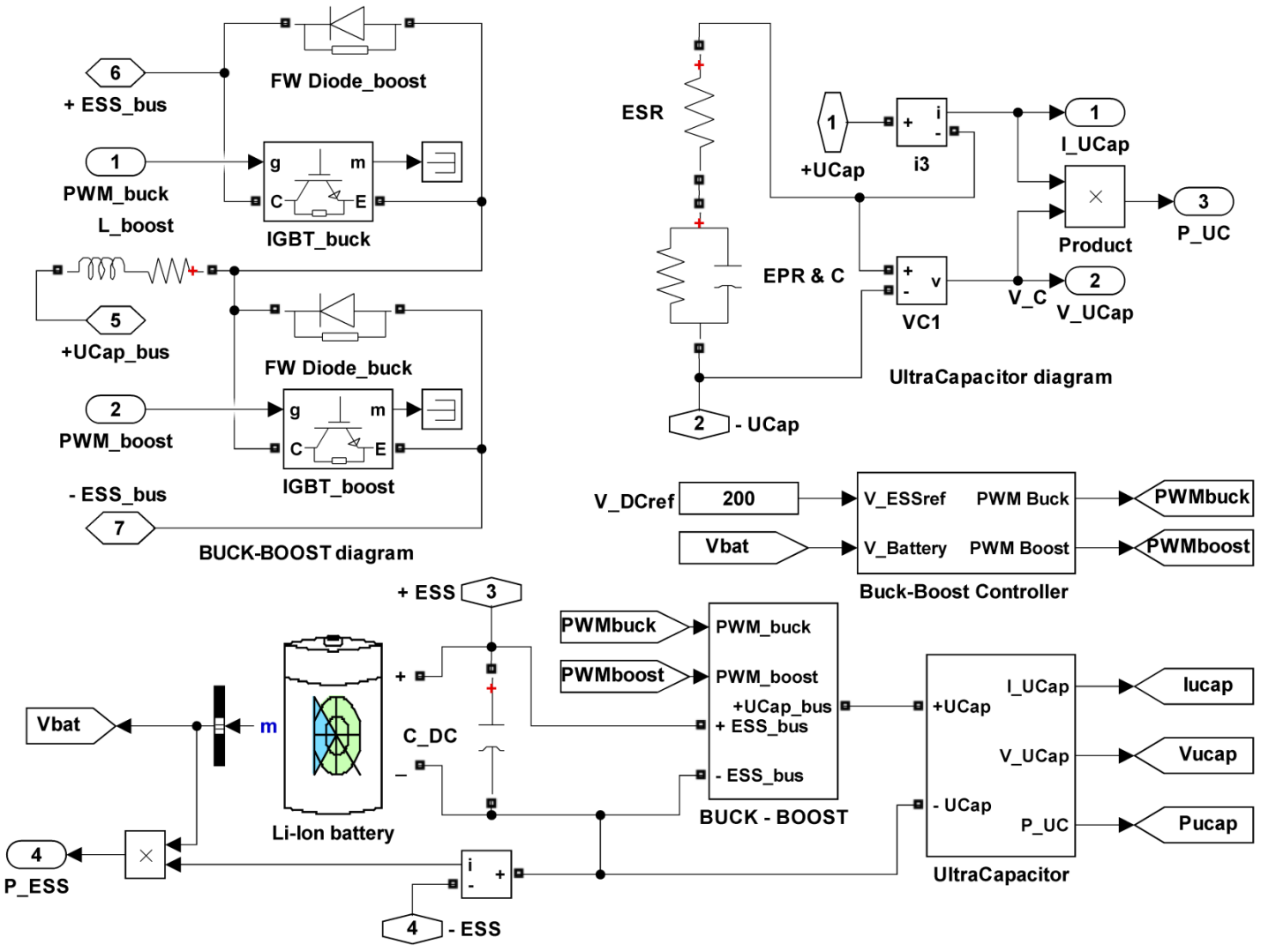

The diagram of the hybrid ESS

Real-time Optimization of FC / Renewable HPS

$$I_L^M = N_p I_L$$
$$I_0^M = N_p I_0$$
$$V_3 = N_s V_2$$
$$I_3 = N_p I_2$$
$$R_s^M = R_s \frac{N_s}{N_p}$$
$$R_p^M = R_p \frac{N_s}{N_p}$$

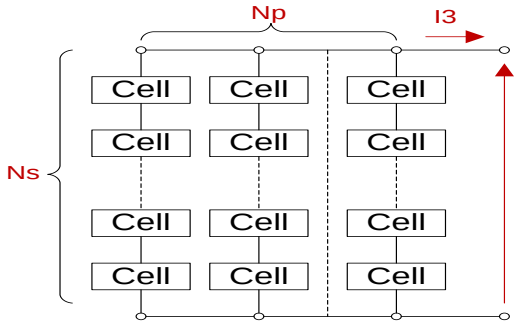

$$I_3 = I_L^M - I_0^M \left(e^{\left(V_3 + I_3 R_s^M\right) / N_s V_T} - 1 \right) - \frac{V_3 + I_3 R_s^M}{R_p^M}$$

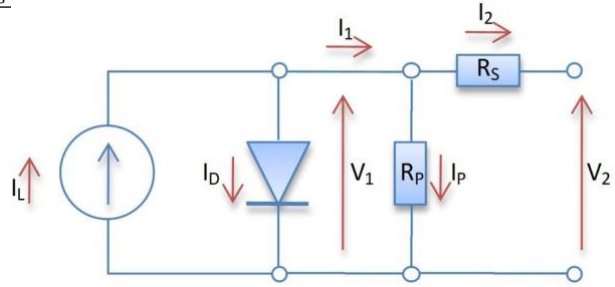

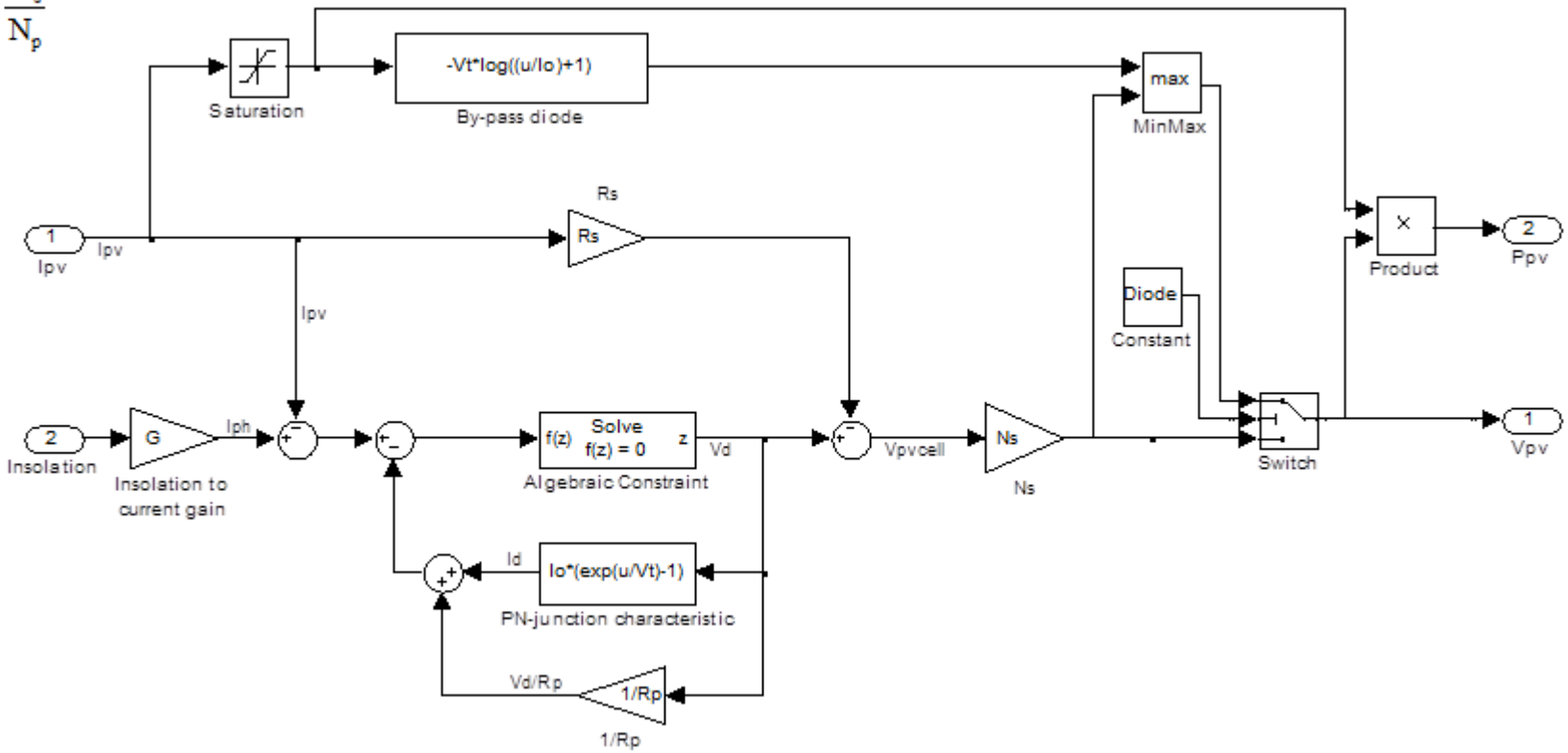

Real-time Optimization of FC / Renewable HPS

$$P_m = c_p(\lambda,\beta)\frac{\rho A}{2}v_{wind}^3 \qquad c_p(\lambda,\beta) = c_1\cdot\left(\frac{c_2}{\lambda_i} - c_3\beta - c_4\right)\cdot\exp\left(-\frac{c_5}{\lambda_i}\right) + c_6\lambda \qquad \frac{1}{\lambda_i} = \frac{1}{\lambda + 0.08\beta} - \frac{0.035}{\beta^3 + 1}$$

$$T_m = \frac{P_m}{\omega_m} \qquad P_{m(pu)} = k_p \cdot c_{p(pu)}(\lambda,\beta)\cdot v_{wind(pu)}^3 \qquad \lambda = \frac{R\omega_m}{v_w}$$

where c_p is WT performance coefficient, ρ is air density (kg/m^3), A=πR^2 is WT swept area (m^2), R is radius of the turbine blade, λ is tip - speed ratio (TST), β is the blade pitch angle (degree), and k_p is the power gain (k_p=0.73, c_1=0.5176, c_2=116, c_3=0.4, c_4=5, c_5=21, and c_6=0.0068 for WT model used (P_m=1500 W, the base power of the electrical generator is 1.5/0.9 MVA, and base wind speed is 12 m/s) and the *pu* values are obtained through normalization of current values to base values)

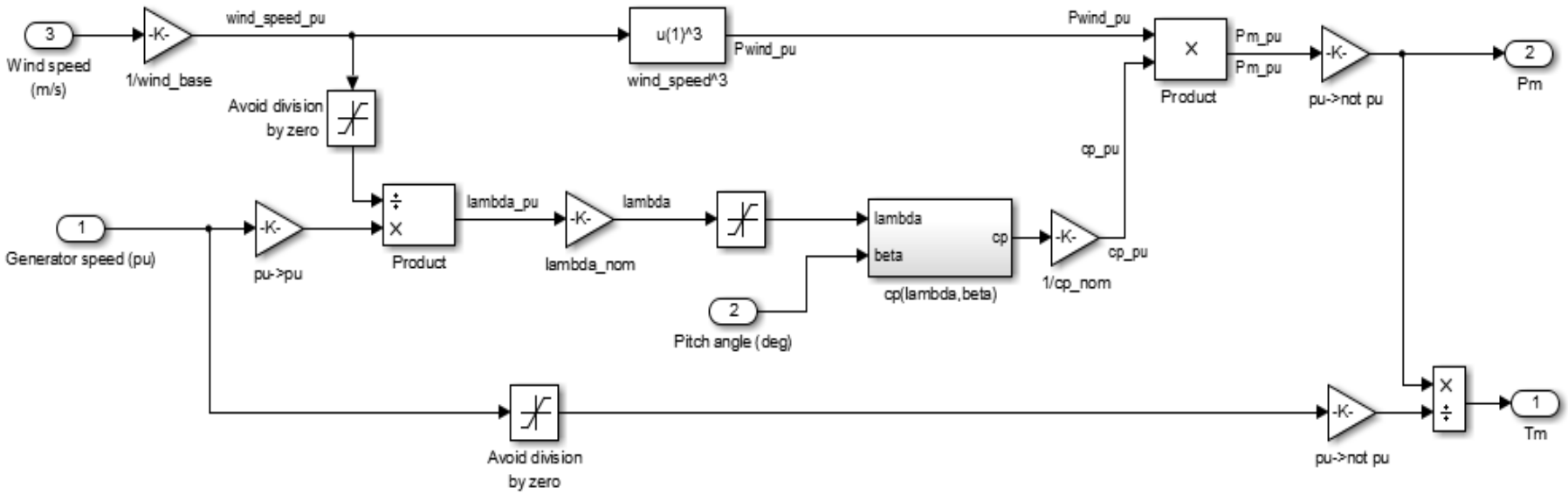

Real-time Optimization of FC / Renewable HPS

The Real-Time Optimization (RTO) strategies are proposed to efficiently operate different nonlinear energy systems such as the mixed heating systems and photovoltaic arrays.

The RTO strategies were recently proposed to increase the fuel economy of the Fuel Cell Hybrid Power Sources (FCHPS), which can also improve their cost, durability and reliability. The RTO strategies must to assure the operation of FCHPS at maximum power efficiency based on efficient control of power flows from renewable energy sources.

As it is known, the RTO strategies can be based on optimization's rules (the rule-based strategies) or optimization's functions.

For example, the tracking efficiencies of 99.60%, 99.41%, and 99.28%, and the tracking times of 12 ms, 33 s, and 25 s are reported for systems of photovoltaic (PV) panels, fuel cell (FC) stacks, and wind turbines (WT).

The deterministic rule-based strategies are of sub-optimal type and cannot guarantee that the optimal solution (the GMP) will be always found. But these strategies are the easiest to be implemented, so these are already available in the market.

On the other hand, even if the optimization-based strategies are difficult to be implemented, the recent RTO applications for FC vehicle (FCV) request advanced RTO strategies because the GMP must be found in any operating condition requested.

Real-time Optimization of FC / Renewable HPS

RTO strategies are based on:

I. the Equivalent Consumption Minimization Strategy (ECMS)
II. the intelligent algorithms
III. the Model Predictive Control (MPC)
IV. the hybrid techniques using

- the wavelet-fuzzy logic control
- the robust-adaptive sliding mode control
- the combinatorial optimisation approach
- the multi-scheme method
- double layer metaheuristic technique
- and so on

The ECMS is most known RTO strategy used for FCHPS considering

- the Pontryagin's Minimum Principle (PMP) or
- Dynamic Programming (DP).

The RTO strategies based on the Extremum Seeking (ES) algorithms have been proposed recently for FCHPS and FC vehicles.

The optimization function (J) is defined as mix of FC net power (P_{FCnet}) and Fuel Consumption Efficiency ($Fuel_{eff}$) using the weighting coefficients k_{net} and k_{fuel} :

$$J(x_1, x_2) = k_{net} P_{FCnet} + k_{fuel} Fuel_{eff}$$

Real-time Optimization of FC / Renewable HPS

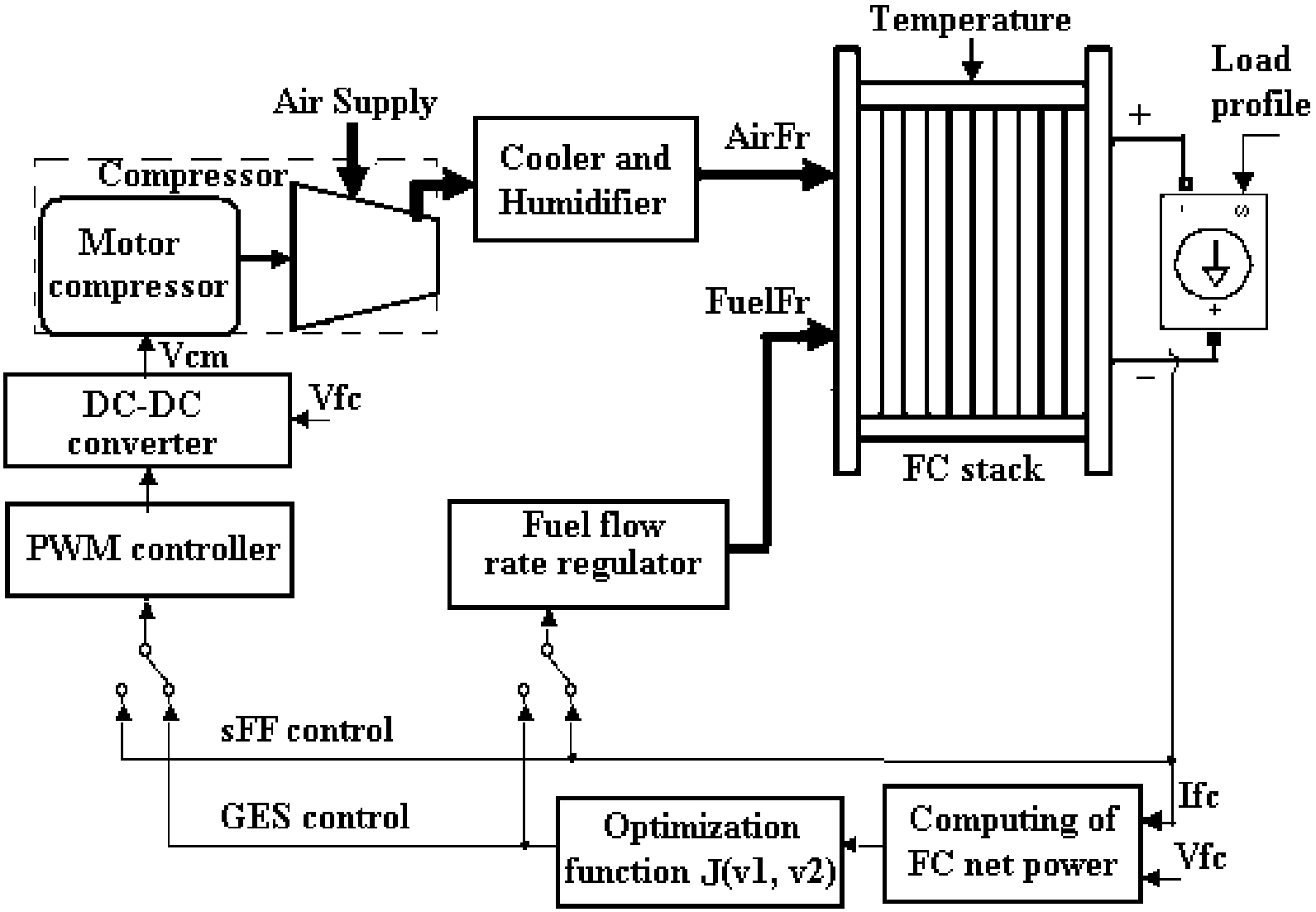

The PEMFC system

Real-time Optimization of FC / Renewable HPS

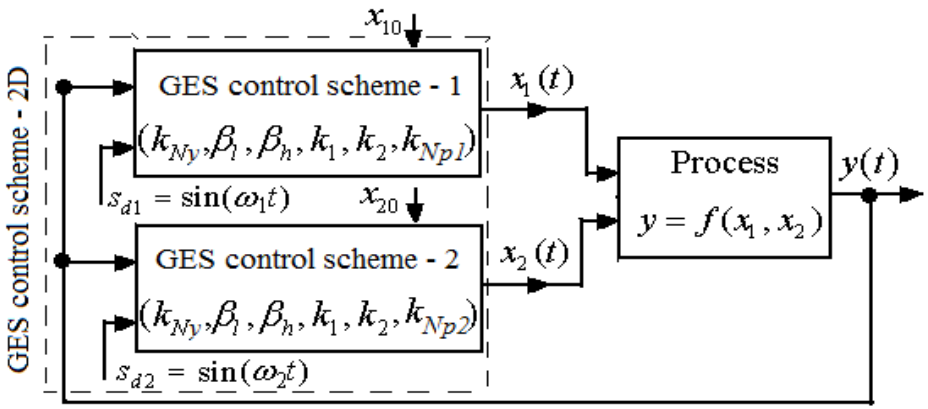

The Global ES control scheme – 2D

Searching of the Extreme Points on Photovoltaic Patterns using a new Asymptotic Perturbed Extremum Seeking Control scheme. Energy Conversion and Management 2017;144:286–302;

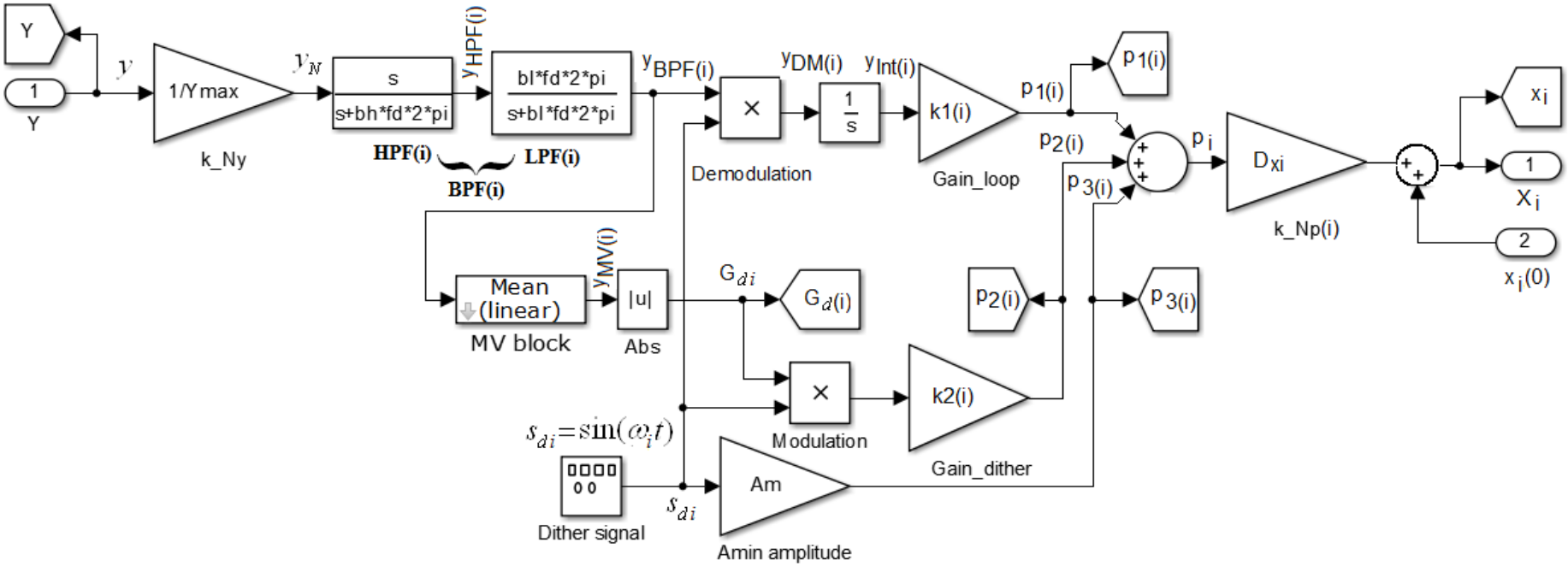

The Global ES control scheme – i, i=1,2

Real-time Optimization of FC / Renewable HPS

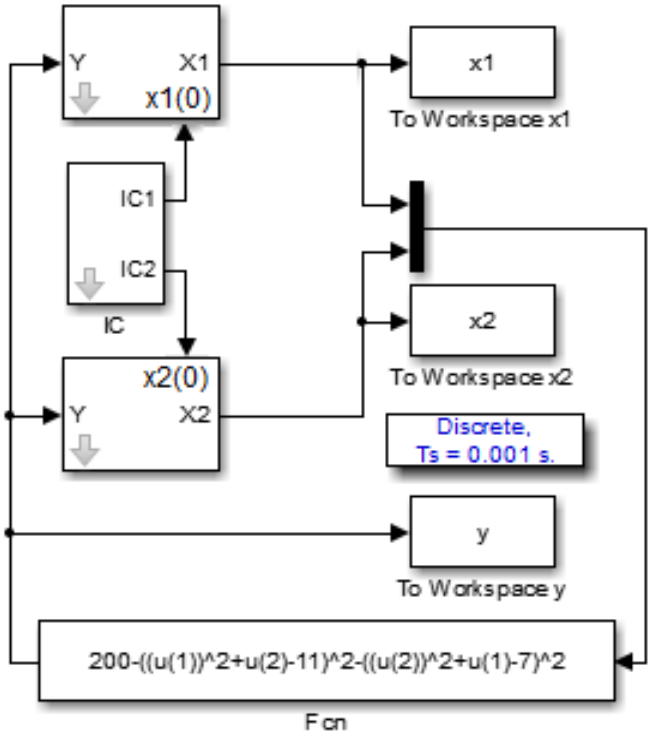

The simulation diagram

The Himmelblau's function

$$f_H(x_1, x_2) = \left(x_1^2 + x_2 - 11\right)^2 + \left(x_1 + x_2^2 - 7\right)^2$$

$$f(x_1, x_2) = GMP - f_H(x_1, x_2)$$

The function f(x1, x2) has four GMPs located at Mi, i=1,2,3,4, in the searching area (top); searching of each GMP starting from initial point close to it (bottom)

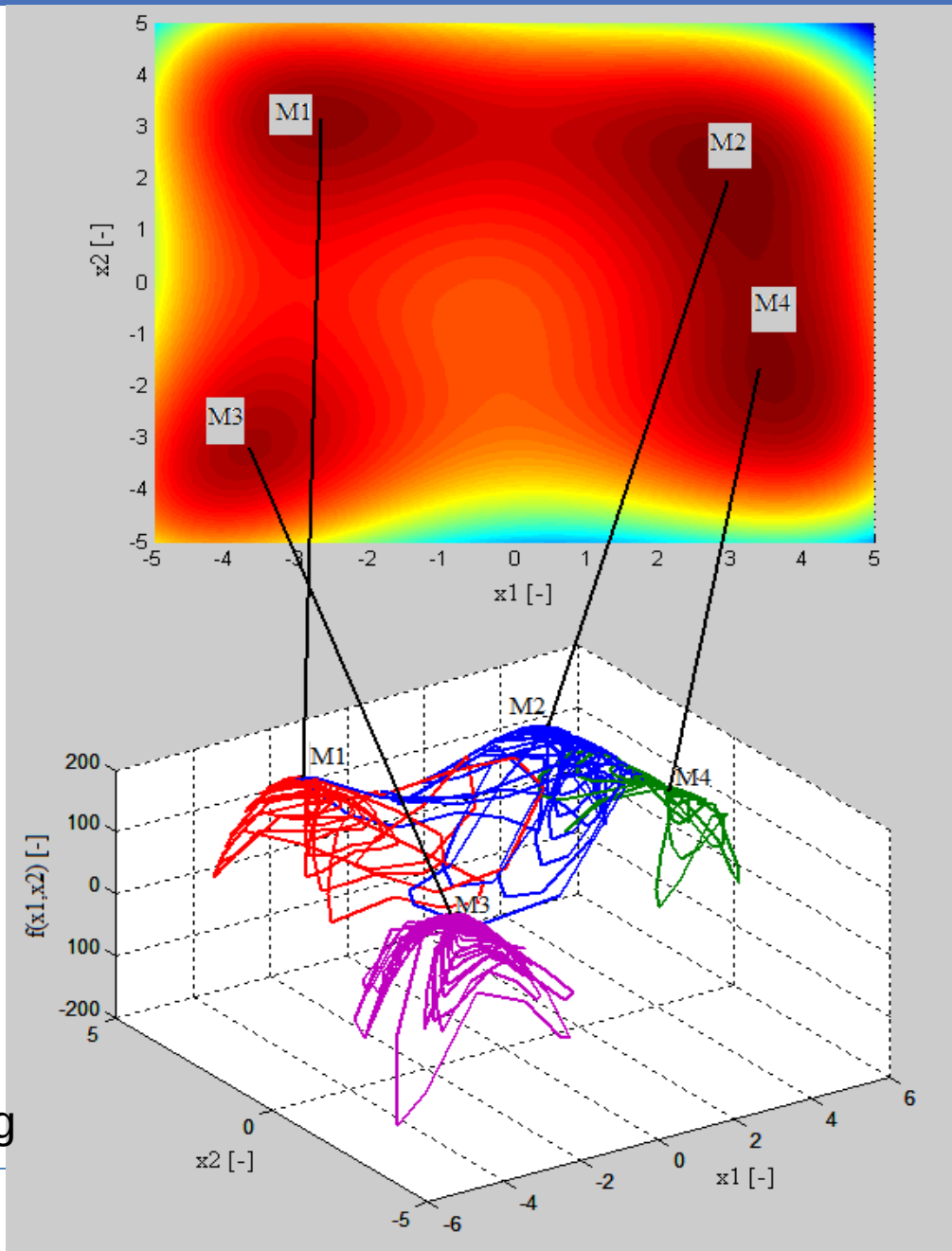

Real-time Optimization of FC / Renewable HPS

The Himmelblau's function has one local maximum point (LMP), f(-0.270845, -0.923039) = 181.617, and four identical local minimum points (LmP): f(-2.805118, 3.283186) = 0.0, f(3.0, 2.0) = 0.0, f(-3.779310, -3.283186) = 0.0, and f(3.554428, -1.848126) = 0.0. So, function f(x1, x2) has four identical GMPs at $(x_{1(M1)}, x_{2(M1)}) = (-2.805118, 3.283186)$, $(x_{1(M2)}, x_{2(M2)}) = (3.0, 2.0)$, $(x_{1(M3)}, x_{2(M3)}) = (-3.779310, -3.283186)$, and $(x_{1(M4)}, x_{2(M4)}) = (3.554428, -1.848126)$, and one LmP, f(-0.270845, -0.923039) = GMP - 181.617, where GMP = 200). The multimodal benchmark patterns must have only one GMP, so four multimodal functions were defined :

$$f_{Mi}(x_1, x_2) = f(x_1, x_2) - r \cdot \left[\left(x_1 - x_{1(Mi)}\right)^2 + \left(x_2 - x_{2(Mi)}\right)^2 \right], \; i = 1, 2, 3, 4$$

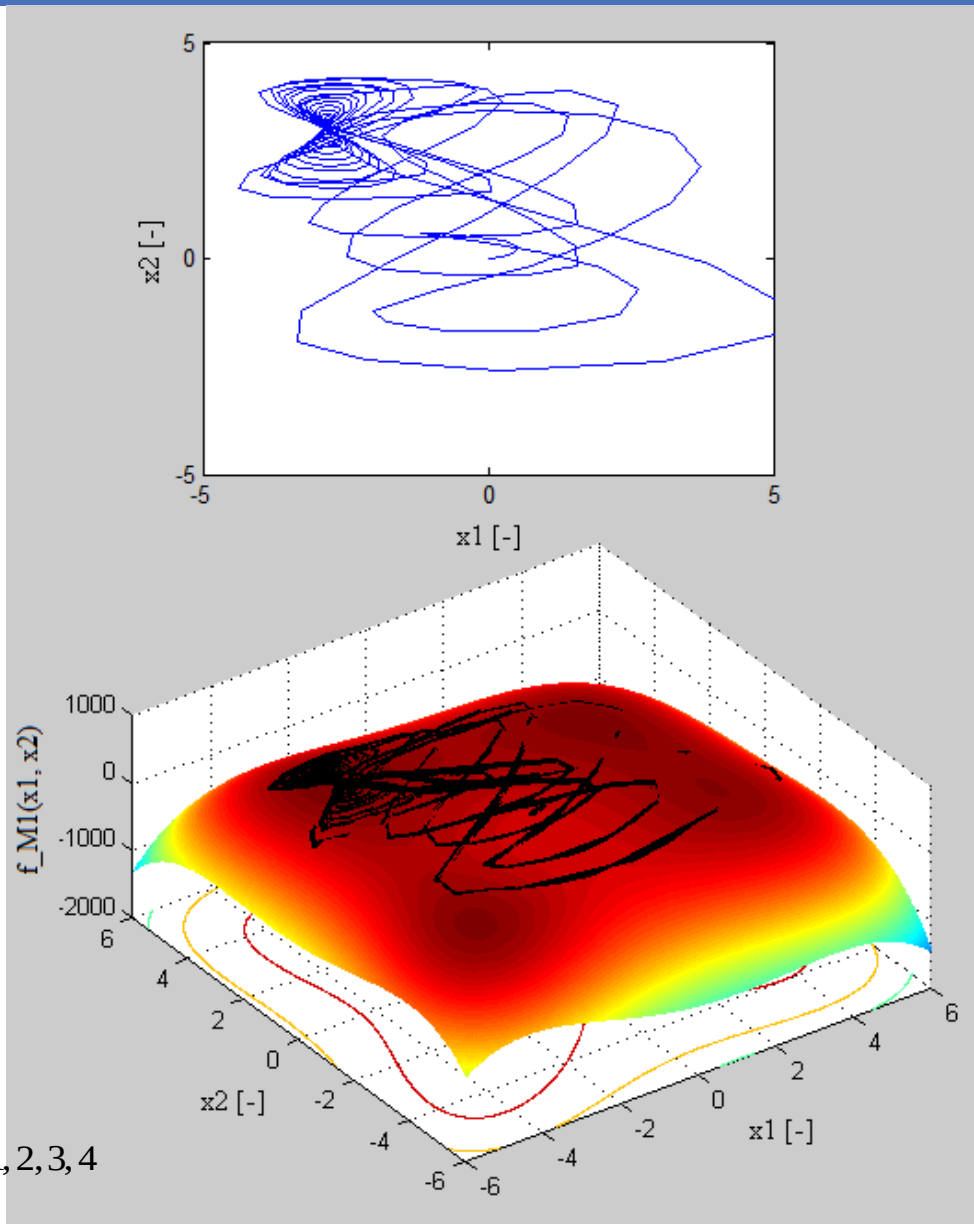

The searching of the GMP_{M1} in the phase plane (top) and on the f_{M1}(x1, x2) (bottom) if the starting point is (0,0).

Real-time Optimization of FC / Renewable HPS

The parameter *r* sets the searching resolution (R_S)

$$R_S = \frac{\min_i |GMP - LMP_i|}{GMP} \cdot 100[\%]$$

Each function f_{Mi} has one GMP and three LMPs in the searching space. The searching resolution is of 8.75%, 3.65%, 10.06%, and 3.79% for f_{Mi} pattern, i=1-4.

Parameters of the GES control scheme (i=1,2):

- the dithers' frequencies:

$\omega_1 = \omega = 50$ Hz, $\omega_2 = 2\omega = 100$ Hz;

- the ESC loops' gains (tuning parameters):

$k_{1(i)} = 4\omega_i$;

- the dithers' gains (tuning parameters):

$k_{2(i)} = 2$;

- the normalization gains:

$k_{Np(i)} = 10$, $k_{Ny(i)} = 200$;

- the BPF cut-off frequencies:

$\omega_{l(i)}=3.5\omega_i$, $\omega_{h(i)}=0.1\omega_i$;

- the minimum amplitude of the dither $p_{3(i)}$:

$A_m = 0.001$.

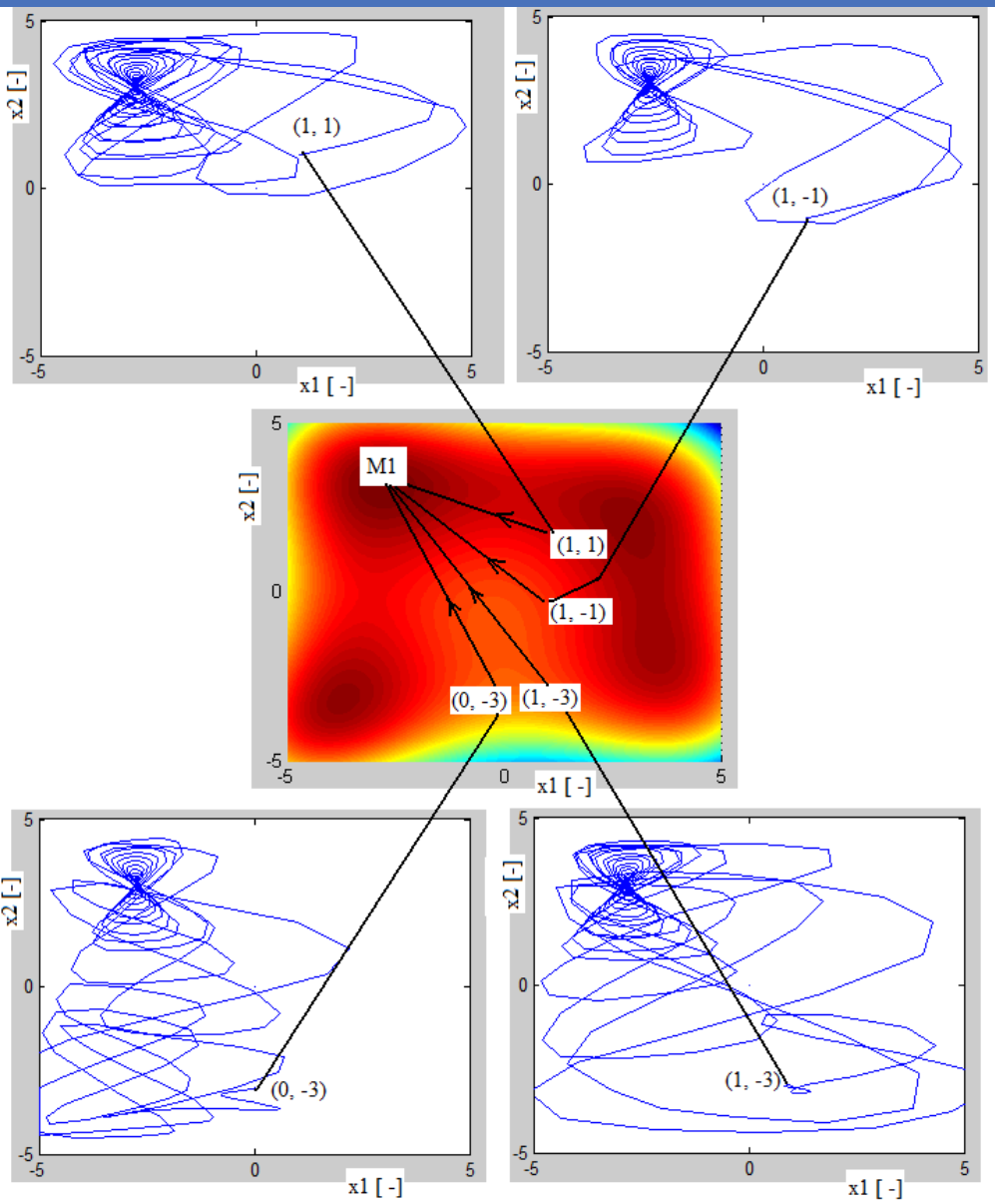

The searching of the GMP_{M1} in the phase plane, starting from different points

Real-time Optimization of FC / Renewable HPS

The tracking speed:
is less than 0.4 seconds;
The tracking accuracy is higher than 99.99%;
The oscillations during the stationary regime are negligible

The tracking accuracy (T_{acc}) is defined by :

$$T_{acc} = \frac{y^*_{GMP}}{y_{GMP}} \cdot 100[\%]$$

where y_{GMP} is the global extreme, $y_{LMP} < y_{GMPP}$ is a local maxima and $y^*_{GMPP} < y_{GMPP}$ is the value tracked with the GMPT algorithm.

N. Bizon. Energy optimization of Fuel Cell System by using Global Extremum Seeking algorithm. Applied Energy 2017;206:458-474
Impact Factor: 7.182

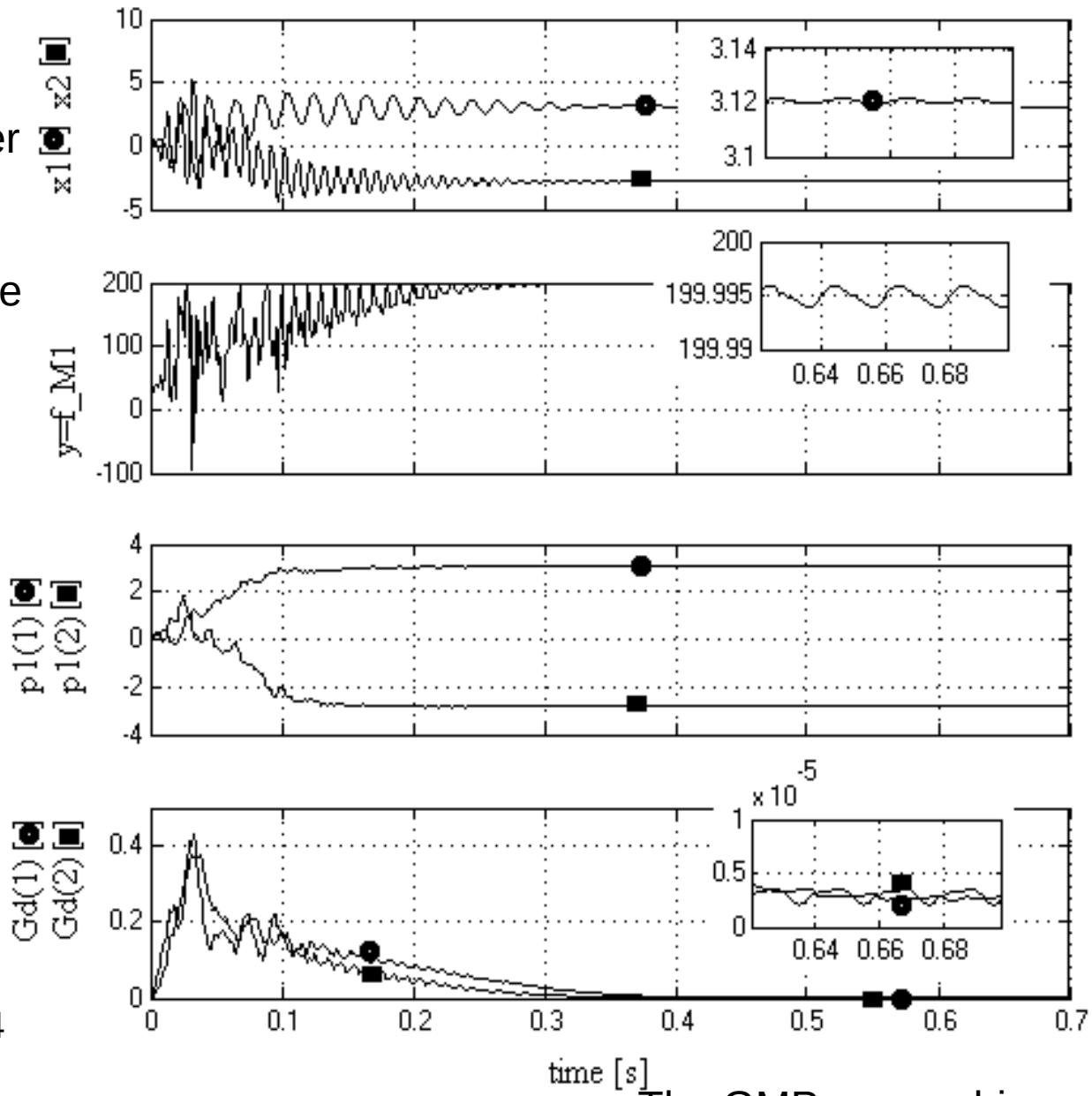

The GMP_{M1} searching

Real-time Optimization of FC / Renewable HPS

RTO Strategy for Fuel Cell Hybrid Power Sources with Load-following Control of the Fuel or Air Flow Rates

$C_{dc}u_{dc}du_{dc}/dt = \eta_{boost}p_{FCnet} + p_{ESS} - p_{Load}$

$0 = \eta_{boost(AV)} \cdot P_{FCnet(AV)} - P_{Load(AV)} \Rightarrow$
$P_{FCnet(AV)} = P_{Load(AV)} / \eta_{boost(AV)}.$

$I_{refLF} = I_{FC(AV)} = P_{Load} / (V_{FC} \cdot \eta_{boost(AV)})$

The performance indicators:

- the fuel consumption efficiency:

$Fuel_{eff} \cong P_{FCnet} / FuelFr$

- the FC system efficiency:

$\eta_{sys} = P_{FCnet} / P_{FC}$

- total fuel consumption:

$$Fuel_T = \int FuelFr(t)dt$$

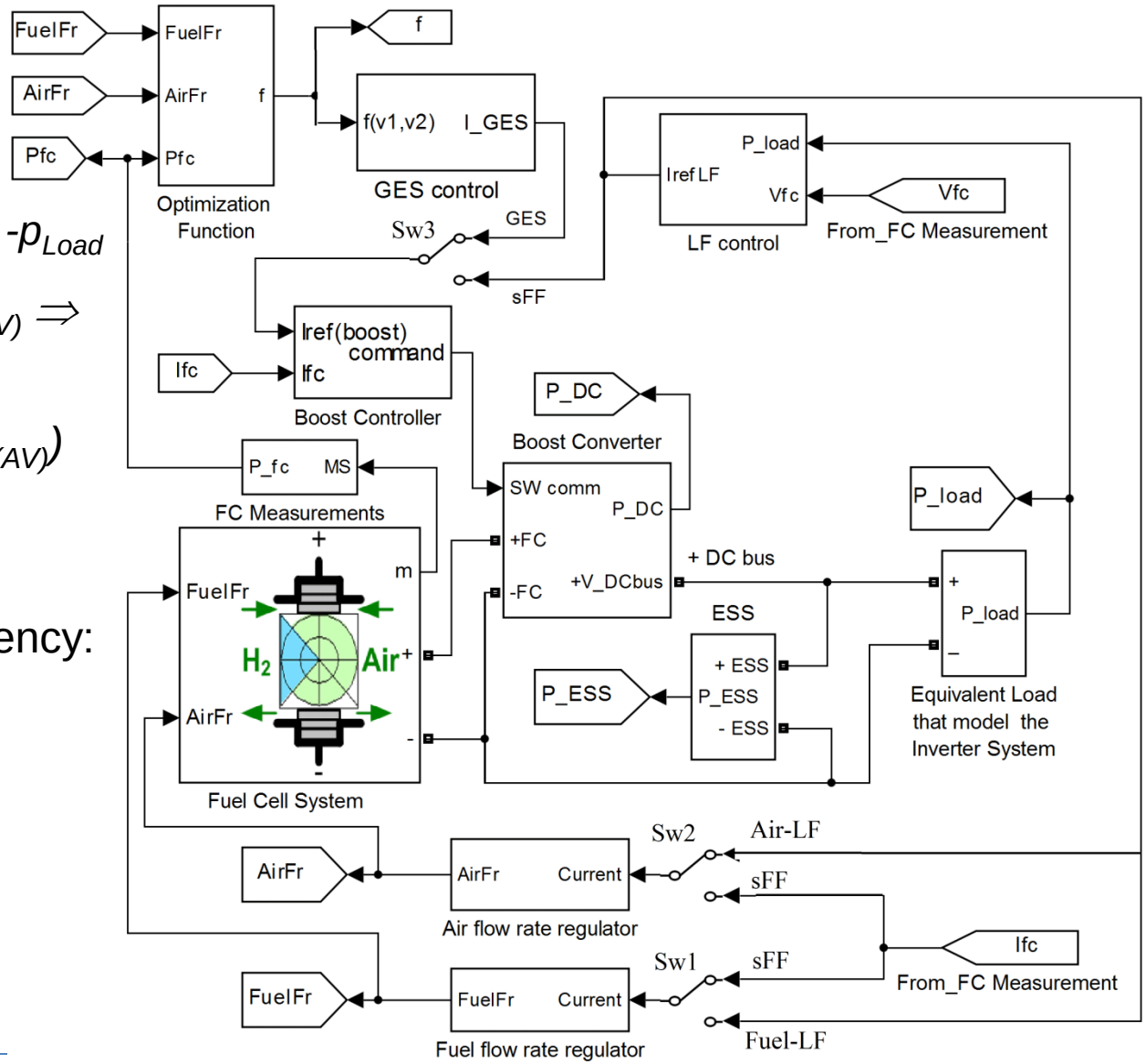

Real-time Optimization of FC / Renewable HPS

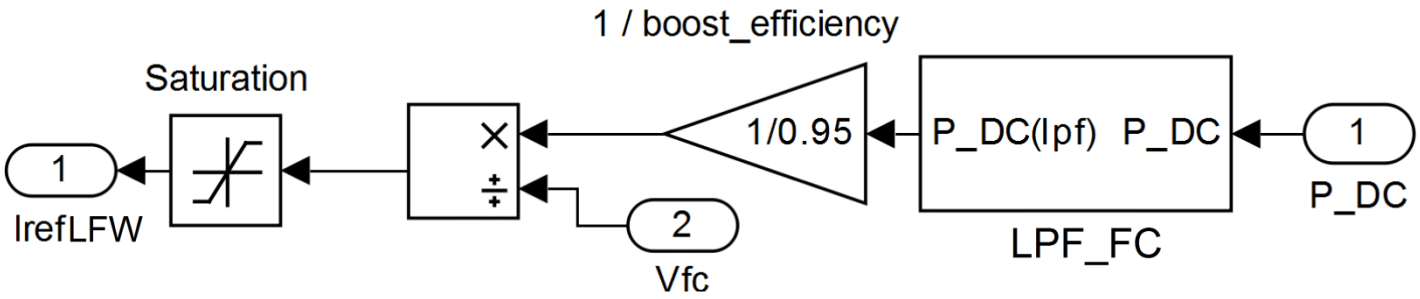

The diagram of the LF control

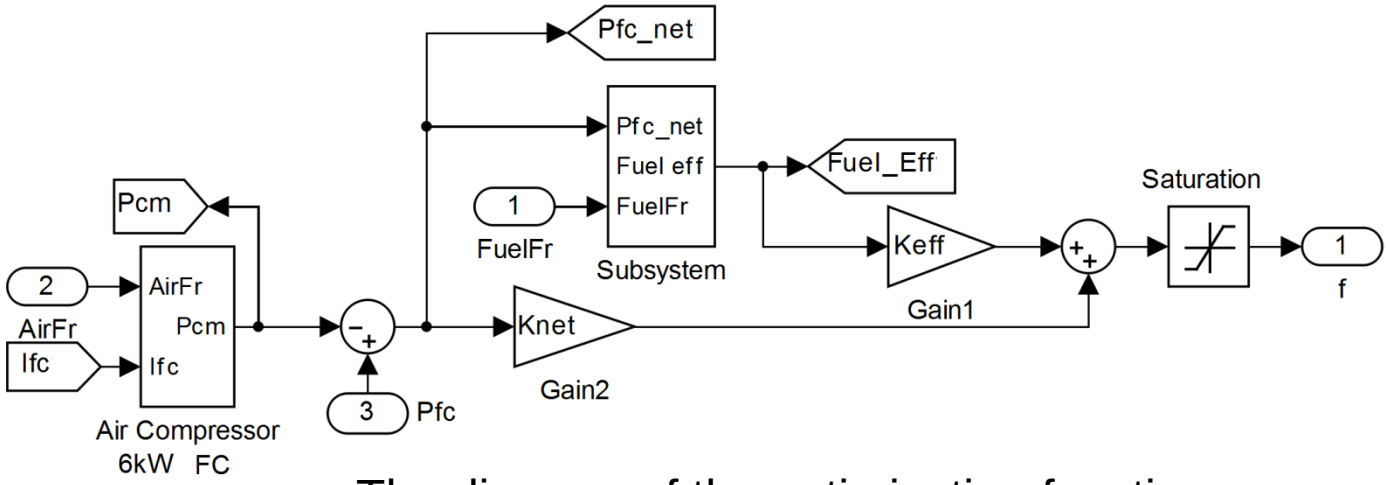

The diagram of the optimization function

Real-time Optimization of FC / Renewable HPS

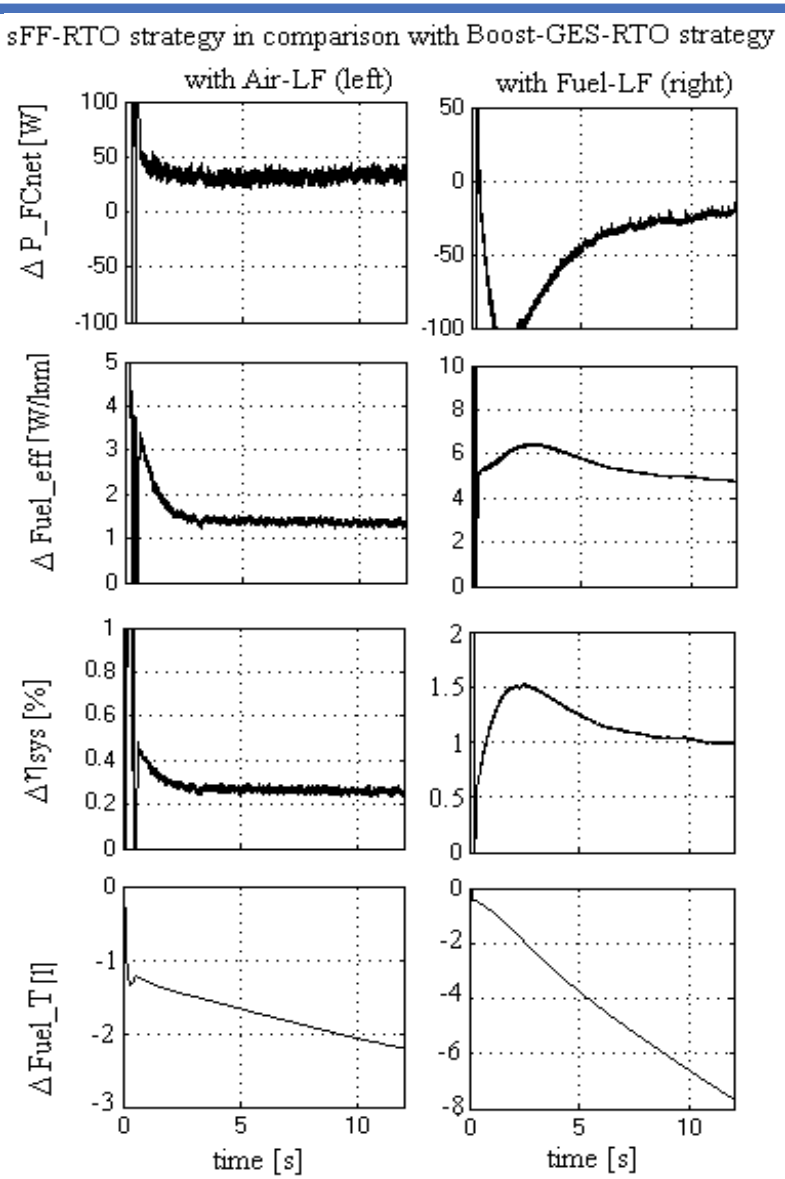

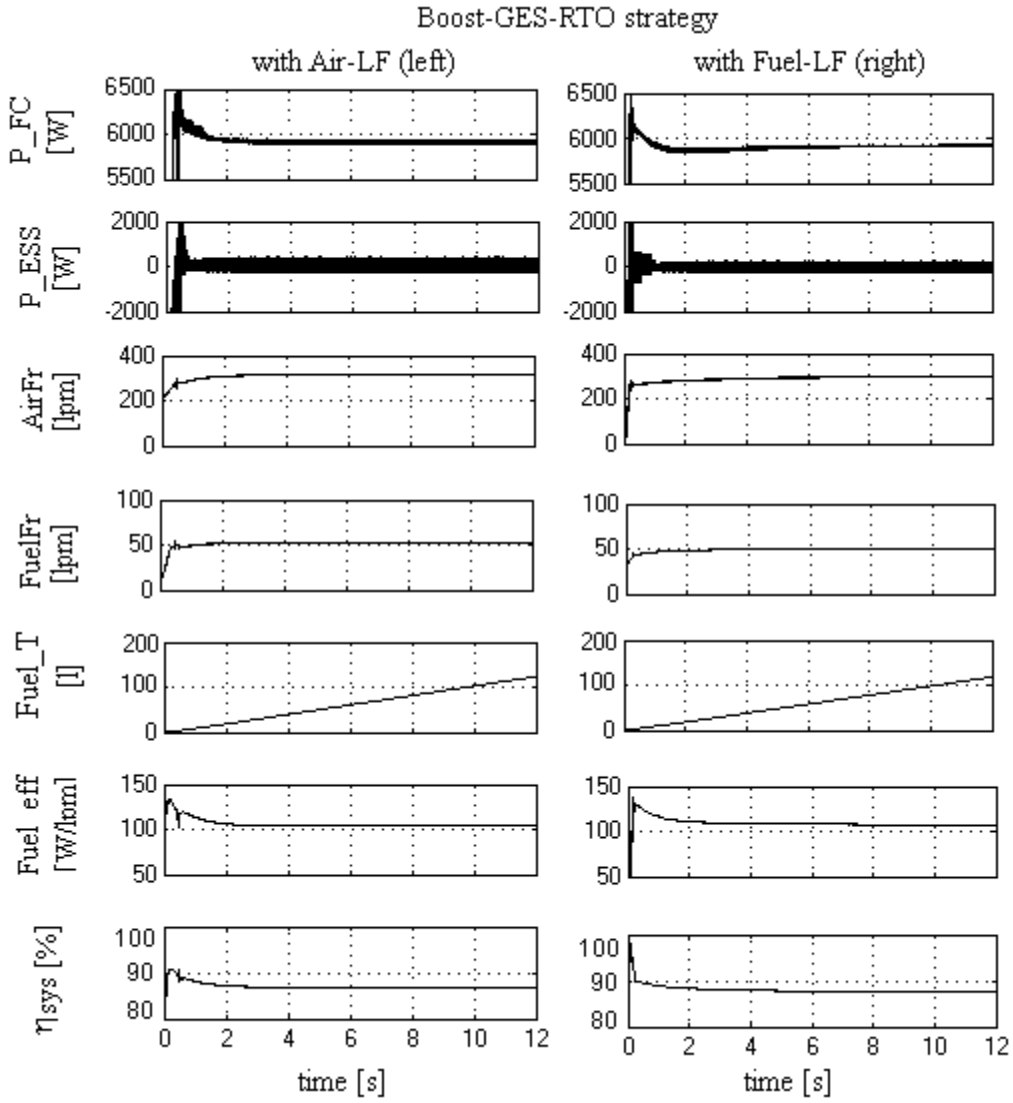

Real-time Optimization of FC / Renewable HPS

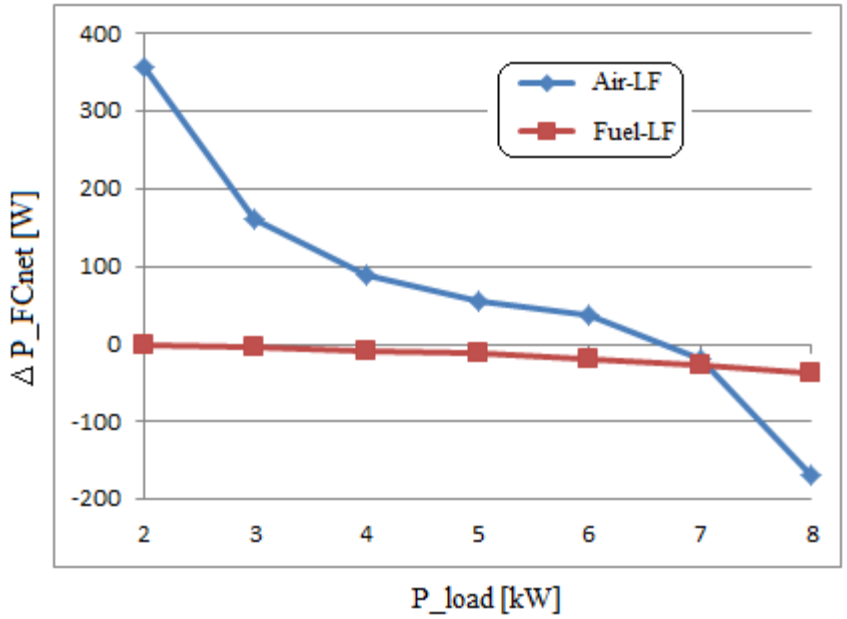

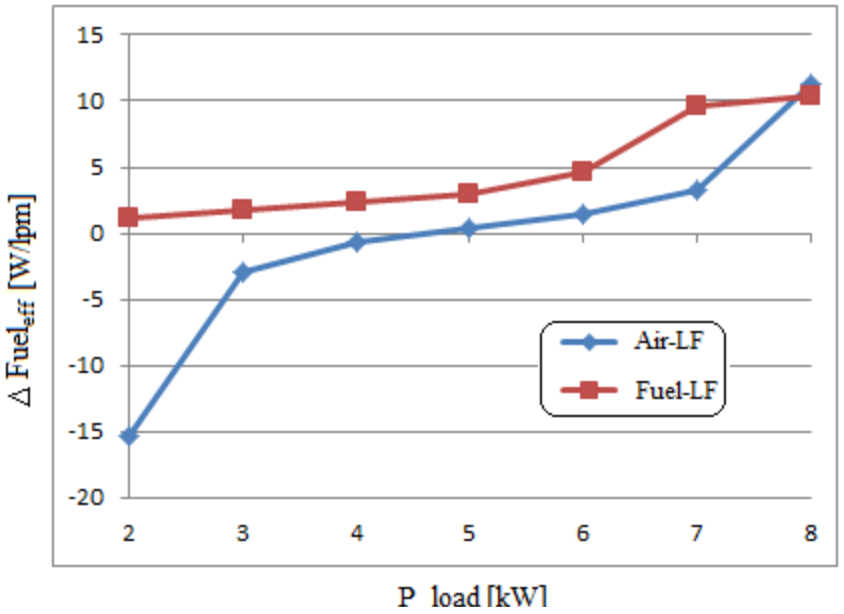

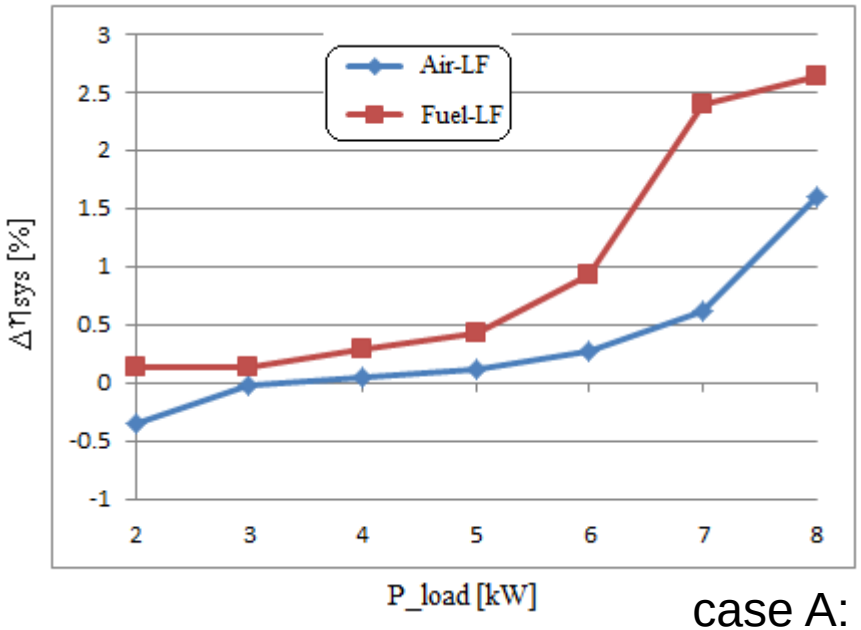

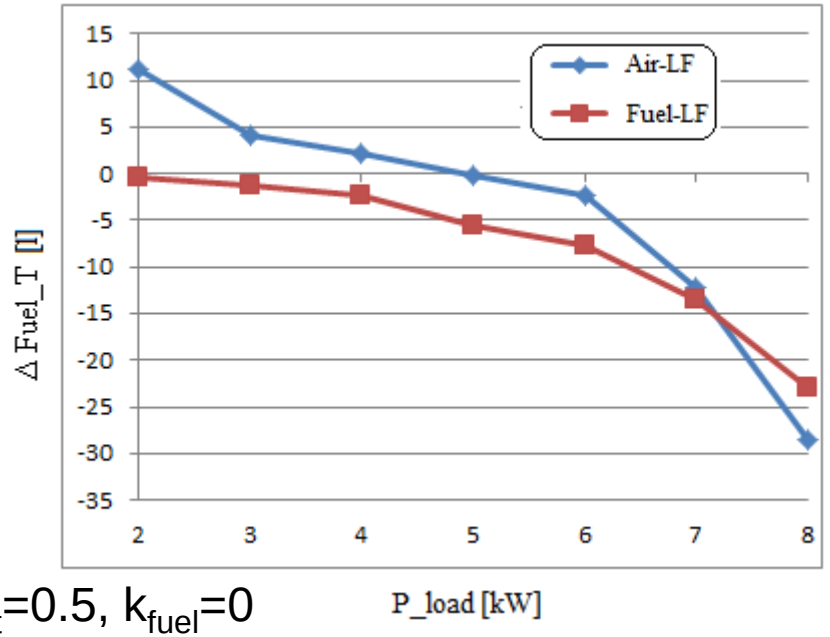

case A: k_{net}=0.5, k_{fuel}=0

Real-time Optimization of FC / Renewable HPS

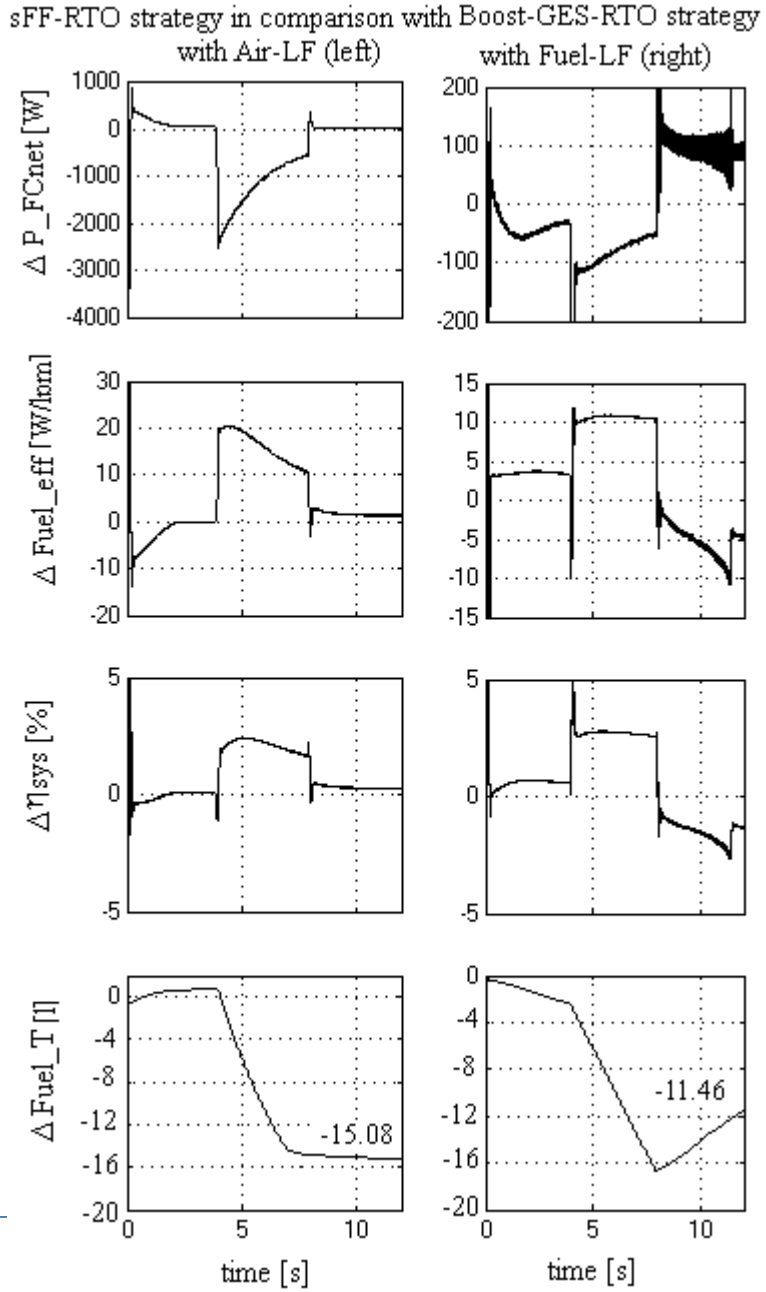

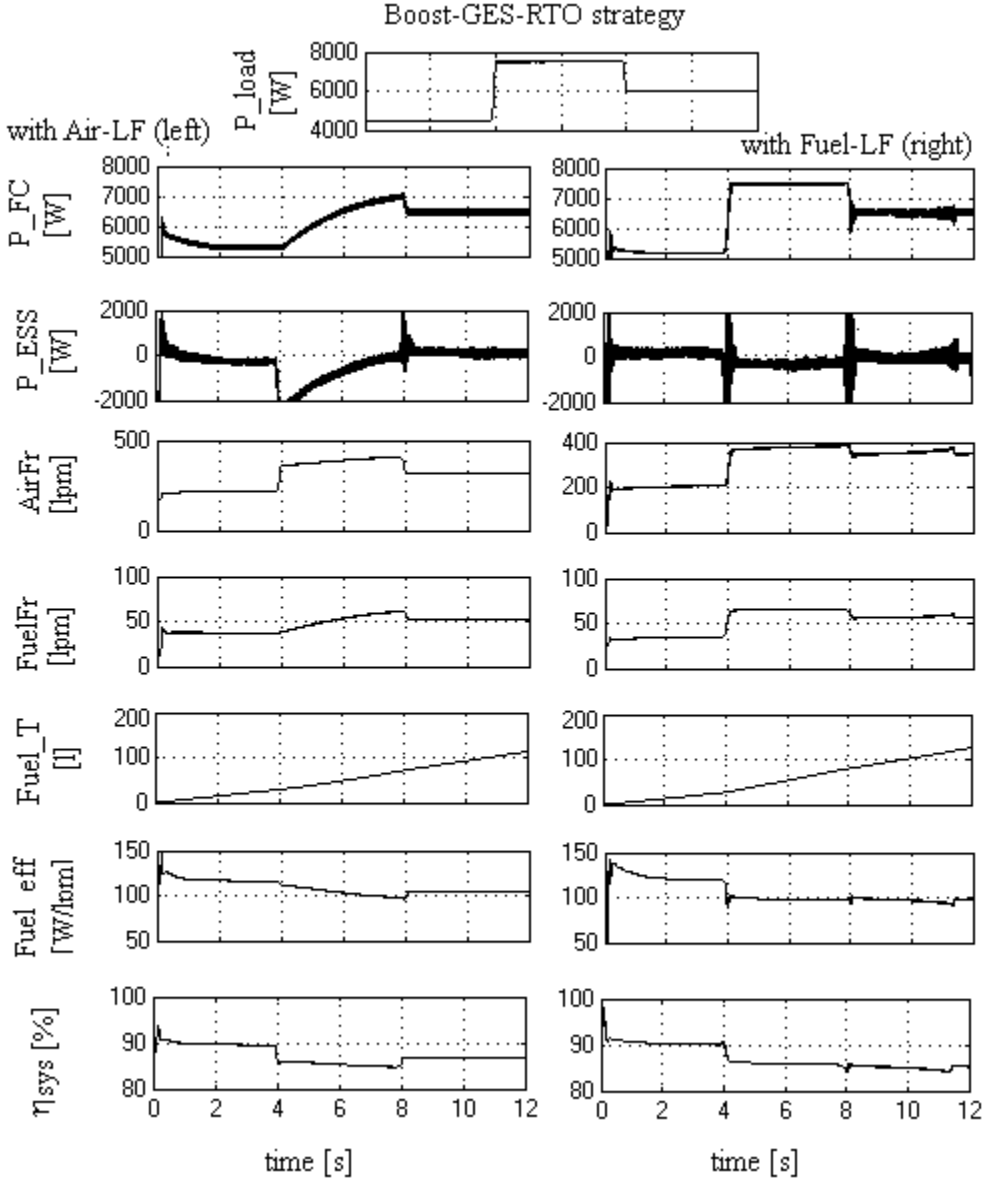

Real-time Optimization of FC / Renewable HPS

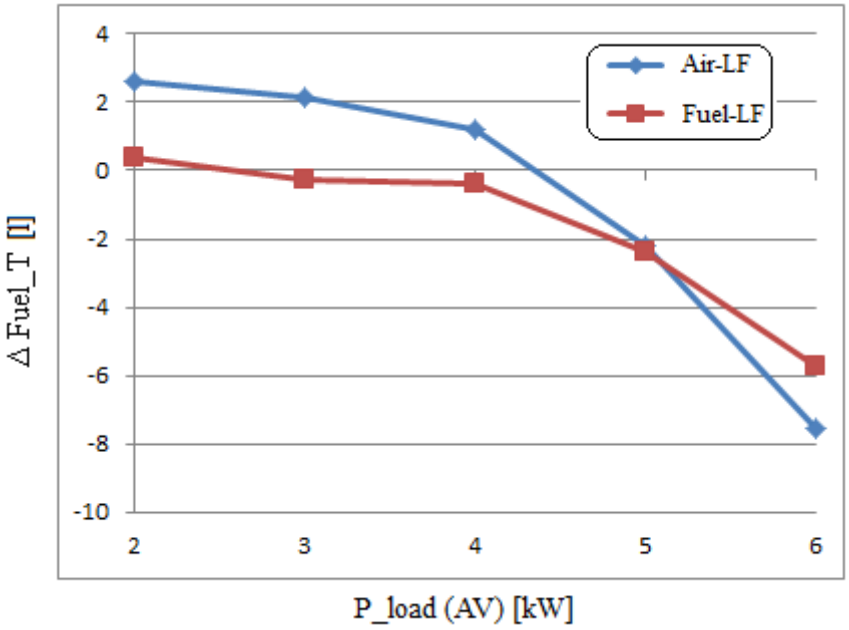

case A: k_{net}=0.5, k_{fuel}=0

Real-time Optimization of FC / Renewable HPS

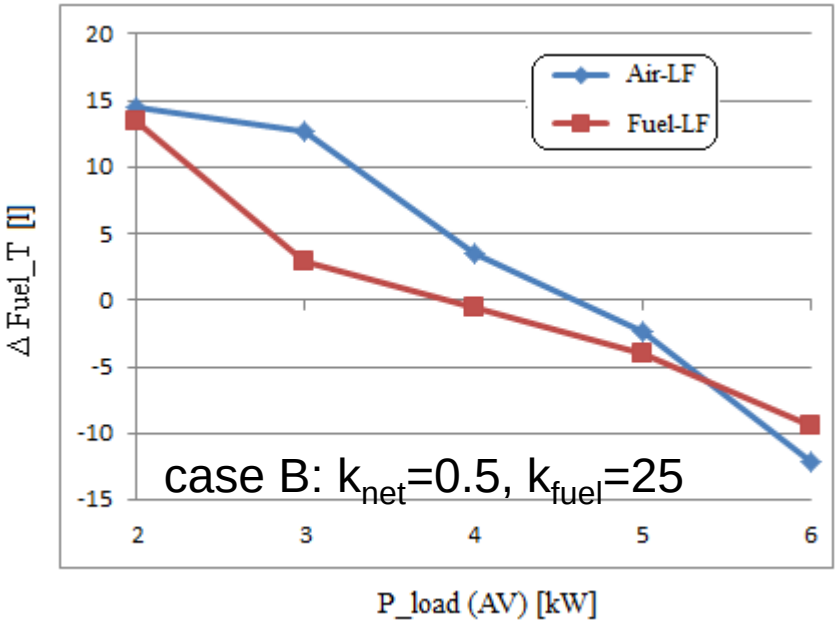

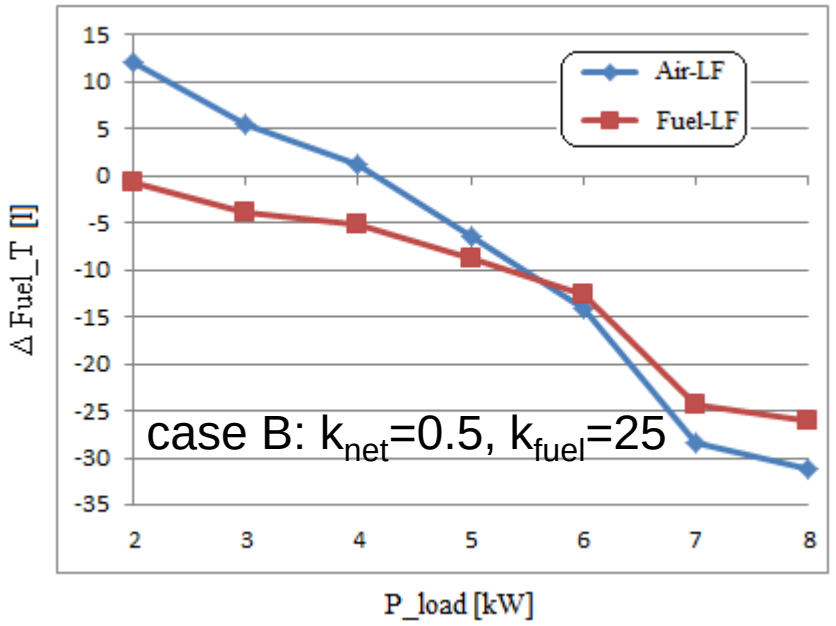

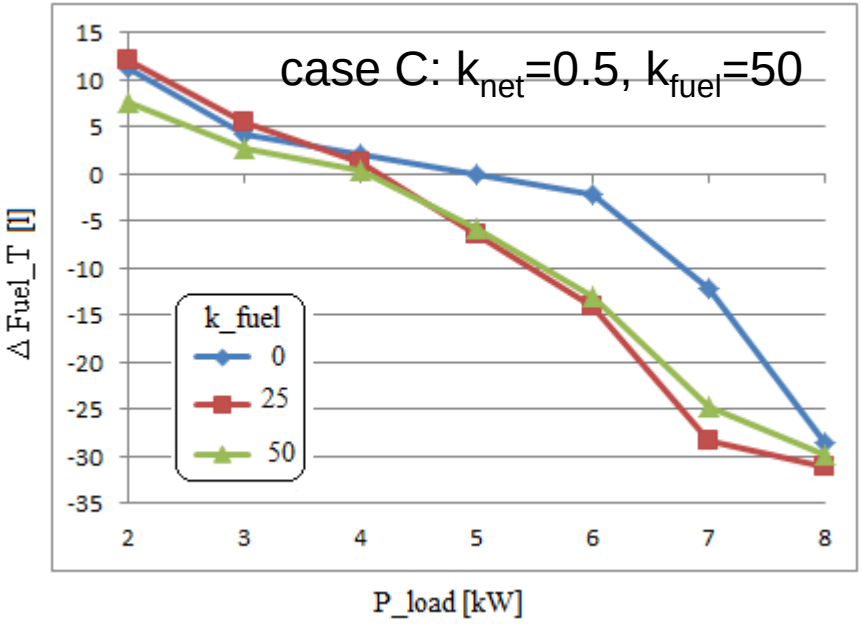

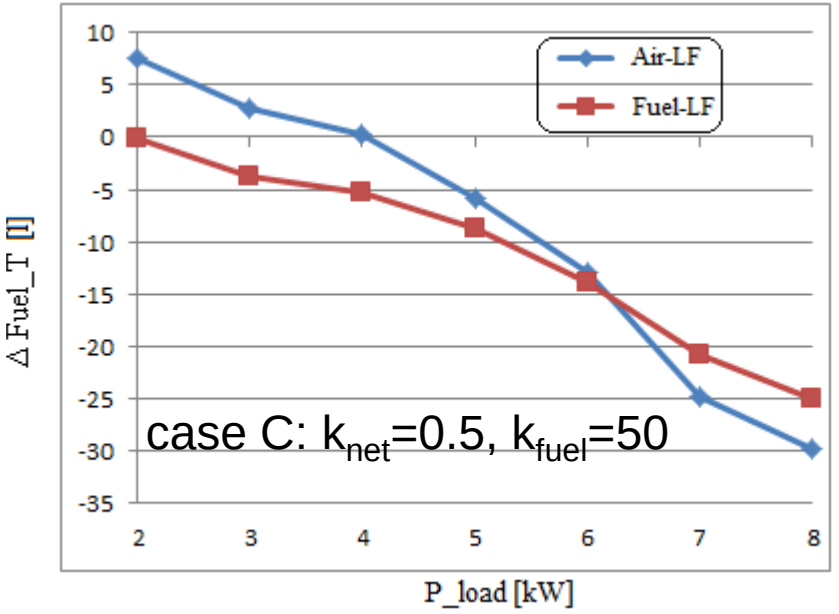

Real-time Optimization of FC / Renewable HPS

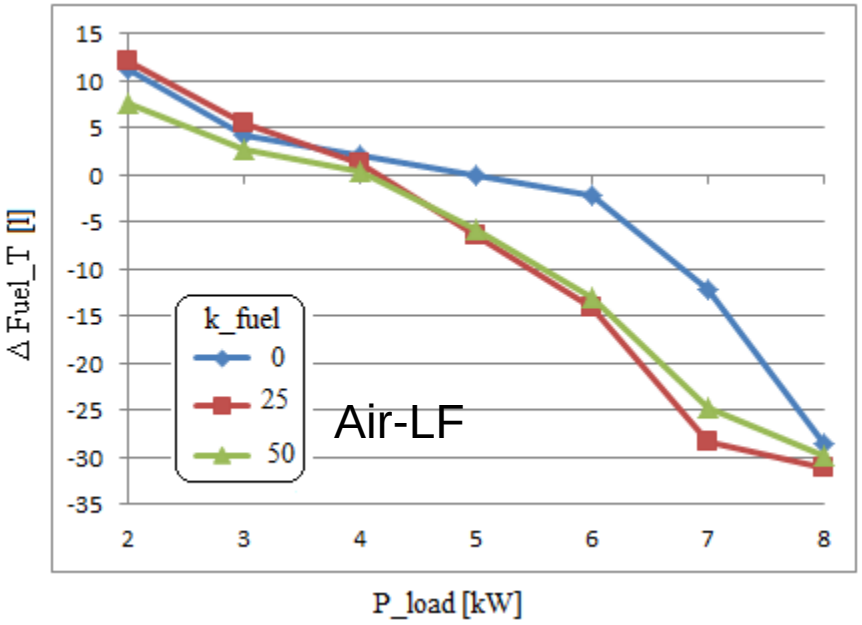

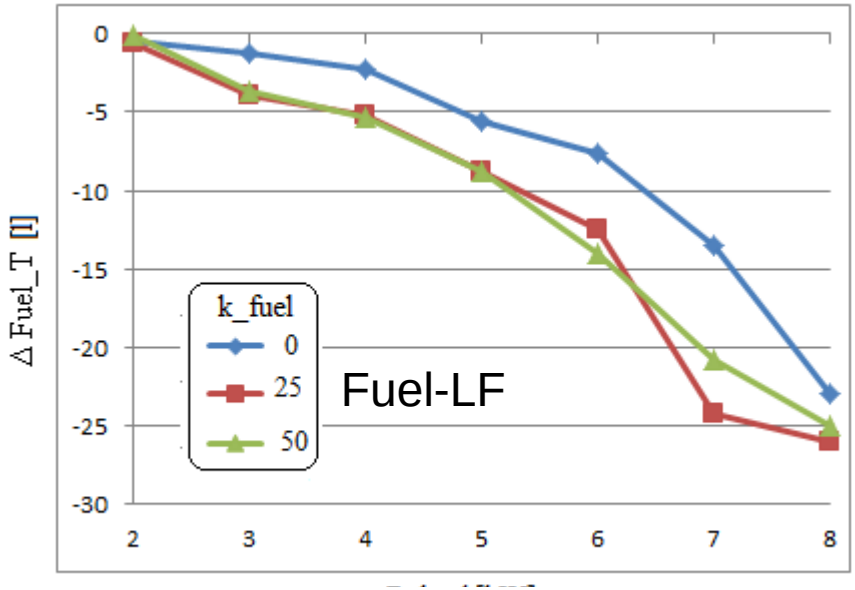

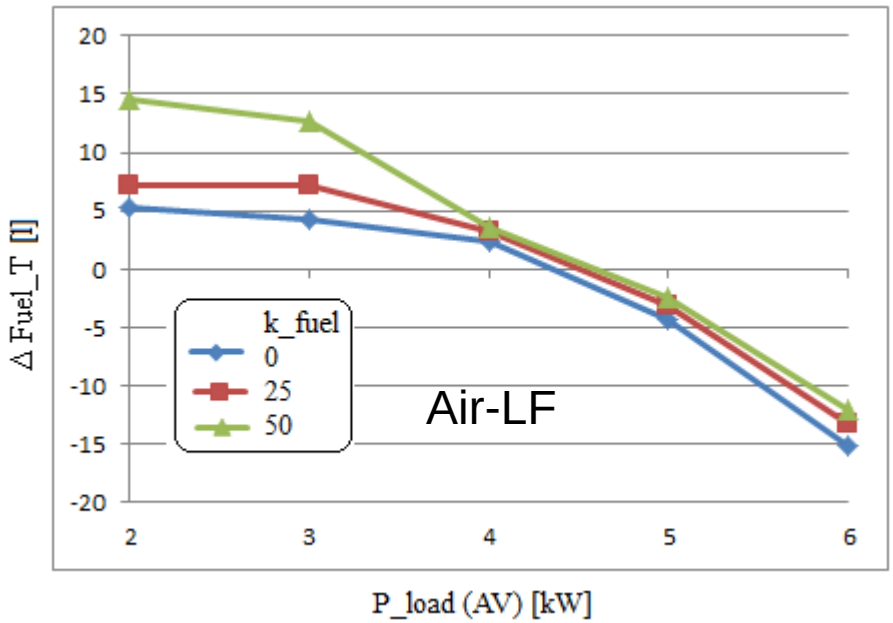

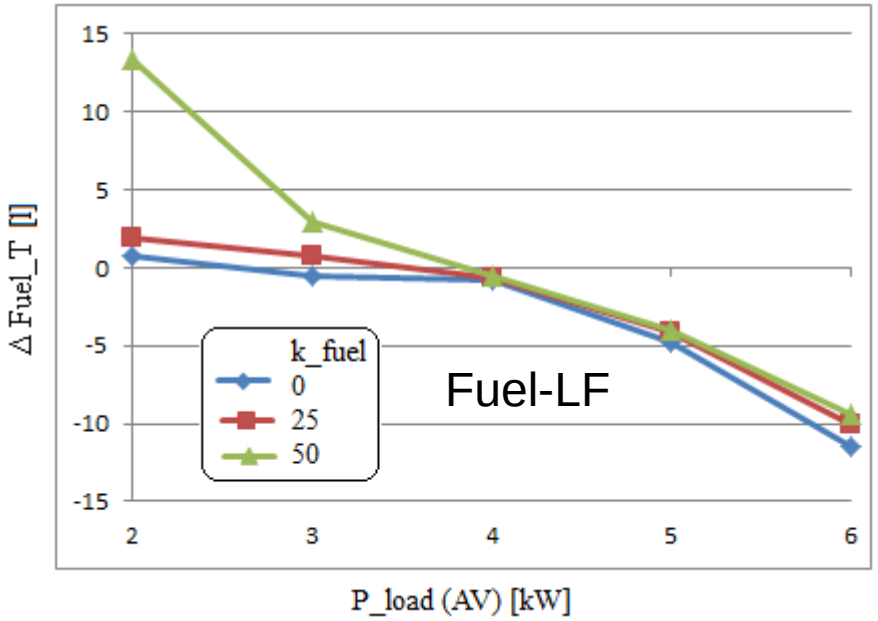

Real-time Optimization of FC / Renewable HPS

The position of optimal points for the Boost-GES-RTO strategies with Air-LF (◊) and Fuel-LF (□), compared to sFF strategy (○)

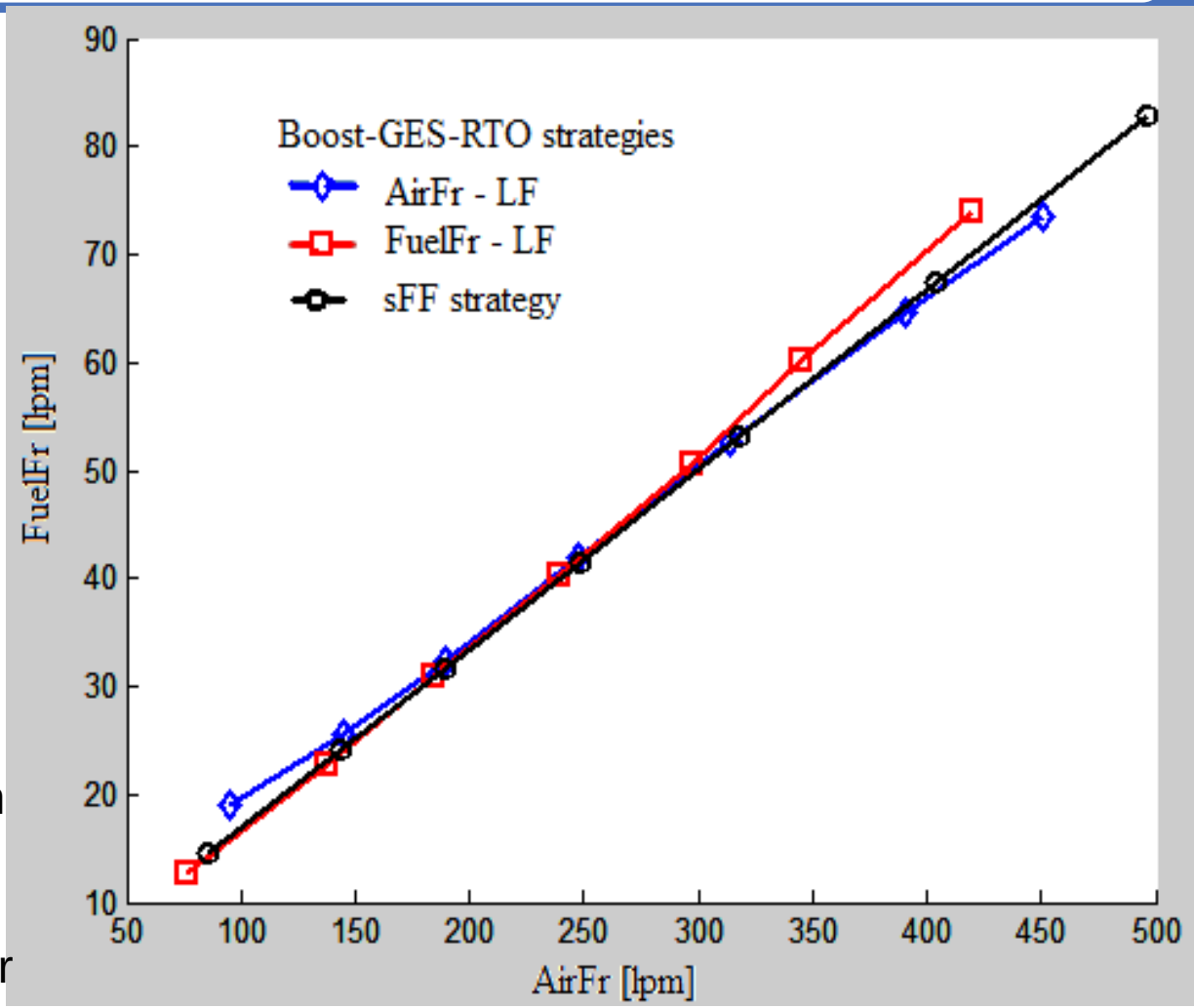

N. Bizon. Real-time optimization strategy for fuel cell hybrid power sources with load-following control of the fuel or air flow. Energy Conversion and Management 2018;157:13–27; impact factor 5.589

Real-time Optimization of FC / Renewable HPS

RTO Strategy for Fuel Cell Hybrid Power Sources with ES CONTROL and LF CONTROL of the Fuel and Air Flow Rates

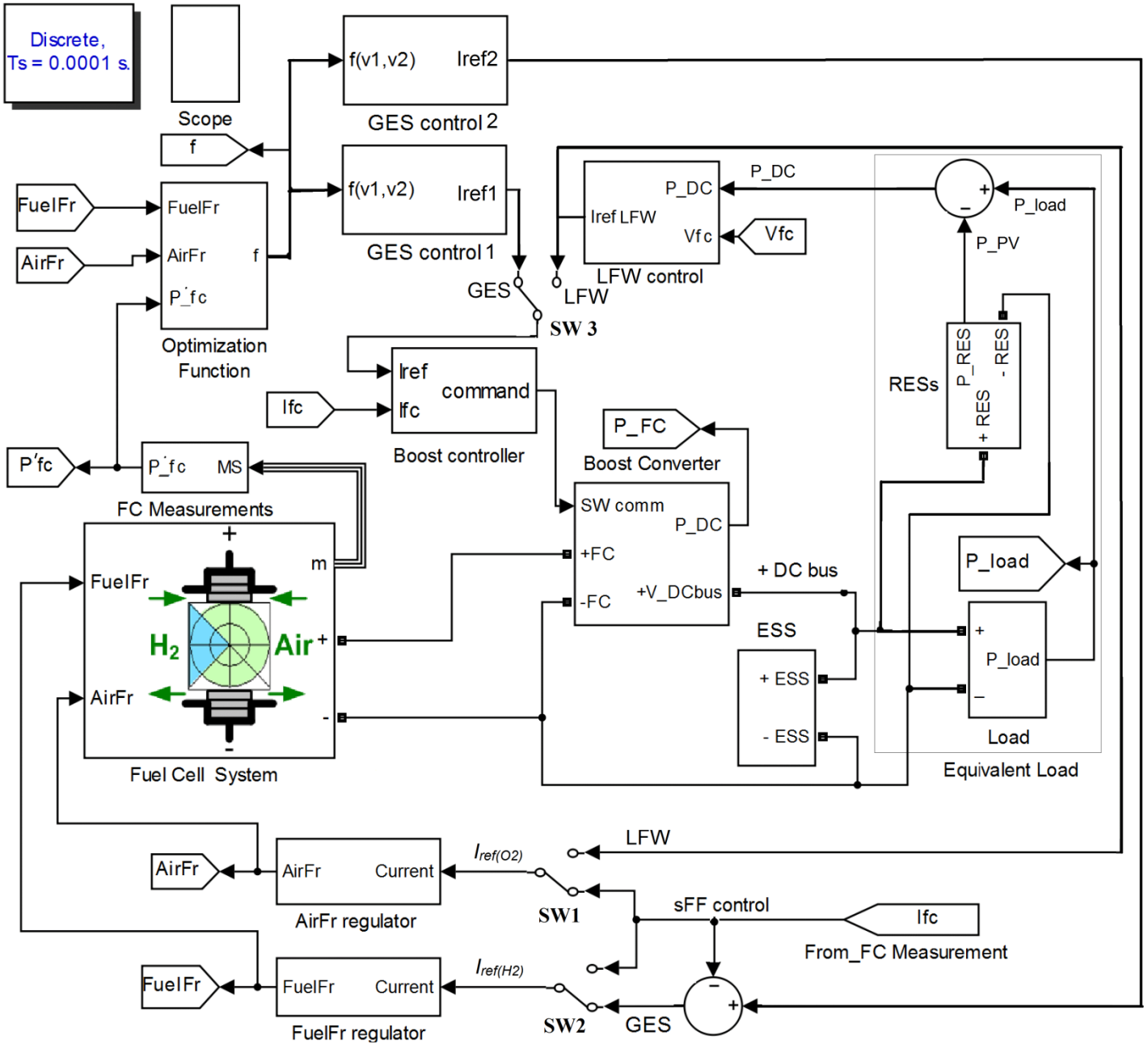

N. Bizon. Optimization of the Proton Exchange Membrane Fuel Cell Hybrid Power System for Residential Buildings. Energy Conversion and Management 2018;163:22–37; impact factor 5.589

Real-time Optimization of FC / Renewable HPS

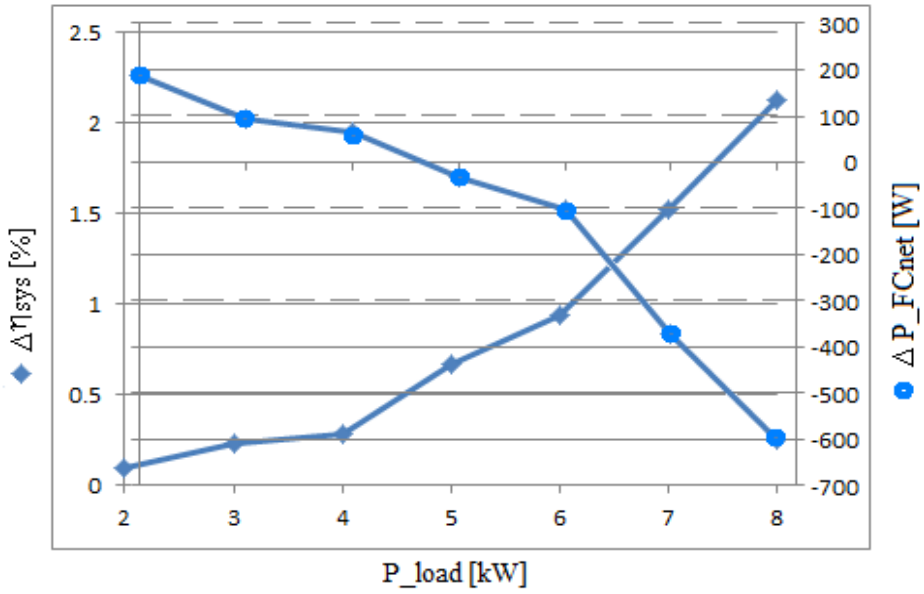

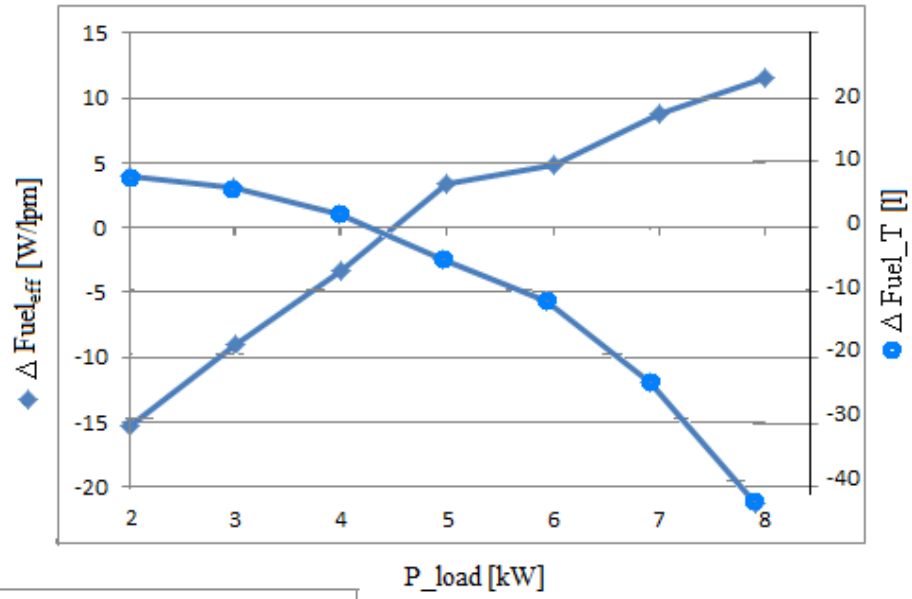

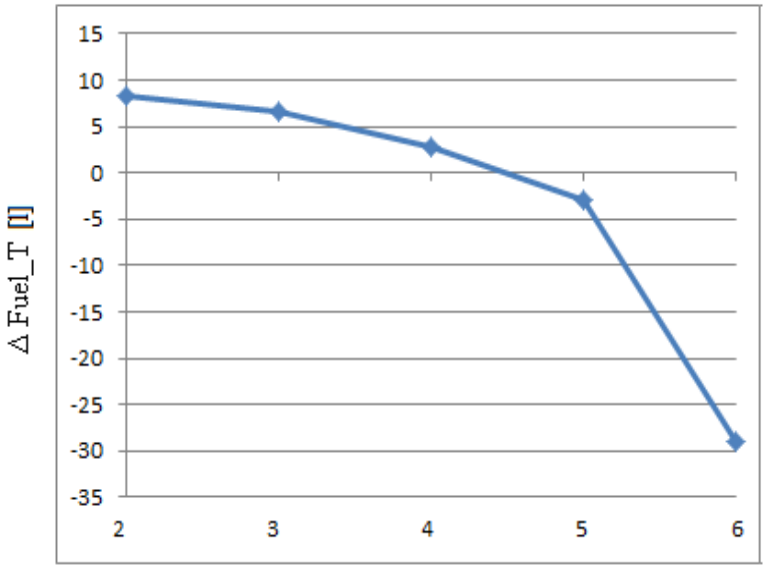

Real-time Optimization of FC / Renewable HPS

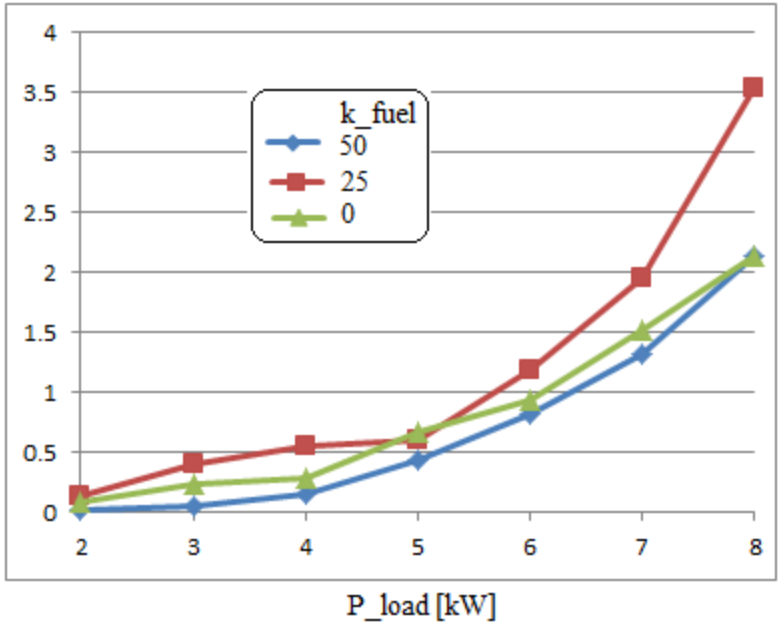

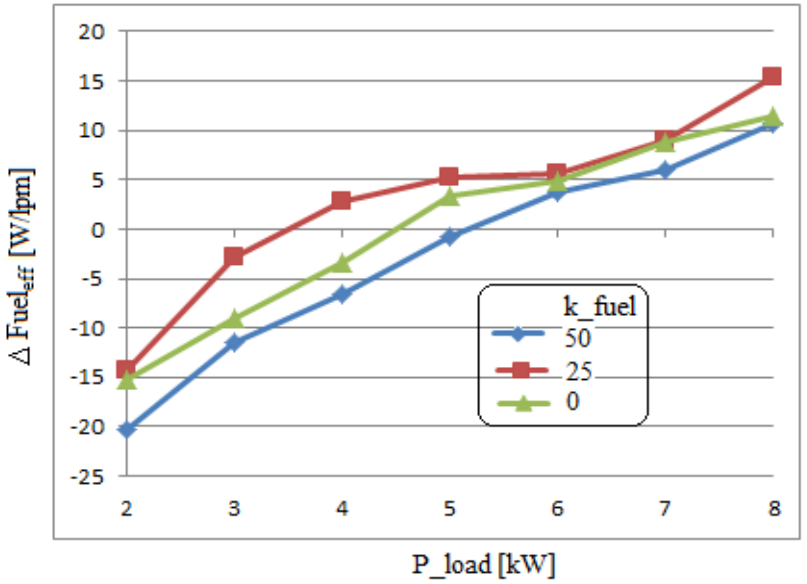

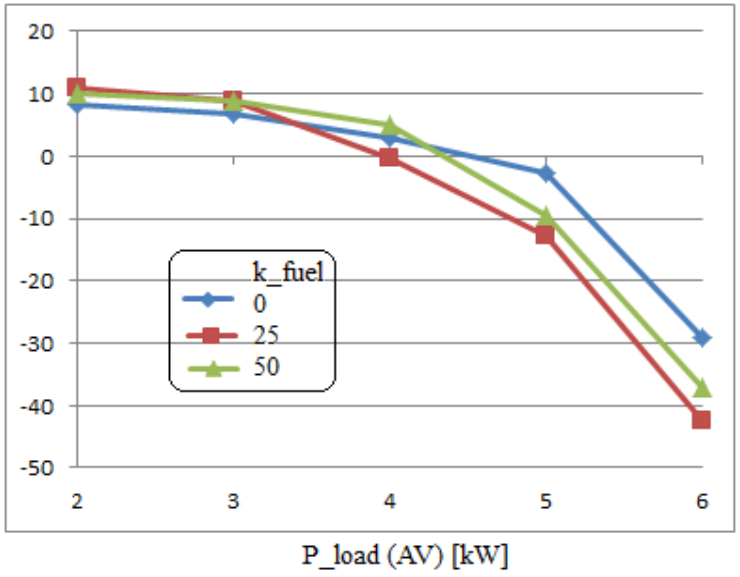

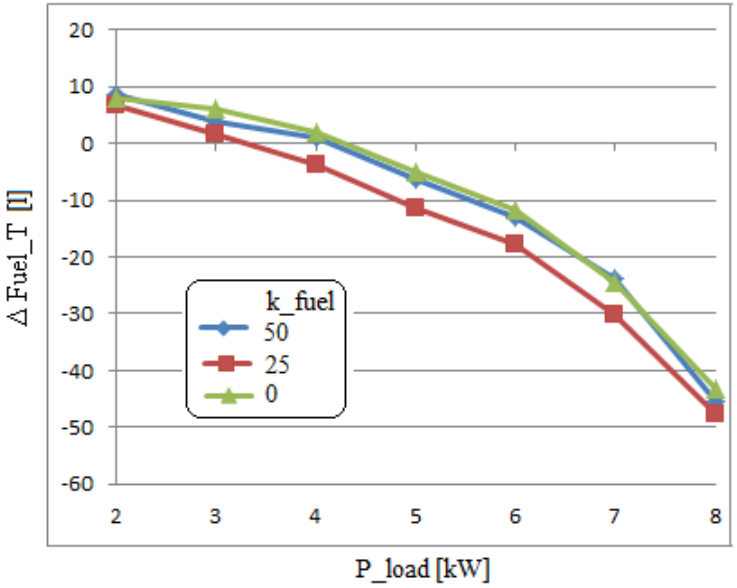

Real-time Optimization of FC / Renewable HPS

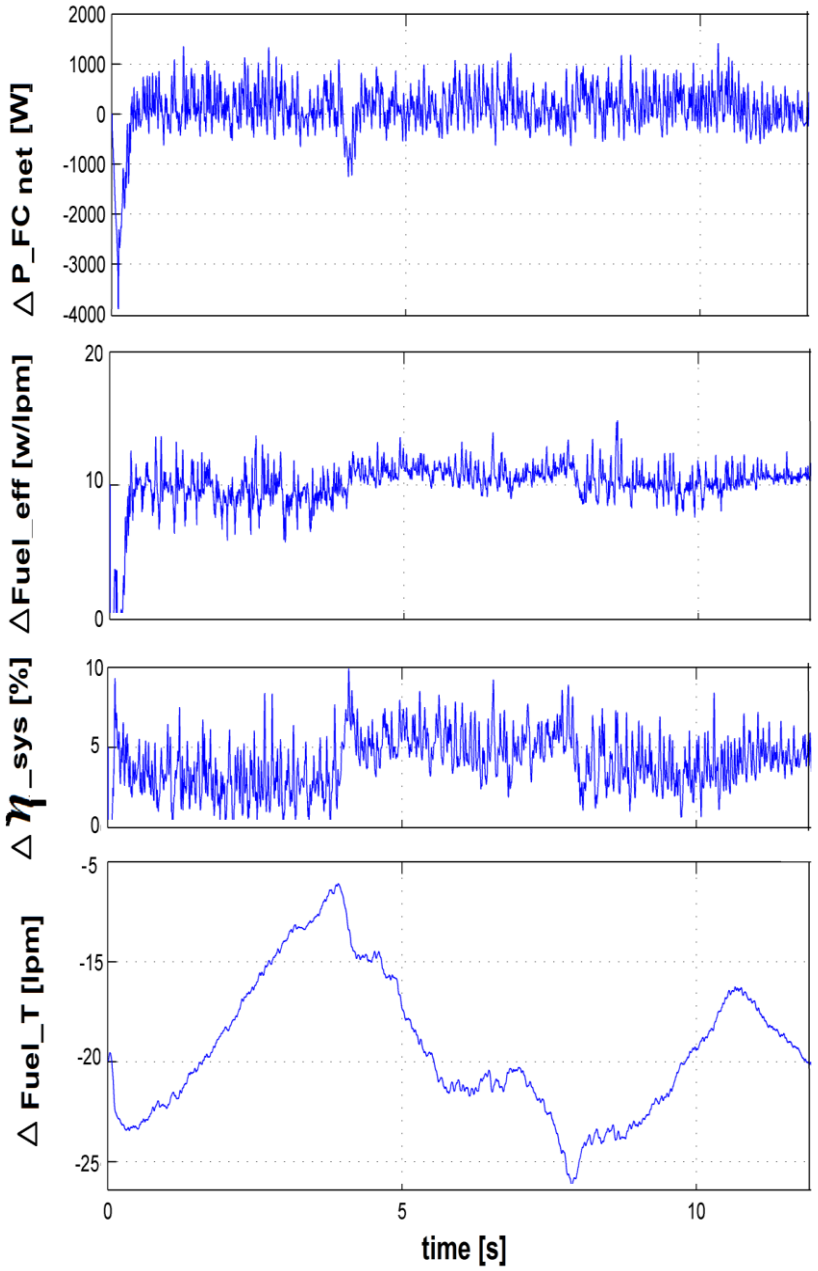

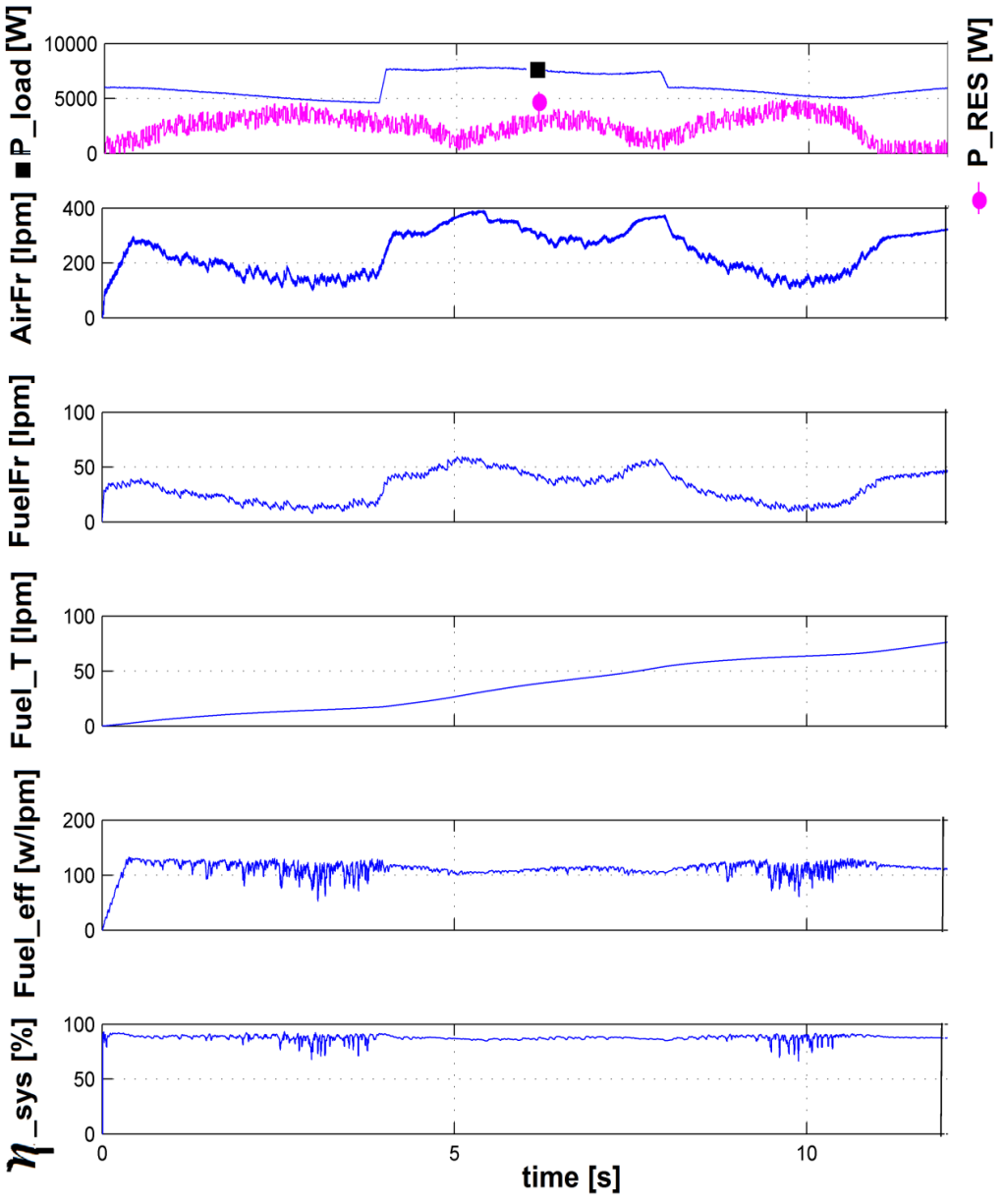

Real-time Optimization of FC / Renewable HPS

RTO Strategy for Fuel Cell / Wind Turbine Hybrid Power System under Turbulent Wind Gusts and Variable Load

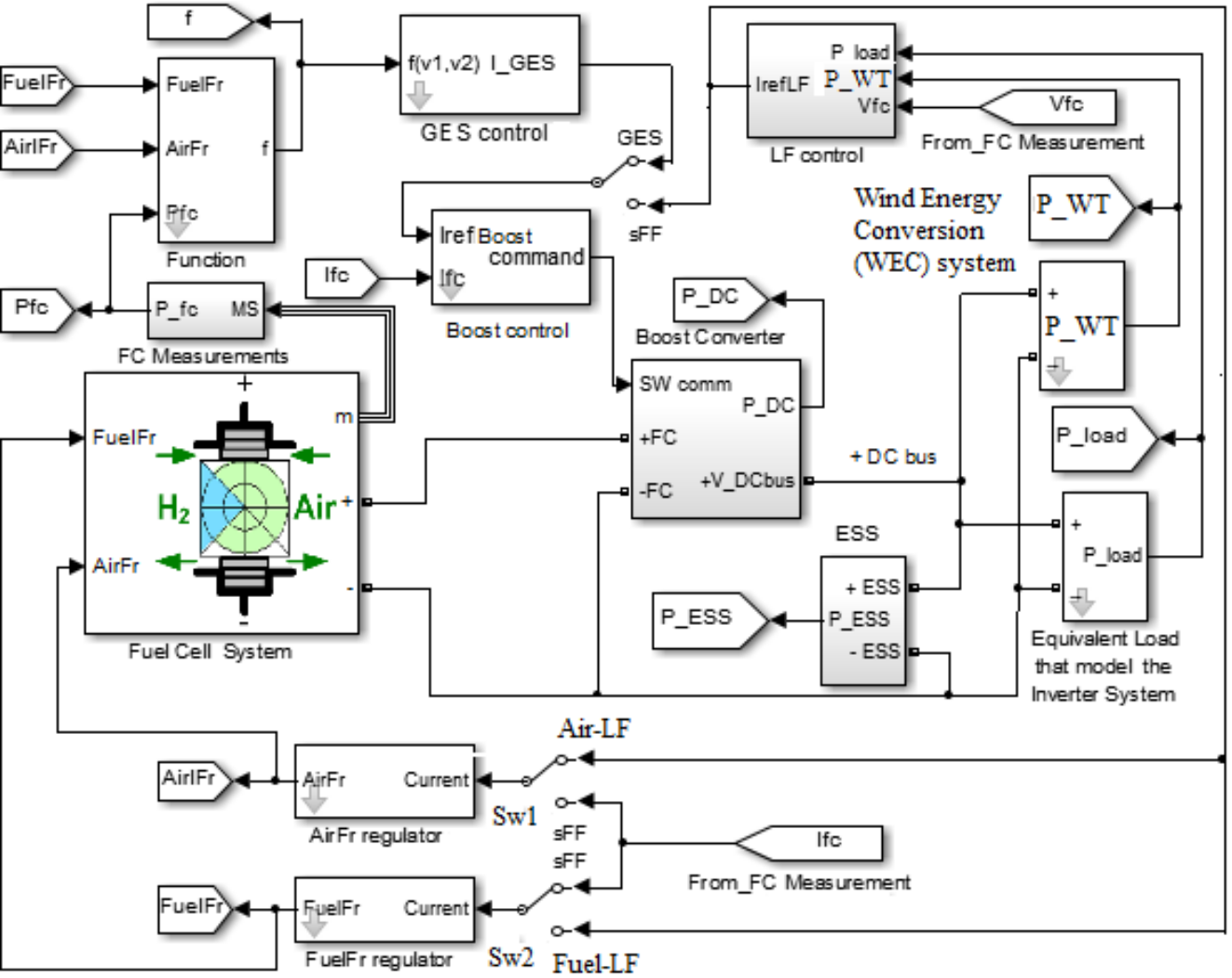

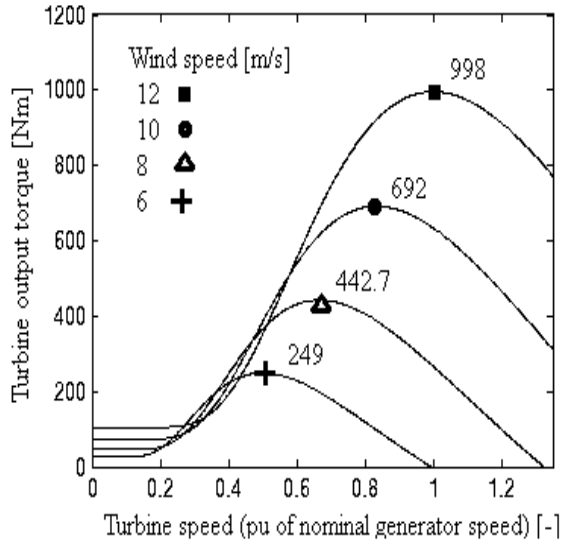

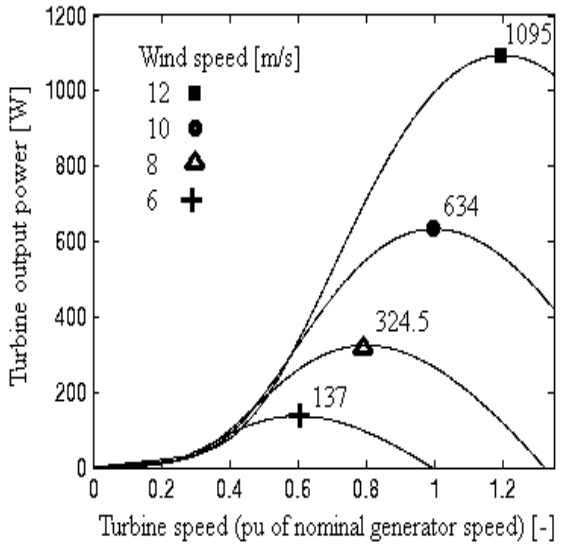

Real-time Optimization of FC / Renewable HPS

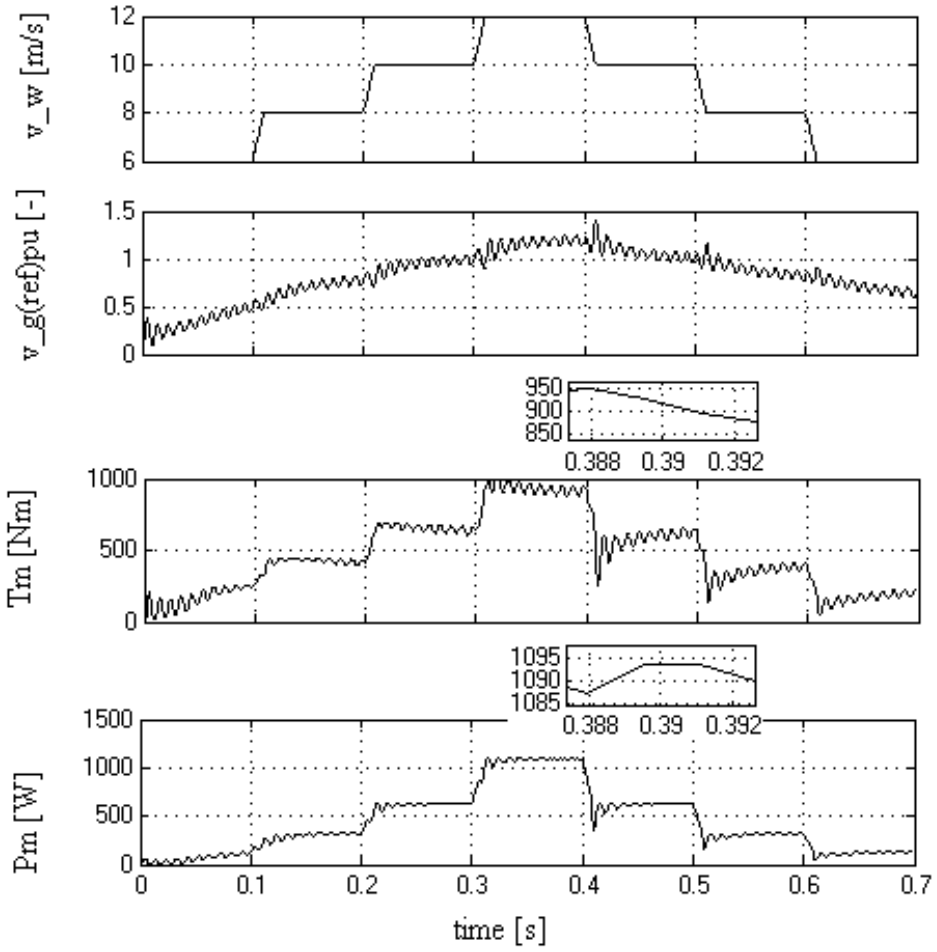

the classic ES control

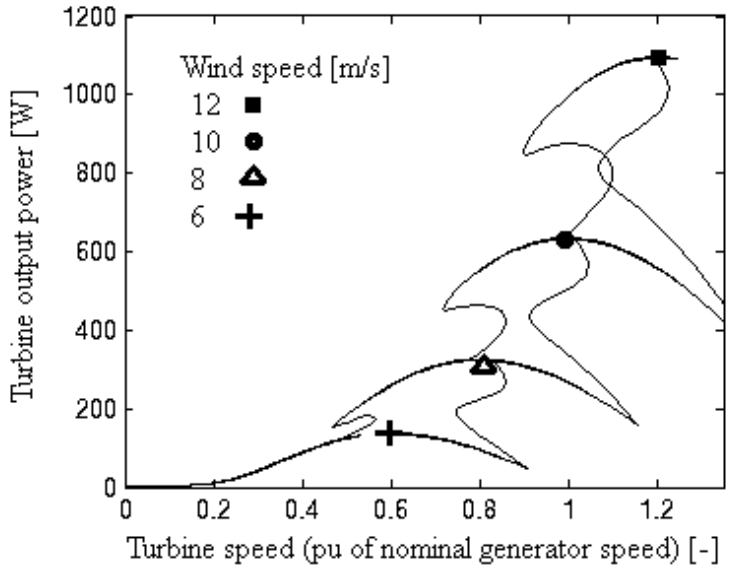

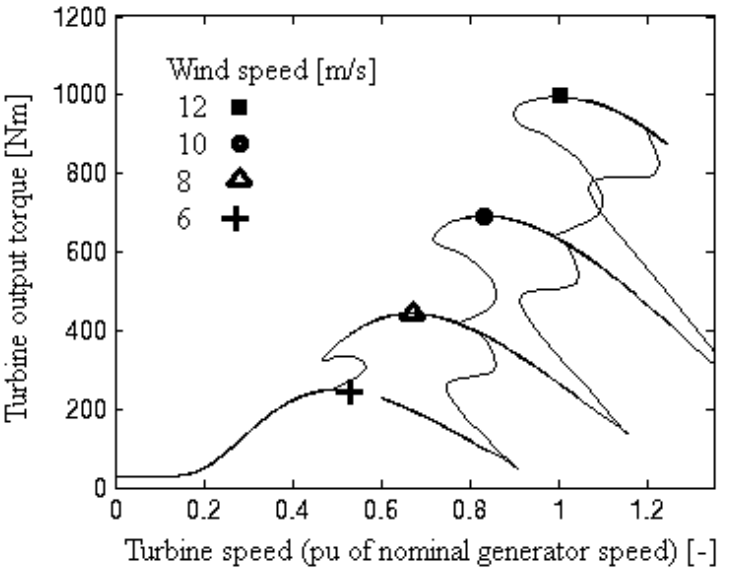

Real-time Optimization of FC / Renewable HPS

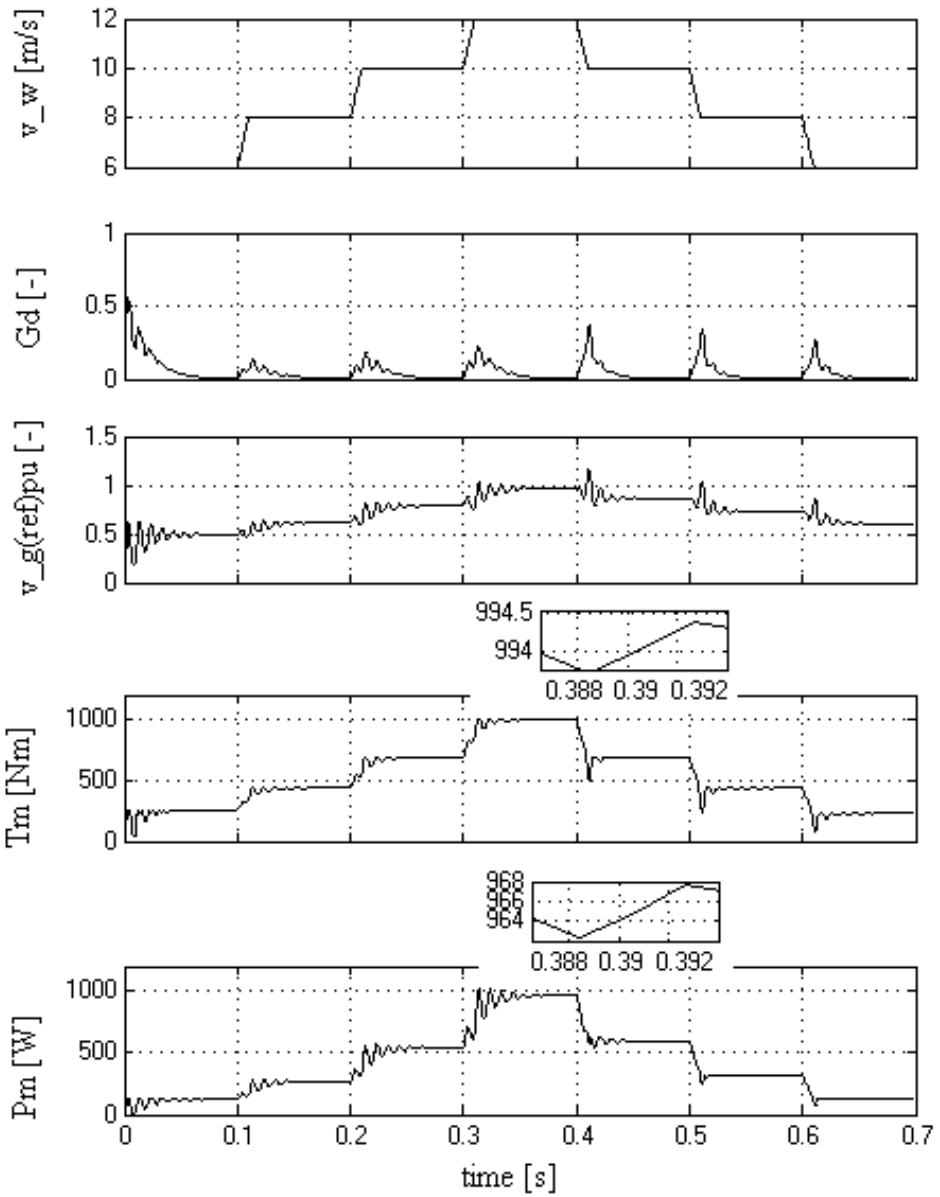

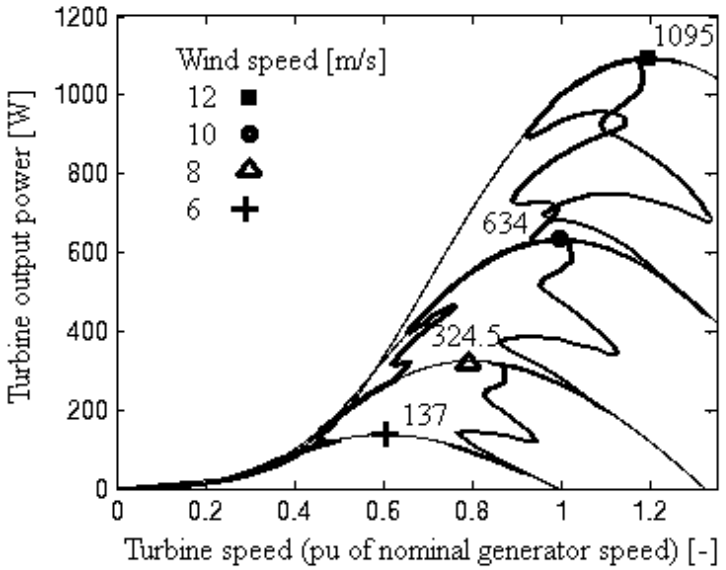

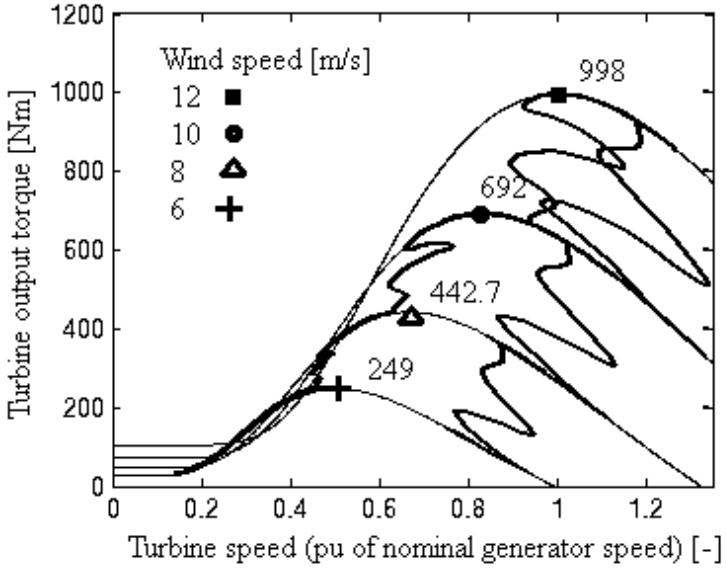

the proposed ES control

Real-time Optimization of FC / Renewable HPS

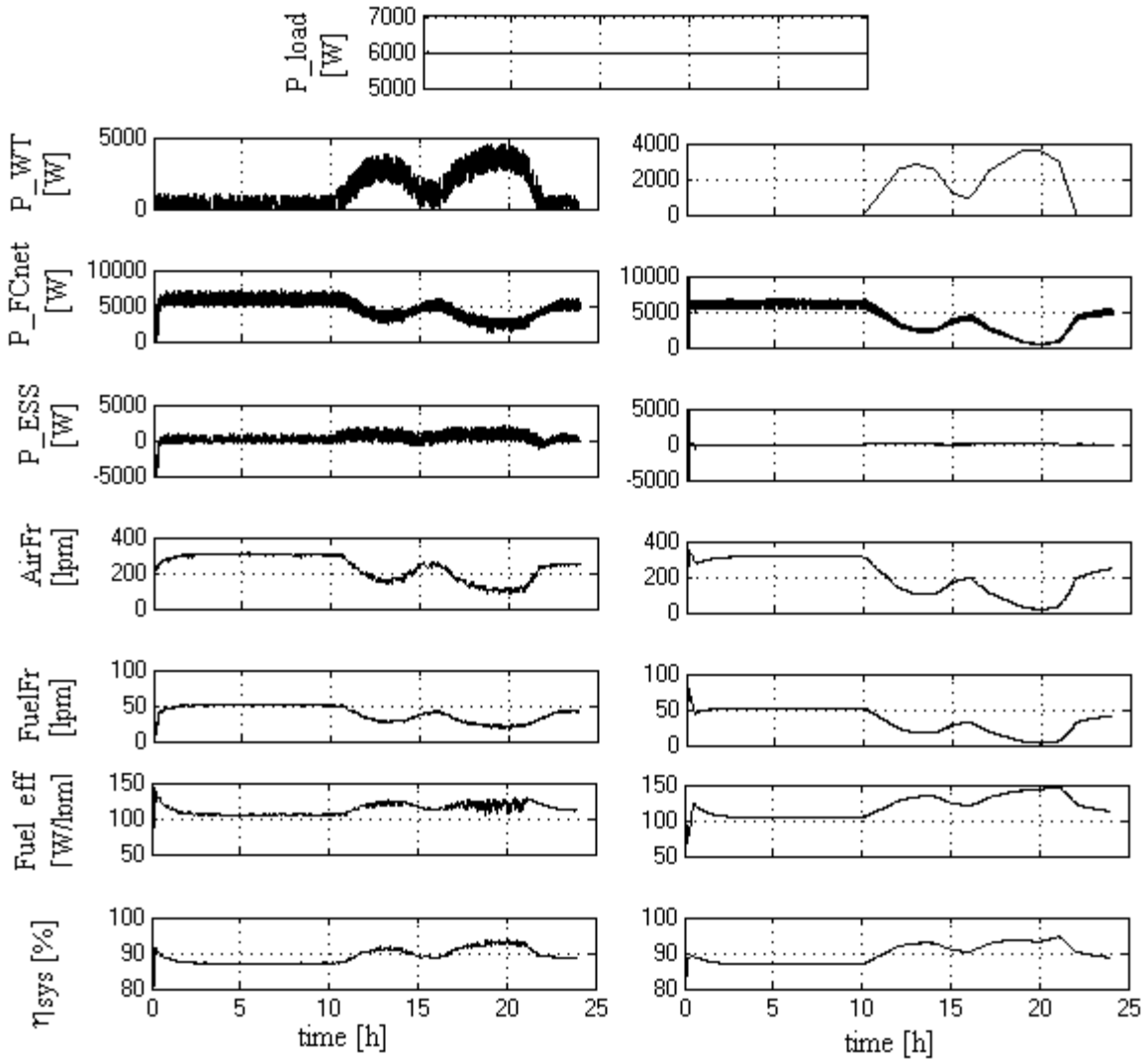

Real-time Optimization of FC / Renewable HPS

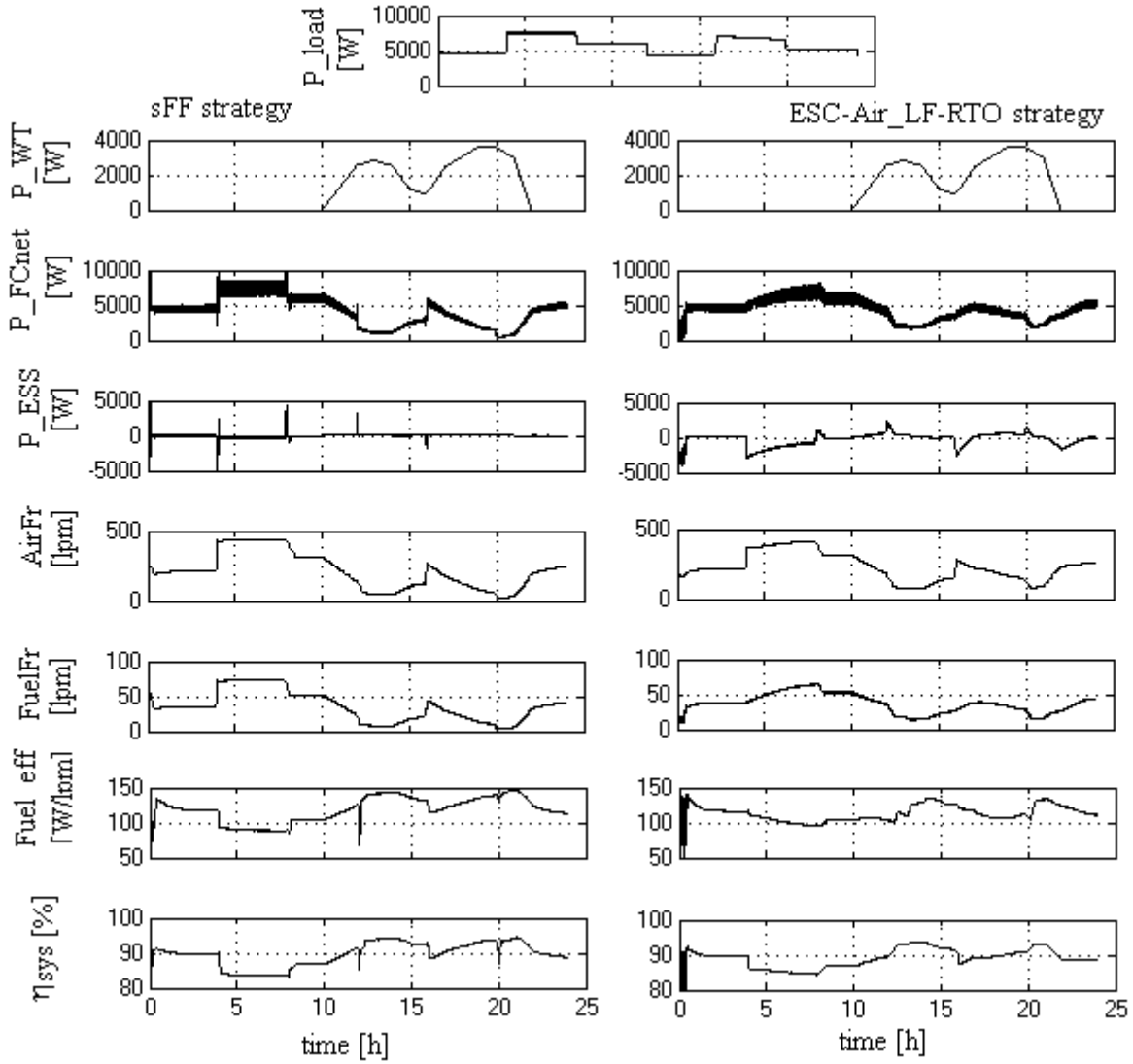

Real-time Optimization of FC / Renewable HPS

Load type	6 kW load		6 kW AV load	
Wind type	turbulent wind	smooth wind	turbulent wind	smooth wind
Gap in fuel economy [lpm]	1.2	1.225	1.275	1.35

Differences in fuel economy for case of turbulent wind and smooth wind are of very small for both sFF and GES-RTO strategies (see Table, being approximately 0.025 lpm and 0.075 lpm for 6 kW load and variable load profile (with AV of 6 kW). It can be noticed that a fuel economy for GES-RTO strategy in comparison with the sFF strategy may be obtained for constant and variable 6 kW load

N. Bizon. Optimal Operation of Fuel Cell / Wind Turbine Hybrid Power System under Turbulent Wind and Variable Load. Applied Energy 2018;212:196-209 Impact Factor: 7.182

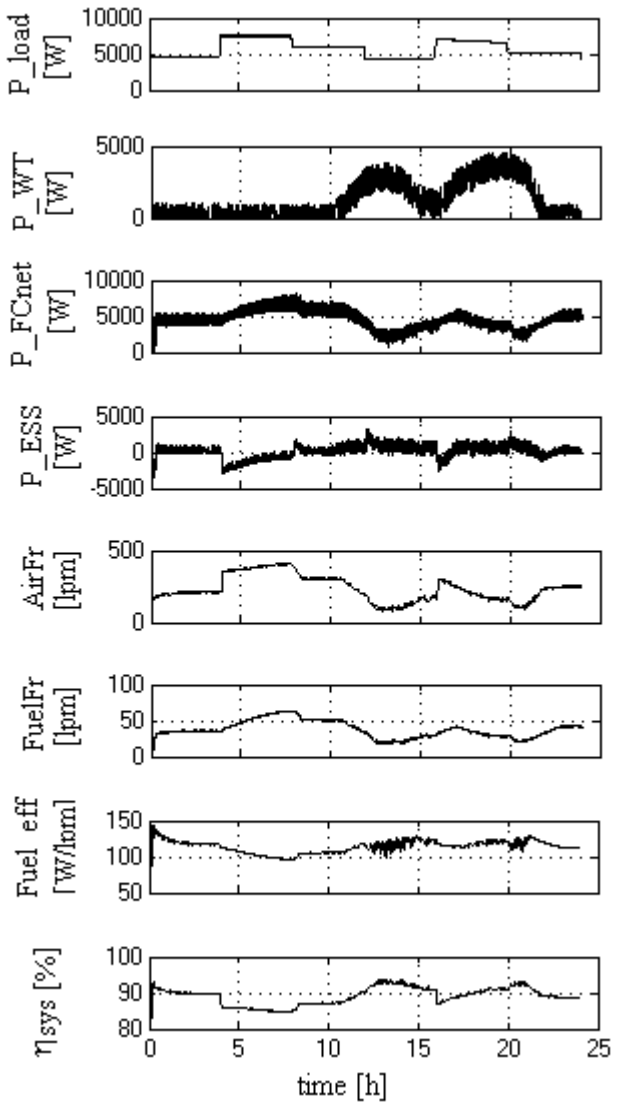

Real-time Optimization of FC / Renewable HPS

RTO Strategy for Fuel Cell Hybrid Power Sources with ES control of the both Fuel and Air Flow Rates

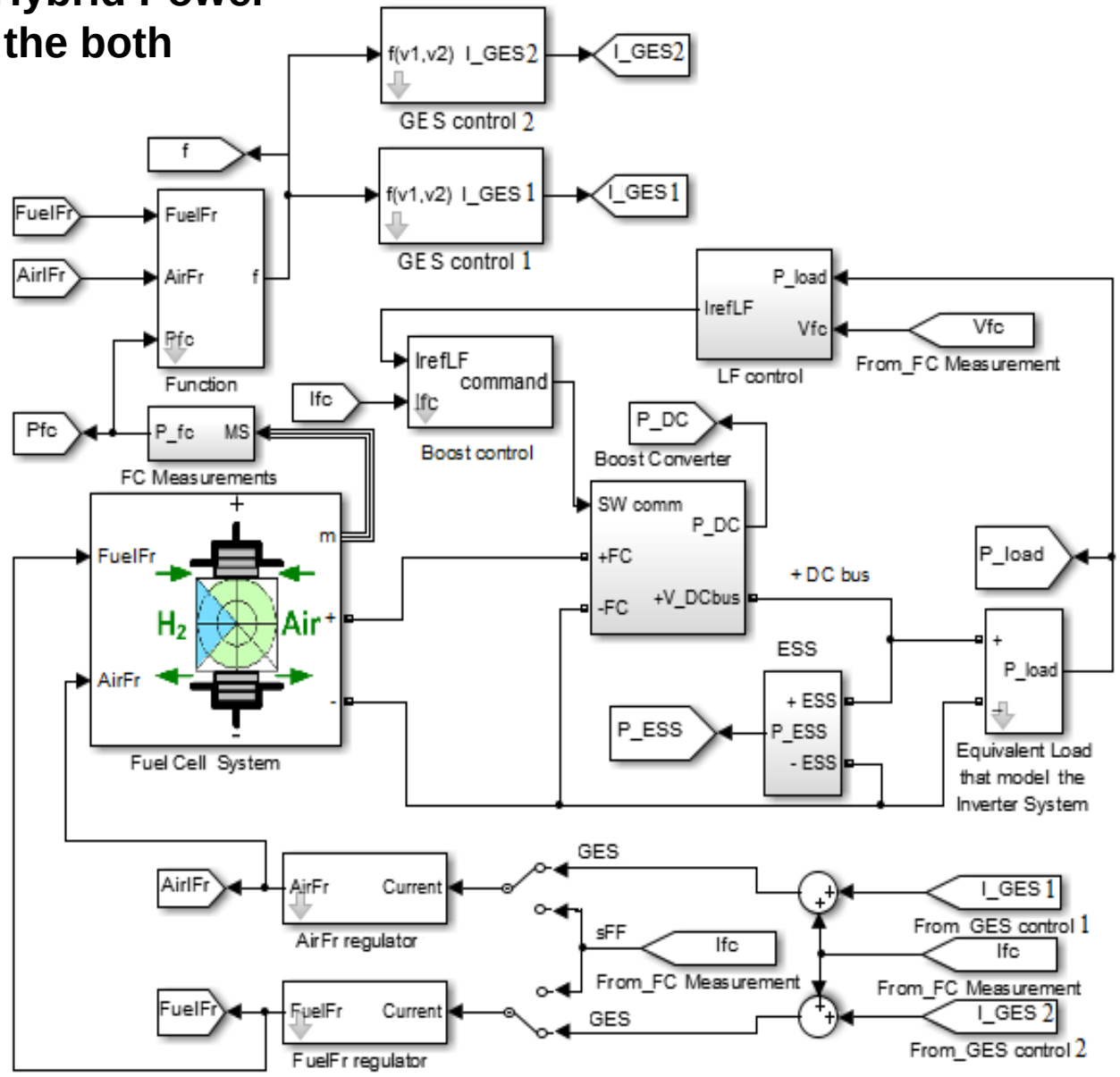

N. Bizon, P. Thounthong. Real-time strategies to optimize the fueling of the fuel cell hybrid power source: A review of issues, challenges and a new approach. Renewable & Sustainable Energy Reviews 2018 (accepted), Impact Factor: 8.05

Real-time Optimization of FC / Renewable HPS

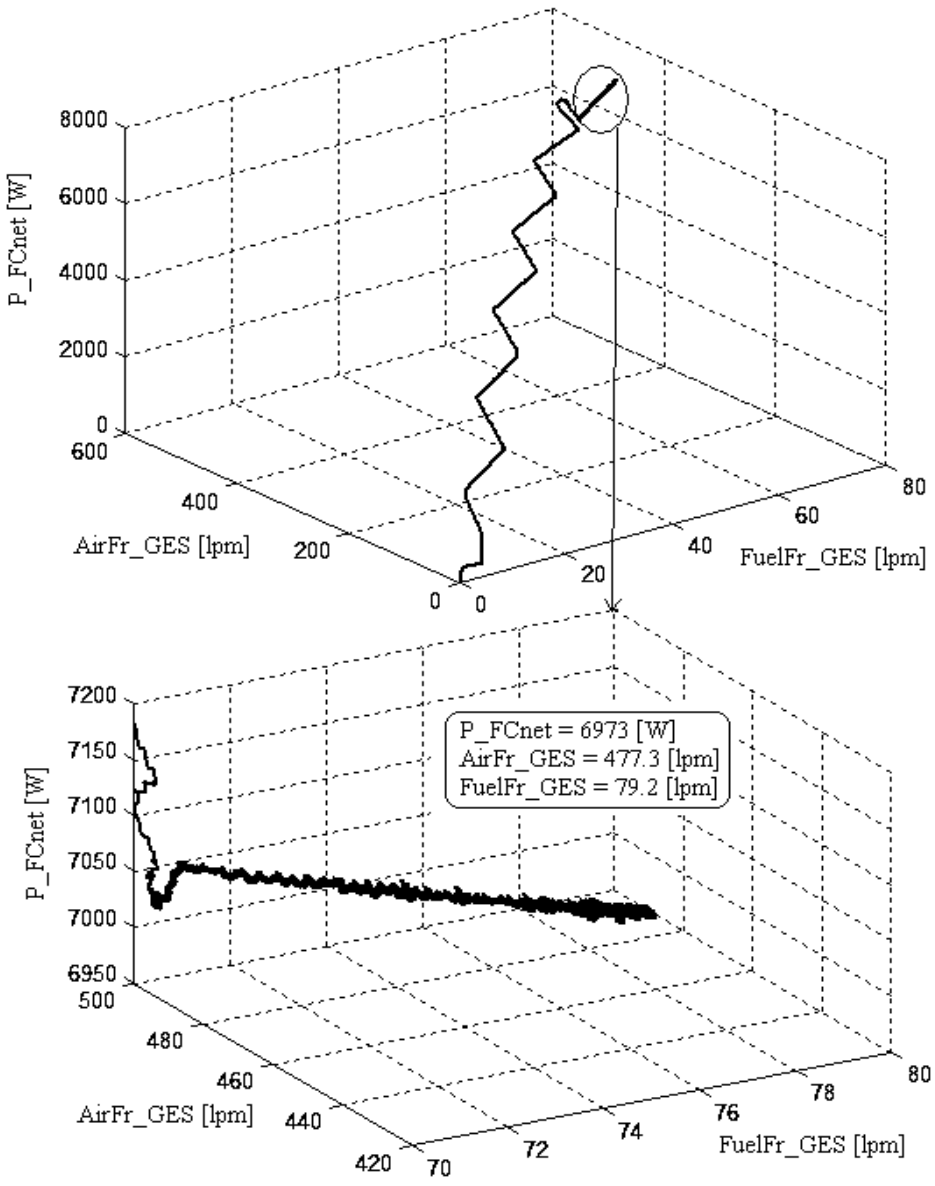

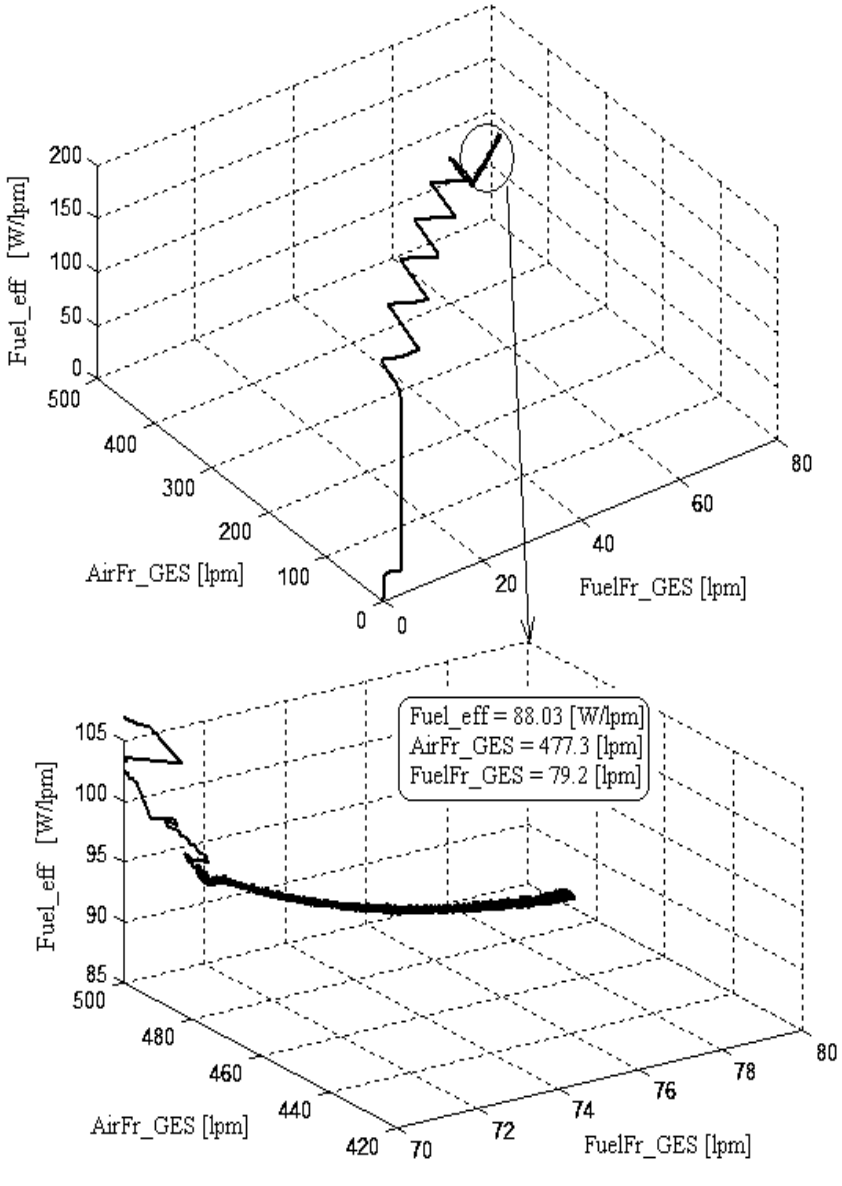

Real-time Optimization of FC / Renewable HPS

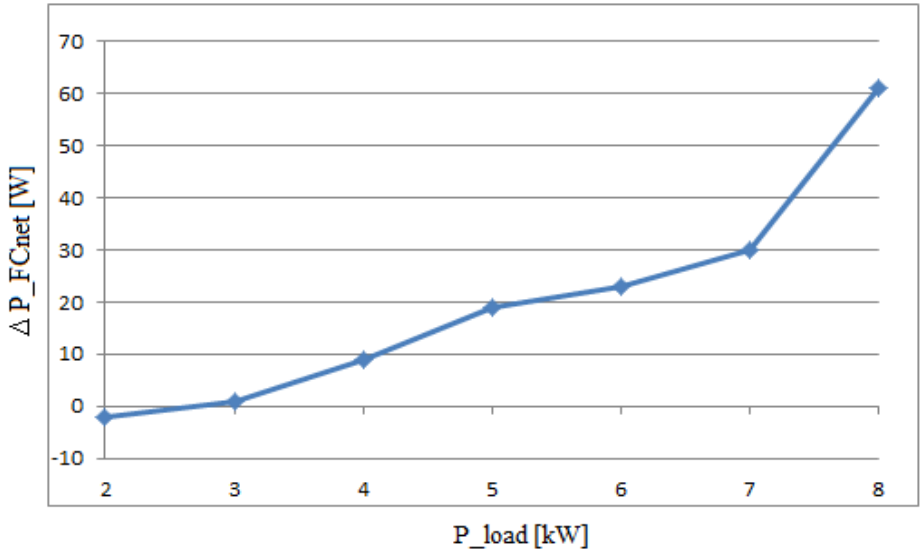

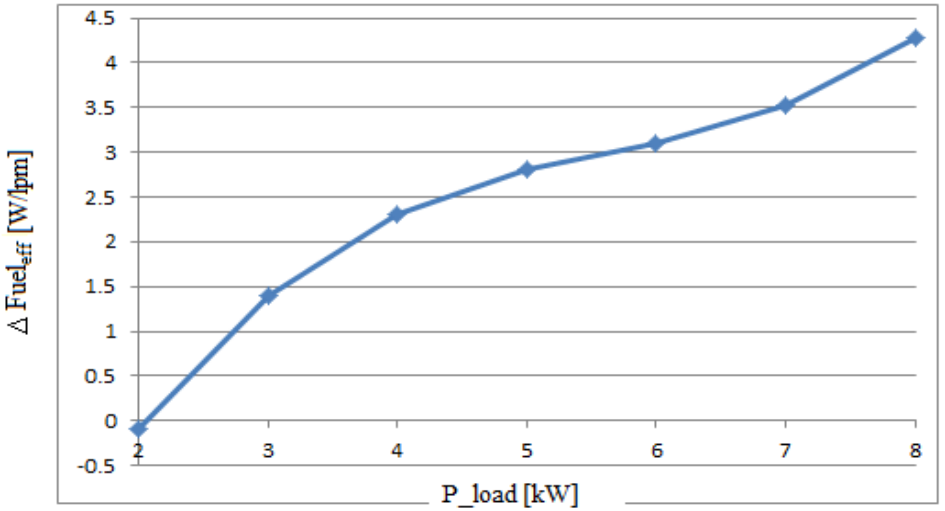

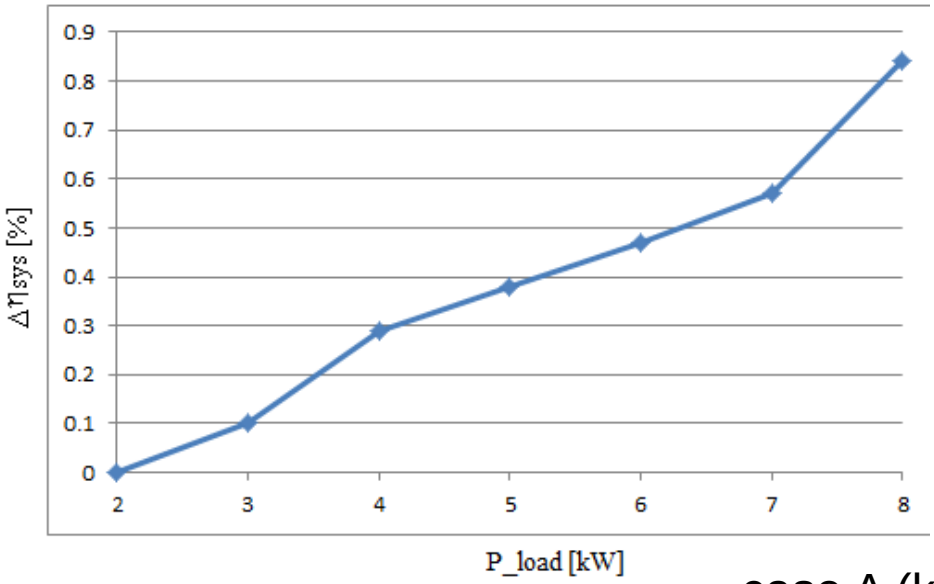

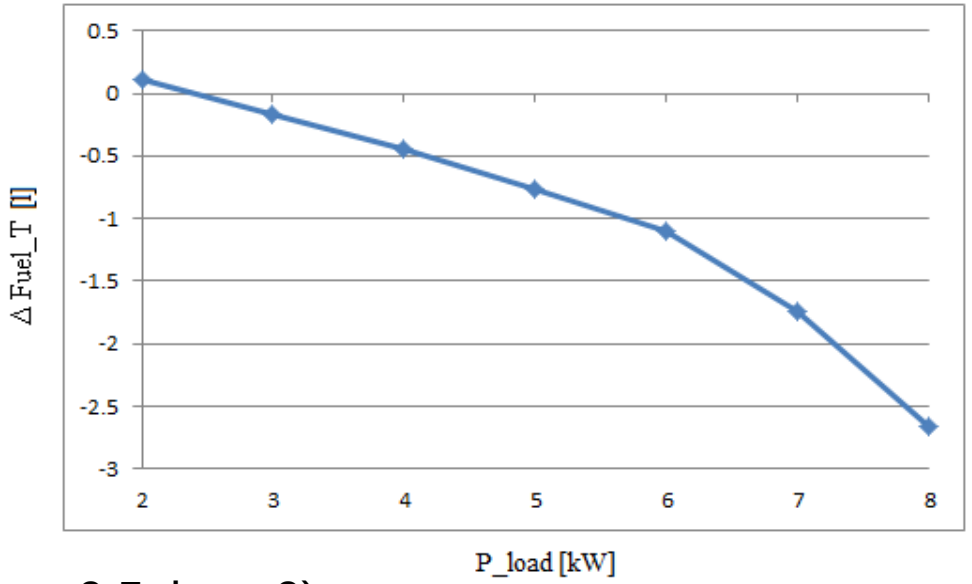

case A (k_{net}=0.5, k_{fuel}=0)

Real-time Optimization of FC / Renewable HPS

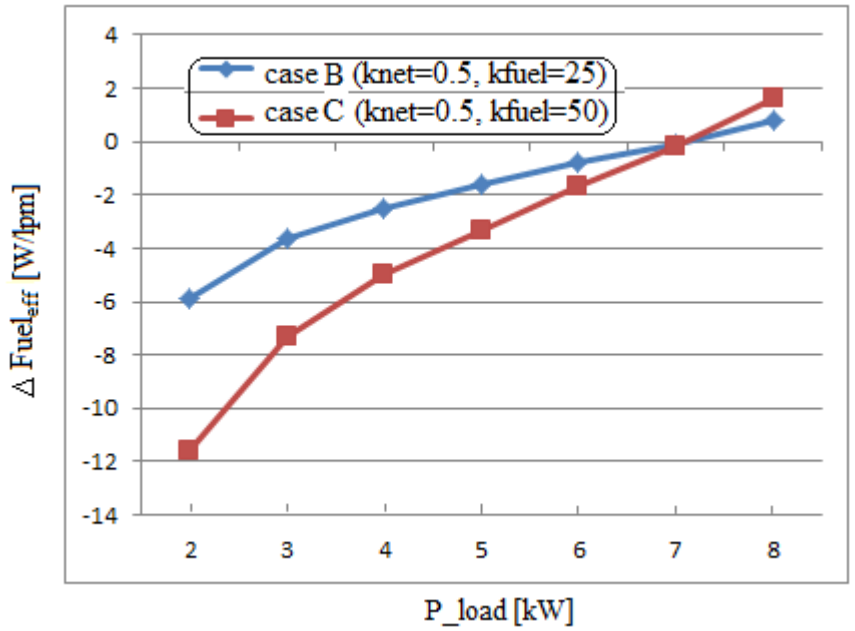

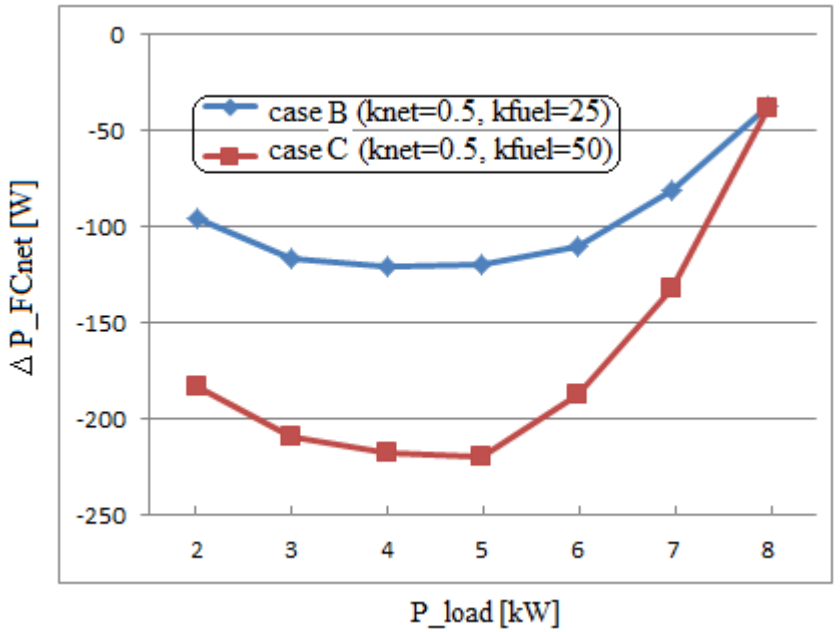

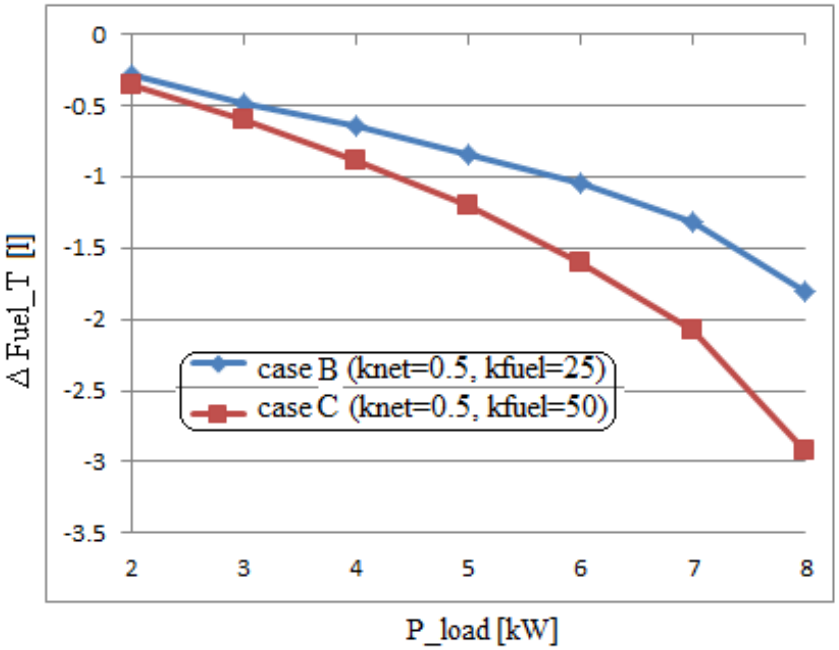

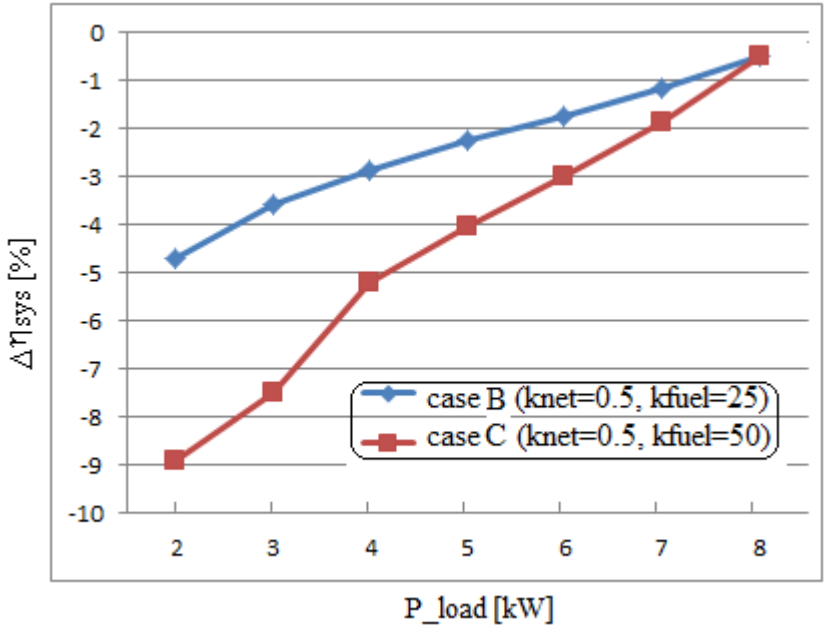

Real-time Optimization of FC / Renewable HPS

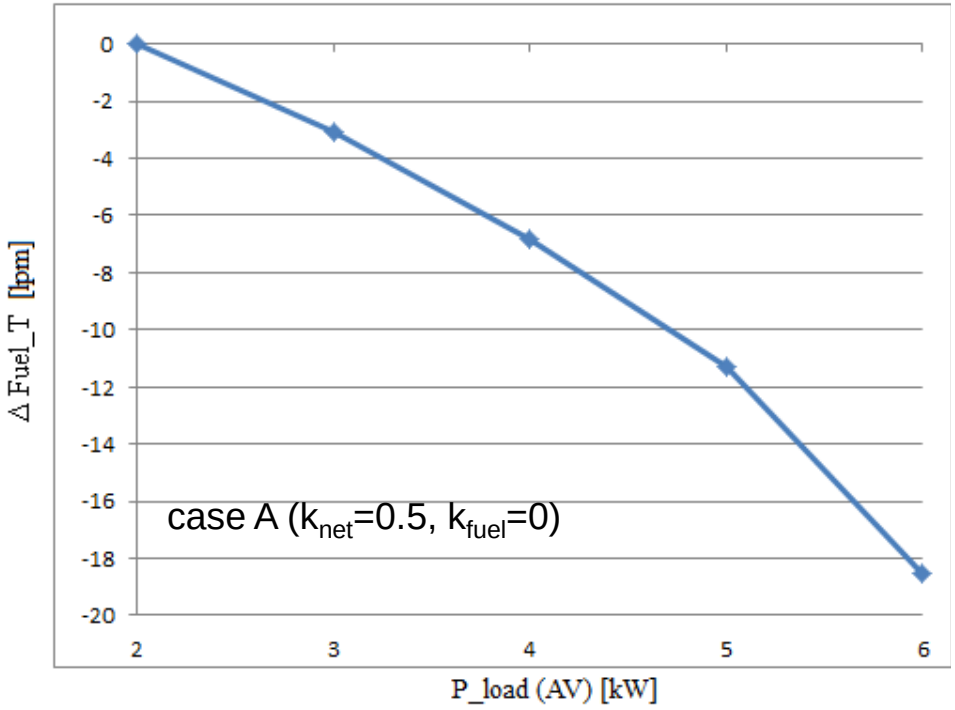

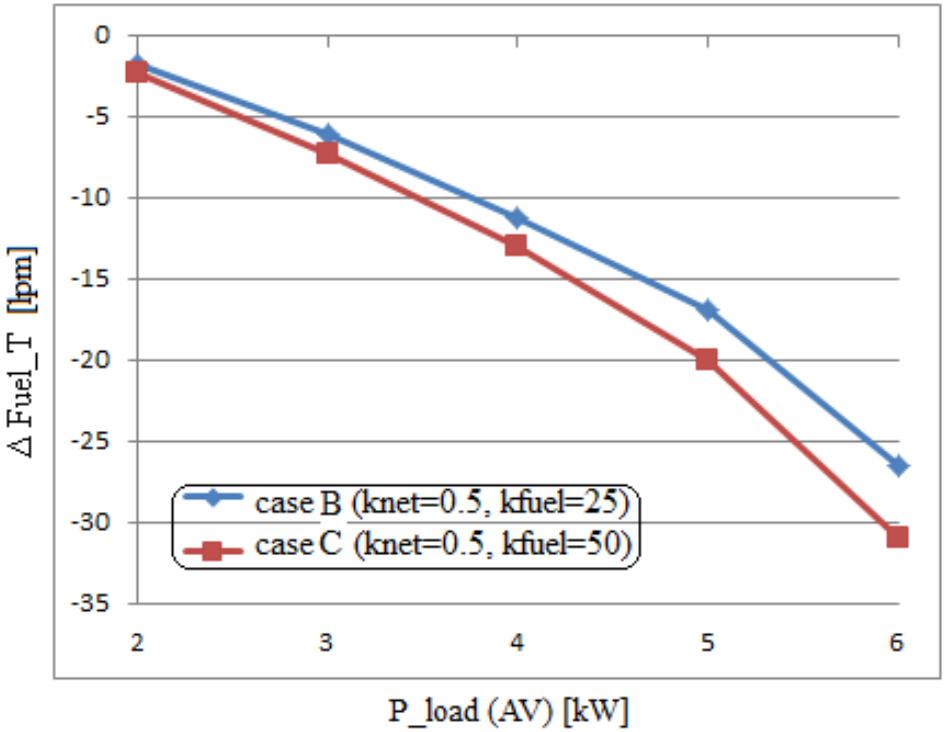

Real-time Optimization of FC / Renewable HPS

Conclusions

No.	$I_{ref(Boost)}$	$I_{ref(Air)}$	$I_{ref(Fuel)}$	RTO strategy	Ref	Class
0	I_{LFW}	I_{FC}	I_{FC}	sFF	[0]	
1	I_{LFW}	I_{FC}	$I_{GES1}+I_{FC}$	RTO1	[1]	C1
2	I_{LFW}	$I_{GES1}+I_{FC}$	I_{FC}	RTO2	[2]	C1
3	I_{GES1}	I_{LFW}	I_{FC}	RTO3	[3]	C2
4	I_{GES1}	I_{FC}	I_{LFW}	RTO4	[4]	C3
5	I_{GES1}	I_{LFW}	$I_{GES2}+I_{FC}$	RTO5	[5]	C2
6	I_{GES1}	$I_{GES2}+I_{FC}$	I_{LFW}	RTO6	[6]	C3
7	I_{LFW}	$I_{GES1}+I_{FC}$	$I_{GES2}+I_{FC}$	RTO7	[7]	C1

[0] Pukrushpan JT, Stefanopoulou AG, Peng H. Control of fuel cell power systems. New York: Springer; 2004.

[1] Bizon N, Culcer M, Iliescu M, Mazare A, Laurentiu I, Beloiu R. Real-time strategy to optimize the Fuel Flow rate of Fuel Cell Hybrid Power Source under variable load cycle. ECAI - 9th Edition of International Conference on Electronics, Computers and Artificial Intelligence. Targoviste, ROMÂNIA, 29 June -01 July, 2017.

Bizon N, Culcer M, Oproescu M, Iana G, Laurentiu I, Mazare A, Iliescu M. Real-time strategy to optimize the Airflow rate of Fuel Cell Hybrid Power Source under variable load cycle, The 22rd International Conference on Applied Electronics - APPEL 2017, University of West Bohemia, Pilsen, Czech Republic, 4 to 6 September 2017.

[3] Bizon N. Energy optimization of Fuel Cell System by using Global Extremum Seeking algorithm. Applied Energy 2017;206:458-474 Impact Factor: 7.182

[4] Bizon N. Real-time optimization strategy for fuel cell hybrid power sources with load-following control of the fuel or air flow. Energy Conversion and Management 2018;157:13–27; impact factor 5.589

[5] Bizon N. Optimization of the Proton Exchange Membrane Fuel Cell Hybrid Power System for Residential Buildings. Energy Conversion and Management 2018;163:22–37; Impact Factor 5.589 , 1 May 2018

[6] Bizon N, Iana G, Kurt E, Thounthong P , Oproescu M, Culcer M, Iliescu M. Air Flow Real-Time Optimization Strategy for Fuel Cell Hybrid Power Sources with Fuel Flow Based On Load-Following. Fuel Cell 2018 (accepted)

[7] Bizon N, Thounthong P. Real-time strategies to optimize the fueling of the fuel cell hybrid power source: A review of issues, challenges and a new approach. Renewable & Sustainable Energy Reviews 2018 (accepted), Impact Factor: 8.05

Real-time Optimization of FC / Renewable HPS

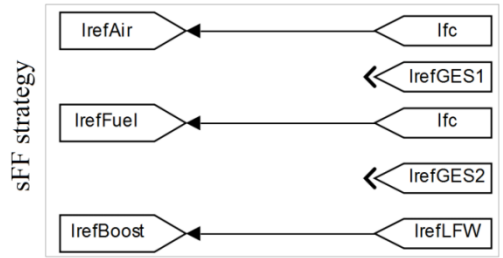

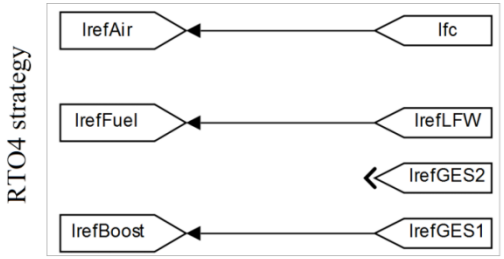

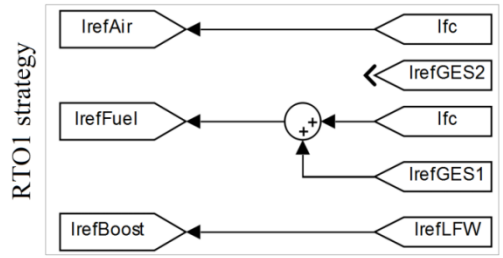

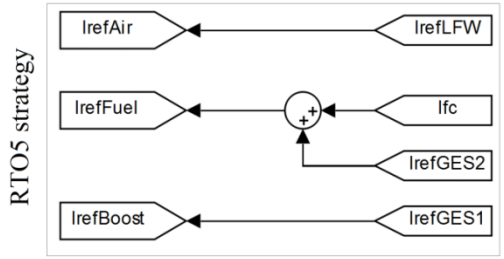

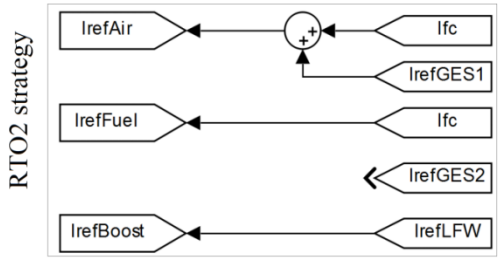

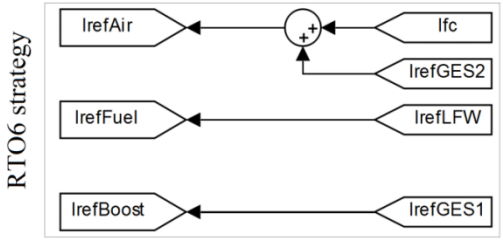

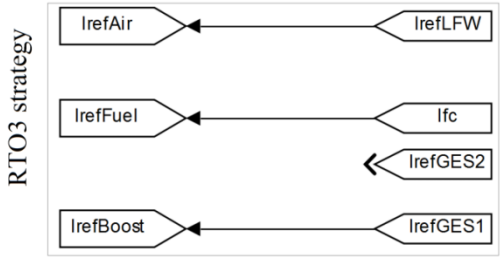

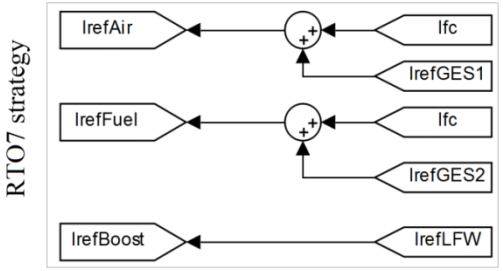

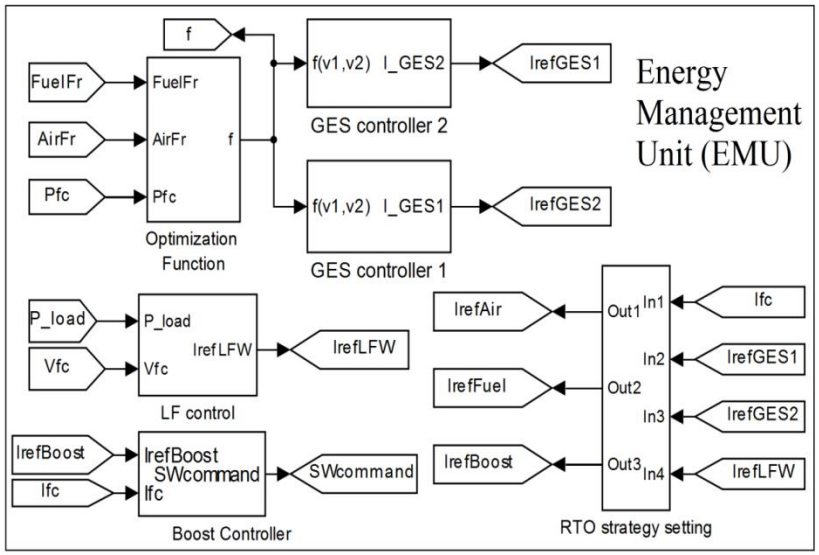

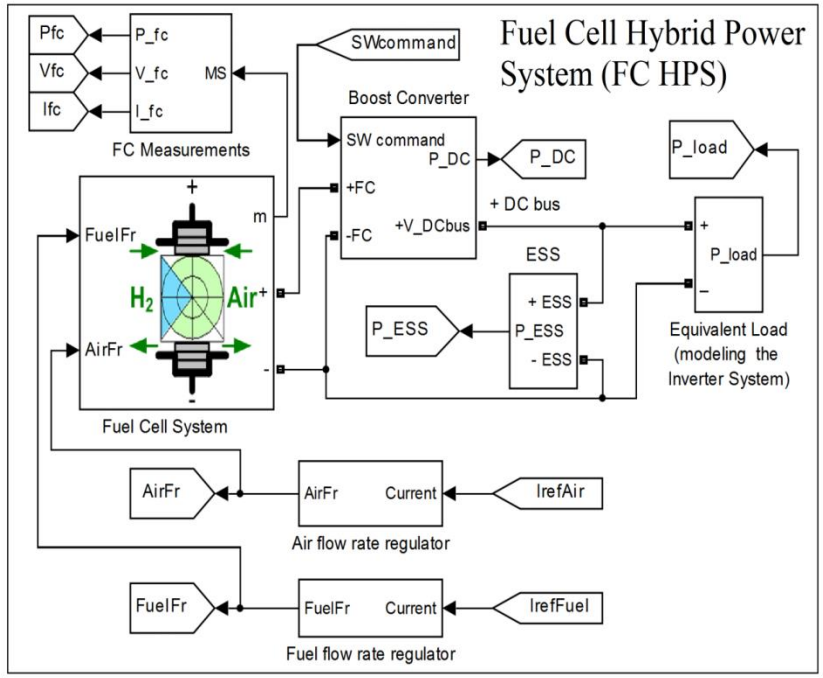

Real-time Optimization of FC / Renewable HPS

No.	$I_{ref(Boost)}$	$I_{ref(Air)}$	$I_{ref(Fuel)}$		RTO strategy
4	I_{GES1}	I_{FC}	I_{LEW}		RTO4
6	I_{GES1}	$I_{GES2}+I_{FC}$	I_{LEW}		RTO6

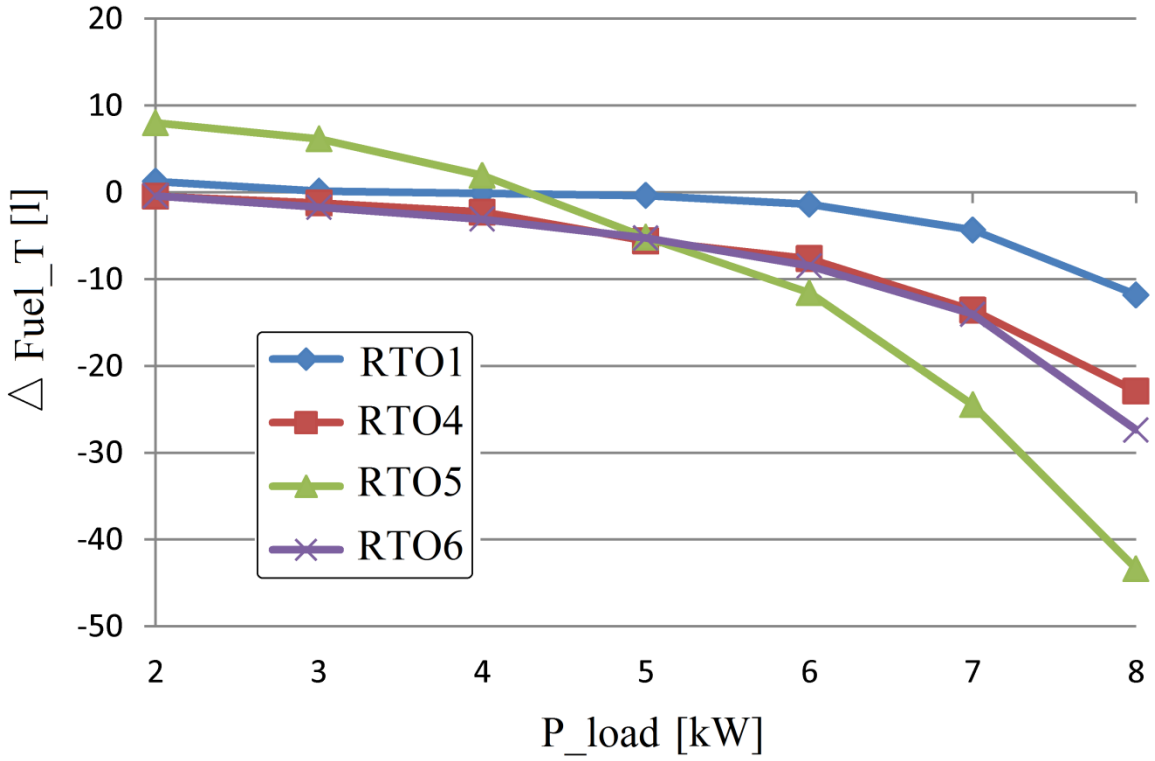

Thank you for your attention
Final questions...